Investigating the role of deubiquitylase enzymes during alphavirus infection

Naomi Coombes

Thesis submitted in accordance with the requirements of the University of Liverpool for the degree of Doctor in Philosophy

April 2019

Declaration

I, Naomi Coombes, confirm that the work presented in this thesis is, except where indicated, the result of my own work and effort. The material contained in the thesis has not been presented, nor is currently being presented, either wholly or in part, for any other degree or other qualification.

Analysis of RSV infection in U2OS-WT and 45KO cell lines was carried out by Shadia Khandaker (University of Liverpool, UK).

Research in this thesis was carried out at the Institute of Infection and Global Health (University of Liverpool, UK).

Abstract

Investigating the role of deubiquitylase enzymes during alphavirus infection

Naomi Coombes

Alphaviruses are a group of arboviruses which include several medically important pathogens including Chikungunya virus (CHIKV). CHIKV is the cause of an extremely debilitating disease, characterised by severe joint pain which can last for months or years. This has a significant impact on the healthcare systems and economies of affected countries. CHIKV has been generating increasing concern as this re-emerging pathogen spreads worldwide. There are currently no vaccines or anti-virals available for CHIKV and with current outbreaks in Asia and the America's escalating, identifying novel drug targets is of increasing importance. As obligate intracellular parasites, viruses depend on host-cell machinery to replicate. Identifying cellular pathways which are hijacked by viruses may provide opportunities to develop novel therapeutics targeting host-factors. Ubiquitylation has been shown to be a key pathway targeted by viruses and the reverse reaction, deubiquitylation, is generating interest for therapeutic intervention. In addition, many viruses have been shown to encode their own deubiquitylase (DUB) which are considered to be highly druggable targets. This thesis investigated the interaction of alphaviruses with host DUBs, a family of ~100 enzymes, and explored the potential for alphaviruses to encode their own DUB.

Prior to this thesis, an initial siRNA screen using the model alphavirus, Semliki Forest Virus (SFV), identified USP45 as a potential pro-viral DUB. Depletion of USP45 resulted in an increase in cell viability post SFV infection. This work was extended to CHIKV using a USP45 knockout cell line in this thesis. USP45 -/- cells are less susceptible to CHIKV infection as reflected by a reduction in viral RNA and protein production. A reduction in the number of cells infected by CHIKV was observed in the absence of USP45, which was partially reversed by direct fusion of virions at the cell membrane. There was also a reduced uptake of transferrin, implying a defect in clathrin-mediated endocytosis, the main method of entry by CHIKV. Thus, these results highlight a role for USP45 during cellular entry by CHIKV and suggest that it could be a potential anti-viral target.

The role of DUBs during alphavirus infection was also investigated using active-site directed probe (ABP) profiling. Utilising ABPs, no probe reactivity was detected for CHIKV implying it was unlikely to possess DUB activity. ABPs were also used to explore changes in host DUB abundance following alphavirus infection by mass spectrometry. This highlighted two DUBs as potentially playing a role in alphavirus infection, USP7 and OTUD6B, which were taken forward for further analysis. This thesis has highlighted the value of generating a greater understanding of the role of DUBs in alphavirus infection. Further analysis of this highly druggable pathway may yield novel treatments for not only alphavirus infections, but a range of diseases, in the future.

Acknowledgements

I would like to express infinite gratitude to my supervisors, Dr. Neil Blake and Professor Judy Coulson, for their continuous support and encouragement throughout this PhD. I am extremely thankful for the opportunities and experiences they provided me with. Without their guidance and constant feedback, this PhD would not have been achievable.

I would also like to thank Dr. Lance Turtle and Dr. Janine Coombes very much for the time they devoted to serving on my advisory panel and for the insightful comments and suggestions provided during our meetings.

I am also indebted to Professor Dario Alessi (University of Dundee) for providing the U2OS-WT and U2OS-45KO cells used in this study. My sincere thanks also to Professor Ian Prior (University of Liverpool) for providing the SILAC labelled HeLa cells.

Special thanks also go to past and present members of both IGH and ITM for our stimulating discussions and their advice throughout this project as well as for all the fun we have had in the last few years. In particular my thanks to: Stacey King, Amer Nubgan, Murad Wali, Charlene Adaken, Lyndsay Mackay, Shadia Khandaker, Ledicia Botas Perez, Sarah Taylor, Francesca Querques and Andrew Fielding.

Last but not least, I would like to thank my parents for their continuous support and always believing in me.

Contents

List of figures

List of tables

List of appendices

Abbreviations

ABP	Activity-based probe
ACTB	Beta-actin
AEC	3-Amino-9-ethylcarbazole
Ago2	Argonaute 2
ANOVA	Analysis of variance
APOBEC	Apoplipoprotein B complex
APS	Ammonium persulfate
Arg 0	L-Arginine
Arg 10	L-Arginine-U13C6-15N4
Arg 6	L-Arginine-U-13C6
Arp3	Actin Related Protein 3
ATP	Adenosine Triphosphate
ATP	Adenosine Triphosphate
ATXN3	Ataxin-3
BAP1	BRCA1 associated protein-1
BFV	Barmah Forest virus
BPB	Bromophenol blue
Br2	Bromoethyl
BRE1B	E3 ubiquitin-protein ligase BRE1B
BUNV	Bunyamwera virus
c-Cbl	Casitas b-lineage lymphoma
CCHFV	Crimean Congo Haemorrhagic Fever Virus
CD4	Cluster of differentiation 4
CDC	Centers for Disease Control and Prevention
cDNA	Complementary deoxyribonucleic acid
CHC	Clathrin heavy chain
CHIKF	Chikungunya fever
CHIKV	Chikungunya virus
CL2	Containment level 2
CL3	Containment level 3

CME	Clathrin-dependent endocytosis
CPE	Cytopathic effect
CRAPome	Contaminant repository for affinity purification
CRISPR	Clustered regularly interspaced short palindromic repeats
CTCF	Corrected Total Cell Fluorescence
Cul5	Cullin 5
CYLD	Cylindromatosis
DAPI	4′,6-diamidino-2-phenylindole
DC-SIGN	Dendritic cell- specific intercellular adhesion molecule-3 grabbing non- integrin
DDX56	DEAD-Box Helicase 56
DENV	Dengue virus
DENV-2	Dengue Virus Type 2
DMARDs	Disease-modifying antirheumatic drugs
DMEM	Dulbecco's modified Eagle's medium
DMSO	Dimethyl sulfoxide
DNA	Deoxyribonucleic acid
DTT	DL-Dithiothreitol
DUB	Deubiquitylating enzymes
DUGV	Dugbe virus
E6AP	E6-associated protein
EAV	Equine Arteritis Virus
EBV	Epstein-Barr virus
ECSA	East, Central and South African
EDTA	Ethylenediaminetetraacetic acid
EEEV	Eastern Equine Encephalitis virus
EEF1A1P5	Eukaryotic Translation Elongation Factor 1 Alpha 1 Pseudogene 5
EGF	Epidermal growth factor
EGFR	Epidermal growth factor receptor
Eps15	Epidermal Growth Factor Receptor Pathway Substrate 15
ERCC1	Excision Repair Cross-Complementation Group 1
ESCRT	Endosomal sorting complexes required for transport

EtBr	Ethidium Bromide
FCS	Fetal Calf Serum
FMDV	Foot-and-Mouth Disease Virus
FUZ	Protein fuzzy homolog
gDNA	Genomic DNA
GMPS	GMP synthase
gRNA	Guide RNA
H1N1	Influenza A virus subtype H1N1
HA	Haemagglutinin
HAUSP	Herpesvirus Associated USP
HBV	Hepatitis B Virus
HBx	Hepatitis B virus X protein
HCC	Hepatocellular carcinoma
HCV	Hepatitis C Virus
HECT	Homologous to E6-AP C-Terminus
HEPES	4-(2-hydroxyethyl)-1-piperazineethanesulfonic acid
HIV-1	Human Immunodeficiency Virus Type 1
HPV	Human Papilloma Virus
HRP	Horseradish peroxidase
Hrs	Hours
HSP90AB2P	Heat Shock Protein 90 Alpha Family Class B Member 2, Pseudogene
HSV-1	Herpes Simplex Virus Type 1
HTLV-1	Human T- cell Leukemia Virus Type 1
IAV	Influenza A Virus
ICAM-1	Intercellular Adhesion Molecule 1
ICP0	Infected Cell Polypeptide 0
IFN	Interferon
IGHA1	Immunoglobulin Heavy Constant Alpha 1
IGHG2	Immunoglobulin heavy constant gamma 2
IGHV1-45	Immunoglobulin heavy variable V1-45
IL	Interleukin
IOL	Indian Ocean lineage

IRES	Internal ribosome entry site
IRF	Interferon regulatory factor
JAMM	Jab1/MPN/MOV34
JCHAIN	Joining Chain Of Multimeric IgA And IgM
JEV	Japanese Encephalitis Virus
KCNK1	Potassium channel subfamily K member 1
KO	Knock-out
KSHV	Kaposi's Sarcoma-associated Herpesvirus
L15	Leibovitz
Lac	β-lactone
LC-MS/MS	Liquid chromatography-tandem mass spectrometry
LPAIV	Low Pathogenicity Avian Influenza Virus
Lys 0	L-Lysine
Lys 4	L-Lysine-2H4
Lys 8	L-Lysine-U13C6-15N2
MAYV	Mayaro virus
MDA5	Melanoma Differentiation-Associated protein 5
MDM2	Mouse double minute 2 homolog
MERS	Middle East respiratory syndrome
MINDY	Motif interacting with Ub-containing novel DUB family
Mins	Minutes
MJD	Machado-Josephin domains
MMTAG2	Multiple myeloma tumor-associated protein 2
MOI	Multiplicity of infection
MOPS	3-(N-morpholino)propanesulfonic acid
mRNA	Messenger ribonucleic acid
MS	Mass spectrometry
MW	Molecular weight
Mxra8	Matrix Remodeling Associated 8
MYDGF	Myeloid Derived Growth Factor
NDS	Normal donkey serum
NF-κB	Nuclear factor kappa light chain enhancer of activated B cells
NGS	Normal goat serum

NHEJ	Non-homologous end joining
NSAID	Nonsteroidal anti-inflammatory drugs
NsP	Non-structural protein
OEtVS	Vinylethoxysulfone
ONNV	O'nyong-nyong virus
ORF	Open reading frame
OTU	Ovarian tumour proteases
OTULIN	OTU Deubiquitinase With Linear Linkage Specificity
p.i.	Post-infection
PA	Propargyl amide
PAHO	Pan American Health Organization
PBS	Phosphate-buffered saline
PCR	Polymerase chain reaction
Pfu	Plaque Forming Units
PIP5K1-α	Phosphatidylinositol-4-Phosphate 5-Kinase Type 1 Alpha
PLK1	Polo Like Kinase 1
PLP2	Proteolipid Protein 2
PLpro	its papain-like protease
Poly-A	Polyadenylate
Pro 0	L-Proline
qPCR	Quantitative PCR
Rac1	Rac Family Small GTPase 1
Rbx-1	RING-box protein 1
RdRp	RNA dependent RNA polymerase
RIG-I	Retinoic acid-inducible gene I
RING	Really interesting new gene
RISC	RNA-inducing silencing complex
RNA	Ribonucleic acid
RNAi	RNA interference
RND3	Rho Family GTPase 3
Rpm	Revolutions per minute
RRV	Ross River virus
SARS-CoV	Severe Acute Respiratory Syndrome Coronavirus

SDS	Sodium Dodecyl Sulfoxide
SDS PAGE	Sodium dodecyl sulfate polyacrylamide gel electrophoresis
SESV	Southern Elephant Seal Virus
SEV	Sendai Virus
SFV	Semliki Forest virus
SILAC	Stable Isotope Labeling by/with Amino acids in Cell culture
SINV	Sindbis virus
siRNA	Small interfering Ribonucleic Acid
SOCS1	Suppressor Of Cytokine Signaling 1
SPDV	Salmon Pancreatic Disease Virus
STAMBPL 1	STAM-binding protein-like 1
STAT	Signal transducer and activator of transcription
STING	Stimulator of interferon genes
SV40	simian virus 40
TAE	Tris-Acetate-EDTA
Taq	Thermus aquaticus
TBE	Tris-Borate-EDTA
TC	Tissue Culture
TEMED	N,N,N',N'-Tetramethylethylenediamene
TF_3BOK	2,6-trifluoromethylbenzyloxymethylketone
Tfn	Transferrin
TIM-1	T-cell immunoglobulin and mucin domain 1
TMEM263	Transmembrane Protein 263
TRAF	TNF receptor-associated factor
TRIM6	Tripartite Motif Containing 6
TSPAN9	Tetraspanin 9
TYMV	Turnip Yellow Mosaic Virus
Ub	Ubiquitin
Ubal	Ubiquitin-aldehyde
UBCH10	Ubiquitin-conjugating enzyme E2 C
Ub-CN	Ubiquitin-nitrile
UBD	Ubiquitin-binding domain

UCH	Ubiquitin C-terminal hydrolases
USP	Ubiquitin-specific proteases
VACV	Vaccinia Virus
VEEV	Venezuelan Equine Encephalitis virus
vIRF1	Viral interferon regulatory factor 1
VLPs	Virus-like particles
VME	Vinyl methyl esters
VS	Vinyl methyl sulfone
VSV	Vesicular Stomatitis Virus
WA	Western African
WEEV	Western Equine Encephalitis virus
WT	Wild-type
ZIKV	Zika Virus
ZnF-UBP	Zinc-finger ubiquitin binding
ZUFSP	Zinc finger with UFM1-specific peptidase domain
β-ME	Mercaptoethanol

Chapter 1: General introduction

1.1 Alphaviruses

Alphaviruses are a globally distributed group of arboviruses (arthropod-borne viruses), transmitted primarily via a mosquito vector (Lim *et al.*, 2018). These single-stranded RNA viruses have a broad host range and include some serious human and animal pathogens which are an economic and public health concern (Weaver & Lecuit, 2015). Most pathogenic alphaviruses cause an acute, febrile illness which is followed by the development of arthralgia or encephalitis, depending on their categorisation as Old World or New World alphaviruses. Old World alphaviruses are typically associated with a rheumatic disease and include: Semliki Forest virus (SFV), Chikungunya virus (CHIKV), Ross River virus (RRV), Barmah Forest virus (BFV), O'Nyong-Nyong virus (ONNV), Sindbis virus (SINV) and Mayaro virus (MAYV). New World alphaviruses are associated more with an encephalitic disease and include: Venezuelan Equine Encephalitis virus (VEEV), Eastern Equine Encephalitis virus (EEEV) and Western Equine Encephalitis virus (WEEV) (Suhrbier *et al.*, 2012; Rupp *et al.*, 2015*a*; Chen *et al.*, 2018). Alphavirus research has intensified over the last decade, largely as a result of several major outbreaks of CHIKV in Africa, Asia, Europe and the Americas (Arankalle *et al.*, 2007; Volk *et al.*, 2010; Weaver & Lecuit, 2015). However, other alphaviruses, such as ONNV which has a similar potential to cause world-wide outbreaks, are generating increasing concern (Rezza *et al.*, 2017). The threat of outbreaks is only likely to increase as factors such as expanding mosquito ranges expose new, immunologically naïve populations to these viruses (Rochlin *et al.*, 2013; Lanciotti & Valadere, 2014; Baylis, 2017). Furthermore, there have also been several outbreaks of alphaviruses in previously unaffected areas introduced by infected travellers (Johansson *et al.*, 2014; Rossini *et al.*, 2016; Wahid *et al.*, 2017). Generating novel therapeutic approaches to target alphaviruses, such as CHIKV, is therefore essential and will be accelerated by forming a comprehensive understanding of alphavirus biology.

1.1.1 Taxonomy

The *Togaviridae* family is a group of enveloped positive-sense RNA viruses which branches into either the *Alphavirus* or *Rubivirus* genera. There is only one known species within the *Rubivirus* genus, Rubella virus. However, the *Alphavirus* genus consists of 31 species which can be split into seven phylogenetic sub-groups (Figure 1.1) (Powers *et al.*, 2001; Chen *et al.*, 2018). It is hypothesised that alphaviruses have a marine origin owing to the discovery of aquatic alphaviruses positioned towards the base of phylogenetic trees (Forrester *et al.*, 2012). Terrestrial alphaviruses are thought to have become established following several geographical introductions and subsequently diverged into Old and New world alphaviruses (Forrester *et al.*, 2012; Rupp *et al.*, 2015*b*).

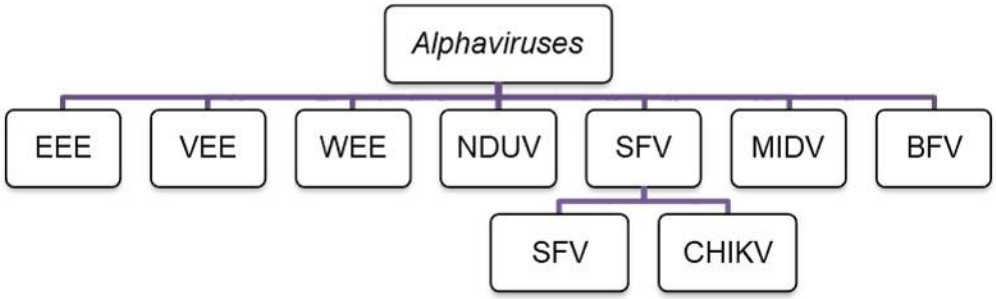

Figure 1.1. Schematic representation of the different alphavirus phylogenetic sub-groups
Alphaviruses can be split into seven sub-groups which have been based on full genome alignment: Eastern equine encephalitis (EEE), Venezuelan equine encephalitis (VEE), Western equine encephalitis (WEE), Ndumu virus (NDUV), Semliki Forest Virus (SFV), Middelburg virus (MIDV) and Barmah Forest virus (BFV). The classification of two alphavirus species, SFV and CHIKV, are highlighted. Figure adapted from Forrester *et al.* (2012).

1.1.2 Structure

Alphavirus virions are approximately 70nm in diameter and built around a positive-sense single-stranded RNA genome which contains a 5' 7-methyl-GpppA cap and a 3' polyadenylated tail. The 5' cap aids initiation of protein synthesis as well as protecting the viral RNA from host degradation

mechanisms (Hefti *et al.*, 1975; Strauss *et al.*, 1984). The genomic RNA of alphaviruses is approximately 11-12 kb in length and is composed of two open reading frames (ORFs) separated by an internal promoter (Strauss *et al.*, 1984). The 5' ORF encodes the non-structural proteins (nsP1-4) and the 3' ORF encodes the structural proteins (E1, E2, E3, capsid and 6K) (Figure 1.2A) (Strauss *et al.*, 1984; Strauss & Strauss, 1994). The genome is enclosed within a protein capsid shell and host-derived lipid bilayer which is interspersed with virally encoded glycoprotein spikes (E1 and E2 proteins, see section 1.1.4). The inner nucleocapsid is formed of a T=4 arrangement of capsid protein, made up of 264 amino acid residues. Capsid protein contains a hydrophobic pocket at residues 400-402 for the E2 protein to interact as well as a highly basic region in the first 100 residues where the viral RNA is thought to bind (Coombs & Brown, 1989; Lee *et al.*, 1996; Mukhopadhyay *et al.*, 2006). The outer envelope is built up of 80 trimers of E1/E2 heterodimers in a T=4 structure (Figure 1.2B) (Holland Cheng *et al.*, 1995; Zhang *et al.*, 2002).

1.1.3 Non-structural proteins

Alphaviruses encode four non-structural proteins, nsP1, nsP2, nsP3 and nsP4, which are first translated as a polyprotein precursor (Strauss *et al.*, 1983; Li & Rice, 1993). This polyprotein plays an important role in genome replication (see section 1.1.5.2), but the individual proteins also perform crucial functions as their separate entities. Cleavage of the polyprotein into its mature protein species is achieved via the autocatalytic activity of nsP2, through its cysteine protease domain (Hahn *et al.*, 1989; Takkinen *et al.*, 1991). NsP1 has been shown to act as a capping enzyme for newly synthesised viral RNA which both aids in translation and protects from degradation (Cross, 1983). It also plays an important role in anchoring replication complexes to cellular membranes to initiate formation of spherules, sites of viral RNA synthesis (Lampio *et al.*, 2000; Spuul *et al.*, 2007). As well as acting as a protease to cleave the nsP polyprotein, nsP2 has been shown to act as an RNA helicase to unwind double-stranded RNA (Gomez De Cedrón *et al.*, 1999). It also possess RNA triphosphatase activity

and works with nsP1 to aid viral mRNA capping (Vasiljeva *et al.*, 2000). NsP2 is considered crucial for shutoff of host transcription and translation which contributes to the inhibition of antiviral responses (Breakwell *et al.*, 2007; Frolov *et al.*, 2009; Bhalla *et al.*, 2016). The role of nsP3 is not as well defined but is thought to play an important role in viral RNA transcription and nucleocapsid assembly (Foy *et al.*, 2013; Rathore *et al.*, 2014). NsP4 is highly conserved and contains the RNA dependent RNA polymerase (RdRp) domain responsible for viral RNA transcription. It is also forms crucial interaction with the P123 polyprotein to initiate formation of the replication complexes (Rubach *et al.*, 2009; Rupp *et al.*, 2011).

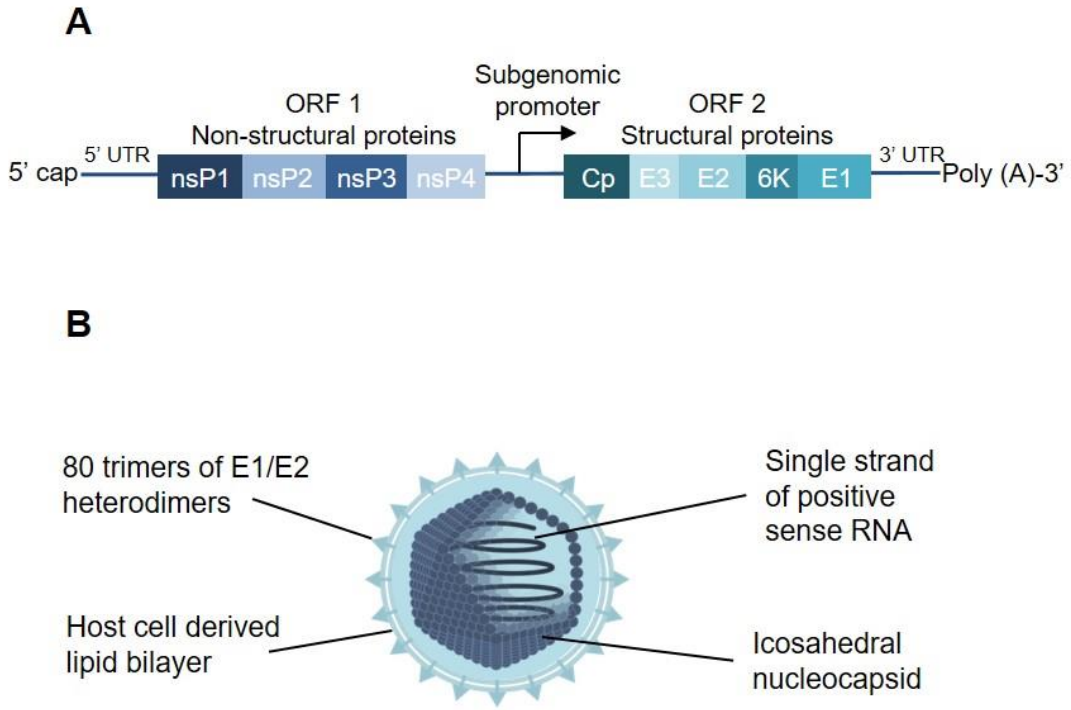

Figure 1.2. Schematic representation of the alphavirus genome and virion

(**A**) The alphavirus genome is 11-12 kb of single stranded positive sense RNA with a 5'cap and 3' poly(A) tail. A region of untranslated RNA (UTR) is present at the 5' and 3' ends. There are two open reading frames (ORFs) separated by an internal subgenomic promoter. The first ORF encodes the non-structural proteins 1 -4 (nsP1-4). The second ORF encodes the structural proteins capsid (Cp), glycoproteins E1-3 and 6K. (**B**) The genome of alphaviruses are contained within an icosahedral nucleocapsid which is surrounded by a host cell derived lipid bilayer. The outer membrane is studded with 80 trimers of E1/E2 heterotrimers.

1.1.4 Structural proteins

There are five structural proteins (E1, E2, E3, capsid and 6K) encoded by alphaviruses (Figure 1.2A). These are not only important for the alphavirus architecture, but also have important functional roles. E1 is composed of 439 amino acids and acts as a fusion protein to control fusion of the viral and endosomal membranes following virus uptake. The E2 protein is 423 amino acids in length and is important for receptor binding and the ensuing receptor-mediated endocytosis. E3 is a small 64 amino acid protein which interacts with E1 fusion protein to ensure proper spike folding and activation in virus entry (Mukhopadhyay *et al.*, 2006; Jose *et al.*, 2009). The capsid protein consists of 264 amino acids and is not only important in forming the icosahedral structure which protects the viral genome but also contains a chymotrypsin-like serine protease (Rice & Strauss, 1981; Choi *et al.*, 1991). The protease function of capsid is essential for its release from the polyprotein pre-cursor but is only active for a single self-cleavage event (Choi *et al.*, 1991). 6K is another small protein present within alphavirus virions, albeit at much lower quantities (approximately 7-30 copies per particle). Less is known about the location and role of 6K. However, when the encoding sequence was deleted, the yield of infectious virus was markedly reduced (Liljeström *et al.*, 1991). It has been suggested that 6K could be involved in ion pore formation in the endoplasmic reticulum thus aiding virus assembly (Liljeström & Garoff, 1991; Melton *et al.*, 2002).

1.1.5 Alphavirus lifecycle

1.1.5.1 Alphavirus binding and entry

The alphavirus lifecycle (Figure 1.3) is initiated upon binding to the surface of a susceptible cell via the E2 glycoprotein. Several receptors have been implicated in alphavirus entry including: laminin, DC-SIGN, heparan sulphate, α1β1 integrin, TIM-1 and Mxra8 (Wang *et al.*, 1992; Smit *et al.*, 2002; Klimstra *et al.*, 2003; La Linn *et al.*, 2005; van Duijl-Richter *et al.*, 2015; Zhang *et al.*, 2018*a*). However, there is no clear evidence for whether these

are directly involved in virus entry or simply promote initial virus binding. Furthermore, although heparan sulphate binding has been shown to increase alphavirus infection, this effect is due to virus adaptation to cell culture and is not seen for circulating virus (Klimstra *et al.*, 1998; Smit *et al.*, 2002). The ability of alphaviruses to bind many cell surface receptors has been suggested as one reason why so many different cell types are susceptible to infection (Jose *et al.*, 2009).

Once bound to the cell surface the virus is then taken up by receptor mediated endocytosis. The type of endocytosis utilised is dependent on the cell type. For example, CHIKV has been shown to be taken up into 293T cells by clathrin-independent endocytosis, whereas in HeLa and U2OS cells clathrin-dependent endocytosis (CME) is utilised (Bernard *et al.*, 2010; Ooi *et al.*, 2013; Hoornweg *et al.*, 2016*b*). It is not thought that alphaviruses trigger endocytosis but instead take advantage of a receptor which is constitutively internalised (Marsh & Helenius, 1980). However, the uptake via receptor-mediated endocytosis has been shown to be very rapid with half of the virus particles taken up within 3-10 mins at 37°C (Kielian *et al.*, 1986; Schmid *et al.*, 1989).

Following uptake, acidification of the endosome leads to fusion of the viral envelope and endosomal membranes (Mellman *et al.*, 1986; Kielian *et al.*, 1986; Glomb-Reinmund & Kielian, 1998). The pH at which alphaviruses fuse can vary depending on the virus. For example SFV and CHIKV have been shown to fuse with early endosomes below ~pH 6.2 (Kielian *et al.*, 1986). However, certain strains of another alphavirus, SINV, have been shown to fuse below ~pH 5.6 (Glomb-Reinmund & Kielian, 1998). Upon endocytic uptake and exposure to low pH, a conformational change occurs triggered by the destabilisation of the E1/E2 heterodimers. This allows formation of E1 homotrimers and exposes the fusion loop of the E1 glycoprotein which inserts into the target membrane (Wahlberg & Garoff, 1992; R Bron, 1993; Gibbons *et al.*, 2004). The trimer then refolds with a hairpin-like conformation and in doing so fuses the endosomal and virus membranes together (Roman-Sosa & Kielian, 2011; Sanchez-San Martin *et al.*, 2013). The nucleocapsid is then delivered to the cytoplasm where it

disassembles. One way this is thought to occur is by binding of ribosomes to the capsid protein which promotes disassembly (Wengler *et al.*, 1992). However, another model proposes that ion channels form in the viral membrane during entry, thereby lowering the pH and priming the nucleocapsid for disassembly when it reaches the cytoplasm (Wengler *et al.*, 1996, 2003; Melton *et al.*, 2002).

Another component important for trafficking and endosomal maturation are the Rab-family of GTPases. Rab5 is a marker for early endosomes and is involved in recycling of receptors and trafficking along microtubules. Rab7 is found in late endosomes and is involved in sorting cargo into the late endosome or lysosome pathway (Schmid *et al.*, 1988). Most alphaviruses, including SFV and CHIKV, have been shown to fuse with Rab5 positive endosomes (Sieczkarski & Whittaker, 2003; Bernard *et al.*, 2010). However, some new world alphaviruses, for example VEEV, preferentially fuse with Rab7 positive endosomes (Kolokoltsov *et al.*, 2006). The efficiency of alphavirus fusion is also increased by the presence of cholesterol and sphingolipid in the target membrane (Waarts *et al.*, 2002; Umashankar *et al.*, 2008; Hoornweg *et al.*, 2016*b*).

1.1.5.2 Alphavirus genome replication

Once the nucleocapsid has disassembled the viral RNA is exposed to the cytoplasm. The first ORF can then be translated into a polyprotein of either nsP1-4 (P1234) or nsP1-3 (P123). The presence of an opal stop codon between nsP3 and nsP4 results in approximately 90% of translation events producing the P123 polyprotein (Strauss *et al.*, 1983; Li & Rice, 1993). Together, P123 and nsP4 form a replication complex and aid synthesis of the minus-strand RNA (Shirako & Strauss, 1994). This acts as a template for both the full-length genomic plus-strand (49S) and a subgenomic (26S) mRNA (Wielgosz *et al.*, 2002). It is thought that this replication complex is short-lived, and further processed into a nsP1/P23/nsP4 complex which initiates synthesis of the positive-sense genomic RNA (Sawicki & Sawicki, 1980; Shirako & Strauss, 1994). These protein-RNA complexes are transported to the plasma membrane where they form membranous spherical

structures. This is facilitated by the membrane binding ability of nsP1 and the formation of invaginations in the inner layer of the plasma membrane. The inside of these spherules remains accessible to the cytoplasm via an open neck to allow continuous RNA synthesis. The formation of these structures occurs rapidly, within 45 mins of infection, and promotes viral replication by concentrating the replication machinery and protecting it from host defence mechanisms (Spuul *et al.*, 2010; Pietilä *et al.*, 2018). Depending on the virus, these spherules are then either transported by endocytosis to cytopathic vacuoles or remain associated with the plasma membrane (Spuul *et al.*, 2010; Frolova *et al.*, 2010; Thaa *et al.*, 2015; Pietilä *et al.*, 2018). Transcription of full-length genomic plus-strand (49S) mRNA and subgenomic (26S) mRNA occurs at a constant rate throughout the replication cycle (Barton *et al.*, 1991).

1.1.5.3 Alphavirus assembly and budding

The subgenomic mRNA contains the ORF which encodes for the structural proteins and is translated as a polyprotein. The capsid protein is a serine protease and auto-catalytically cleaves itself from the rest of the polyprotein (Choi *et al.*, 1991, 1997). The remaining structural proteins are released by host signal peptidase as 6K, E1 and p62 (a pre-cursor to E2 and E3) (Liljeström & Garoff, 1991). The glycoproteins E1 and p62 translocate across the endoplasmic reticulum membrane and are transported through the Golgi network where they undergo a series of post-translational modifications. These include addition of high-mannose chains, palmitoylation and phosphorylation which ensure correct folding and transport to the plasma membrane (Sefton, 1977; Ivanova & Schlesinger, 1993; Knight *et al.*, 2009). During the translocation through the Golgi network, furin is recruited to cleave p62 to produce mature E2 and E3 proteins (Zhang *et al.*, 2003).

Assembly of the alphavirus occurs in the cytoplasm and is initiated by formation of capsid protein dimers which bind to a molecule of genomic RNA (Forsell *et al.*, 1995; Perera *et al.*, 2001). The nucleocapsid then diffuses towards the plasma membrane where it associates with viral glycoproteins. The interaction between the nucleocapsid and the C-terminal of E2

glycoprotein which is thought to allow the capsid to pass through the plasma membrane. As the virus particle moves through the plasma membrane it acquires a full set of glycoproteins to complete virion assembly (Garoff & Simons, 1974; Lu & Kielian, 2000). This process is also dependent on cholesterol in the plasma membrane and is pH sensitive with an optimal pH of ~7.5-8.0 (Lu *et al.*, 1999, 2001; Lu & Kielian, 2000).

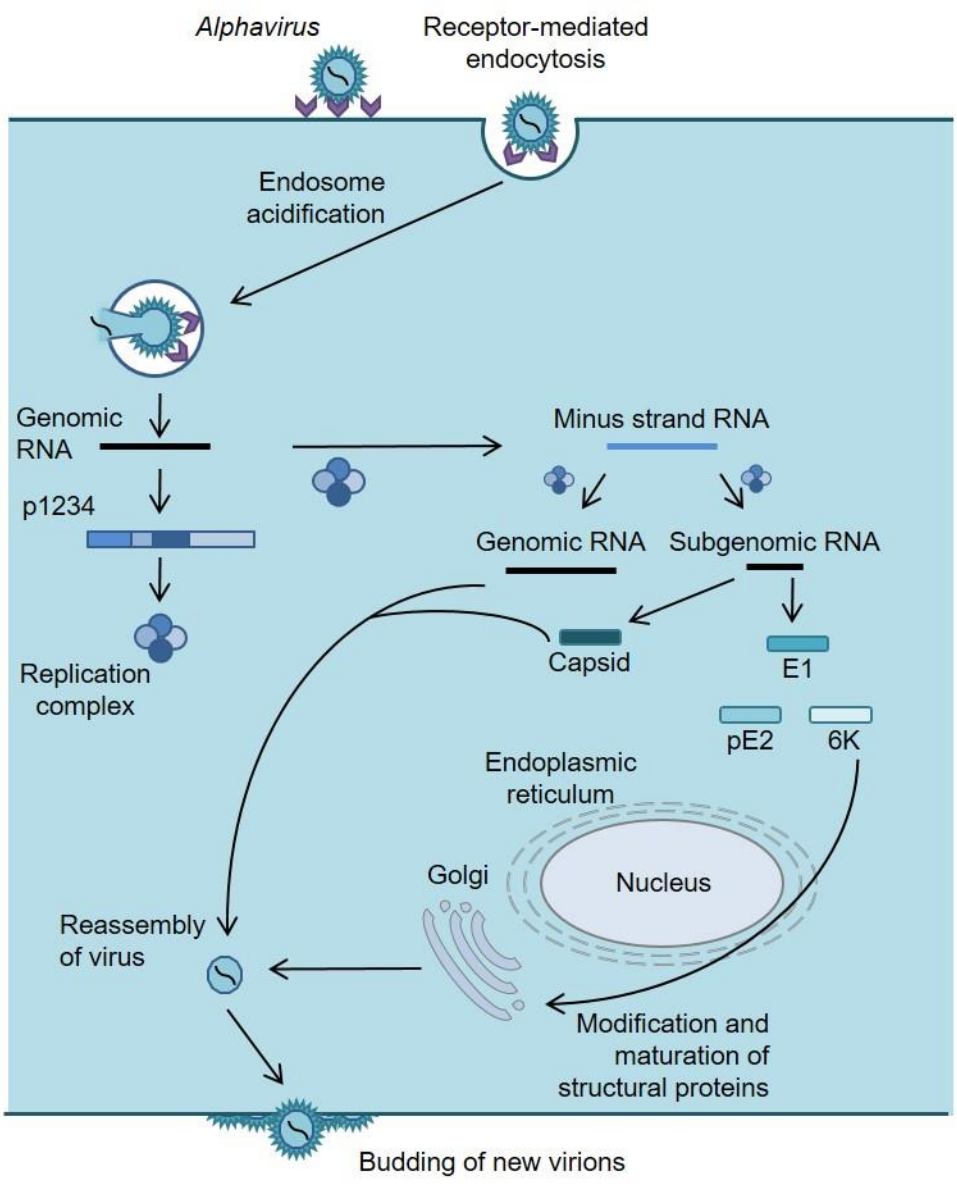

Figure 1.3. The alphavirus lifecycle
Alphaviruses bind to host-cell receptors to allow uptake by receptor-mediated endocytosis. Acidification of the endosome triggers a conformational change in the E1 protein resulting in fusion with the endosomal membrane and release of the genome into the cytoplasm. The non-structural proteins are translated into a polyprotein before cleavage to form the replication complex. The replication complex aids synthesis of the minus strand RNA which allows for production of additional copies of the genomic RNA as well as the subgenomic RNA. The structural proteins are translated from the subgenomic RNA and are transported to the plasma membrane via the endoplasmic reticulum and golgi to undergo post-translational modifications. New virions can then assemble before budding from the host-cell to infect neighbouring cells.

1.1.6 Alphavirus transmission

Alphaviruses are arboviruses which are dependent on repeated cycling between their insect vector and host for maintenance in the wild (Gould *et al.*, 2017). The majority of alphaviruses are transmitted by mosquitoes, with the exception of two aquatic alphaviruses: Salmon Pancreatic Disease Virus (SPDV) and Southern Elephant Seal Virus (SESV) (Weston *et al.*, 2002). A different arthropod vector, *Lepeophtherius salmonus*, a species of sea louse, is thought to be involved in transmission for both of these viruses (La Linn *et al.*, 2001). In addition, alternative transmission routes such as aerosol or bodily secretions have been shown to be possible for some alphaviruses including: SFV, CHIKV, WEEV and VEEV (Hanson *et al.*, 1967; Willems *et al.*, 1979; Gardner *et al.*, 2015). Indeed, the potential for transmission via aerosols allowed for the weaponisation of VEEV as a biological warfare agent during the Cold War (Hawley & Eitzen Jr, 2001; Weaver *et al.*, 2004). However, the most important mode of transmission is via mosquitoes, commonly those of the *Aedes* genus (Lim *et al.*, 2018). For example, *Aedes aegypti* and *Aedes albopictus* have been responsible for large scale outbreaks of CHIKV owing to their existence in close proximity with humans (Lounibos & Kramer, 2016).

It is only the female mosquitoes which feed on blood as they require the protein and iron to make their eggs. Following a bloodmeal from an infected individual, the virus replicates in the epithelial cells of the mosquito midgut before making its way back to the salivary glands (Hardy *et al.*, 1983). When the mosquito next bites an individual for another bloodmeal, it injects saliva as a vasodilator and anticoagulant (Hardy *et al.*, 1983; Dubrulle *et al.*, 2009). The virus is then not only introduced to a new host, but the immune response to the bite can also act to promote virus replication and dissemination (Fong *et al.*, 2018). For example, an edema initiated by mosquito saliva was demonstrated to promote alphavirus replication through initial retention of the virus at the bite site, thus promoting infection of local cutaneous cells (Pingen *et al.*, 2016). In addition, mosquito saliva is known to supress the innate immune response of the host and disrupt the endothelial barrier function at the bite site. This provides a delay in early

detection of the virus as well as enhancing the dissemination of the virus into the blood vessels (Her *et al.*, 2010; Schmid *et al.*, 2016; Pingen *et al.*, 2016). Furthermore, immune cells recruited to the site of infection can become hijacked themselves and contribute to the dissemination of virus around the body (Her *et al.*, 2010; Pingen *et al.*, 2016).

The target host must develop a high enough viraemia to infect the next mosquito. The natural hosts for alphaviruses are usually susceptible vertebrates such as birds, small mammals or nonhuman primates. alphaviruses typically circulate amongst these hosts in an enzootic cycle with occasional spillover in to human hosts (Weaver & Barrett, 2004). Humans are often dead-end hosts as they generally do not generate a sufficient viraemia. However, in some epidemics, mosquito-human-mosquito transmission has been recorded. For example, this was an important factor in the spread of RRV, ONNV and CHIKV in recent epidemics (Weaver & Barrett, 2004; Go *et al.*, 2014).

As alphaviruses are dependent on their vector for transmission, the environmental conditions can have a large impact on virus spread. Indeed, outbreaks often coincide with seasonal conditions which promote the mosquito life cycle (Anyamba *et al.*, 2014; Grossi-Soyster *et al.*, 2017). For example, warmer temperatures are more conducive to mosquito development and allow them to complete their life cycle in standing water in urban environments (Rueda *et al.*, 1990; Weaver & Barrett, 2004). This not only leads to seasonal outbreaks in susceptible areas, but as global warming becomes more of an issue, results in expansion of the mosquitoes geographical range (Rochlin *et al.*, 2013; Baylis, 2017). Furthermore, the rise in global temperature taken together with an increase in global travel has facilitated the spread of alphaviruses to novel areas. This is exemplified by the spread of CHIKV across the globe, including to Europe and the USA, since its emergence in Africa (Johansson *et al.*, 2014; Wahid *et al.*, 2017).

Control of alphavirus vectors is seen as one way to prevent alphavirus spread and reduce the scale of epidemics. For example, it is common practice to spray insecticides in areas where mosquito-borne diseases are

prevalent (McGraw & O'Neill, 2013; Chanda *et al.*, 2015). However, there are concerns around environmental and human health as well as increasing resistance issues with the use of insecticides (Kamgang *et al.*, 2011; Muturi & Alto, 2011; McGraw & O'Neill, 2013). Other measures such as the use of bed nets and elimination of mosquito breeding sites have proven effective at reducing disease burden. However, these techniques are not considered sustainable and the targeted disease rapidly returns if these measures are not maintained (Zaim *et al.*, 2000; Rigau-Pérez *et al.*, 2002). Recent advances have led to the development of other techniques such as biological control which are considered to be less environmentally damaging (Christodoulou, 2011). For example, release of mosquitoes infected with Wolbachia, a bacteria which halves the lifespan of adult mosquitoes. This has recently been shown to reduce the capacity of mosquitoes to spread CHIKV, without eliminating the mosquito population completely (Aliota *et al.*, 2016; Ahmad *et al.*, 2017). Another technique which has been trialled is the release of mosquitoes which have been sterilised by radiation or genetic modification (Benedict & Robinson, 2003; Alphey *et al.*, 2010; Wise de Valdez *et al.*, 2011). These trials have also shown promising results, for example with release of genetically modified *A. aegypti*, one of the main vectors of CHIKV, significantly reducing wild-type populations (Benedict & Robinson, 2003; Lounibos & Kramer, 2016). However, public resistance to the release of artificially altered mosquitoes has hindered the progression of these techniques (Christodoulou, 2011).

1.2 Chikungunya virus

CHIKV is a medically important Old World alphavirus which has resulted in large outbreaks in recent years. There are three main lineages of CHIKV: Western African (WA); East, Central and South African (ECSA); and Asian (Tsetsarkin *et al.*, 2011). In addition an important sub-lineage, the Indian Ocean lineage (IOL), emerged from the ECSA lineage as the result of a point mutation (Tsetsarkin *et al.*, 2007). This sub-lineage first appeared in 2004 and was responsible for the re-emergence of CHIKV with explosive

epidemics throughout Africa and Asia (Arankalle *et al.*, 2007; Volk *et al.*, 2010). Similarly, another sub-lineage, the Asian/American lineage, arose from the Asian lineage due to the introduction of two point mutations (Sahadeo *et al.*, 2017). This lineage is currently circulating around the Americas and is responsible for large outbreaks in immunologically naïve populations (Lanciotti & Valadere, 2014; Sahadeo *et al.*, 2017). In the UK, CHIKV is categorised as a hazard group 3 pathogen and as such, all work with CHIKV must be carried out under containment level 3 (CL3) conditions (Health and Safety Executive, 2013). The US army also considers CHIKV a potential biological warfare agent (Thiboutot *et al.*, 2010). Therefore, SFV or SINV are commonly used as a model alphavirus owing to their classification as a hazard group 2 pathogen allowing for it to be worked with under containment level 2 (CL2) (Health and Safety Executive, 2013).

1.2.1 Chikungunya fever

Chikungunya fever (CHIKF) is the debilitating disease caused by CHIKV. Upon infection with CHIKV, the virus undergoes initial replication within the dermal fibroblasts before transmission to the rest of the body including the liver, lymphoid tissue, brain, skeletal muscles and joints (see section 1.2.2). Consequently, the symptoms of CHIKV infection manifest mainly as fever, maculopapular rash and severe joint pain (Burt *et al.*, 2017; McFee, 2018). Typically, 90% of people who become infected exhibit symptoms (De Brito, 2017). The name Chikungunya is derived from the Makonde word for ‘that which bends up’ owing to the hunched over posture of the afflicted as a result of this defining joint pain. Disease symptoms are typically observed 3-7 days post-infection with the acute phase of infection lasting 1-2 weeks (Burt *et al.*, 2017; McFee, 2018). In addition, some individuals continue to experience recurrent joint pain, clinically similar to the autoimmune disease rheumatoid arthritis, for months or years after the acute phase. Varying rates of these recurring symptoms have been reported following CHIKV outbreaks with some recording relapsing arthralgia in up to 60% of patients (Schilte *et al.*, 2013). The cause of this persistent joint pain once the virus has been cleared from the blood is poorly understood. One

suggestion is that the virus persists in the cells of the muscles and joints, however to date live virus has not been detected at these sites (Hoarau *et al.*, 2010; Hawman *et al.*, 2013). Another possibility is the presence of defective viral particles which do not produce infectious virus but are able to stimulate an immune response (Burt *et al.*, 2017). Furthermore, recent research into CHIKV antivirals demonstrated that favipiravir was able to reduce viral RNA in the acute but not the chronic phase which suggests that the viral nucleic acid detected at these later stages is not a consequence of replicating virus (Abdelnabi *et al.*, 2018).

Severe disease or death following CHIKV infection is rare but infants, elderly or immunocompromised individuals may be at increased risk. A death rate of 1 for every 1,000 cases has been reported but it is thought that this is likely to be an underestimate due to CHIKV associated deaths not being identified as such (Josseran *et al.*, 2006; De Brito, 2017). Severe symptoms which have been reported in these populations include encephalitis, myocarditis and multiple organ failure. Mother-to-child transmission has been reported with the infected neonates having a particularly poor prognosis including suffering from long-term neurological disorders such as microcephaly and cerebral palsy (Gérardin *et al.*, 2014). Transmission is thought to occur via maternal-foetal blood exchange during birth (Chen *et al.*, 2010*a*; Gérardin *et al.*, 2014).

1.2.2 CHIKV pathogenesis

Following a bite from an infected mosquito, CHIKV initially replicates at the site of inoculation in skin-resident cells such as keratinocytes, dendritic cells and dermal fibroblasts (Figure 1.4). From here, infected dendritic cells traffic to the draining lymph nodes where viral replication continues before CHIKV is disseminated to other tissues and organs in the body (Couderc *et al.*, 2008; Puiprom *et al.*, 2013; Ong *et al.*, 2014). It has been suggested that viral dissemination during the acute phase may be mediated by infected blood monocytes which are able to distribute CHIKV to the peripheral organs (Her *et al.*, 2010). The primary sites of replication include the lymph nodes, muscle, joints, spleen and skin (Couderc *et al.*, 2008; Morrison *et al.*, 2011).

In more serious presentations of the disease, viral replication can also occur in the brain and the liver (Chua *et al.*, 2010; Chusri *et al.*, 2011; Acevedo *et al.*, 2017). A combination of the effects of viral replication and the immune response at these sites cause the symptoms characteristic of CHIKV infection (section 1.2.1).

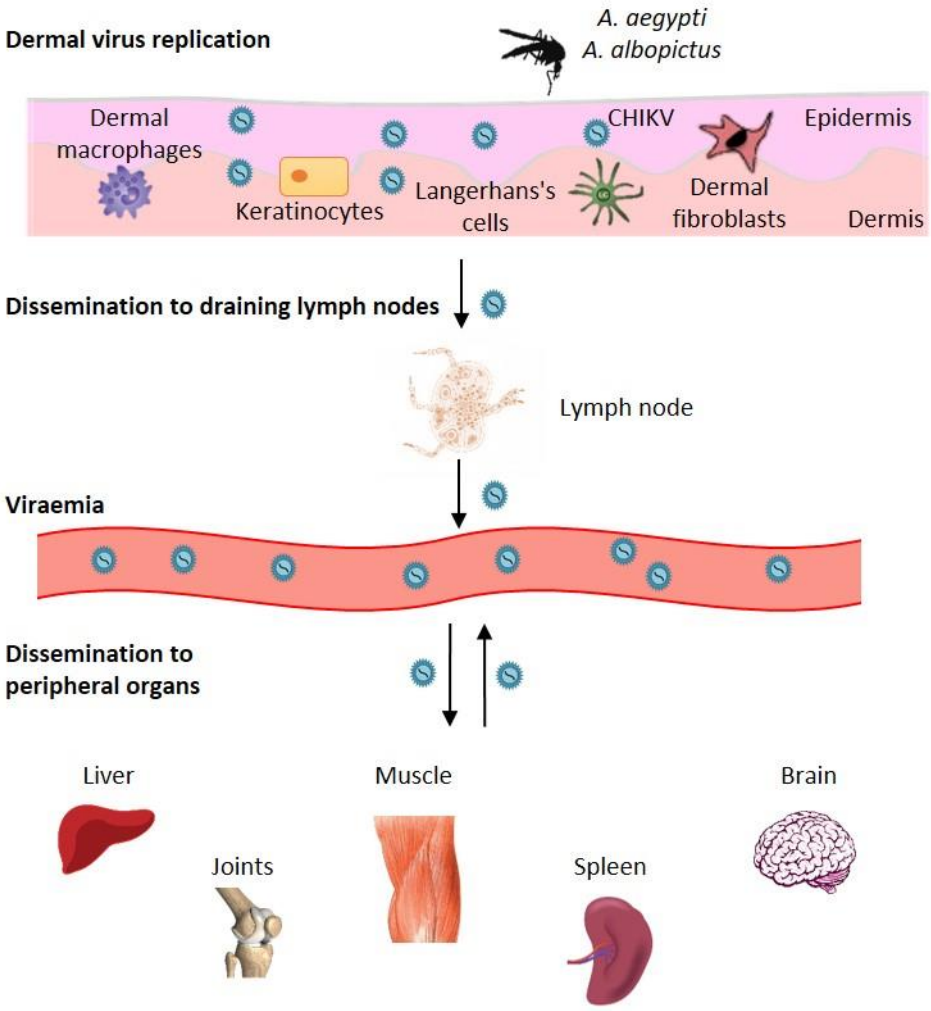

Figure 1.4. CHIKV pathogenesis
CHIKV is transmitted to host organisms via the bite of an infected mosquito (*A*. aegypti or *A. albopictus*). Initial CHIKV replication occurs within skin-resident cells before the virus disseminates to draining lymph nodes where CHIKV replication continues. Subsequent induction of viraemia results in circulation of CHIKV to peripheral organs which become additional sites of replication. Adapted from (Ong *et al.*, 2014).

In response to CHIKV infection, a robust innate immune response is triggered which has both protective and pathological consequences. The primary infiltrating cells of infected tissues are activated macrophages and elevated levels of monocyte chemotactic protein-1 (MCP-1), a monocyte/ macrophage chemo-attractant, are correlated with high viral loads (Labadie *et al.*, 2010; Hoarau *et al.*, 2010; Rulli *et al.*, 2011). Although depletion of macrophages in mice was associated with a reduction in arthritic symptoms, there was also a significantly prolonged viraemia (Gardner *et al.*, 2010). Natural killer (NK) cells are also activated upon CHIKV infection and are thought to play a key role in contributing to the production of IFNγ (Hoarau *et al.*, 2010; Teo *et al.*, 2015). Furthermore, persistence of NK cells is correlated with the development of chronic arthralgia (Petitdemange *et al.*, 2016). One group of innate immune cells associated predominantly with a protective role in CHIKV infection are dendritic cells. These are believed to be resistant to CHIKV infection and mice deficient in the dendritic cell immunoreceptor developed more severe disease symptoms (Sourisseau *et al.*, 2007; Long *et al.*, 2013). Overall, the innate immune response acts to produce significant quantities of pro-inflammatory cytokines such as: IFNα, IFNβ, IL-6, and IFNγ (Ng *et al.*, 2009).

Although the innate immune response can rapidly suppress viral replication, it cannot completely clear CHIKV infection. The adaptive immune response is also critical for clearance of CHIKV, exemplified by studies showing that mice lacking T and B cells exhibit a persistent, high viraemia (Teo *et al.*, 2013; Hawman *et al.*, 2013). It has also been reported that CD8+ T cells are more prominent during the early stages of CHIKV infection with CD4+ T cells playing an important role at a later stage (Wauquier *et al.*, 2011). Cytotoxic CD8+ T cells destroy infected cells and levels peak at 1 day post-infection then remain elevated for 7-10 weeks (Wauquier *et al.*, 2011; Miner *et al.*, 2015). The role of CD4+ cells appears to be both beneficial, by aiding production of a humoral response, as well as harmful, by exacerbating joint swelling (Wauquier *et al.*, 2011). Further analysis of the T-cell response suggests a potential pathogenic role for the subset of T cells, Th17 T cells, in CHIKV infection. These have been shown to have a pathogenic role in other

alphavirus infections and IL-17, a cytokine produced by Th17 cells, has repeatedly been detected in CHIKF patients (Ng *et al.*, 2009; Chow *et al.*, 2011; Kulcsar *et al.*, 2014; Teng *et al.*, 2015). In contrast, another subset of T cells, regulatory T cells (Tregs), have been shown to limit CHIKV-induced pathology in mice (Lee *et al.*, 2015).

There is also a good antibody response to CHIKV infection and early appearance of anti-CHIKV IgG is associated with reduced severity of chronic complications from infection (Kam *et al.*, 2012*b*). The majority of antibodies produced, by both humans and mice, appear to be targeted against the E2 envelope glycoprotein (Kam *et al.*, 2012*a*; Weber *et al.*, 2015; Smith *et al.*, 2015). Administration of anti-CHIKV antibodies to mice lacking B and T cells was sufficient to control CHIKV infection and prevent persistent CHIKV symptoms (Hawman *et al.*, 2013). Provision of antibodies against CHIKV has also been shown to prevent virus spread when given therapeutically to rhesus monkeys after infection (Broeckel *et al.*, 2017). The provision of anti-CHIKV antibodies from convalescent plasma is a strategy which has also been suggested for protecting and treating neonates born to viraemic mothers (Couderc *et al.*, 2009). While, inducing a neutralising antibody response is an essential feature of potential vaccine candidates, there are concerns that sub-neutralising levels of CHIKV antibodies could enhance CHIKV pathology (Lum *et al.*, 2018). While it is not clear if this antibody dependent enhancement can occur in CHIKV infections, a more severe disease was reported during a prime-boost immunisation study (Hallengärd *et al.*, 2014).

1.2.3 Epidemiology

Chikungunya virus was first isolated in modern day Tanzania in 1952; however potential outbreaks may have been recorded as early as 1779 and mistaken for Dengue due to the similarity in symptoms (Robinson, 1955; Lumsden, 1955; Carey, 1971; Ng & Hapuarachchi, 2010). This was shortly followed by the first isolation of CHIKV in Bangkok in 1958 with the first documented epidemic in India in 1963 and subsequent large outbreaks throughout Asia (Hammon & Sather, 1964; Sarkar *et al.*, 1965).

Sporadic outbreaks have since been recorded throughout Africa with recent epidemics of note including the re-emergence of CHIKV in Kenya in 2004 which escalated and resulted in 5,000 cases in the Comoros before reaching the French Indian Ocean island, La Réunion (Borgherini *et al.*, 2007; Gérardin *et al.*, 2008). The 2005 outbreak in La Réunion caused particular concern due to the high infection and mortality rate. Of a population of 785,000 nearly 40% were infected with CHIKV and 237 deaths were recorded (Josseran *et al.*, 2006; Renault *et al.*, 2007). The severity of this outbreak is linked to the emergence of a new strain of CHIKV which allows for transmission by a new species of mosquito, *Aedes Albopictus*, which has a much wider geographical range. The increased ability to infect *A. albopictus* is believed to be due to the presence of the point mutation Ala226Val in the E1 glycoprotein (Tsetsarkin *et al.*, 2007). This outbreak spread to India by the end of 2005 where approximately 1.5 million individuals were reported to have been infected. However the actual number of cases is estimated to be much higher with potentially 6.5 million infected (Mavalankar *et al.*, 2007).

CHIKV was first detected in the Western hemisphere on the Caribbean island of Saint Martin in 2013 then rapidly spread throughout the Caribbean and South America with a substantial outbreak in 2014 which recorded over one million cases (PAHO, 2018). There remains large ongoing outbreaks in these regions and as of May 2018 local transmission of CHIKV has been recorded in 112 countries, including the USA and Europe (Figure 1.5) (CDC, 2018). This includes recent outbreaks in Europe the most recent of which occurring in France and Italy during 2017 with 15 and 238 autochthonous cases reported, respectively (Calba *et al.*, 2017; Venturi *et al.*, 2017).

There is growing concern that with the increasing threat of global warming, the geographical range of the mosquitoes will expand and consequently result in outbreaks in areas not normally considered at risk (Rochlin *et al.*, 2013; Tjaden *et al.*, 2017). This coupled with an increase in international travel of individuals from these areas makes the introduction of arboviruses into these areas more likely (Semenza *et al.*, 2016).

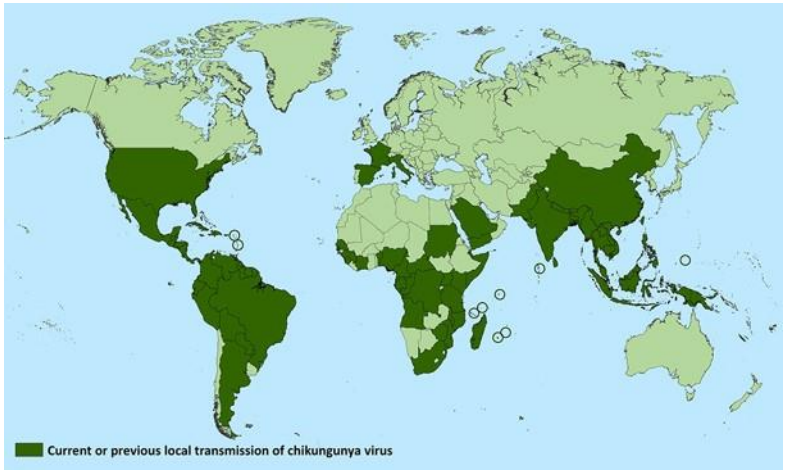

Figure 1.5. Geographical distribution of CHIKV
Countries where local transmission of CHIKV has been recorded as of May 2018 (CDC, 2018).

1.2.4 Treatment

There are currently no approved antivirals for CHIKF and treatment is limited to relieving symptoms. However, an antiviral drug which has been used in past outbreaks with some success includes Ribavirin which decreased the joint swelling and pain associated with CHIKV in a small group of patients during an outbreak in India (Ravichandran & Manian, 2008). The standard course of treatment revolves around giving pain relief and anti-inflammatory drugs such as acetaminophen, tramadol, codeine or oxycodone during the acute phase of infection (Simon *et al.*, 2015). However, prior to administering drugs which have anticoagulant side effects, such as aspirin or NSAIDs, it is important to ensure that the patient is not infected with DENV due to the risk of haemorrhaging in DENV patients (Lum *et al.*, 2014; McFee, 2018). It is also not advised to give corticosteroids due to the risk of return of severe arthritis upon withdrawal of the treatment (Simon *et al.*, 2015). Non-pharmaceutical approaches can also prove beneficial with provision of fluids, application of cold compress to joints and maintaining mobility during the acute phase assisting in the relief of symptoms (Mohammad Arif, 2017; McFee, 2018). Patients who go on to suffer from chronic joint pain following CHIKV infection are often referred to rheumatologists and treated similarly to those with rheumatoid arthritis owing to the similarity in symptoms.

Treatment is with Disease-modifying antirheumatic drugs (DMARDs) such as Methotrexate to relieve inflammation (Amaral *et al.*, 2018).

However, the treatments described above are generally non-specific anti-inflammatories and do not target the specific CHIKV induced pathogenesis. Recent advances are attempting to address this, for example by using immune based therapies which target the $CD4^+$ T cells which exacerbate the CHIKV-induced joint inflammation (Miner *et al.*, 2017; Teo *et al.*, 2017). The drug fingolimod was shown to reduce CHIKV-induced joint swelling in mice during the acute phase of infection by inhibiting migration of $CD4^+$ T cells into the joints (Teo *et al.*, 2017). Another study showed that a combined approach of targeting the virus with monoclonal antibodies at the same time as interfering with T-cell activity with drugs such as abatacept was effective at reversing acute CHIKV arthralgia in mice (Miner *et al.*, 2017). Fingolimod is used routinely in the treatment of multiple sclerosis and abatacept for rheumatoid arthritis (Vital & Emery, 2006; Brinkmann *et al.*, 2010). However, to date the use of these drugs to treat CHIKF has only been investigated in murine models (Miner *et al.*, 2017; Teo *et al.*, 2017). Safety or efficacy has not been demonstrated in human patients which is especially important when considering immunomodulatory approaches in the treatment of infectious diseases.

A number of antivirals are also under investigation which target either the virus itself or host cell processes which are essential for virus replication. For example, several targeted approaches have been used to look for specific inhibitors of CHIKV nsP2 based on its structure which identified a number of compounds for future therapeutic development (Bassetto *et al.*, 2013; Nguyen *et al.*, 2015; Das *et al.*, 2016). Some of these have been taken forward for further validation and while many were quickly eliminated due to toxicity and lack of efficacy, some promising candidates have been identified (Das *et al.*, 2016; Rashad *et al.*, 2018).

Other compounds selected for further investigation have been selected based on their efficacy in treating other diseases. One compound which has shown encouraging results is Suramin, an approved

trypanosomiasis treatment, which inhibited CHIKV entry and transmission in vitro (Nok, 2003; Ho *et al.*, 2015). This is supported by *in vivo* work demonstrating that CHIKV infected mice treated with Suramin had a lower viraemia and a reciprocal reduction in joint swelling (Kuo *et al.*, 2016). In another study imipramine, a known inhibitor of cholesterol biosynthesis and trafficking, was shown to reduce CHIKV replication *in vitro* via its restriction of intracellular cholesterol trafficking thereby hindering multiple stages of the virus lifecycle (Underwood *et al.*, 1996; Wichit *et al.*, 2017). An encouraging finding was that this approach was shown to inhibit other arboviruses which often co-circulate with CHIKV, potentially eliminating the need for a definitive diagnosis prior to commencing treatment (Wichit *et al.*, 2017).

1.2.5 Vaccine development

Ultimately, the ideal solution would be to develop a vaccine against CHIKV to protect “at risk” populations; however there are currently no licensed CHIKV vaccines available. Early attempts in the 1960s to develop a formalin inactivated virus vaccine did not show much potential (Harrison *et al.*, 1971; Hoke *et al.*, 2012). However, a live attenuated virus developed by the US army appeared promising in both phase I and II trials (Levitt *et al.*, 1986; McClain *et al.*, 1998; Edelman *et al.*, 2000; Hoke *et al.*, 2012). Further development was halted due to lack of funds and interest, although this vaccine candidate is still under consideration for future development (Hoke *et al.*, 2012). However, concerns remain over the safety of this attenuated virus due to the presence of only two point mutations, thus presenting the risk of reversion to the wild-type strain (Gorchakov *et al.*, 2012). Other attenuated virus vaccines have been developed in the intervening years with perhaps the most promising of these being the CHIK-IRES vaccine. CHIKV was attenuated via the addition of an internal ribosome entry site (IRES) from encephalomyocarditis virus between the two ORFs of a CHIKV cDNA clone (Plante *et al.*, 2011). Vaccination with CHIK-IRES induced strong immunogenicity in both mouse and nonhuman primates (Chu *et al.*, 2013; Roy *et al.*, 2014). Interestingly, cross-protective immunity against the related alphavirus, O’Nyong-Nyong virus was also induced (Partidos *et al.*, 2012).

More recent vaccine options include the use of subunit vaccines, virus-like particles (VLPs), chimeric vaccines and nucleic acid vaccines. For example, another promising vaccine is the VLP-based vaccine produced by transfection of HEK293 cells. Nonhuman primates given three doses were protected from viraemia following a challenge and it was recently shown to be immunogenic and safe in phase I trials (Akahata *et al.*, 2010; Chang *et al.*, 2014). Another option being explored is the use of chimeric vaccines using a variety of combinations of different virus backbones combined with selected CHIKV proteins. One candidate with encouraging results is a chimeric of the insect alphavirus, Eilat virus, containing the structural proteins of CHIKV. The resulting virus is structurally identical to CHIKV but unable to replicate and induced protective immunity in nonhuman primates (Erasmus *et al.*, 2017).

1.3 Ubiquitin system

Ubiquitylation, the addition of ubiquitin moieties to protein substrates, was originally classified as a signal for protein degradation (Goldknopf *et al.*, 1977; Chau *et al.*, 1989; Hershko & Ciechanover, 1998). However, accumulating evidence points towards the ubiquitin system being a key regulator in many cellular processes (Xu *et al.*, 2009). Importantly, this is a reversible process and dynamic ubiquitylation is crucial for the physiological functioning of cells (Clague *et al.*, 2013; Heride *et al.*, 2014). Consequently, it is now generating interest as a source of potential drug targets for a number of diseases, including virus infections (de Chassey *et al.*, 2014; Huang & Dixit, 2016).

1.3.1 Ubiquitin

Ubiquitin is a highly conserved 8.6 kDa protein consisting of 76 amino acids found in all eukaryotic cells (Goldstein *et al.*, 1975; Wilkinson & Audhya, 1981; Vijay-kumar *et al.*, 1987). It is encoded for by four genes, UBA52, RPS27A, UBB and UBC, which are believed to have originated from prokaryotic equivalents ThiS and MoaD (Lund *et al.*, 1985; Baker & Board,

1991; Nicholson *et al.*, 2001; Lake *et al.*, 2001). Ubiquitin is synthesised as a pre-cursor of either ubiquitin conjugated to a ribosomal subunit or as polyubiquitin (Wiborg *et al.*, 1985; Lund *et al.*, 1985; Redman & Rechsteiner, 1989; Baker & Board, 1991). Therefore, it must first be proteolytically cleaved from these precursors to produce free ubiquitin before it can be utilised by the cell (Grou *et al.*, 2015).

1.3.2 Ubiquitin conjugation

Ubiquitylation is a post-translational modification involving covalent attachment of ubiquitin moieties to lysine residues of target proteins (Figure 1.6). This is achieved through the sequential action of three enzymes: Ub-activating enzymes (E1), Ub-conjugating enzymes (E2) and Ub ligases (E3). There are two E1 enzymes, approximately 40 E2 conjugating enzymes and over 600 E3 ligases encoded for within the human genome (Clague *et al.*, 2015; Zheng & Shabek, 2017). The process of ubiquitin conjugation begins with activation of the C-terminal glycine of Ub by an E1 enzyme in an ATP and Mg^{2+}-dependent manner (Ciechanover *et al.*, 1981, 1982). This results in the formation of a thioester bond between ubiquitin and the E1 enzyme which facilitates transfer to a cysteine residue on an E2 enzyme (Hershko *et al.*, 1983). The E3 enzyme is then able to transfer the ubiquitin molecule to a lysine residue on the target substrate. The final transfer of ubiquitin to its substrate occurs in one of two ways, indirectly or directly, depending on the type of E3 enzyme involved. HECT (homologous to E6-AP C-Terminus) ligases acts as an intermediary by forming a thioester bond with ubiquitin prior to transfer to the substrate (Huibregtse *et al.*, 1995). Whereas, RING (really interesting new gene) ligases have no catalytic activity and simply act as a scaffolding protein to bring the E2 and substrate together, thereby allowing direct transfer of ubiquitin from E2 to target protein (Seol *et al.*, 1999).

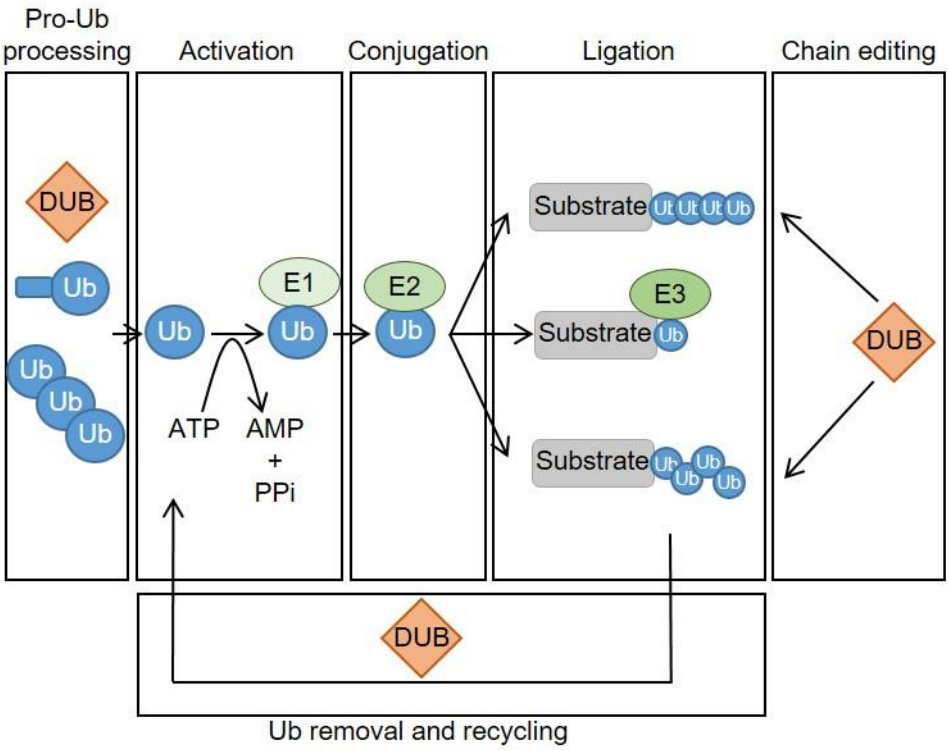

Figure 1.6. The ubiquitin system
Free ubiquitin (Ub) is generated by cleavage from pro-Ub precursors by deubiquitylating enzymes (DUBs). Ub is activated by E1 enzymes which allows for transfer to an E2 conjugating enzyme. The E3 ligases then complete the ubiquitylation process by transferring the Ub molecule to a lysine residue of a target protein. Ub can either be added as single moieties (monoubiquitin) or this process can be repeated to form Ub chains (polyubiquitin). Many chain topologies are possible with both linear and branched chains formed. The DUBs can then act to either edit Ub chains or to remove and recycle Ub.

1.3.3 Ubiquitin chain topologies

Addition of ubiquitin as a single moiety is known as monoubiquitylation and addition at multiple lysine residues is referred to as multi-monoubiquitylation (Figure 1.7A) (Robzyk *et al.*, 2000; Lai *et al.*, 2001). However, ubiquitin also contains seven lysine residues (K6, K11, K27, K29, K33, K48 and K63) to which additional ubiquitin moieties can be added, forming homotypic chains of polyubiquitin (Figure1.7B) (Peng *et al.*, 2003). Linear polyubiquitin chains (M1) can also be created by conjugation to the N-terminal methionine of Ub (Kirisako *et al.*, 2006). Ubiquitin chains can

become highly complex via formation of heterotypic chains which contain branches via multiple linkages within the same chain (Figure 1.7C) (Hyoung *et al.*, 2007). These chains can also be further modified by post-translational modifications of ubiquitin itself. For example, ubiquitin can be phosphorylated or acetylated providing additional layers of complexity and regulation to the ubiquitin system (Swaney *et al.*, 2013; Ohtake *et al.*, 2015).

Ubiquitylation was first identified as a signal for protein degradation upon tagging of proteins with K48 linked polyubiquitin chains, the most abundant linkage (Goldknopf *et al.*, 1977; Chau *et al.*, 1989; Hershko & Ciechanover, 1998; Xu *et al.*, 2009). Soon after, K63 polyubiquitin chains were recognised as playing a non-degrading role in DNA repair. As the diversity in chain linkages were uncovered more recent research has begun to uncover the roles of these 'atypical' chains. For example, K11 polyubiquitin linkages have been shown to play a role in both proteasomal degradation and cell cycle control (Bremm & Komander, 2011; Wickliffe *et al.*, 2011). In addition, K33 linked chains have been implicated in protein trafficking of membrane proteins through the Golgi-network (Yuan *et al.*, 2014). Polyubiquitin chains can also play important roles when not anchored to a protein substrate. Unanchored ubiquitin and polyubiquitin chains have been shown to serve as second messengers in cell signalling pathways (Xia *et al.*, 2009).

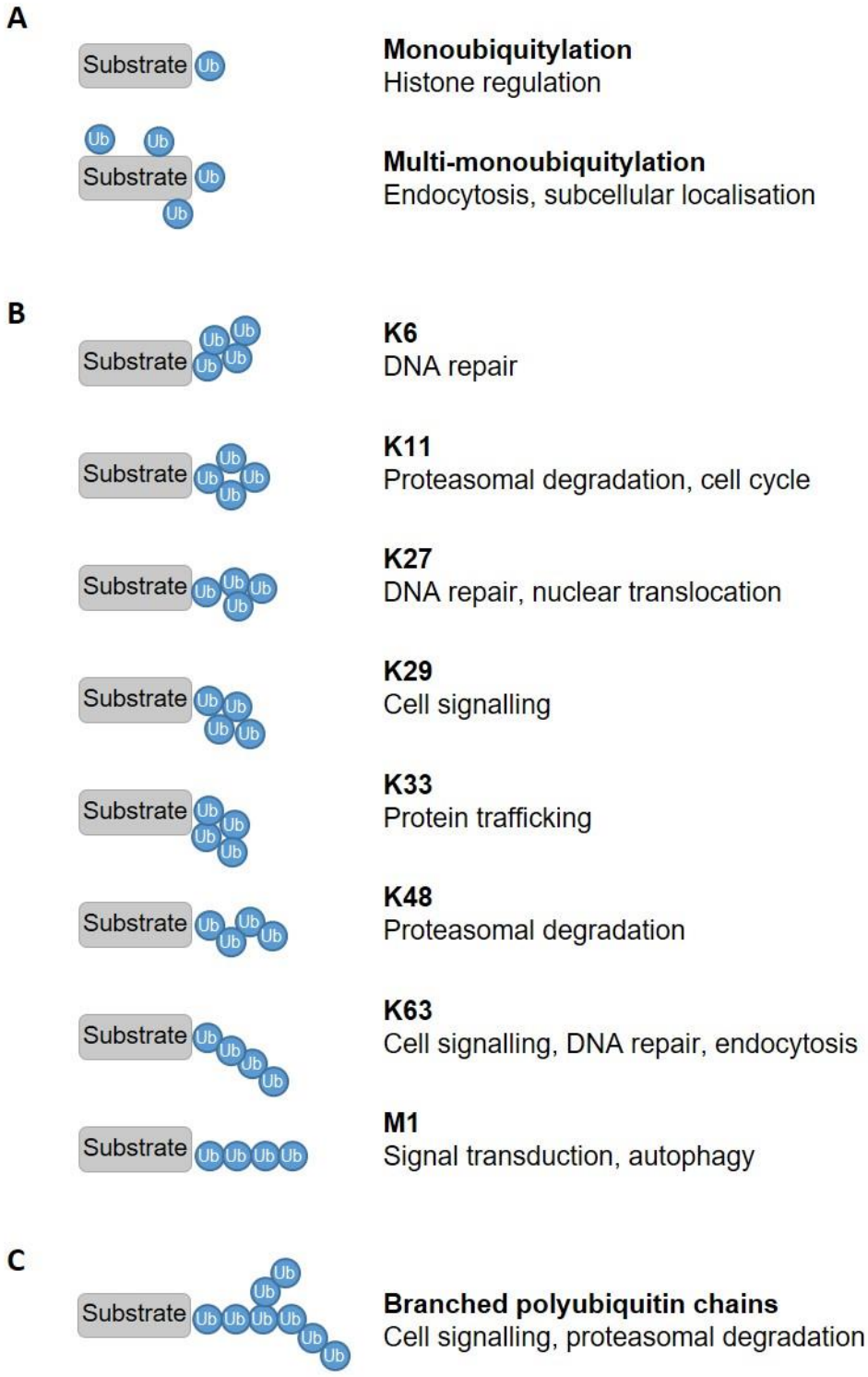

Figure 1.7. Forms of ubiquitylation
Ubiquitin can be added to substrates as single moieties (**A**), homotypic polyubiquitin chains (**B**) or heterotypic polyubiquitin chains (**C**). Examples of the roles for each topology are also shown. Figure adapted from Ye & Rape, (2009).

1.4 Deubiquitylase enzymes

Ubiquitylation is a reversible process with its antithesis, deubiquitylation, being catalysed by deubiquitylating enzymes (DUBs). In addition to reversing ubiquitylation, DUBs also play important roles in generating free ubiquitin from immature precursors as well as editing ubiquitin chains to modify the fate or function of the substrate (Figure 1.6) (Clague *et al.*, 2013; Heride *et al.*, 2014).

1.4.1 DUB families

To date, over 100 human DUBs have been identified which can be split into two classes: cysteine proteases and metalloproteases. The cysteine proteases represent the largest class of DUBs and can be divided further into separate families: ubiquitin-specific proteases (USPs), ubiquitin C-terminal hydrolases (UCHs), ovarian tumour proteases (OTUs), Machado-Josephin domains (MJDs), motif interacting with Ub-containing novel DUB family (MINDYs) and zinc finger with UFM1-specific peptidase domains (ZUFSPs) (Nijman *et al.*, 2005; Abdul Rehman *et al.*, 2016; Haahr *et al.*, 2018; Kwasna *et al.*, 2018). The metalloproteases consists only of the Jab1/MPN/MOV34 family (JAMMs) (Figure 1.8) (Nijman *et al.*, 2005).

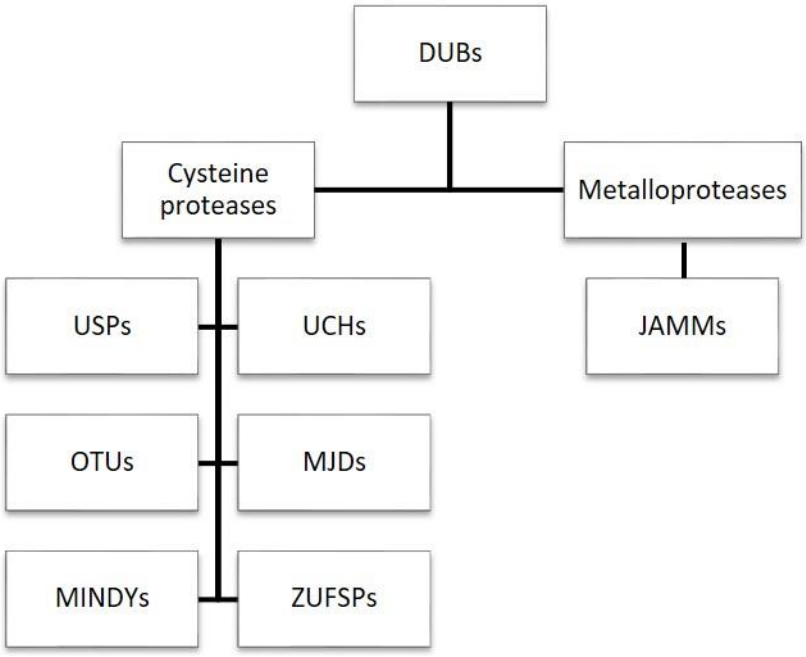

Figure 1.8 Schematic representation of DUB families
DUBs can be divided into two main groups: cysteine proteases and metalloproteases. The cysteine proteases consist of ubiquitin-specific proteases (USPs), ubiquitin C-terminal hydrolases (UCHs), ovarian tumour proteases (OTUs), Machado-Josephin domains (MJDs), motif interacting with Ub-containing novel DUB family (MINDYs) and zinc finger with UFM1-specific peptidase domains (ZUFSPs). The metalloproteases consist of the Jab1/MPN/MOV34 family (JAMMs) only.

1.4.2 DUB catalytic activity

DUBs are categorised into the families described in section 1.4.1 based on the structure of their catalytic domains. The cysteine proteases contain a highly conserved catalytic triad of cysteine, histidine and aspartate/ asparagine residues. The aspartate/ asparagine residue polarises and aligns the histidine residue which then acts to lower the pK_a and deprotonate the cysteine residue. This allows for a nucleophilic attack by the cysteine residue on the isopeptide bond between ubiquitin and its substrate (Komander & Barford, 2008; Clague *et al.*, 2013). In contrast, the metalloprotease catalytic site consists of histidine, aspartame and serine residues with a core zinc ion. The mechanism for metalloproteases is dependent on the presence of a water molecule which, when deprotonated by the zinc ion, is able to attack

the isopeptide bond linking the ubiquitin moiety (Tran *et al.*, 2003; Clague *et al.*, 2013).

It has also been shown that some DUBs have preferences for certain ubiquitin chains (Ritorto *et al.*, 2014). For example, OTUB1 and OTUB2, despite structural similarities, will preferentially cleave K63 and K48 chains, respectively (Edelmann *et al.*, 2009; Mevissen *et al.*, 2013). Another OTU DUB, OTULIN, exhibits specificity for linear ubiquitin chains (Fiil *et al.*, 2013; Keusekotten *et al.*, 2013). The USP DUBs are largely thought to be indiscriminative with regards to their chain linkage preferences (Faesen *et al.*, 2011*b*). For example, the proteasome associated DUB, USP14, is capable of removing ubiquitin from a diverse range of linkages (Lee *et al.*, 2011). However, there are certain exceptions such as CYLD, a USP DUB with a preference for K63 and linear ubiquitin chains (Komander *et al.*, 2009).

In addition to linkage-specificity, DUBs can also have ‘endo’ or ‘exo’ preferences which cleave either within or from the end of chains, respectively. Endo-DUBs, for example CYLD and USP9X, are capable of removing entire polyubiquitin chains, thereby providing an efficient way to rapidly reverse ubiquitination (Komander *et al.*, 2008; Al-Hakim *et al.*, 2008). Exo-DUBs, such as USP14, remove the terminal ubiquitin from a chain and recycle polyubiquitin chains to restore pools of free monoubiquitin (Hu *et al.*, 2005).

Another layer of specificity is provided by DUB selectivity for its substrate protein. These interactions can either be controlled by protein interacting domains within the DUB itself or by physical location within the cell. For instance, USP25 requires a ubiquitin-interaction motif (UIM) for efficient hydrolysis of ubiquitin chains (Meulmeester *et al.*, 2008). In addition, USP30 has been demonstrated to be a transmembrane protein which localises at the mitochondria, thereby limiting its exposure to certain substrates (Nakamura & Hirose, 2008).

1.4.3 Regulation of DUB activity

It is crucial for DUB activity to be tightly controlled to prevent potential harm coming to the cell as a result of dysregulated ubiquitin signalling. This is achieved through multiple layers of regulation, some of which comes at the transcriptional level. For example, DUB transcript levels have been shown to differ between cell and tissue type as well as in pathophysiological states (Clague *et al.*, 2013). However, most control appears to be provided at the protein level (Sahtoe & Sixma, 2015).

One way in which certain DUBs can regulate their activity is through intramolecular control of specific structural conformations. For example USP7, in its native state, exists as an inactive DUB with the catalytic triad misaligned resulting in a closed conformation (Hu *et al.*, 2002). Binding of ubiquitin alters the configuration of USP7 to realign the catalytic triad and stabilise the active conformation. The catalytic activity of USP7 can also be increased further by folding back of a C-terminal domain to allow it to come in contact with the switching loop (Faesen *et al.*, 2011*a*).

DUB activity can also be influenced by interactions with external factors. For example, the recruitment of USP14 to the proteasome via its ubiquitin-like (Ubl) domain has been shown to increase its activity 500-fold (Hu *et al.*, 2005). Another illustration of increased catalytic activity via interacting with an external protein partner is the stabilisation of the active conformation of USP7 by GMP synthase (GMPS) (Van Der Knaap *et al.*, 2005; Faesen *et al.*, 2011*a*). Although less common, inhibition of DUB activity through interactions with external factors has also been documented. For example, UCHL5 can be inhibited by the binding of INO80G, a component of chromatin-remodelling complexes. By binding to the ubiquitin-docking site, INO80G reduces the affinity of UCHL5 for ubiquitin thereby inhibiting its role in DNA repair mechanisms until this restriction has been alleviated (Yao *et al.*, 2008; VanderLinden *et al.*, 2015).

Post-translational modifications are also increasingly being seen as an important mechanism for increasing or decreasing DUB activity. For example, phosphorylation of the OTU DUB, DUBA, at Ser177 is essential for

its activity (Huang *et al.*, 2012). Conversely, phosphorylation at Tyr56 of OTULIN inhibits DUB activity and thereby interrupts the NK-κB signalling pathway (Elliott *et al.*, 2014; Schaeffer *et al.*, 2014). DUBs can also be ubiquitylated themselves, as has been shown for ATXN3, for which addition of ubiquitin moieties increases its catalytic activity (Todi *et al.*, 2009). In contrast, monoubiquitylation near the active site of UCHL1 has been demonstrated to decrease activity (Meray & Lansbury, 2007). The ubiquitylation status of DUBs can also affect their location within the cell. For example, monoubiquitylation of BAP1 by UBE20 leads to its exclusion from the nucleus, where the majority of its target substrate is present. However, BAP1 is also capable of autodeubiquitylating itself to antagonise this effect (Mashtalir *et al.*, 2014). Indeed, the ability of some DUBs to autodeubiquitylate themselves is vital for their protein stability, as is the case for USP4. Phosphorylation of USP4 is essential for both its relocation to the cytoplasm and catalytic activity to enable it to autodeubiquitylate and maintain its protein stability (Zhang *et al.*, 2012).

1.5 Viruses and the ubiquitin system

Viruses are obligate intracellular parasites which depend on their host in order to replicate. Given the involvement of the ubiquitin system in such a wide-range of cellular functions, it is unsurprising that viruses have evolved to exploit it. Indeed, viruses have been shown to take advantage of the ubiquitin system in a variety of ways, particularly through manipulation of host E3 enzymes and DUBs (Gustin *et al.*, 2011; Zhang *et al.*, 2018*b*). In addition, viruses have been shown to mimic their host and encode their own E3 enzymes or DUBs (Wimmer & Schreiner, 2015; Zhang *et al.*, 2018*b*).

1.5.1 Viral manipulation of host E3 enzymes

The first example of a virus redirecting a host cell E3 ligase came from HPV which was shown to recruit E6AP, an E3 ligase, via its E6 oncoprotein. This interaction induces the ubiquitylation and subsequent degradation of p53, thereby promoting malignant transformation (Scheffner *et al.*, 1990).

Adenoviruses are another example of viruses which promote the degradation of p53. The viral proteins, E1B-55K and E4orf6, recruit the E3 ligases, Cul5 and Rbx-1, and target p53 for ubiquitylation (Querido *et al.*, 2001; Blanchette *et al.*, 2004). As well as altering the cell cycle of infected cells, viruses have been shown to hijack host E3 ligases to inhibit cellular anti-viral mechanisms. For example, HIV manipulates the host anti-viral response by targeting an apolipoprotein B complex (APOBEC) for degradation. APOBEC proteins are a group of cytidine deamination proteins which induce hypermutations in the viral genome, thereby inhibiting its propagation (Sheehy *et al.*, 2002; Malim, 2009). The HIV accessory proteins, Vif and Vpr, redirect the APOBEC3G complex to cullin-RING finger ubiquitin ligases to induce its degradation (Yu *et al.*, 2003; Mehle *et al.*, 2004). In a similar manner, the rubulavirus V protein alters the substrate specificity of a host E3 ligase to promote degradation of STAT proteins and dampen the anti-viral response (Ulane & Horvath, 2002; Goodbourn *et al.*, 2005). For example, the Mumps V protein was shown to recruit the E3 ligases, Cullin4A and Rbx1, to target STAT3 for degradation and suppress cytokine signalling (Ulane *et al.*, 2003).

While the majority of examples for viral hijacking of E3 ligases results in protein degradation, some viruses manipulate E3 ligases in order to prevent the degradation of their target. For example, the HPV E5 protein was shown to subvert the E3 ligase, c-Cbl, to prevent degradation of EGFR (Zhang *et al.*, 2005). Subsequent signalling through the EGFR pathway contributes to the transformation and anchorage-independent growth of infected cells (Pim *et al.*, 1992; Straight *et al.*, 1993). Another example includes the SV40 Large T antigen, which binds the host SCF ligase to inhibit degradation of cyclin E, thereby promoting progression of the cell cycle (Welcker & Clurman, 2005). There are also several examples of viruses which manipulate E3 ligases to promote ubiquitylation of their own proteins to aid the virus lifecycle. For example, monoubiquitylation of the retroviral Gag proteins by Nedd4 E3 ligase is required for virus budding. Tsg101 and ESCRT proteins are recruited to monoubiquitylated Gag during retroviral budding instead of their usual cargo (Blot *et al.*, 2004; Sette *et al.*, 2013). Similarly, Ebola VP40 protein is ubiquitylated by Nedd4, thereby facilitating

virion budding and release (Yasuda *et al.*, 2003). Another Ebola protein, VP35, is ubiquitylated by the TRIM6 host E3 ligase to promote virus replication (Bharaj *et al.*, 2017).

1.5.2 Virus encoded E3 enzymes

Some viruses have also evolved to encode their own E3 ligases, particularly the large DNA viruses such as herpesviruses and poxviruses. For example, ICP0 of HSV-1 features two E3 ligase domains which induces ubiquitylation and degradation of a range of cellular targets to promote its replication (Boutell *et al.*, 2002; Hagglund *et al.*, 2002). Another virus with two E3 ligases is KSHV, which encodes K3 and K5 to ubiquitylate class I MHC proteins, ICAM-1 and B7-2 (Coscoy & Ganem, 2001; Boname & Lehner, 2011). These are proteins important for antigen presentation and stimulation of T cells (Dubey *et al.*, 1995; Neefjes *et al.*, 2011). Therefore, ubiquitylating these and consequently promoting their degradation is tactic utilised by KSHV to overcome the host immune response. Another virus encoded E3 ligase shown to interfere with the host anti-viral response is the ORF61 protein of VZV. This RING finger E3 ligase specifically ubiquitylates phosphorylated IRF3 to promote its degradation and inhibit immune signalling (Zhu *et al.*, 2011). Other viral E3 ligases have a more direct impact on viral replication such as the adenovirus encoded E1B-55k and E4orf6 which were shown to be required for viral nuclear mRNA export (Woo & Berk, 2006).

1.5.3 Changes in expression of cellular DUBs during viral infection

One of the most commonly associated roles for DUBs is stabilisation of proteins by removal of ubiquitin, thereby preventing degradation by the proteasome (Glickman & Adir, 2004). Indeed this aspect has been shown to be exploited by viruses (Table 1.1). For example, USP7 is known to be upregulated in response to HIV-1 infection resulting in stabilisation of the viral Tat protein and enhancement of virus gene transcription (Ali *et al.*, 2017). In comparison, the upregulation of USP25 by Sendai virus (SeV) and Vesicular Stomatitis Virus (VSV) has been suggested to promote the antiviral response

by stabilising the scaffolding proteins TRAF3 and TRAF6, allowing signalling complexes to form as part of the pro-inflammatory response (Lin *et al.*, 2015). However, this study is in contradiction to earlier findings which suggest that USP25 is a negative regulator of the type I IFN response by removing K63-linked polyubiquitin chains from TRAF6 which are important for signalling (Zhong *et al.*, 2013).

It is now known that DUBs play a role in many more biological processes other than protein stability and that DUBs can be utilised by the host to fight infection or by the virus to divert the normal cellular pathways. For example, downregulation of the DUB USP11 by influenza A results in an increase in monoubiquitylation of the NP protein, resulting in more efficient replication by increasing interactions with RNA (Liao *et al.*, 2010). Another example includes the upregulation of A20 following EBV infection (Laherty *et al.*, 1992). The DUB activity of A20 leads to a decrease in IRF7 activity by removing K63 linked polyubiquitin chains and thereby inhibiting transcriptional activity and the resulting type I IFN production (Ning & Pagano, 2010).

Dysregulation of DUB expression not only affects acute viral infections, but can also play a role in chronic virus infections. A common mutation in a HBV protein during integration into hepatic cells results in a truncated version of the HBx protein (Ct-HBx) which has been shown to downregulate USP16. This results in promotion of cell growth and leads to hepatocellular carcinoma (HCC) (Qian *et al.*, 2016). Another interesting example involving HBV deregulation of the cell cycle is the increased expression of USP37 in HBV infected cells. In this instance the viral protein, HBx, physically interacts with the DUB and acts as a chaperone to translocate USP37 from its normal location within the nucleus to the cytoplasm. This protects USP37 from degradation and results in an increase in ubiquitination of cyclin A thereby promoting progression of the cell cycle (Saxena & Kumar, 2014).

1.5.4 Viral interference with cellular DUB function

Viruses do not only modulate DUB expression levels upon infection, they can also modulate activity by direct and indirect interactions. For example, following KSHV infection, the viral protein vIRF1 interacts with and blocks USP7 activity so it is no longer able to remove ubiquitin from p53 to stabilise it. Consequently, the p53-mediated antiviral response is inhibited and KSHV can progress to latency (Chavoshi *et al.*, 2016). Interactions with DUBs are not only inhibitory. For example, interaction of the HSV-1 protein ICP0 with USP7 does not inhibit the activity of either protein, indeed this interplay ensures efficient deubiquitination of ICP0 to stabilise it (Boutell *et al.*, 2005).

Another method for modification of DUB activity during virus infection is via post-translational modifications to alter the DUB's catalytic capacity. Indeed, DUB activity has been shown to be tightly regulated during normal physiological processes by several post-translational modifications, including phosphorylation, acetylation, sumoylation and ubiquitination (see section 1.4.3) (Kessler *et al.*, 2011). It is therefore inevitable that viruses will have developed ways to manipulate this regulation to subvert DUBs for their own benefit. For example, CYLD acts as a negative regulator of HTLV-1 infection by removing K63-linked ubiquitin chains from the viral Tax protein to prevent NF-κB signalling (Wu *et al.*, 2011). This inhibition is overcome in infected cells via the HTLV-1-induced phosphorylation of CYLD by the IKK complex, a known negative regulator of CYLD catalytic activity (Reiley *et al.*, 2005; Wu *et al.*, 2011).

Table 1.1. Viral manipulation of host cell DUBs during virus replication

DUB	Virus	Role	Reference
USP1, USP12, USP46	HPV	Interacts with HPV genome to promote HPV replication via an unknown mechanism	(Lehoux *et al.*, 2014)
CYLD	HIV-1	Negatively regulates HIV replication and reactivation via the NF-κB pathway.	(Manganaro *et al.*, 2014)
USP7	HIV-1	Promotes viral transcription by protecting Tat from proteasomal degradation	(Ali *et al.*, 2017)
USP7	KSHV	The viral protein vIRF1 binds to and inhibits USP7 to prevent stabilisation of p53 and promote virus replication.	(Chavoshi *et al.*, 2016)
USP8	ZIKV	Recruited by the viral protein NS1 to deubiquitylate and stabilise caspase-1 to enhance inflammasome activation and promote virus replication	(Zheng *et al.*, 2018)
USP11	Influenza A	Increased monoubiquitylation of the viral NP protein resulting in increased influenza A replication following USP11 down-regulation	(Liao *et al.*, 2010)
USP15	HBV	Stabilises the viral protein HBx to promote virus replication and oncogenic signalling	(Su *et al.*, 2017)
USP15	HIV-1	Promotes degradation of HIV-1 Nef and Gag thereby inhibiting virus replication	(Pyeon *et al.*, 2016)

chUSP18	LPAIV	Promotes virus replication by an unknown mechanism	(Tanikawa *et al.*, 2017)
USP18	HBV	Promotes HBV replication and cell proliferation in infected hepatic cells	(Kim *et al.*, 2008; Cai *et al.*, 2017)
A20	EBV	Inhibits IRF7 via its DUB activity to interfere with immune response	(Laherty *et al.*, 1992; Ning & Pagano, 2010)
CYLD	HPV	Promotes NF-κB signalling leading to cell proliferation and angiogenesis	(An *et al.*, 2008)
CYLD	HTLV-1	Inhibits Tax ubiquitylation to prevent IKK activation. Phosphorylation of CYLD by HTLV-1 can counteract this effect by inhibiting CYLD	(Wu *et al.*, 2011)
CYLD	VSV	Involved in IFNR signalling in antiviral response	(Zhang *et al.*, 2011*a*)
JOSD1	VSV	Stabilises SOCS1 resulting in down-regulation of the IFN antiviral response	(Wang *et al.*, 2017*b*)
MYSM1	VSV	Negative regulator of innate immune signalling which increases susceptibility to virus infection	(Panda *et al.*, 2015)
MCPIP1	HCV	Simultaneously inhibits viral replication and antiviral immune response	(Lin *et al.*, 2014)
MCPIP1	JEV, DENV	Inhibits viral replication by promoting viral RNA degradation	(Lin *et al.*, 2013)
MCPIP1	IAV	Inhibits RIG-I expression following IAV infection to suppress innate	(Sun *et al.*, 2017*b*)

		immune signalling	
STAMBPL1	HTLV-1	Promotes NF-κB signalling resulting in enhanced nuclear export of the viral tax protein	(Lavorgna & Harhaj, 2012)
UCHL1	HPV	Negatively regulates innate immune response in keratinocytes	(Karim *et al.*, 2013)
USP10	SFV	USP10 negatively regulates stress granule formation.	(Panas *et al.*, 2015)
USP13	HSV-1	Deubiquitylates STING to inhibit the immune response by reducing IRF3 and NFκB activation, thereby allowing virus replication	(Sun *et al.*, 2017*a*)
USP13	DENV-2	Deubiquitylates STAT1 to prevent degradation and promote DENV2 replication	(Yeh *et al.*, 2013)
USP15	SeV	Negatively regulates antiviral RIG-I signalling in a DUB-dependent and -independent manner	(Zhang *et al.*, 2015)
USP17	SeV	Deubiquitylates RIG-I and MDA5 to promote the type I IFN response following virus infection	(Chen *et al.*, 2010*b*)
USP18	HBV	Inhibits interferon signalling in response to HBV infection	(Li *et al.*, 2016)
USP18	HIV	Inhibits antiviral activity of p21 and increases intracellular pool of dNTPs to promote HIV-1 and HIV-2.	(Osei Kuffour *et al.*, 2018)
USP18	VACV and Influenza B	Negatively regulates the IFN response	(Ketscher *et al.*, 2015)

USP18 USP20	HSV-1	Recruitment of USP20 by USP18 stabilises STING to promote antiviral response	(Zhang *et al.*, 2016)
USP19	H1N1	Negatively regulates RIG-I mediated type I IFN response	(Jin *et al.*, 2016)
USP20	HTLV-1	Lower expression of USP20 prevents inhibition of NF-κB signalling	(Yasunaga *et al.*, 2011)
USP21	VSV	Inhibits antiviral response by deubiquitylating RIG-I thereby inhibiting antiviral signalling	(Fan *et al.*, 2014)
USP25	SeV	Interferes with type I IFN response by deubiquitylating RIG-I, TNF, TRAF2 and TRAF6	(Zhong *et al.*, 2013)
USP25	SeV and VSV	Protects TRAF3 and TRAF6 from proteasomal degradation to promote antiviral response	(Lin *et al.*, 2015)
USP2a	VSV, SeV DENV, H1N1	Prevents degradation of phosphorylated STAT1 to promote the antiviral response	(Ren *et al.*, 2016)

Abbreviations: Chicken USP18 (chUSP18), Dengue Virus (DENV), Dengue Virus Type 2 (DENV-2), Epstein-Barr virus (EBV), Influenza A virus subtype H1N1 (H1N1), Hepatitis B Virus (HBV), Hepatitis C Virus (HCV), Human Immunodeficiency Virus Type 1 (HIV-1), Human Immunodeficiency Virus Type 2 (HIV-2), Herpes Simplex Virus Type 1 (HSV-1), Human Papilloma Virus (HPV), Human T- cell Leukaemia Virus Type 1 (HTLV-1), Influenza A Virus (IAV), Japanese Encephalitis Virus (JEV), Kaposi's Sarcoma-associated Herpesvirus (KSHV), Low Pathogenicity Avian Influenza Virus (LPAIV), Sendai Virus (SeV), Semliki Forest Virus (SFV), Vaccinia Virus (VACV), Vesicular Stomatitis Virus (VSV)

1.5.5 Virus encoded DUBs

It is known that viruses can mimic their host and encode their own DUBs which act on both viral and cellular proteins (Table 1.2). An important tool in the discovery of virus-encoded DUBs has been the use of activity based probes (ABPs) which are designed to bind the active site of DUBs (see section 4.1 for more detail on ABPs) (Kattenhorn *et al.*, 2005). Indeed, the first viral DUB identified, adenovirus L3 23K proteinase (Avp), was through the use of an ABP (Balakirev *et al.*, 2002). These provide an advantage over previous techniques such as homology screening as the sequence variability compared to host cell DUBs can be high (Kattenhorn *et al.*, 2005; Schlieker *et al.*, 2007).

There are now several examples of virus encoded DUBs. One of the more extensively studied viral DUBs is the Herpes-Simplex Virus protein, UL36. This DUB has now been shown to be conserved across other *Herpesviridae* subfamilies, for example UL48 of human cytomegalovirus (HCMV) and BPLF-1 of Epstein-Barr virus (EBV), are the UL36 homologs for their respective viruses (Schlieker *et al.*, 2005; Wang *et al.*, 2006; Sompallae *et al.*, 2008). Other DUBs encoded within the herpes genome have also now been identified including: ORF64 of Kaposi's sarcoma-associated herpesvirus (KSHV), BSLF-1 and BXLF-1 of EBV and M48 of murine cytomegalovirus (Schlieker *et al.*, 2005; Sompallae *et al.*, 2008; González *et al.*, 2009).

DUB activity has also been described in several plus-strand RNA viruses. For example, the Severe Acute Respiratory Syndrome Coronavirus (SARS-CoV) has been shown to have deubiquitinating activity in its papain-like protease (PLpro) protein which is thought to play a role in suppressing the innate immune response (Barretto *et al.*, 2005; Ratia *et al.*, 2014). The closely related Middle East respiratory syndrome (MERS) coronavirus also encodes a PLpro with DUB activity, but with distinct ubiquitin cleavage preferences (Békés *et al.*, 2015). Other viruses encoding proteins with DUB activity include Hepatitis E protein pORF1, Foot-and-Mouth Disease Virus (FMDV) protein L^{pro} and arteriviruses such as Equine Arteritis Virus (EAV)

protein PLP2, all thought to be involved in inhibiting the innate immune response (Karpe & Lole, 2011; Wang *et al.*, 2011*a*; van Kasteren *et al.*, 2013, 2015; Nan *et al.*, 2014). The PRO domain of the polyprotein of the alphavirus-like Turnip Yellow Mosaic Virus (TYMV) has also been shown to contain DUB activity important for stabilising its RNA-dependent RNA polymerase (Chenon *et al.*, 2012; Lombardi *et al.*, 2013).

Viral DUBs have also been identified in the minus-strand RNA viruses, for example of the Nairovirus and Tenuivirus genera. This includes the important human pathogen, Crimean Congo Haemorrhagic Fever Virus (CCHFV) which has DUB activity within its RNA polymerase which is utilised to suppress innate immune responses (Honig *et al.*, 2004; Scholte *et al.*, 2017). The related Dugbe virus (DUGV) has also been shown to display similar DUB activity (Bakshi *et al.*, 2013). In addition, analysis of the rice stripe virus genome revealed an OTU-like cysteine protease domain within its RNA1 protein (Zhang *et al.*, 2007).

Table 1.2. Virus encoded DUBs

Virus	Viral protein	Role	Reference
AdV	Avp	Promotes viral replication	(Balakirev *et al.*, 2002)
HSV-1	pUL36	Inhibits innate immune response	(Kattenhorn *et al.*, 2005; Ye *et al.*, 2016)
MDV	pUL36	Promotes viral replication and tumorigenesis	(Jarosinski *et al.*, 2007; Veiga *et al.*, 2013)
PRV	pUL36	Involved in neural invasion	(Lee *et al.*, 2009; Huffmaster *et al.*, 2015)
HCMV	pUL48	Enhances cellular metabolism and inhibits innate immune response	(Wang *et al.*, 2006; Kumari *et al.*, 2017)
EBV	BPLF1	Inhibits innate immune response, disrupts DNA damage repair	(Schlieker *et al.*, 2005; Saito *et al.*, 2013)
KSV	ORF64	Inhibits innate immune response, required for virus replication	(González *et al.*, 2009; Inn *et al.*, 2011)
MHV-68	ORF64	Inhibits innate immune response and promotes delivery of viral DNA to nucleus	(Gredmark *et al.*, 2007; Sun *et al.*, 2015)
PEDV	PLP2	Inhibits innate immune response	(Xing *et al.*, 2013)
TGEV	PL1	Inhibits innate immune response	(Hu *et al.*, 2017)
SARS-CoV	PLpro	Inhibits innate immune response	(Barretto *et al.*, 2005; Chen *et al.*, 2014)
MERS-CoV	PLpro	Inhibits innate immune response	(Mielech *et al.*, 2014; Yang *et al.*, 2014)

MHV	PLP2	Inhibits innate immune response	(Zheng *et al.*, 2008; Wang *et al.*, 2011*b*)
IBV	PLpro	Inhibits innate immune response	(Kong *et al.*, 2015; Yu *et al.*, 2017)
EAV	PLP2	Inhibits innate immune response	(van Kasteren *et al.*, 2013)
PRRSV	nsp2	Inhibits innate immune response	(Sun *et al.*, 2010)
LDV	nsp2	Inhibits innate immune response	(van Kasteren *et al.*, 2012)
SHFV	nsp2	Inhibits innate immune response	(van Kasteren *et al.*, 2012)
CCHFV	L-protein	Inhibits innate immune response	(Honig *et al.*, 2004; Scholte *et al.*, 2017)
DUGV	L-protein	Inhibits innate immune response	(Bakshi *et al.*, 2013)
NSDV	L-protein	Inhibits innate immune response, interferes with cell signalling	(Holzer *et al.*, 2011)
FMDV	Lpro	Inhibits innate immune response	(Wang *et al.*, 2011*a*)
TYMV	PRO	Stabilises TYMV RdRp	(Chenon *et al.*, 2012)

Abbreviations: Human Adenovirus (HAdV), L3 23K proteinase (Avp), Herpes Simplex Virus type 1 (HSV-1), Marek's disease virus (MDV), pseudorabies virus (PRV), Human cytomegalovirus (HCMV), Epstein-Barr Virus (EBV), Kaposi's sarcoma-associated herpesvirus (KSHV), murine gammaherpesvirus 68 (MHV68), porcine epidemic diarrhoea virus (PEDV), papain-like protease 2 (PLP2), transmissible gastroenteritis virus (TGEV), papain-like protease 1 (PL1), severe acute respiratory syndrome coronavirus (SARS-CoV), papain-like protease (PLpro), Middle East respiratory coronavirus (MERS-CoV), mouse hepatitis virus (MHV), infectious bronchitis virus (IBV), equine arteritis virus (EAV), porcine reproductive and respiratory syndrome virus (PRRSV), lactate dehydrogenase elevating virus (LDV), simian haemorrhagic fever virus (SHFV), Crimean-Congo haemorrhagic fever virus (CCHFV), Dugbe virus (DUGV), Nairobi sheep disease virus (NSDV), foot-and-mouth disease virus (FMDV), leader proteinase (Lpro), Turnip yellow mosaic virus (TYMV)

1.6 DUBs as therapeutic targets

Attempts to target the ubiquitin proteasome system in the past have demonstrated potential with some inhibitors making it to clinical practice. For example, the proteasome inhibitor, bortezomib, which was approved for use in treating certain cancers (Richardson *et al.*, 2005; Manasanch & Orlowski, 2017). However, resistance to bortezomib is increasingly becoming an issue as cancer cells upregulate other proteins to counteract the effects of the drug (Lü & Wang, 2013). Work is now beginning to focus on regulators of the ubiquitin system which are upstream of the proteasome in order to overcome issues such as these (Colland, 2010; Farshi *et al.*, 2015).

DUBs are increasingly becoming the focus of attention for the development of drugs to target the ubiquitin system. This is, in part, due to their specificity in substrate selection making them key checkpoints of protein fate. In addition, there are fewer DUBs encoded by the human genome (~100), compared to E3 ligases (600-1000), which increases the feasibility of their functional analysis (Ye & Rape, 2009; Zheng & Shabek, 2017; Clague *et al.*, 2019). Indeed, several compounds targeting DUBs are under investigation for treatment of a range of diseases. The most intensively studied example is USP7 as a target for cancer therapies due to the critical role it plays in regulating p53 function (Li *et al.*, 2002). Several small molecule inhibitors targeting USP7 are currently under investigation as oncotherapies, for example HBX41108, P5091 and P22077 (Colland *et al.*, 2009; Reverdy *et al.*, 2012; Weinstock *et al.*, 2012). Therapeutic inhibition of DUBs is also being considered for infectious diseases. For example, the DUB inhibitors P22077 and PR-619, have been shown to block HIV-1 replication *in vitro* (Setz *et al.*, 2017). However, the complexity and diversity of the ubiquitin system has frustrated attempts to develop effective and specific therapeutics which make it to clinical practise. Progress has therefore been slow, with many compounds exhibiting unacceptably low potency and poor selectivity (Ritorto *et al.*, 2014). Thus, to date no compounds targeting DUBs have successfully completed clinical trials. An inhibitor targeting the proteasomal DUBs UCHL5 and USP14, VLX1570, intended for multiple myeloma treatment, commenced clinical trials in 2015

(Wang *et al.*, 2016). However, these were suspended in 2017 during phase 1/2 due to dose limiting toxicity (ClinicalTrials.gov identifier: NCT02372240).

Despite these setbacks, new technologies such as activity-based probes (ABPs), are aiding development of highly specific inhibitors (Kramer *et al.*, 2012). The use of ubiquitin derived ABPs in high-throughput screening experiments has accelerated the identification of potential drug targets from pools of lead compounds by determining the selectivity and potency of DUB inhibitors (Altun *et al.*, 2011; Ritorto *et al.*, 2014; McLellan *et al.*, 2016). In addition, for viruses which encode their own DUB, efforts are being made to develop drugs to target these. For example GRL0617, which was demonstrated to inhibit the SARS-CoV deubiquitylase, PLpro, *in vitro* without inhibiting host DUBs (Ratia *et al.*, 2008). Alternative techniques are also being explored, such as the use of ubiquitin variants to screen for and identify potent inhibitors of the viral DUB of Crimean-Congo haemorrhagic fever virus (CCHFV) (Zhang *et al.*, 2017).

1.7 Project aims

Recent large scale outbreaks of diseases caused by alphaviruses, such as CHIKV, highlight the requirement to develop novel drugs against these threats. The ubiquitin system has been demonstrated to play a key role in virus infections in both a pro- and anti-viral manner. Viruses have even evolved the capacity to encode their own components of the ubiquitin machinery, further highlighting the importance of this system in viral replication. The ubiquitin system is therefore generating interest as a target for therapeutic intervention. DUBs in particular are seen as highly druggable and the feasibility of targeting these enzymes has been demonstrated for other diseases. However, a targeted approach to investigate the role of DUBs in alphavirus infection has yet to be published. Generating a more detailed understanding of the role of DUBs in alphavirus infection would aid the development of therapeutics and potentially identify novel drug targets. Thus, the overall aim of this thesis was to investigate the involvement of DUBs in alphavirus infection using both the CL2 model virus, SFV, and the more clinically relevant CL3 virus, CHIKV.

Chapter 2: Materials and Methods

2.1 Chemical reagents and solutions

Reagents and solutions used in this thesis were sourced as detailed in Tables 2.1 to 2.4.

Table 2.1 Chemical reagents

Item	Brand
7.5% Sodium bicarbonate	Sigma, UK
Ammonium persulfate (APS)	Sigma, UK
Dimethyl sulfoxide (DMSO)	Sigma, UK
DL-Dithiothreitol (DTT)	Sigma, UK
Ethidium Bromide (EtBr)	Sigma, UK
Fetal Calf Serum (FCS)	Sigma, UK
L-Glutamine	Sigma, UK
Mercaptoethanol (β-ME)	Sigma, UK
N,N,N',N'-Tetramethylethylenediamene (TEMED)	Sigma, UK
Penicillin/streptomycin	Sigma, UK
Ponceau S Stain	Sigma, UK
Sodium Dodecyl Sulfoxide (SDS)	Sigma, UK
Sucrose	Sigma, UK
Trypsin-EDTA	Sigma, UK
UltraPure™ Agarose	Thermo Fisher Scientific, UK
UltraPure™ Low Melting Point Agarose	Thermo Fisher Scientific, UK

Table 2.2 Enzymes and Commercial Kits

Item	Brand
2x PCR Reddy Mix	Thermo Fisher Scientific, UK
5x reverse transcription buffer	Thermo Fisher Scientific, UK
AllStars Negative Control	Qiagen, Germany
Amersham ECL Rainbow Molecular Weight Markers	GE Healthcare Life Sciences, UK
CellTiter-Glo® Luminescent Cell Viability Assay	Promega, USA
Color Prestained Protein Standard, Broad Range (11–245 kDa)	New England Biolabs, USA
Ethyl alcohol, Pure, 200 proof	Sigma, UK
iTaq™ Universal SYBR Green supermix	BioRad
Oligo (dT) 15 primers	Promega, USA
Pierce™ BCA Protein Assay Kit	Thermo Fisher Scientific, UK
Pierce™ ECL Western Blotting Substrate	Thermo Fisher Scientific, UK
Plasmid purification kit	Qiagen, Germany
QIAquick PCR purification kit	Qiagen, Germany
Quick-Load® 100 bp DNA Ladder	New England Biolabs, USA
RevertAid™ M-MuLV reverse transcriptase	Thermo Fisher Scientific, UK
RNAiMax	Invitrogen, UK
RNase-free DNase	Qiagen, Germany
RNeasy Plus Mini Kit	Qiagen, Germany

Table 2.3 Solutions and Buffers

Item	Brand
2.3% crystal violet stain	Sigma, UK
2-Propanol	Sigma, UK
5x Agarose Gel Loading Dye	New England BioLabs, USA
Acetone	Sigma, UK
Bromophenol blue (BPB)	Sigma, UK
Butanol	Sigma, UK
Formalin solution, neutral buffered, 10%	Sigma, UK
Glycerol 99%	Sigma, UK
Isopropanol	Fisher Scientific, UK
Methanol	Fisher Scientific, UK
Nuclease free ddH2O	Sigma, UK
NuPAGE® MOPS SDS Running Buffer (20X)	Thermo Fisher Scientific, UK
Opti-MEM media	Thermo Fisher Scientific, UK
PCR Nucleotide Mix	Promega, USA
Protogel Acrylamide solution	GeneFlow, UK
Protogel Resolving buffer	GeneFlow, UK
Protogel Stacking buffer	GeneFlow, UK
RNasin® Plus Rnase Inhibitor	Promega, USA
SDS PAGE Tank Buffer (10x) Tris-Glycine SDS	Geneflow, UK
Tris Glycine Electroblotting Buffer (10x)	Geneflow, UK
Tris-Acetate-EDTA (TAE)	Geneflow, UK
Tris-Borate-EDTA (TBE)	Thermo Fisher Scientific, UK
Tween 20	Sigma, UK

Table 2.4 Mass spectrometry reagents

Item	Brand
Iodoacetamide	Sigma, UK
MS-grade Methanol	VWR chemicals, USA
MS-grade Chloroform	VWR chemicals, USA
MS-grade Water	VWR chemicals, USA
HEPES	Sigma, UK
Ethyl acetate	Merck, USA
Acetonitrile	VWR chemicals, USA
Trifluoroacetic acid	VWR chemicals, USA
Formic acid	VWR chemicals, USA
Trypsin Gold	Promega, USA

2.2 Cell biology

2.2.1 Cell culture

The following cell lines were used in this study: U2OS-WT, U2OS-45KO, HeLa S3, Vero-E6, and C6/36. The U2OS-WT and U2OS-45KO cells, an osteosarcoma cell line, were provided by Dario Alessi (University of Dundee, UK). These are wild type U2OS cells, an osteosarcoma cell line of osteoblast origin, and a USP45 KO version generated by CRISPR/Cas9 deletion (Perez-Oliva *et al.*, 2015). Unlabelled and SILAC labelled HeLa-S3 cells, a human cervical cancer cell line, were provided by Ian Prior (University of Liverpool, UK). HeLa and U2OS cells are epithelial cells and both represent cell types in which alphaviruses replicate in infected individuals and are readily used in alphavirus research. Vero-E6 (African Green Monkey Kidney) cells were provided by Alain Kohl (University of Glasgow, UK). This line is a clone of Vero cells which exhibits some contact inhibition. C6/36 (*Aedes albopictus*) cells were provided by Lance Turtle (University of Liverpool, UK). All mammalian cells were cultured in: high glucose (4.5g/L) Dulbecco's modified Eagle's medium (DMEM) supplemented with 10% heat-

inactivated Foetal Calf Serum (FCS), 2 mM Glutamine, 100 IU/ml Penicillin and 100 µg/ml Streptomycin (all Sigma, UK), termed DMEM growth medium. C6/36 cells were cultured in L15 growth medium: L15 media with 10% heat-inactivated FCS, 2 mM Glutamine, 100 IU/ml Penicillin and 100 µg/ml Streptomycin (all Sigma, UK)

For SILAC experiments, Light, Medium or Heavy labelled HeLa cells were used, as detailed in Table 2.5. Labelled HeLa cells were cultured in arginine and lysine free DMEM which was supplemented with 10% heat-inactivated dialysed FCS (both Dundee Cell Products, UK). The supplemented amino acids were added for a final concentration of: 200mg/L L-Proline, 84mg/L L-arginine and 146mg/L L-lysine (all Sigma, UK).

Mammalian cell lines were maintained at 37°C with 5% CO_2. C6/36 cells were maintained at 28°C without CO_2. All cell lines were passaged regularly when they reached 80-100% confluency. Media was removed from the cells before washing once with PBS (Gibco Life Technologies, USA) then cells detached using Trypsin-EDTA (Sigma, UK) at 37°C for 5 mins. The trypsin was neutralised with growth media and the detached cells transferred to fresh flasks/ TC dishes at a ratio of 1:5 or 1:10.

Table 2.5. Labelling strategy for SILAC labelled HeLa S3 cells

	L-Proline	L-Lysine	L-Arginine
Light	Pro 0	Lys 0	Arg 0
Medium	Pro 0	Lys 4	Arg 6
Heavy	Pro 0	Lys 8	Arg 10

Abbreviations: L-Proline (Pro 0), L-Lysine (Lys 0), L-Arginine (Arg 0), L-Lysine-2H4 (Lys 4), L-Arginine-U-13C6 (Arg 6), L-Lysine-U13C6-15N2 (Lys 8), L-Arginine-U13C6-15N4 (Arg 10)

2.2.2 Cell viability assay

Cell viability was monitored using the CellTiter-Glo Luminescent Cell Viability Assay (Promega, USA) as a readout for levels of cellular ATP. Cells

were seeded into opaque-walled, 96-well plates in triplicate and processed according to individual experimental protocols. To quantify ATP, 100 µl CellTiter-Glo (Promega, USA) reagent was added to each well and plates incubated at room temperature for 10 mins followed by orbital shaking for 120 seconds. Luminescence was measured using a Fluostar Omega luminometer (BMG Labtech) with excitation and emission filters 485 nm and 520 nm, respectively.

2.2.3 DUB siRNA knockdown

The USP7 siRNAs used in this study were purchased from Dharmacon and the OTUD6B siRNAs from Qiagen; further details are shown in Table 2.6. The Qiagen All Stars Negative Control (siC, SI03650318) was used as a control. siRNAs were resuspended in DNase/RNase-free H_2O to a final concentration of 20 µM then 10 µl aliquots prepared and stored at -20°C to minimise freeze-thaw deterioration.

Table 2.6. Details of DUB siRNAs used in this study

siRNA	Sequence (5'-3')	Product code
siUSP7#1	AAGCGUCCCUUUAGCAUUA	J-006097-05
siUSP7#3	UAAGGACCCUGCAAAUUAU	J-006097-07
siOTUD6B#1	AGGGTCATTGATAGCAAGTAA	SI00344939
siOTUD6B#2	TTCGGTTACACGGTTGGTAA	SI04172420

To transiently knock-down endogenous USP7 or OTUD6B, HeLa cells were reverse transfected with individual siRNAs at 10 nM in 10 cm dishes. Briefly, a reaction mix of 1350 µl OptiMEM (Thermo Fisher Scientific, UK) with 8 µl RNAiMAX lipofectamine reagent (Invitrogen, Thermo Fisher Scientific, UK) and 4 µl of individual DUB siRNAs or siC was prepared then incubated at room temperature for 20 mins. HeLa cells were harvested and resuspended at $3x10^5$ cells/ml in antibiotic-free DMEM supplemented with 10% heat-inactivated FCS and 2 mM Glutamine. The reaction mix was then

added to $2x10^6$ cells and seeded into 10cm dishes at a final siRNA concentration of 10 nM. Cells with no transfection reagents added were also included as a mock transfection control. Cells were incubated at 37°C, 5% CO_2 for 48 hrs with a further 6ml antibiotic-free growth DMEM supplemented with 10% heat-inactivated FCS and 2 mM Glutamine after 24 hrs. At 48 hrs cells were harvested and re-seeded into 6 well-plates at $1x10^6$ cells/ well and incubated for a further 24 hrs at 37°C, 5% CO_2. Following the 24 hr incubation period (72 hrs post-transfection) cells were counted and infected with SFV at 5 MOI as described in section 2.3.2. Infected cells were harvested at 8 hrs post-infection (p.i.) as described in section 2.2.4 and processed for RNA and protein extraction as described in sections 2.4.1 and 2.5.1.1, respectively.

2.2.4 Harvesting cells for RNA and protein extraction

Cells were harvested for RNA or protein extraction by removing culture media and washing monolayers with ice-cold PBS. Cells were scraped into ice-cold PBS, transferred to 15 ml tubes and pelleted by centrifugation at 600 x g for 3 mins at room temperature. Cell pellets were washed a further three times with ice-cold PBS. For RNA or protein extraction, cell pellets were either processed immediately or stored at -20°C prior to processing. For active-site directed probe experiments (see section 2.6) cell pellets were snap-frozen in liquid nitrogen and stored at -80°C until required.

2.2.5 Immunofluorescence microscopy

For immunofluorescent staining cells were cultured in 8-well Falcon™ chamber slides and infected or treated as appropriate then fixed (4% w/v paraformaldehyde in PBS) (Sigma, UK) for 20 mins at room temperature. For internal staining cells were permeabilised in a 1:1 mixture of methanol: acetone at -20°C for 10 mins then rehydrated in PBS at room temperature for 5 mins. Cells were blocked for 30 mins with either 5% normal goat serum (NGS) or 5% normal donkey serum (NDS) in a humidified atmosphere at 37°C. The primary antibody was then diluted in the blocking buffer (see

Table 2.7) and incubated with the cells in a humidified box at 37°C for 60 mins. The slide was then washed three times with PBS and the secondary Alexa Fluor® 488 conjugated secondary antibody (see Table 2.8) was incubated with the cells at 37°C in a humidified box for 60 mins. After a further three PBS washes, coverslips were mounted using antifade mounting medium with DAPI (Vector Laboratories, USA) and observed with a Nikon Eclipse 80i microscope (Plan Fluor 20x N.A. 0.50, W.D. 2.1mm). Photos were taken with a Hamatsu ORCA 100 Series Digital camera and further analysed using Fiji.

Table 2.7. Primary antibodies used for immunofluorescence microscopy

Target	Species	Source	Code	Incubation conditions
USP45	Sheep	University of Dundee, UK	S109D 3rd bleed	1:100 in 5% NDS
Pan-alphaviruses	Mouse	Virostat, USA	3582-Viro	1:50 in 5% NGS

Table 2.8. Secondary antibodies used for immunofluorescence microscopy

Name	Source	Code	Incubation conditions
Donkey anti-Sheep IgG, Alexa Fluor ® 488	Abcam, UK	ab150177	1:1000 in 5% NDS
Goat anti-Mouse IgG (H+L), Alexa Fluor ® 488	Invitrogen, Thermo Fisher Scientific, UK	A-11001	1:1000 in 5% NGS

2.2.6 Transferrin internalisation assay

For transferrin (Tfn) uptake experiments cells were cultured in 8-well Falcon™ chamber slides to approximately 50% confluency. Cells were serum-starved for 45 mins at 37°C in DMEM (Sigma, UK) with no additions then incubated on ice for 10 mins. Alexa594-conjugated Tfn (Thermo Fisher Scientific, UK) was added at 50 µg/ml in DMEM (Sigma, UK) with no additions and cells incubated on ice for 30 mins. For internalised samples, cells were then transferred to 37°C for 5 mins then returned to ice, washed once with ice-cold PBS. Cells were acid-washed (0.2M Acetic acid, 0.5M NaCl, pH 2.5) on ice for 10 mins to strip surface bound Tfn, then washed a further three times with ice-cold PBS. As a control an acid-stripped only sample, without internalisation at 37°C, was included with cells washed and acid-stripped as above but kept on ice throughout. Cells were fixed (4% w/v paraformaldehyde in PBS) at room temperature for 20 mins then coverslips mounted using antifade mounting medium with DAPI (Vector Laboratories, USA) and observed with a Nikon Eclipse 80i microscope (Plan Fluor 40x N.A. 0.75, W.D. 0.72mm). Photos were taken with a Hamatsu ORCA 100 Series Digital camera and merged and quantified in Fiji. Quantification of microscopy images was performed by measuring the fluorescence for five random microscopic views then calculating the Corrected Total Cell Fluorescence (CTCF) according to the equation: CTCF = Integrated Density – (Area x Mean fluorescence of background). The CTCF was divided by the number of nuclei in that view to give an average for each cell.

2.3 Viruses and virus assays

2.3.1 Virus stocks

SFV4 clone 4 was provided by Dr Sareen Galbraith (Leeds Beckett University, UK) (Liljeström & Garoff, 1991). SFV stocks were produced in Vero-E6 cells by infecting with SFV at 0.01 MOI diluted in high glucose (4.5g/L) DMEM maintenance media: DMEM supplemented with 2.5% heat-inactivated FCS, 2 mM L-Glutamine, 100IU/ml Penicillin and 100 µg/ml

Streptomycin (all Sigma, UK). The virus was allowed to adsorb to the cells for 1 hr before the media was replaced and cells incubated at 37°C with 5% CO_2 for 48 hrs. Supernatant was collected and cleared by centrifuging at 400xg for 3 mins then stored as single use aliquots at -80°C.

The CHIKV strain used was SV0451-96 from Thailand, a human isolate provided by Dr Christopher Logue (Public Health England, UK). This is a pre-A226V mutation strain. All work with CHIKV was carried out in biosafety level 3 (BSL3) facilities at the University of Liverpool. Virus stocks were produced in C6/36 cells by infecting with CHIKV at 1 MOI diluted in L15 maintenance media: L15 supplemented with 2.5% heat-inactivated FCS, 2 mM Glutamine, 100 IU/ml Penicillin and 100 µg/ml Streptomycin (all Sigma, UK). The virus was allowed to adsorb to the cells for 1 hr before the media was replaced and cells incubated at 28°C without CO_2 for 5 days. Supernatant was collected and cleared by centrifuging at 400xg for 3 mins then stored as single use aliquots at -80°C.

The vaccinia virus (VACV) used was the western reserve (WR) strain expressing green fluorescent protein (GFP) (Lautscham *et al.*, 2001). Virus stocks of known titre were provided by Dr. N Blake.

The Respiratory Syncytial Virus (RSV) used was the Human RSV type A2 strain. Virus stocks were provided by Prof. J Schwarze (University of Edinburgh, UK)

2.3.2 SFV and CHIKV infections

For infection of cells with SFV or CHIKV cell monolayers were allowed to reach approximately 90% confluency and on the day of infection cells were counted to allow accurate calculation of MOI. Virus stock was diluted to the appropriate MOI in DMEM maintenance media. The minimum volume of virus inoculum was added to the cells and allowed to adsorb for 1 hr at 37°C, 5% CO_2. The virus inoculum was removed and fresh media added after 1 hr. Cells were returned to 37°C, 5% CO_2 for the time indicated for each experiment. For all experiments a mock infected control was included with the DMEM maintenance media only without virus.

2.3.3 Virus plaque assays

Virus plaque assays were used to quantify virus titre in Vero-E6 cells and monitor the ability of the virus to infect U2OS-WT and -45KO populations following SFV, CHIKV and VACV infection. Monolayers of cells were infected with a 10-fold serial dilution of virus in DMEM maintenance media. The virus was allowed to adsorb to the cells for 1 hr at 37°C before the media was removed and overlaid with a 1% (w/v) low melting point agarose in DMEM supplemented with 5% heat-inactivated FCS, 2mM Glutamine, 100IU/ml Penicillin and 100µg/ml Streptomycin (all Sigma, UK). Plaques were allowed to form at 37°C for 72 hrs or 48 hrs for SFV/ CHIKV and VACV, respectively. Cells were fixed with 10% neutral buffered formalin (Sigma, UK), overlay removed and cells stained with 2.3% crystal violet solution (Sigma, UK). Once dry, plaques were counted and plaque forming units per ml (pfu/ml) calculated using the formula:

$$\text{pfu/ml} = \frac{\text{no. of plaques}}{\text{dilution factor x volume of virus added}}$$

2.3.4 RSV syncytia formation assay

RSV syncytia formation assays to monitor the number of infected U2OS-WT and -45KO cells were carried out by Shadia Khandaker (University of Liverpool, UK). Monolayers of cells were infected with a 2-fold serial dilution of RSV in serum free DMEM growth media (all Sigma, UK) and the virus was allowed to adsorb to the cells for 2 hrs at 37°C. After 2 hrs media was replaced and cells incubated at 37°C for 16 hrs. Cells were washed once with PBS and fixed with methanol containing 2% hydrogen peroxide then washed once with PBS. To visualise plaques cells were incubated with biotinylated anti-RSV antibody (AbD Serotec, UK) diluted 1:200 in PBS and incubated at room temperature for 1 hr. Cells were washed twice with PBS then extravidin peroxidase (Sigma, UK) diluted 1:500 in PBS added and incubated for 30 mins at room temperature then washed twice with PBS. A 3-Amino-9-ethylcarbazole (AEC) stain (Sigma, UK) was prepared according to manufacturer's instructions, added to cells and

incubated at room temperature for 20 mins to stain the plaques. To terminate the reaction the AEC stain was removed and cells washed twice with PBS then plaques observed by light microscopy under a CETI microscope (Plan PH 20x N.A. 0.40, W.D. 1.2 mm) and photos taken. Images representing four fields of view were taken, syncytia counted and the average calculated.

2.3.4 Endosome bypass assay

U2OS-WT and -45KO cells were cultured in 8-well Falcon™chamber slides and pre-cooled on ice for 10 mins. Cells were infected with CHIKV at 10 MOI in DMEM maintenance media on ice for 1 hr to allow virus to adsorb to the cell surface. Cells were washed once with PBS pH7.2 then incubated for 10 mins in either PBS pH 7.2 or pH 5.5 at 37°C followed by another wash with PBS pH7.2. Fresh maintenance media was then added and cells incubated at 37°C. Cells were then fixed after 24 hrs (4% w/v paraformaldehyde in PBS) at room temperature for 20 mins. Cells were stained for pan-alphavirus antibodies as described in section 2.2.5. Coverslips were mounted using antifade mounting medium with DAPI (Vector Laboratories, USA) and observed with a Nikon Eclipse 80i microscope (Plan Fluor 20x N.A. 0.50, W.D. 2.1 mm). Photos of 10 fields of view for both DAPI and virus staining in each condition were taken with a Hamatsu ORCA 100 Series Digital camera. The DAPI and virus staining images were merged in Fiji and the percentage of infected cells calculated.

2.4 Molecular biology

2.4.1 RNA extraction and quantification

Cell pellets were lysed and total RNA extracted using the Qiagen RNeasy plus kit according to the manufacturer's instructions (Qiagen, Germany). To remove any potential genomic DNA contamination, an on-column gDNA digest was also included by addition of 27 Kunitz units of RNase-free DNase (Qiagen, Germany) and incubation at room temperature for 15 mins. RNA quantification was performed using the NanoDrop ND-100 Spectrophotometer (Thermo Fisher Scientific, UK). The optical density at

230, 260 and 280 nm was measured to monitor RNA quality. The 260/ 280 ratio was used to asses RNA purity and protein contamination. The 260/ 230 ratio was used to monitor potential contamination with salts or solvents. For both, a ratio between 1.8 and 2.0 was considered satisfactory, with lower ratios being indicative of contamination. Analysis of RNA integrity was further analysed by agarose gel electrophoresis and visualised by staining with ethidium bromide. Briefly, a 1.5% agarose gel made with 0.5 x TBE buffer was made to analyse 1.0 µg RNA. RNA was resolved by gel electrophoresis and stained with Ethidium Bromide (Sigma, UK). The RNA integrity was judged by the quality of the bands, with two distinct bands representing 18S and 28S RNA being indicative of good quality RNA without degradation. RNA samples were stored at -80°C until required.

2.4.2 Reverse transcription

RNA was converted to cDNA using Oligo(dT) primers to allow investigation of all cellular transcripts as well as viral genome RNA. For reverse transcription 1.0 µg RNA was incubated with 0.5 µg of Oligo(dT) 15 (Promega, USA) at 70°C for 5 mins then chilled on ice. Next, 8 µl of mastermix (1mM dNTP (Promega, USA), 20units of RNasin (Promega, USA) and 4 µl 5X reverse transcription buffer (Thermo Fisher Scientific, UK)) was added and reaction tubes were incubated at 37°C for 5 mins. For reverse transcription 200 U M-MuLV reverse transcriptase (Thermo Fisher Scientific, UK) was added to make the final volume 20µl then incubated at 42°C for 1 hr. The reaction was terminated at 70°C for 10 mins. RT- samples were prepared simultaneously in the absence of reverse transcriptase as a control for genomic DNA contamination. Final cDNA was diluted 1:5 with nuclease free ddH_2O (Thermo Fisher Scientific, UK) and stored at -20°C.

2.4.3 Endpoint PCR

Endpoint PCR with cDNA was carried out using 2x PCR Reddy Mix (Thermo Fisher Scientific, UK) and specific primer pairs (see Table 2.9) at a concentration of 750nM in a final volume of 20 µl. A three-step process was used as follows: 95°C/ 5 mins; [95°C/ 30 secs, 55°C/ 30 secs, 72°C/ 30 secs]

x35; 72°C/ 10 mins. PCR products were resolved on a 2% agarose (Thermo Fisher Scientific, UK) gel made using 0.5 x TAE (Geneflow, UK) buffer and stained with Ethidium Bromide (Sigma, UK).

2.4.4 qPCR

For qPCR the cDNA was amplified using specific primer pairs (see Table 2.9) at a concentration of 200 nM in a final volume of 12 µl. Prior to setting up qPCR, cDNA was diluted with nuclease free ddH_2O (Thermo Fisher Scientific, UK) 1:4 for detection of host genes or 1:10^{-4} for detection of viral genomes. Gene expression was analysed by incorporation of the BioRad iTaq Universal SYBR Green Supermix (BioRad, USA) into the PCR product. Each reaction contained 4 µl of diluted cDNA. A two-step process was used as follows: 94°C/ 3 mins; [94°C/ 15 secs, 55°C/ 30 secs] x40. For quantification of gene expression the comparative Ct method was used to calculate the fold change ($2^{-\Delta\Delta Ct}$) using 18S to normalise the data, as described by Schmittgen and Livak (Schmittgen & Livak, 2008). Melt curves were monitored for the presence of primer dimers or secondary products by looking for additional peaks.

Table 2.9. PCR primer sequences used in this project

Target		Sequence (5'-3')	Reference
SFV	For	CGCATCACCTTCTTTTGTG	(Fragkoudis *et al.*, 2007)
	Rev	CCAGACCACCCGAGATTTT	
CHIKV	For	TCGACGCGCCCTCTTTAA	(Edwards *et al.*, 2007)
	Rev	ATCGAATGCACCGCACACT	
18S	For	GGATGCGTGCATTTATCAGA	(Chan *et al.*, 2005)
	Rev	GTTGATAGGGCAGACGTTCG	
USP45	For	GCGGGTGAAAGATCCAACTAA	Designed during this project
	Rev	TCCAAGTCCACAGAGCCCAGG	
USP7	For	ATGGCCTGGAGTGAAGTGACC	(Darling, 2017)
	Rev	CGGTTGGCATCATGTACACAGC	
OTUD6B	For	GAGCTTGATGAGGAAGAGCAG	(Xu *et al.*, 2011)
	Rev	GTCATTCTTGGGAACAGCATTC	

2.4.5 Sequencing

A PCR product for USP45 was amplified with 2x PCR Reddy Mix (Thermo Fisher Scientific, UK) and specific primer pairs at a final concentration of 10 µM in a final volume of 50 µl. A three-step process was used as follows: 95°C/ 5 mins; [95°C/ 30 secs, 55°C/ 30 secs, 72°C/ 30 secs] x35; 72°C/ 10 mins. The PCR product was then purified using the QIAquick PCR purification kit (Qiagen, Germany) according to manufacturer's instructions then DNA was quantified by measuring the optical density at 230, 260 and 280 nm using the NanoDrop ND-100 Spectrophotometer. 10% of the purified PCR elute was resolved on a 2% agarose (Thermo Fisher Scientific, UK) gel made using 0.5x TAE (Geneflow, UK) buffer and stained with Ethidium Bromide (Sigma, UK). Sanger Sequencing of both the forward and reverse strand was carried out by SourceBioscience with either the forward primer 5'-GAGAAAGCCAAAAGAAGTAAAAGG-3' or reverse primer 5'-TCCAAGTCCACAGAGCCCAGG-3'. Purified PCR products were sent at 2.96 ng/µl and primers at 3.2 pmol/µl.

2.5 Protein biochemistry

2.5.1 Protein extraction

2.5.1.1 Laemmli lysis

Cells were harvested as described in section 2.2.4. Depending on cell number, pellets were lysed in 50 – 200 µl 1x Laemmli buffer (50 mM Tris-Base (pH6.8), 2% SDS, 10% glycerol – without BPB and DTT) then boiled at 95°C for 10 mins. Lysates were cleared by centrifugation for 10 mins at 13,226 x g and soluble protein extracts stored at -20°C.

2.5.1.2 Non-denaturing homogenisation

For lysates to be used for active site-directed ubiquitin-based probes, cells were harvested as described in section 2.2.4. Cell pellets were resuspended in 100 – 400 µl (depending on cell number) of ice-cold K-buffer

(50 mM Tris-base pH 7.5, 5 mM $MgCl_2$, 250 mM sucrose, 1 mM DTT, 2 mM ATP). Homogenisation was performed by progressively passing the sample through 23G, 26G and 30G needles. Phosphatase inhibitors (PhosStop, Roche) were then added to each sample to give a final concentration of 1X. Lysates were cleared by centrifugation at 4°C for 20 mins at 13,226 x g. Aliquots of lysate were then snap-frozen in liquid nitrogen and stored at -80°C.

2.5.2 Protein quantification

Protein quantification was determined using the microplate procedure of the Pierce, UK BCA Protein Assay Kit (Thermo Fisher Scientific, UK) according to the manufacturer's instructions. Briefly, Calf serum albumin (BSA) diluted in 1x Laemmli buffer (without BPB or DTT) was used to generate a set of standards from 2000 µg/ml to 25 µg/ml and samples were diluted 1:10 with 1x Laemmli buffer. 25 µl of each standard (including blank wells of 1x Laemmli buffer only) and sample were added to duplicate wells in a 96-well plate. 200 µl BCA working reagent (50:1 ratio of reagent A: reagent B) was added to each well and the plate incubated at 37°C for 30 mins. Absorbance was measured at 562 nm using a MultiSkan Plate Reader (Thermo Fisher Scientific, UK). The blank measurement was subtracted from all readings and a standard curve created to provide the concentration of the samples.

2.5.3 SDS-PAGE

From whole cell lysate, 20 µg protein (unless otherwise stated) was made up to the same volume with 1x Laemmli buffer (50 mM Tris-Base pH6.8, 2% SDS, 10% glycerol) then supplemented with 1% bromophenol blue and 100 mM DTT. The protein extract was run through a 4% stacking gel and resolved in a 10% SDS-PAGE gel alongside the colour prestained protein standard (11 – 245 kDa) (New England Biolabs). Gels were run in SDS-PAGE running buffer (25 mM Tris Base, 192 mM glycine, 0.1% w/v SDS) (Geneflow, UK) for approximately 90 mins at 100V using the BioRad Mini-PROTEAN 3 System (BioRad, USA).

Non-denatured cell lysate from active site-directed ubiquitin-based probe assays was supplemented with the appropriate volume of 5x sample buffer (15% w/v SDS, 312.5 mM Tris-HCl (pH 6.8), 50% w/v glycerol, 16% β-mercaptoethanol, 1% bromophenol blue) to give a final concentration of 1x following DUB activity assays. 15 µg protein (unless otherwise stated) was loaded onto NuPAGE® Novex™ Bis-Tris 4-12% gradient gels (Invitrogen, Thermo Fisher Scientific, UK) alongside Amersham ECL Rainbow Molecular Weight Marker (GE Healthcare Life Sciences). Gels were run in NuPAGE® MOPS (3-(N-morpholino)propanesulfonic acid) SDS Running Buffer (50 mM MOPS, 50 mM Tris Base, 0.1% SDS, 1 mM EDTA, pH 7.7) for approximately 45 mins at 165V using the Bolt® Mini Gel system (all Thermo Fisher Scientific, UK).

2.5.4 Immunoblotting

The BioRad Mini Trans-Blot System (BioRad, USA) was used to transfer the protein to Amersham Protran Premium nitrocellulose 0.45NC filters (GE Healthcare Life Sciences). Proteins were transferred in Tris-Glycine Electro-Blotting Buffer (20 mM Tris Base, 150 mM glycine) (Geneflow, UK) supplemented with 20% methanol (Fisher Scientific) for 2 hrs at 250 mAmp. Proteins were stained with Ponceau-S (Sigma, UK Aldrich) to monitor loading and transfer efficiency. Filters were blocked for 2 hrs in 5% skimmed milk in PBS-T (PBS supplemented with 0.05% Tween-20). Primary antibodies were diluted in the blocking buffer (see Table 2.10 for details) and incubated with the filters either at 4°C overnight or at room temperature for 1-2 hrs with continuous rocking. Secondary antibodies, either conjugated to horseradish peroxidase (HRP) or immunofluorescent dyes, were diluted in the blocking buffer (see Table 2.11 for details). Filters were incubated with secondary antibodies for 1 hr at room temperature with continuous rocking then washed three times with PBS-T.

Proteins labelled with HRP-conjugated secondary antibodies were visualised with HRP substrate according to manufacturer's instructions (Pierce, UK™ ECL Western Blotting Substrate, Thermo Fisher Scientific, UK). For proteins labelled with immunofluorescent secondary antibodies,

filters were washed another two times with PBS then visualised on a LI-COR Odyssey® 2.1 scanning system.

Table 2.10. Primary antibodies

Target	Company	Catalogue number	Species	Dilution
ACTB	Abcam, UK	ab6276	Mouse	1:10,000
ACTB	Abcam, UK	ab8266	Rabbit	1:1000
HA	Biolegend, USA	901501	Mouse	1:1000
SFV-nsP1	Johan Peränen (University of Helsinki)	n/a	Rabbit	1:2000
SFV-nsP2 2C7	Johan Peränen (University of Helsinki)	n/a	Mouse	1:2000
SFV-nsP3	Johan Peränen (University of Helsinki)	n/a	Rabbit	1:2000
SFV-capsid	Johan Peränen (University of Helsinki)	n/a	Rabbit	1:2000
CHIKV-nsP1	Andres Merits (University of Tartu)	n/a	Rabbit	1:2000
CHIKV-nsP2	Andres Merits (University of Tartu)	n/a	Rabbit	1:2000

CHIKV-nsP3	Andres Merits (University of Tartu)	n/a	Rabbit	1:2000
USP7	Abcam, UK	Ab4080	Rabbit	1:1000
USP15	Abnova. Taiwan	H00009958-M01	Mouse	1:1000
OTUD6B	Proteintech, USA	25430-1-AP	Rabbit	1:1000

Table 2.11. Secondary antibodies

Name	Detection method	Source	Dilution
IRDye® 800CW Donkey anti-Mouse IgG (H + L)	Immunofluorescence	Licor, USA 926-32212	1:15,000
IRDye® 800CW Donkey anti-Rabbit IgG (H + L)	Immunofluorescence	Licor, USA 926-32213	1:15,000
IRDye® 680LT Donkey anti-Rabbit IgG (H + L)	Immunofluorescence	Licor, USA 926-68023	1:15,000
Goat anti-mouse IgG-HRP	Chemiluminescence	Santa Cruz, USA sc-2005	1:5,000
Goat anti-rabbit IgG-HRP	Chemiluminescence	Santa Cruz, USA sc-2004	1:5,000

2.6 Active-site directed probe assays

2.6.1 For analysis by SDS-PAGE

Snap-frozen cell lysates were thawed on ice and adjusted to 1 mg/ml with ice-cold K-buffer. Cell lysate was incubated with HA-Ub-VME (UbiQ-035) or HA-Ub-PA (UbiQ-078) at the ratio and time indicated for each individual experiment at 37°C with shaking at 300rpm. For each experiment a negative control was included with 1 µl 50 mM Tris-base (pH 7.5) added in place of the probe. Reactions were terminated with 5x sample buffer (15% SDS, 312.5 mM Tris-HCl pH 6.8, 50% glycerol, 16% β-ME, 5% BPB) then boiling at 95°C for 5 mins.

2.6.2 For analysis by mass spectrometry

Snap-frozen cell lysates (as described in Section 2.5.1.2) were thawed on ice and 500 µg diluted to 250 µl with ice-cold K-buffer. 5 µg HA-Ub-PA (UbiQ-078) was added and samples incubated at 37°C for 45 mins with shaking at 37°C. Reactions were terminated by adding SDS to a final concentration of 0.4% (v/v) and incubating at room temperature for 20 mins before proceeding with immunoprecipitation as described in section 2.7.

2.7 Immunoprecipitation to enrich for ABP bound proteins

500 µg of non-denatured cell lysate was incubated with the activity-based probe and terminated with SDS to a final concentration of 0.4% as described in section 2.6.2. Ice-cold NET buffer (50 mM Tris pH 7.5, 5 mM EDTA, 150 mM NaCl, 0.5% NP-40) was added to dilute SDS concentration to 0.1%. 40 µg Protein G Sepharose® beads (Sigma, UK) per sample and 140 µg anti-HA-Agarose beads (Sigma, UK) were prepared separately by washing three times with ice-cold NET buffer with centrifugation at 4°C for 1 min at 9,000 x g all centrifugation steps utilise these conditions unless otherwise stated). Following washes the beads were diluted with ice-cold NET buffer to make a 50% slurry. Equal amounts of 50% Protein G

Sepharose® bead slurry (~40 µg) were added to each sample and incubated at 4°C for 30 mins with vertical rotation at 15 rpm. Beads were pelleted and pre-cleared supernatant transferred to new tubes then equal amounts of 50% anti-HA-Agarose bead slurry (~140 µg) was added to each pre-cleared sample and incubated at 4°C for 16 hrs with vertical rotation at 15rpm. Beads were pelleted and the unbound fraction removed then washed three times with ice-cold NET buffer as above and supernatant removed. Beads were then washed once with ice-cold wash buffer (10 mM Tris pH 7.5, 2 mM $MgCl_2$) before eluting bound protein. Elution buffer (1% SDS, 1% β-ME, 0.1M Tris-HCl pH 6.8) equal to 2x volume of beads was added and beads boiled at 95°C for 5 mins with regular vortexing. Beads were pelleted at 16,000 x g for 1 min and supernatant containing eluted proteins transferred to a fresh tube for further processing. Samples were taken from the supernatant at the following stages of the IP: input, pre-clear, flow-through, each of the 4 HA-bead washes and elution. Beads were also stripped following elution by adding 2x sample buffer (6% SDS, 12 5mM Tris-HCl pH 6.8, 20% glycerol, 6.4% β-ME 2% BPB), boiling at 95°C for 5 mins with regular vortexing. Beads were pelleted as above and a sample of supernatant kept allowing analysis of efficiency of elution. These samples were then kept for quality control analysis by immunoblotting for HA.

2.8 Mass spectrometry

2.8.1 In-solution digest and preparing samples for mass spectrometry

Eluted protein from the immunoprecipitation from the SILAC triplet lysate incubated with HA-Ub-PA probe (described in section 2.7) was mixed at a 1:1:1 ratio. The mixture of SILAC triplets were then made up to 1ml total volume with elution buffer (1% SDS, 1% β-ME, 0.1 M Tris-HCl pH 6.8). Samples were reduced with 5mM DTT at 60°C for 25 mins then alkylated with 20 mM iodoacetamide for 30 mins at room temperature in the dark. Alkylation was terminated by bringing the final DTT concentration to 10mM and incubating for a further 5 mins at room temperature in the dark. Samples

were concentrated on Amicon® Ultra-4 10K Centrifugal Filter Units for 30 mins at 1,800 x g at 4°C then transferred back to Eppendorf tubes.

Methanol-chloroform precipitation of proteins was carried out by addition of 400 µl MS-grade methanol, then addition of 100 µl MS-grade chloroform before addition of 300 µl MS-grade water. Samples were centrifuged at 16,000 x g for 10 mins at 4°C to allow formation of the interphase and the upper aqueous layer was removed. 500 µl MS-grade methanol was added, protein pelleted at 16,000 x g for 10 mins at 4°C and supernatant removed. The methanol wash was repeated three times then samples dried by evaporation in a Speedvac. The protein pellet was resuspended in 50 µl 50 mM HEPES pH 8 then 500 ng trypsin gold added and incubated at 37°C for 16 hrs to digest protein.

Following protein digestion triton was removed by ethyl acetate extraction by addition of 1 ml water-saturated ethyl acetate (1:10, H_2O: ethyl acetate), mixing thoroughly then centrifuging at 16,000 x g for 5 mins at room temperature. The ethyl acetate layer was removed and the extraction step was repeated another two times. Residual ethyl acetate was evaporated at 60°C before samples were dried completely by evaporation in a Speedvac. Peptide pellets were resuspended in 200 µl equilibration buffer (5% acetonitrile, 0.5% trifluoroacetic acid).

C-18 Spin Columns (Pierce, UK) were prepared by washing twice with 50% acetonitrile then twice with equilibration buffer (all centrifugation steps at 1,466 x g for 1 min at room temperature). Peptides were bound to the column and flow-through re-loaded three times. The column was then washed three times with equilibration buffer before samples were eluted in 50 µl 50% acetonitrile.

Samples were either stored at -20°C after elution in 50% acetonitrile or dried completely by evaporation in a Speedvac.

For samples analysed by Warwick Scientific Services (University of Warwick, UK) (see section 2.8.2) peptides were stored at -20°C after elution

in 50% acetonitrile. For samples to be analysed in Liverpool, peptides were dried completely by evaporation in a Speedvac.

2.8.2 Mass Spectrometry

Peptides were analysed by LC-MS/MS either in-house at the University of Liverpool or by Warwick Scientific Services (University of Warwick, UK).

For samples to be analysed in Liverpool, pellets of peptides (as described in section 2.8.1) were resuspended in 5 µl 5% formic acid and sonicated for 5 mins. Samples were diluted to 1% formic acid with 20 µl MS-grade-water and sonicated for a further 5 mins. Debris was pelleted at 16,000 x g for 10 mins at 4°C then 17 µl of supernatant transferred to clear glass Qsert vials (Waters, USA) and analysed immediately. Peptides in 1% formic acid were separated using a nanoACQUITY UPLC system (Waters, USA), coupled to an LTQ Orbitrap XL mass spectrometer (Thermo Fisher Scientific, UK) with a Proxeon nano-electrospreay source. Next, 4 µl of the digest was injected into a 180 µm x 20 mm, 5 µm BEH-C18 symmetry trapping column (Waters, USA) at 15 µl/ min. Samples were resolved on a 25 cm x 75 µm BEH-C18 column (Waters, USA), in an acetonitrile gradient in 0.1% formic acid, with a flow rate of 400 nl/ min. Full scan MS spectra (m/z 300-2000) were generated at 30,000 resolution and the top five most intense ions were fragmented and subjected to MS/MS in the linear quadrapole ion trap (collision energy 35%, 30 ms). All spectra were acquired using Xcalibur software (version 2.0.7; Thermo Fisher Scientific, UK) prior to in-depth analysis of RAW files for peptide identification as described in section 2.9.1.

For samples to be analysed by Warwick Scientific Services (University of Warwick, UK), eluted peptides in 50% acetonitrile were sent on dry ice for analysis by LC-MS/MS spectrometry. Here, samples were loaded onto an Acclaim PepMam µ-precolumn cartridge 300µm i.d. x 5 mm, 5 µm, 100 Å (Thermo Fisher Scientific, UK) in 2% aqueous acetonitrile containing 0.1% trifluoroacetic acid for 8 mins at 10 µl min^{-1}. Next they were loaded onto an Acclaim PepMap RSLC 75 µm i.d. x 25 cm, 2 µm, 100 Å (Thermo Fisher

Scientific, UK) at 300 nL min^{-1}. Peptides were analysed using an Orbitrap Fusion instrument (Thermo Fisher Scientific, UK) with survey scans (m/z 375-1500) generated at 120,000 resolution. MS/MS was performed using the quadrupole, HCD fragmentation (normalised collision energy of 33, max. injection times 200 ms) and rapid scan MS analysis in the ion trap. RAW files were returned and analysed for peptide identification as described in section 2.9.1.

2.9 Bioinformatics and statistical analysis

2.9.1 MaxQuant analysis

RAW files from LC-MS/MS were analysed using MaxQuant version 1.5.3.8 (Http://www.maxquant.org) with all datasets for SILAC experiments processed simultaneously. Peptides were identified using the UniProtKB/Swiss-Prot *H. sapiens* proteome (up000005640) with one unique peptide being required for protein identification. The minimum peptide length was set to 7 and the maximum peptide mass was set to 4600 Da. The minimum and maximum peptide for unspecific search was set to 8 and 25, respectively.

2.9.2 Statistical analysis

Statistical analyses were performed using GraphPad Prism 5 for all experiments carried out for least three biological repeats. All error bars represent standard deviation. When comparing the means of two populations a paired two-tailed t-test was used. For comparing the means of more than two populations a one-way ANOVA analysis coupled with a Dunnett's multiple comparison test was used.

Chapter 3: Characterising the role of the deubiquitylase USP45 in alphavirus infection

3.1 Introduction

One method of identifying host factors involved in virus infection which could make promising drug targets is through loss-of function screens, either targeting the entire genome or specific pathways (Hirsch, 2010; Perwitasari *et al.*, 2013). A commonly used technique is to knockdown genes through RNA interference (RNAi) then monitor the effect on cells after virus infection using a suitable assay (Cherry, 2009). RNAi experiments allow for silencing of a target gene by inducing degradation of mRNA through the introduction of small double-stranded interfering RNAs (siRNAs) (Elbashir *et al.*, 2001). The siRNA is designed to be complimentary to the target mRNA. Upon introduction to the cell, the siRNA is incorporated into the RNA-inducing silencing complex (RISC) and is separated into single-stranded siRNAs. The passenger strand undergoes degradation while the guide strand remains associated with the RISC complex and binds to complementary mRNA when it is encountered in the cell. When the target mRNA has been located, Argonaute 2 (Ago2) of the RISC complex, induces cleavage of the mRNA molecule. The cell then recognises the cleaved mRNA as abnormal, thereby resulting in its degradation. Turnover of the existing protein in the absence of new synthesis depletes the cellular levels of the protein. As such, RNAi has proven to be a valuable tool in scientific research due its ease of use and applicability to most mammalian cell types (Fire *et al.*, 1998; Hamilton & Baulcombe, 1999; Wilson & Doudna, 2013).

Several large-scale siRNA screens have identified genes which are involved in alphavirus infection. For example, a genome wide siRNA screen identified the host proteins TSPAN9 and FUZ as important for alphavirus entry (Ooi *et al.*, 2013). Another screen covering the entire genome identified 156 pro-viral and 41 anti-viral host factors involved in CHIKV infection. These data were then used to identify fatty acid synthesis as essential to

CHIKV and subsequently demonstrated the anti-viral activity of drugs targeting this pathway (Karlas *et al.*, 2016). Furthermore, pathway specific siRNA screens have identified host factors involved in alphavirus infection which may be overlooked in larger screens. For example, an siRNA screen against 140 genes known to be involved in trafficking was used to identify Rac1, PIP5K1-α and Arp3 as essential for alphavirus infection. These were shown to be involved in intracellular actin cytoskeleton remodelling and were suggested to be potential alphavirus therapy targets (Radoshitzky *et al.*, 2016). Pathway specific siRNA screens have also been used in the context of the ubiquitin system to identify DUBs as potential drug targets for several viruses. For example, a screen which utilised a DUB siRNA library identified the DUB, STAM-binding protein-like 1 (STAMBPL1), as a key regulator of HTLV-1 mediated pathogenesis (Lavorgna & Harhaj, 2012). However, this approach has yet to be extended to alphaviruses.

Although there are many examples of DUBs playing important roles during virus infection, as described above and in section 1.5, little is known about the role DUBs may play in alphavirus infection. Therefore, a study previously carried out in our lab sought to utilise a DUB siRNA library to identify DUBs which may be involved in virus infection (Coombes *et al.*, 2019, unpublished). Briefly, an siRNA library targeting 92 DUBs was used to knockdown expression in HeLa cells and identify potential pro- and anti-viral DUBs in relation to alphaviruses. Using the model alphavirus, SFV, it was possible to identify DUBs which were potentially pro- or anti-viral using cell viability as a readout. The results from this screen are displayed in Figure 3.1A as percentage change in cell viability ratio of infected versus uninfected cells relative to the mean of the data. DUBs, which when knocked down resulted in an increase in cell viability ratio following SFV infection, were considered to represent a decrease in SFV replication and therefore predicted to be pro-viral. Similarly, DUBs which when knocked down resulted in a decrease in cell viability ratio were anticipated to be anti-viral DUBs due to an increase in virus replication following their depletion. For the identification of potential drug targets, it is initially the pro-viral DUBs which are of most interest. One of the top ten hits from the screen for potential pro-

viral DUBs was USP45, which displayed a mean increase in cell viability ratio of 63% compared to uninfected cells. Deconvolution assays were performed by repeating the original cell viability assay with each of the four individual siRNAs separately (Coombes *et al.*, 2019, unpublished) (Figure 3.1B). Two individual siRNAs (3 and 4) replicated the initial finding with increases in cell viability of 50% and 47% respectively. USP45 therefore satisfied the criteria for a positive hit with a change in cell viability of 30% or more in the original screen which was replicated by at least two individual siRNAs following deconvolution.

USP45 is a member of the USP family of DUBs and is a poorly characterised DUB, yet is highly conserved between *H. sapiens, D. reiro, D. melanogaster* and *S. pombe* (Clague *et al*., 2013). The USP45 protein is 814 amino acids in length and contains a zinc finger-ubiquitin binding (Znf-UBP) domain within the N-terminus followed by the catalytic (USP) domain (Figure 3.2A). The catalytic domain, unusually, contains a serine as the third catalytic residue rather than aspartate or asparagine. The biochemical role of this serine reside has not been investigated however this is a characteristic shared by the DUBs USP16 and USP30 which have been reported to retain enzymatic activity (Nijman *et al.*, 2005; Zhang *et al.*, 2011*b*). USP45 is therefore predicted to be an enzymatically active DUB. Prior to commencement of this thesis there was only one study which had investigated a mechanistic role for USP45 in detail (Perez-Oliva *et al*., 2015). Perez-Oliva *et al* selected USP45 for investigation on the basis of cancer genome analyses showing that 12% of prostate cancers and 5% of diffuse large B-cell lymphomas have deletions within the USP45 gene (http://www.cbioportal.org). For their investigations they developed a diploid USP45 knock-out in U2OS cells using CRISPR/Cas9. They went on to demonstrate that cells lacking USP45 displayed hypersensitivity to UV irradiation and were less capable of repairing DNA damage. The mechanism by which USP45 promoted DNA repair was through interacting with and deubiquitylating the DNA repair endonuclease subunit, ERCC1 (Perez-Oliva *et al*., 2015). Taken together, as a poorly characterised DUB, with no known

role in the context of virus infection, USP45 warranted further investigation as a novel pro-viral DUB.

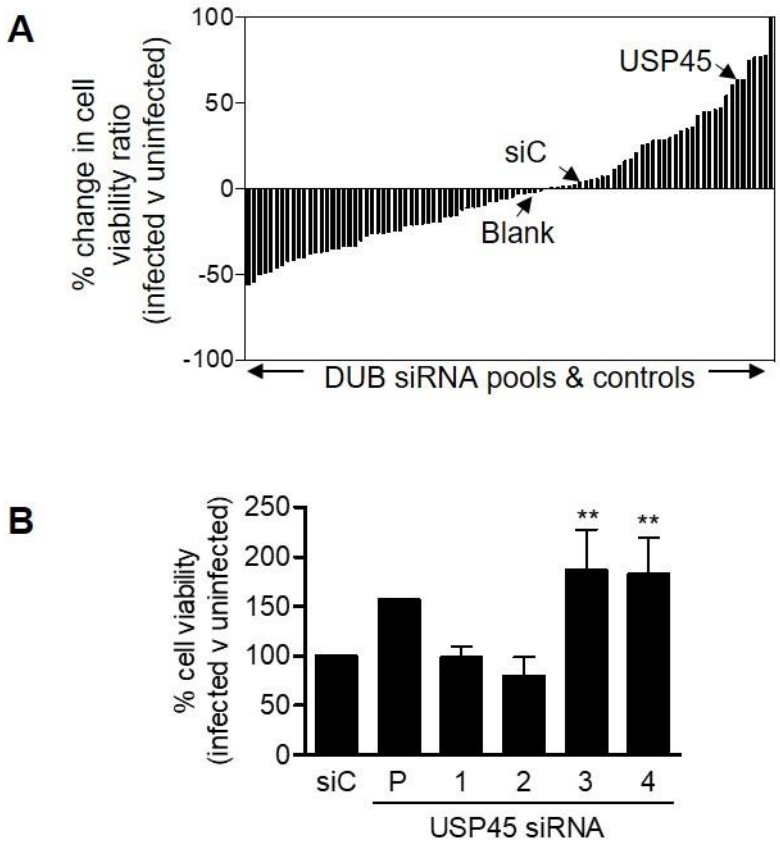

Figure 3.1. Knockdown of USP45 results in an increase in cell viability following SFV infection

(**A**) An siRNA library of pools of 4 siRNAs targeting 92 human DUBs identified DUBs which when knocked down resulted in a decrease (anti-viral) or increase (pro-viral) in cell viability following SFV infection. The mean data from two independent screens are presented as the percentage change in cell viability ratio (infected v uninfected) relative to the mean of the data (**B**) The pool of USP45 siRNAs was deconvoluted by repeating the cell viability assay following knockdown with individual siRNAs. Data are presented as the percentage cell viability of infected v uninfected, relative to siC which was set to 100%. Data represents three independent experiments with the exception of the pool for USP45 which is presented as the mean of two (± SD). Data were analysed against siC by one-way ANOVA with Dunnett's post-hoc test (** = $p \leq 0.01$). Data provided by Dr. N Blake

3.2 Aims

This preliminary data suggested that USP45 was required for efficient SFV infection. As described, this data was generated by utilising siRNA to deplete USP45 from target cells prior to infection with SFV. The availability of the U2OS USP45 knockout and corresponding wild type cell line (U2OS-45KO and U2OS-WT (Perez-Oliva *et al.*, 2015), both kindly provided by Prof D. Alessi, University of Dundee) allowed for the opportunity to further explore the role of USP45 during alphavirus infection. The aims of this chapter were two-fold:

1. To first validate the role of USP45 during alphavirus infection using a USP45 knockout cell line.
2. Then to investigate at which stage(s) during the alphavirus lifecycle USP45 plays a critical role, using both SFV and extending to the pathogenic CHIKV.

3.3 Genotypic and phenotypic analysis of the U2OS45KO cell line

Before investigating the role of USP45 during alphavirus infection, it was important to confirm the genotype and phenotype of the WT and 45KO lines. These cells were developed using CRISPR/Cas9 technology to generate a diploid USP45 knock-out in U2OS cells by Perez-Oliva *et al* (Perez-Oliva *et al.*, 2015). A guide RNA (gRNA) was designed to target the end of exon 2, the first coding exon, of USP45 to deplete protein expression. For their study the genotyping strategy utilised was selection of clones resistant to digestion by the restriction enzyme Hpy1881 (Perez-Oliva *et al.*, 2015). To confirm the genotype of the cell clone that was supplied for our study, RNA was extracted from both WT and 45KO cells and reverse transcribed to cDNA. PCR primers were designed to amplify across the relevant region of USP45 and the resulting PCR product was purified and sequenced using Sanger sequencing, performed by SourceBioscience (Figure 3.2B). Analysis was repeated for three separate PCR amplifications

to ensure any observed changes were not due to introduction of a random mutation during the PCR by Taq polymerase. The reverse strand was also sequenced once to ensure the same was seen on the opposite strand. The same mutation was observed each time, a single thymine deletion at the end of exon 2 in 45KO cells, which results in a frame-shift mutation and a premature stop codon. When comparing the sequence generated for the 45KO line here with the genotyping strategy described by Perez-Oliva *et al*, it was noted that a different mutation was observed (Perez-Oliva *et al.*, 2015). The 45KO clone used by Perez-Oliva *et al* was selected based on the absence of an Hpy188I restriction site to indicate USP45 ablation. This restriction site is still present in the clone used for the work described in this thesis indicating that a different clone is being used (Figure 3.2C).

Whilst the sequencing data indicated the presence of the mutation that would lead to production of a truncated protein or nonsense-mediated decay, given the different mutation found it was important to confirm the lack of USP45 protein. Several commercially available USP45 antibodies were tested by immunoblot but these did not detect endogenous USP45. However the S109D anti-USP45 antibody described by Perez-Oliva *et al* has been demonstrated to detect endogenous USP45 by immunofluorescence (Perez-Oliva *et al.*, 2015). Therefore to check the expression of USP45 at the protein level, WT and 45KO cells were analysed by immunofluorescence. Cells were seeded onto a chamber slide at 50% confluency and processed for immunofluorescence staining with S109D anti-USP45 antibody (residues 29-80). Representative images are presented in Figure 3.2D which demonstrate clear staining for USP45 in the WT cells which is lacking in the 45KO cells. The pattern of staining seen here is comparable to that demonstrated by Perez-Oliva *et al* and confirms the efficiency of USP45 knock-out in this clone of U2OS cells (Perez-Oliva *et al.*, 2015).

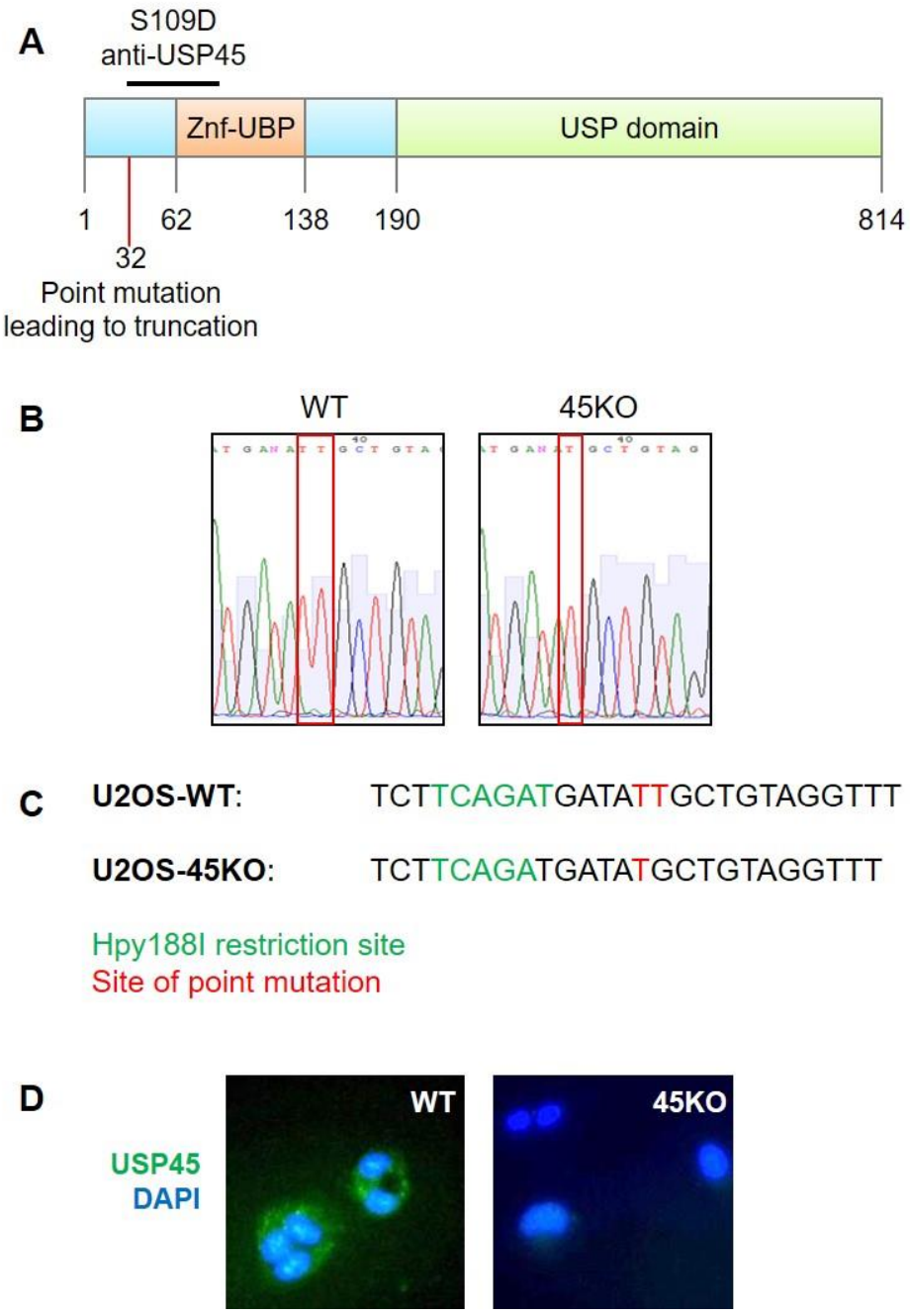

Figure 3.2. Validation of U2OS-45KO cells

(**A**) The domain structure of the deubiquitylase enzyme USP45. The mutation site identified in this thesis and S109D anti-USP45 antibody binding site are indicated. The zinc-finger ubiquitin binding (ZnF-UBP) and ubiquitin-specific peptidase (USP) domains are shown. (**B**) RNA extracted from U2OS-WT and-45KO cells was converted to cDNA and a USP45 PCR product was amplified to encompass the guide RNA binding site. Purified PCR products were sequenced by SourceBioscience. Red boxes highlight site of mutation. (**C**) A section of sequence from U2OS-WT and -45KO cells with the Hpy188I restriction site highlighted in green and the point mutation highlighted in red. (**D**) U2OS-WT and -45KO cells were verified by immunostaining for USP45 with S109D antibody. The nuclei were counterstained with DAPI (40X objective).

Amongst the phenotypes observed due to knock-out of USP45 in this cell background was a reduced cell growth (Perez-Oliva *et al.*, 2015). Therefore to analyse the phenotype of these cells in our lab, their growth was monitored over the course of 96 hrs. To quantify this, cells were seeded into a 6-well plate at $1x10^5$ cells per well, then cells in one well were trypsinised and counted every 24 hrs (Figure 3.3). After the first 24 hrs there was little difference in the number between the two cell lines. However, by 48 hrs post-seeding there were twice as many WT than 45KO cells and by 96 hrs there were ~3 fold more WT cells compared to 45KO cells. This confirmed that the knockout of USP45 resulted in a slower cell growth but the difference does not become apparent until 48 hrs.

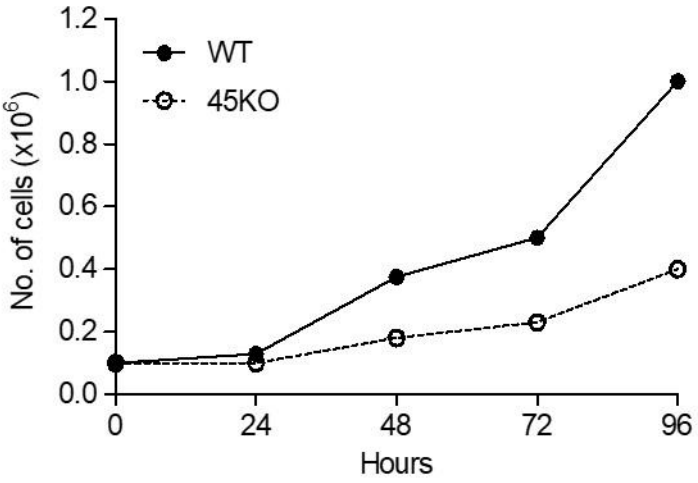

Figure 3.3. Analysis of the growth characteristics of U2OS-WT and -45KO cells
The growth of U2OS-WT and -45KO cells was monitored over 96 hrs. $1x10^5$ cells were seeded into a 6-well plate for both cell lines at 0 hrs then one well counted every 24 hrs (n=1).

3.4 Monitoring cell viability in alphavirus infected WT and 45KO cells

The WT and 45KO cells represent a different cell background to HeLa cells and have also been manipulated by CRISPR knock-out rather than siRNA knock-down. It was therefore next important to confirm the effect of USP45 ablation on cell viability in the context of viral infection of WT and 45KO cells. Initially, cell viability in the DUB siRNA screen was analysed using the MTS assay which produces a colorimetric readout corresponding to the ability of viable cells to reduce the MTS tetrazolium compound to the coloured formazan product (Goodwin *et al.*, 1995). However follow up experiments utilised the CellTiter-Glo cell viability assay which produces a luminescent signal relating to the amount of ATP produced by the cells present (Wang *et al.*, 2010). The effect on virus induced cytotoxicity in WT and 45KO cells was also observed visually. The cytopathic effect (CPE), the morphological changes in cell monolayers following virus infection, was monitored for both SFV and CHIKV.

3.4.1 Cell viability

Prior to confirming the cell viability phenotype in virus infected WT and 45KO cells, it was important to optimise the appropriate number of cells to seed per well to ensure the luminescent signal produced was within the linear range of the assay. This would also allow further characterisation of the cells and determine if there were any differences in cell viability in the uninfected 45KO cells compared to WT. Cells were seeded into a 96-well plate at increasing cell densities from $1x10^4$ – $2x10^5$ per well in triplicate and incubated at room temperature for 30 mins before addition of CellTiter-Glo Reagent and measurement of luminescent signal. The mean luminescence of triplicate wells is presented in Figure 3.4, which shows a linear relationship with r^2=0.98, for both WT and 45KO cells. From this it was decided to continue with a cell density of $5x10^4$ cells per well for subsequent virus experiments as this would provide the capacity to reliably measure any increase in cell viability.

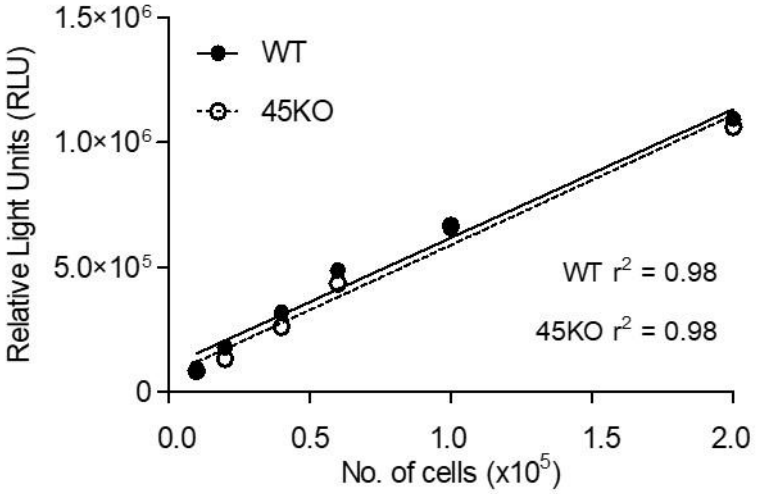

Figure 3.4. Optimisation of U2OS-WT and -45KO cell plating density using the CellTiter-Glo luminescent assay
U2OS-WT and -45KO cells were seeded into a 96-well plate at the indicated densities and cell viability was monitored 30 mins later using the CellTiter-Glo Luminescent assay (n=1).

To investigate the effect of USP45 ablation on cell viability following virus infection, WT and 45KO cells were infected with SFV at 10 MOI for 17 hrs. A high MOI was used in this instance to ensure that every cell was infected within the first round of replication. The mean data from three independent experiments are presented in Figure 3.5A as percentage cell viability relative to mock-infected cells. The relative number of viable WT cells infected with SFV decreased to 55% relative to mock. However, for 45KO cells infected with SFV, the relative number of viable cells was significantly higher at 80% which represents a 69% increase compared to WT. This is in line with the original siRNA screen data where USP45 siRNA knock-down in HeLa cells resulted in an increase of 63% for the relative number of viable cells. These results therefore provide initial confirmation that USP45 is required for efficient alphavirus replication or initiation of CPE in this different cell background, as there were more viable U2OS-45KO cells following SFV infection than WT cells.

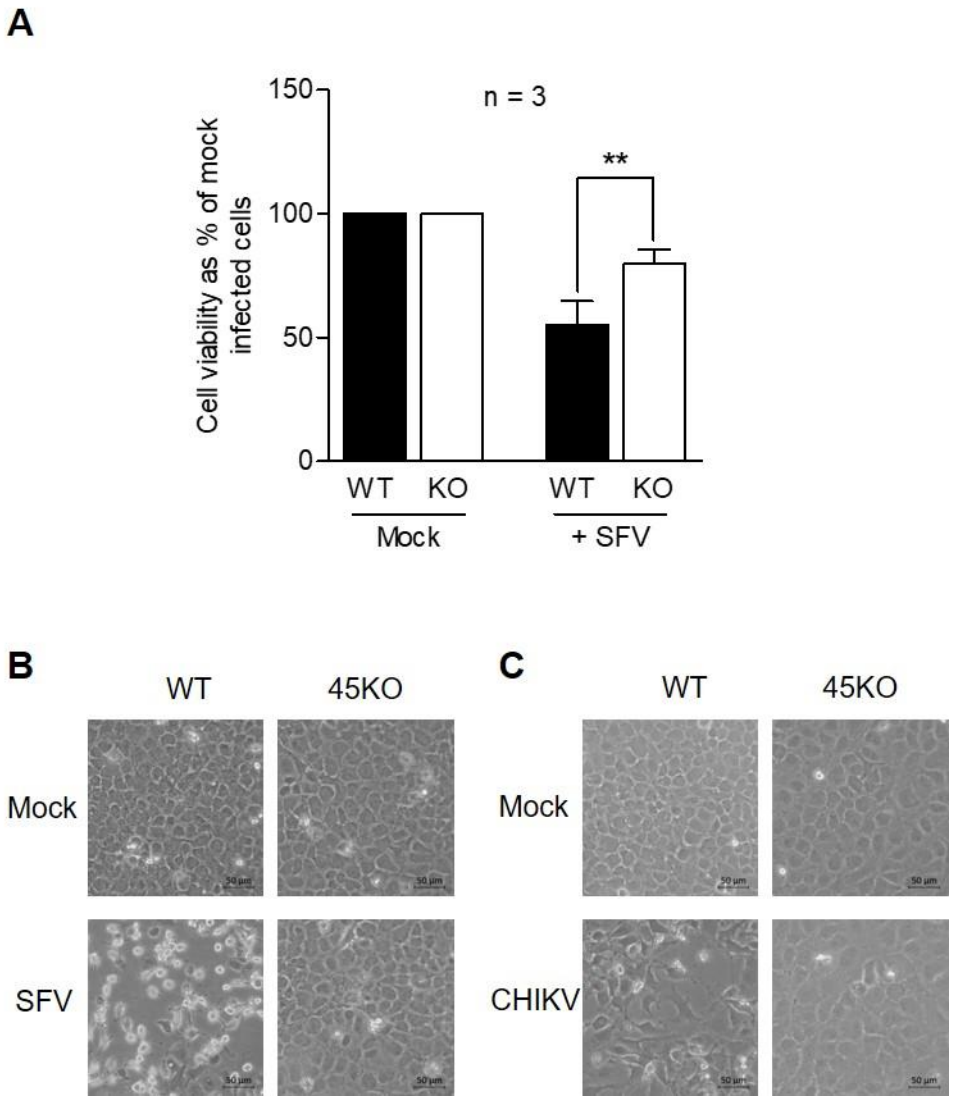

Figure 3.5. Reduced CPE in SFV and CHIKV infected U2OS-45KO cells compared to WT

(**A**) U2OS-WT and -45KO cells were infected in triplicate with SFV at 10 MOI. Cell viability was measured 17 hrs p.i. using the CellTiter-Glo Luminescent assay. Cell viability data are presented as the percentage of mock infected cells and are the mean of three independent experiments. Data are presented as cell viability as % of mock infected cells (±SD, **p= 0.034, two-tailed unpaired student's t-test). U2OS-WT and -45KO cells were infected with SFV (**B**) and CHIKV (**C**) and CPE observed. Phase-contrast images taken 24 hrs p.i. Representative phase-contrast images at 20X magnification are shown.

3.4.2 Cytopathic effect

Virus induced cytotoxicity can also be observed visually by monitoring CPE. First, WT and 45KO cells were infected with SFV at 0.1 MOI then fixed at 24 hrs p.i. and CPE observed. Representative images are shown in Figure 3.5B. WT cells show substantial CPE with the majority of cells exhibiting the characteristic 'rounded up' phenotype and death associated with alphavirus infection of mammalian cells (Li *et al.*, 2013). In contrast, the 45KO cells displayed markedly reduced CPE. However, as CHIKV is the more clinically interesting virus, it was next important to see if USP45 ablation had a similar effect on cell viability following CHIKV infection. WT and 45KO cells were infected with CHIKV at 10 MOI then fixed 24 hrs p.i. and CPE observed. Representative images are presented in Figure 3.5C. A higher MOI was used here as, although SFV and CHIKV are closely related, they are two distinct viruses and a higher MOI is often required for efficient replication of CHIKV (Powers *et al.*, 2001; Briolant *et al.*, 2004). Again, following CHIKV infection the WT cells show substantial CPE compared to 45KO cells. These results complement the cell viability assay and confirm that SFV and CHIKV both replicate more efficiently when USP45 is present.

3.5 Discriminating the points in the virus lifecycle at which USP45 is playing a role

The data presented in the previous section indicated that USP45 was important for alphavirus infection. However, these assays measuring cytopathic effect provide readouts at a relatively late stage in the viral lifecycle. Furthermore, using these assays, it was not possible to make any predictions as to when USP45 may be playing an important role during the lifecycle of alphaviruses. The next aim was therefore to identify at which point in the virus lifecycle USP45 could be playing a role in order to gain an insight into potential mechanism. The focus was to investigate viral genome replication, viral protein production and the number of infected cells. These readouts were selected to explore progressively earlier stages of virus replication.

3.5.1 Monitoring the level of alphavirus genome replication in WT and 45KO cells

To monitor alphavirus genome replication, WT and 45KO cells were first infected with SFV at 5 MOI, then RNA extracted 8 hrs p.i.. As discussed in section 1.1.2, alphaviruses contain a poly-A tail at the 3' end of their genomic RNA. Therefore, to permit analysis of both viral and cellular transcripts, cDNA was synthesised using oligo d(T) primers. Viral genome levels were analysed by qPCR and normalised to the house-keeping gene, 18S. Fold-change relative to WT cells was calculated using the $2^{-\Delta\Delta Ct}$ method (Schmittgen & Livak, 2008). A significant reduction in SFV genome production in the 45KO cells can be seen with a 60% decrease in the level of viral RNA compared to WT (Figure 3.6A). This was then extended to CHIKV by infecting WT and 45KO cells with CHIKV at 10 MOI. RNA was extracted 8 hrs p.i. and qPCR analysis of viral genome performed as above. A similar decrease of 60% in viral RNA was seen in the 45KO cells following CHIKV infection (Figure 3.6B). This indicated that the role of USP45 is likely to precede production of viral genomic RNA.

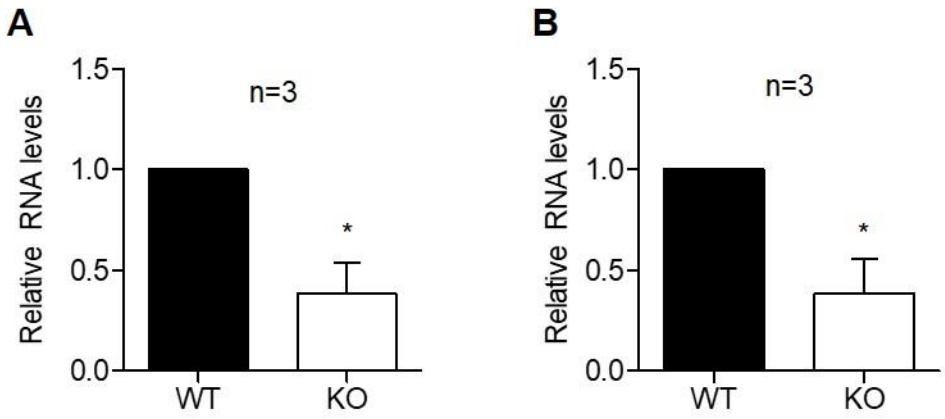

Figure 3.6. U2OS-45KO cells produce less SFV and CHIKV RNA
U2OS-WT and 45-KO cells were infected with (**A**) SFV at an MOI of 5 or (**B**) CHIKV at an MOI of 10 and harvested 8 hrs p.i.. Viral RNA was analysed by qPCR and fold-change calculated using the $2^{-\Delta\Delta Ct}$ method to calculate fold-change relative to WT, normalised to 18S. Data represent the mean of three independent experiments. Error bars represent SD, (paired, two-tailed student's t-test SFV* p=0.021, CHIKV* p=0.026).

3.5.2 Analysis of viral protein production in WT and 45KO cells following SFV or CHIKV infection

To explore a slightly earlier stage of the virus lifecycle, the production of viral proteins in WT and 45KO cells infected with either SFV or CHIKV was assessed next. Initially, cells were infected with SFV at an MOI of 5 then harvested 8 hrs p.i. and whole cell lysate generated. Total protein was resolved by SDS-PAGE and immunoblot analysis of SFV nsP1, nsP2, nsP3 and capsid proteins was performed. There was efficient production of all viral proteins in the WT cells, but this was markedly reduced in the 45KO cells (Figure 3.7A). Blots were quantified by densitometry using Fiji and are presented as density relative to WT normalised to the loading control, ACTB (Figure 3.7B). For nsP1, nsP2 and nsP3 a significant reduction in expression of 4-, 4- and 3-fold was observed in 45KO cells compared to WT, respectively. Expression of capsid in 45KO cells also displayed a mean 2-fold decrease relative to WT, but with more variability between experiments and it was therefore not statistically significant.

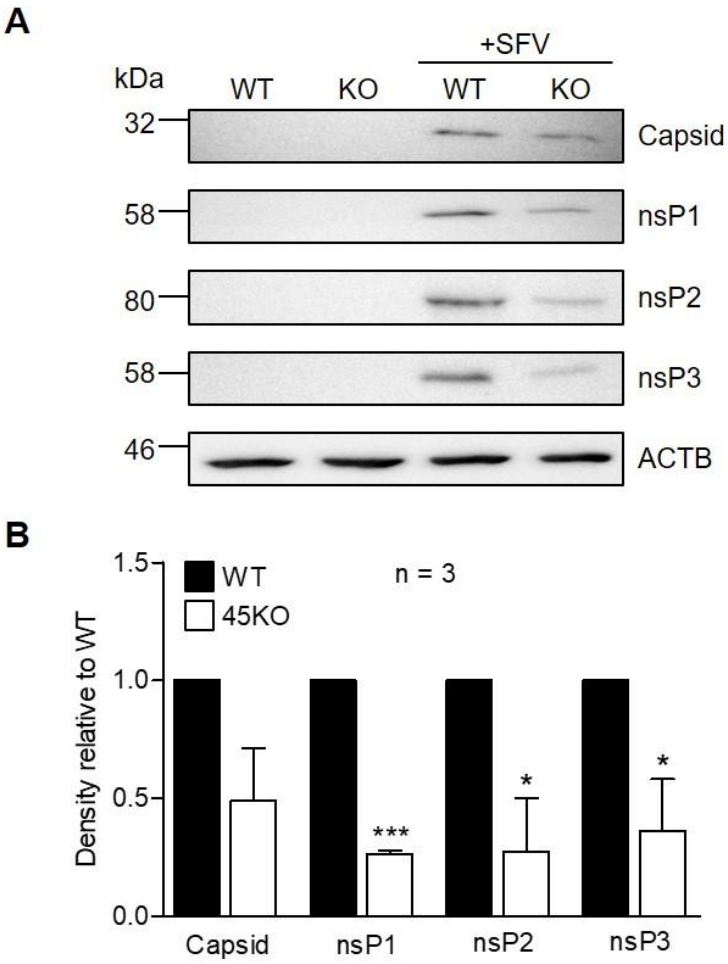

Figure 3.7. U2OS-45KO cells produce less SFV proteins
U2OS-WT and -45KO cells were infected with SFV at an MOI of 5 and harvested 8 hrs p.i.. Protein was extracted for analysis of the SFV viral proteins capsid, nsP1, nsP2 and nsP3 by immunoblot. (**A**) Representative blot **(B**) Viral protein expression was calculated using densitometry and is presented as density relative to WT normalised to ACTB. Data represent the mean of three independent experiments. Error bars represent SD, (paired, two-tailed student's t-test, nsP1*** p = 0.0001, nsP2 * p = 0.0308, nsP3* p = 0.0367).

For analysis of CHIKV proteins, WT and 45KO cells were infected at 10 MOI and harvested 24 hrs p.i.. As described in section 3.4.2, SFV and CHIKV are two closely related, but distinct, viruses which require different infection conditions. Therefore, a higher MOI and later time-point was used for CHIKV, to allow sufficient production of viral proteins to permit accurate quantification. Lysate was prepared and protein resolved, as described above, followed by immunoblot analysis of CHIKV nsP1, nsP2 and nsP3.

Capsid protein expression was not investigated here, as we did not have access to an anti-capsid antibody and the SFV antibody used above does not have pan-alphavirus specificity. Again, good production of CHIKV proteins can be seen in the WT cells but with a significant reduction in the 45KO cells (Figure 3.8A). For nsP1, nsP2 and nsP3 there was a 15-, 6-, and 8-fold decrease in 45KO cells, respectively (Figure 3.8B). Taken together these experiments demonstrated that 45KO cells produce significantly less viral proteins upon infection with either SFV or CHIKV. Thus, it was likely that the defect in cells deficient of USP45 was at an early stage of infection.

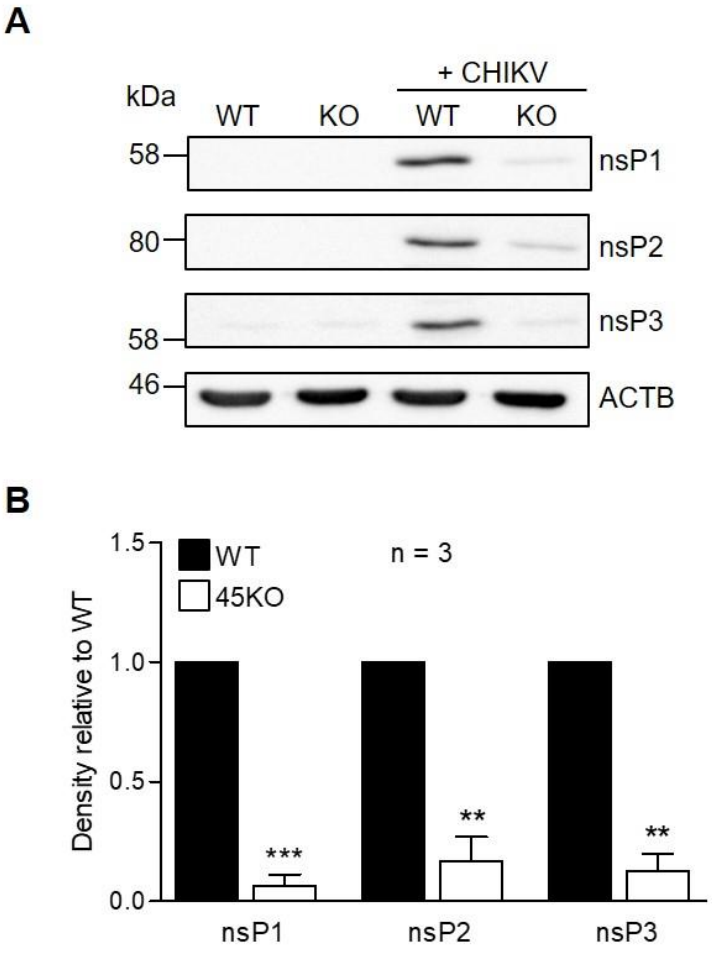

Figure 3.8. U2OS-45KO cells produce less CHIKV proteins
(**A**) U2OS-WT and -45KO cells were infected with CHIKV at an MOI of 10 and harvested 24 hrs p.i.. Protein was extracted for analysis of the CHIKV viral proteins nsP1, nsP2 and nsP3 by immunoblot. (**A**) Representative blot (**B**) Viral protein expression was calculated using densitometry and is presented as density relative to ACTB. Data represent the mean of three independent experiments. Error bars represent SD, (paired, two-tailed student's t-test, nsP1*** p = 0.0009, nsP2** p = 0.005, nsP3** p = 0.0022).

3.5.3 Investigating the effect of USP45 KO on the number of infected U2OS cells

The data to this point are indicative of a potential role for USP45 early in alphavirus infection. To explore the earlier stages of virus infection, plaque assays and immunofluorescence microscopy were used to monitor the ability of both SFV and CHIKV to infect WT and 45KO cells.

Firstly, the capacity of SFV and CHIKV to infect and spread in WT and 45KO cells was analysed by their ability to form plaques on monolayers of cells with an agarose overlay. This allows for analysis of efficiency of infection, as the number of cells infected is represented by the number of plaques formed within the cell monolayer. In addition, the ability of the virus to replicate and spread can be implied by monitoring the plaque phenotype. Confluent monolayers of WT and 45KO cells were infected in triplicate with 10-fold serial dilutions of SFV, then plaque formation counted 72 hrs later using crystal violet staining (Figure 3.9A). Although a mixed plaque phenotype can be seen in both the WT and 45KO cells following SFV infection, meaning firm conclusions about plaque sizes cannot be drawn, any potential changes in plaque size were minor. Importantly though, the number of plaques formed following SFV infection was significantly reduced in the 45KO cells, with 70% fewer plaques than in the WT cells (Figure 3.9B). This analysis was repeated for CHIKV infection. Again, a mixed plaque phenotype was observed making it hard to draw conclusions on the plaque size between WT and 45KO cells (Figure 3.9A). However, a similar reduction in the number of plaques was seen, with 60% fewer plaques in the 45KO cells relative to WT (Figure 3.9B). The reduction in plaque number in 45KO cells may suggest that the virus is less able to initially infect the cells. Taken together, this was suggestive of a potential role for USP45 in virus entry.

To determine if the absence of USP45 also affects the ability of other viruses to infect target cells, two unrelated viruses were tested for their ability to infect U2OS WT and 45KO lines. These were the negative sense RNA virus, respiratory syncytial virus (RSV) and the dsDNA virus, vaccinia virus

(VACV). RSV induces syncytia formation in infected cells rather than producing holes in cell monolayers (Kahn *et al.*, 1999). Thus, plaque formation could not be used as the readout for this experiment, as it was with SFV and CHIKV. Instead immunostaining of syncytia was performed. Briefly, monolayers of WT and 45KO cells were infected with RSV then fixed and visualised 24 hrs p.i. by immunostaining with a biotinylated anti-RSV antibody (Figure 3.9C). Syncytia were observed and images representing four fields of view were used to quantify syncytia formation. Data are presented in Figure 3.9D as syncytia formation as percentage of WT. RSV was equally capable of infecting and replicating in WT and 45KO cells with no significant difference in syncytia phenotype or number observed in the 45KO cells compared to WT. VACV efficiently induces plaque formation, thus the WT and 45KO lines were tested for the ability of VACV to form plaques in a similar manner to that for SFV and CHIKV. The plaques formed by VACV are smaller than expected when compared to other studies (Panda *et al.*, 2017), however the plaque phenotype in WT and 45KO cells was very similar (Figure 3.9C). Furthermore, the number of plaques in WT and 45KO cells displayed no significant difference (Figure 3.9D).

In summary, RSV and VACV were able to infect and replicate efficiently in both WT and 45KO U2OS cells, whilst SFV and CHIKV were significantly inhibited when USP45 was absent. Although the presence of a mixed plaque phenotype for SFV and CHIKV hinders the accurate analysis of plaque size, any differences between WT and 45KO were minor. Taken together, this demonstrates that USP45 is not essential for all viruses to infect and replicate. Furthermore, the number of plaques formed following SFV and CHIKV infection was significantly reduced, rather than an effect on plaque size. This points towards a role for USP45 in cell entry for these viruses.

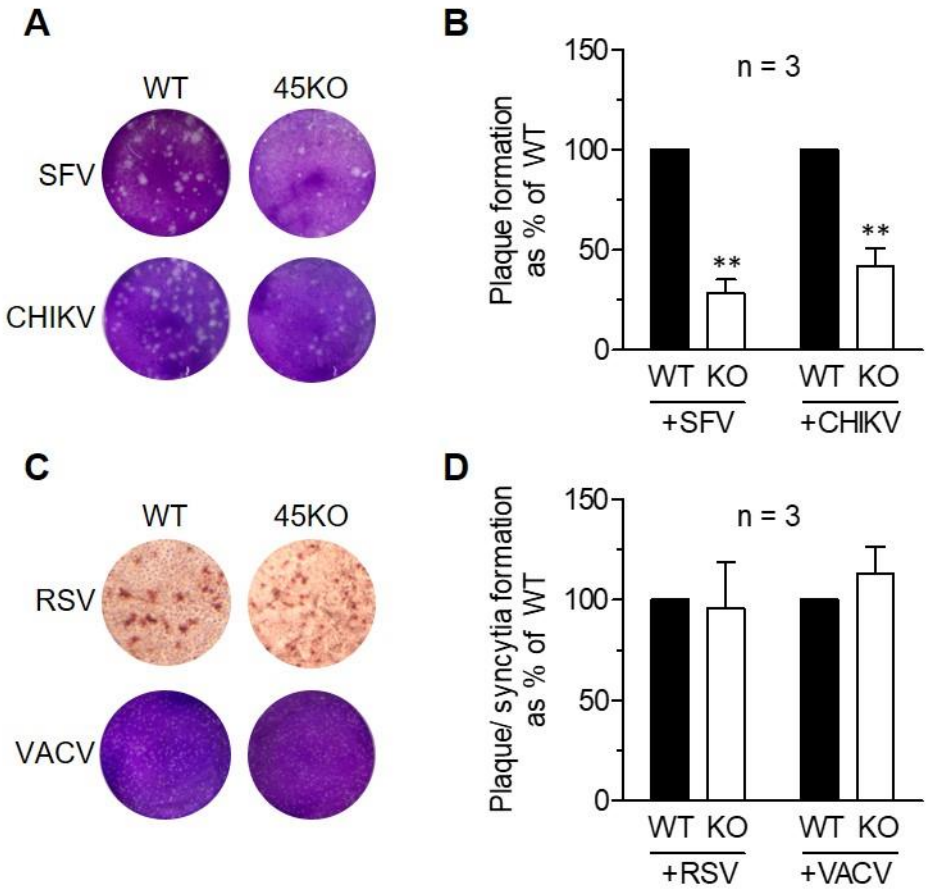

Figure 3.9. U2OS-45KO are less susceptible to alphavirus replication
(**A** and **B**) U2OS-WT and -45KO cells were infected in triplicate with either SFV or CHIKV. Plaques were visualised and counted at 72 hrs by staining monolayers with crystal violet. (**A**) Representative images are shown (**B**) Plaques were counted and are presented as plaque formation as % of WT ± SD. (SFV** p =0.0031, CHIKV** p =0.008, paired, two-tailed Student's t-test). Data are the mean of three independent experiments. (**C** and **D**) U2OS-WT and -45KO cells were also infected with RSV and syncytia visualised at 24 hrs by immunostaining with a biotinylated anti-RSV antibody. For VACV infection, U2OS-WT and -45KO cells were infected then plaques visualised and counted at 48 hrs by staining monolayers with crystal violet. (**C**) Representative images are shown (**D**) Plaque/ syncytia number is presented as plaque/ syncytia formation as % of WT ± SD. Data are the mean of three independent experiments.

In a complementary approach the ability of CHIKV to infect the WT and 45KO cells was monitored by immunofluorescence staining. CHIKV infected cells were detected by staining with a pan-alphavirus monoclonal

antibody. WT and 45KO cells were seeded on to chamber slides at 50% confluency. Cells were infected with CHIKV at 10 MOI then fixed 16 hrs p.i. and processed for immunofluorescence staining. Efficient staining of CHIKV infected cells can be seen in WT cells, but with a notable reduction in 45KO cells (Figure 3.10A). Images representing ten fields of view were taken using the same microscope setting, and used to calculate the percentage of infected cells (Figure 3.10B). This reveals a significant 75% reduction in the number of virus infected cells following 45KO compared to WT.

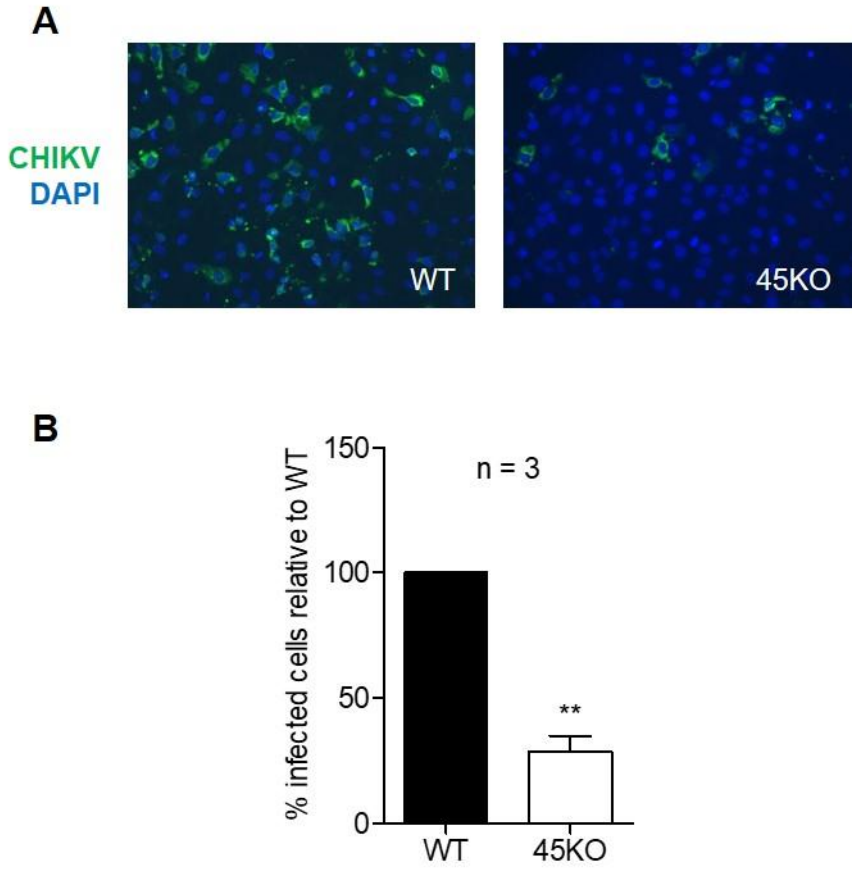

Figure 3.10. There is a reduction in the number of CHIKV infected U2OS cells following USP45 KO

(**A**) U2OS-WT and -45KO cells were infected with CHIKV at 10 MOI and fixed 24 hrs p.i.. Immunostaining with a pan-alphavirus antibody was used to visualise infected cells (20X objective). (**B**) The percentage of CHIKV was calculated for 10 fields of view and is presented relative to WT. Error bars represent SD (** p = 0.0028, paired, two-tailed student's t-test). Data are the mean of three independent experiments.

3.6 Evaluating the role of USP45 in virus entry

Taken together, the data point towards a defect early in the alphavirus lifecycle in 45KO cells. The syncytia formation and plaque assay data demonstrated that RSV and VACV infect both WT and 45KO cells equally well, while the alphaviruses were significantly less able to infect when USP45 is absent. When considering the differences between RSV and VACV with alphaviruses it was noted that one of the defining features is their mode of entry. For alphaviruses, the main route of entry is CME, whereas RSV and VACV largely enter by macropinocytosis (Mercer & Helenius, 2008; Mercer *et al.*, 2010; Krzyzaniak *et al.*, 2013; Ooi *et al.*, 2013). It should be noted that the type of endocytosis utilised by alphaviruses is also dependent on the cell type, as entry has been shown via both clathrin dependent and independent mechanisms (Bernard *et al.*, 2010; Ooi *et al.*, 2013). However previous published data has demonstrated that in U2OS cells alphaviruses enter by CME (Ooi *et al.*, 2013). Therefore the next aim was to explore whether USP45 could be involved in virus entry by playing a role in CME.

3.6.1 Endosome bypass assay

First, to determine if USP45 is indeed involved in virus entry the endosome bypass assay was utilised, which was first described by Ari Helenius in 1980 (Helenius *et al.*, 1980). This assay relies on the ability to release the viral genome directly into the cytoplasm of cells by using low pH to induce viral membrane fusion with the plasma membrane, thus bypassing the normal CME and release of viral genome in to the cytoplasm after acidification of endosomes (Figure 3.11). If, as predicted, USP45 is involved in uptake of alphavirus particles by CME, then acid bypass should rescue the infection defect in 45KO cells.

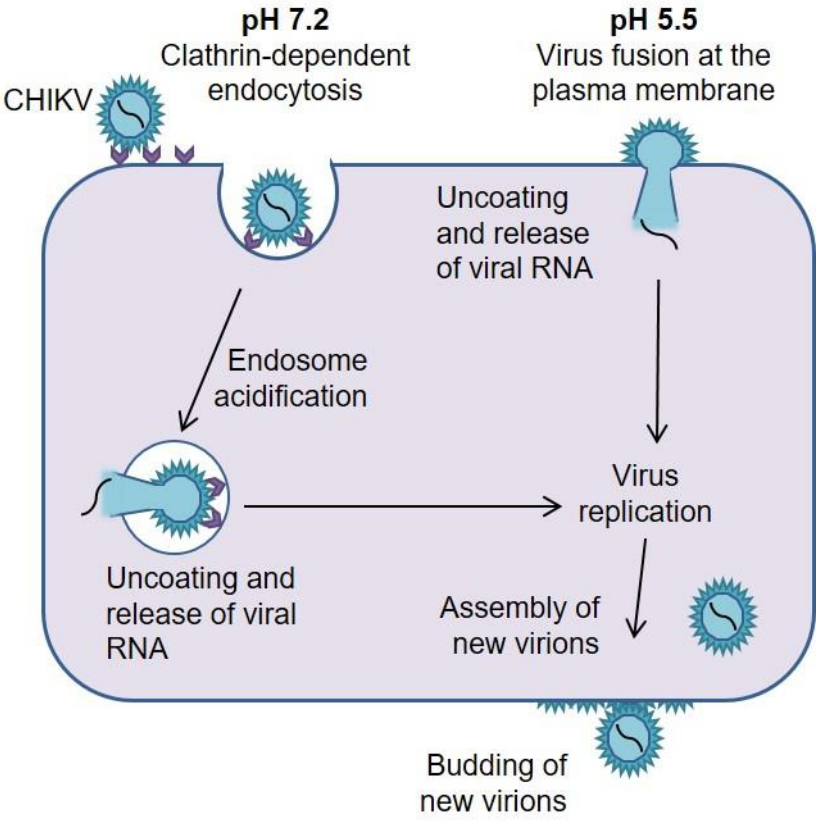

Figure 3.11. Schematic of endosome bypass experiment
U2OS-WT and -45KO cells are infected with CHIKV at 10 MOI at 4°C for 1 hr to allow binding without internalisation. Cells are then incubated with PBS pH7.2 or pH5.5 for 10 mins at 37°C to allow CME or force the virus to fuse at the cell membrane, respectively. Cells are incubated in media at 37°C for 16 hrs to allow the virus to replicate before fixing 16 hrs p.i.. Immunostaining with a pan-alphavirus antibody is used to visualise infected cells.

WT and 45KO cells were seeded into chamber slides to 50% confluency and infected with CHIKV at 10 MOI for 1 hr at 4°C to synchronise virus binding to the cell surface before allowing internalisation. Cells were then incubated with PBS at pH 7.2 or pH 5.5 for 10 mins at 37°C to allow entry via the endosome or plasma membrane, respectively. The PBS is then replaced with media and the infection allowed to progress for 16 hrs before fixing and immunostaining for quantification as previously described. Representative images are shown in Figure 3.12A and quantitation presented as percentage of infected cells (Figure 3.12B).

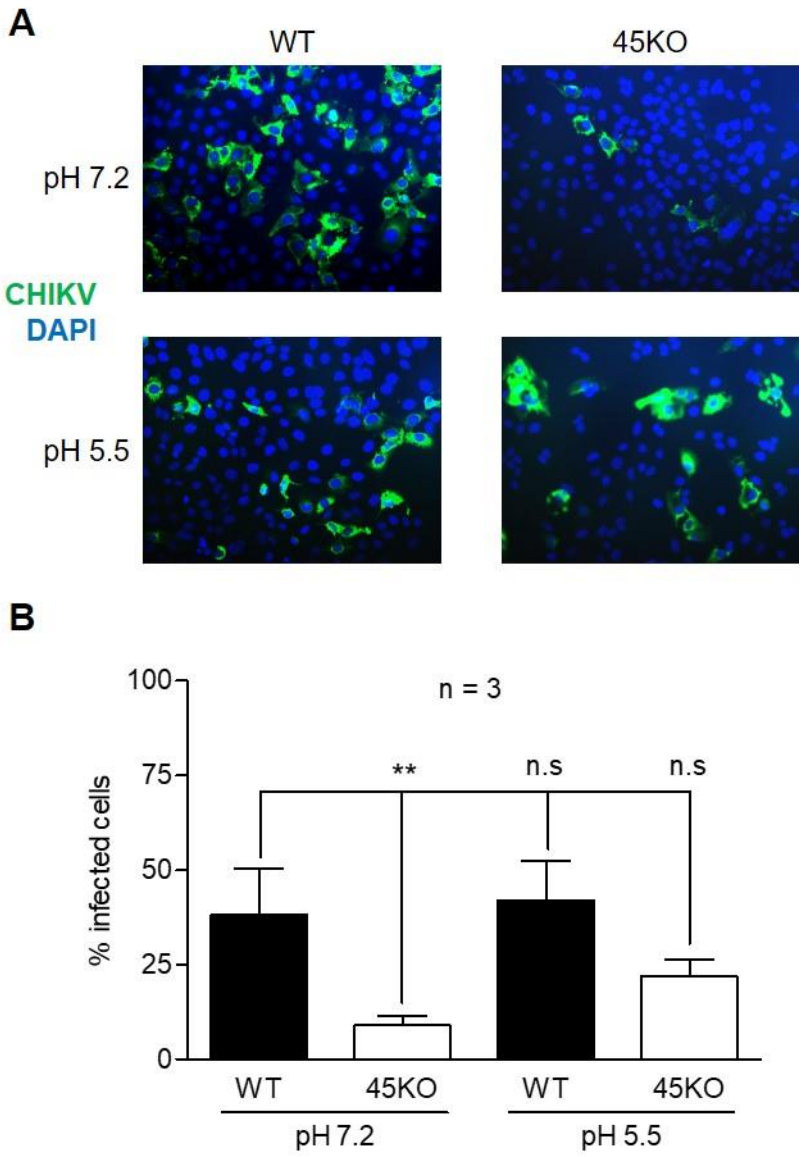

Figure 3.12. Bypassing the endosomal pathway in U2OS-45KO cells increases the percentage of CHIKV infected cells

(**A**) U2OS-WT and -45KO cells were infected with CHIKV at 10 MOI at 4°C for 1 hr then incubated with PBS (pH 7.2 or pH 5.5) for 10 mins. Cells were incubated in media at 37°C and fixed 16 hrs p.i.. Immunostaining with a pan-alphavirus antibody was used to visualise infected cells (20X objective). (**B**) The percentage of CHIKV infected cells was calculated for 10 fields of view. Error bars represent SD (**= $p < 0.01$ relative to WT pH 7.2, one way ANOVA with Dunnetts' multiple comparison test). Data are the mean of three independent experiments.

As previously observed, depletion of USP45 at neutral pH (pH 7.2) lead to a significant decrease of 80% in the percentage of CHIKV infected cells (Figure 3.12B). In comparison, following the acidic treatment in the bypass assay (pH 5.5), USP45 depletion had less effect on CHIKV infection. Under these acidic conditions 45KO cells exhibited a decrease of 50% in the percentage of CHIKV infected cells compared to WT cells. Although there is still a trend towards fewer infected cells, the difference between the WT and 45KO cells following incubation with acidic PBS was not significant. This suggests that USP45 is involved in CHIKV entry as the percentage of infected cells was increased after the virus was forced to fuse at the plasma membrane. However, the data could also be indicative of an additional role down-stream of virus entry as the percentage of infected cells was not completely rescued to the level seen in WT cells.

3.6.2 Tfn internalisation in WT and 45KO cells

In order to look more specifically at CME the transferrin (Tfn) uptake assay was utilised. Tfn is a serum glycoprotein which plays a crucial role in transporting iron into cells. It circulates in serum as apo-Tfn (iron-free) and can bind to up to two Fe^{3+} ions, becoming holo-Tfn (iron-bound), before binding to a Tfn receptor on the cell surface. The complex is then transported into the cell by CME and the endocytic vesicle begins to acidify. After approximately five mins the pH has reduced to pH 5.5 triggering release of Fe^{3+} from the Tfn complex which is subsequently reduced to Fe^{2+}. Free Fe^{2+} can now be transported out of the early endosome by metal ion transporters. Apo-Tfn remains bound to its receptor at the low pH and is recycled back to the cell surface. Here the neutral pH triggers release of Tfn to allow scavenging of more Fe^{3+} (Baravalle *et al.*, 2005; Mayle *et al.*, 2012).

The Tfn uptake assay takes advantage of this process by using an Alexa Fluor® tagged Tfn to monitor CME (Fielding *et al.*, 2012; Hackett *et al.*, 2015). WT and 45KO cells were seeded into chamber slides at 50% confluency and starved for 45 mins at 37°C. After pre-cooling the cells, Alexa Fluor ® tagged Tfn was added and cells incubated at 4°C for 30 mins to synchronise binding to the cell surface, while preventing internalisation. The

cells were then warmed to 37°C to allow endocytosis to proceed and after 5 mins, when Tfn should have reached early endosomes, cells were returned to 4°C to prevent endocytosis from proceeding further. After internalisation, surface bound Tfn was removed by washing with acetic acid buffer for 10 mins at 4°C then fixed and nuclei counterstained with DAPI. Cells were observed by fluorescence microscopy and representative images captured (Figure 3.13A). In WT cells, a strong signal can be seen representing accumulation of Tfn in early endosomes which is markedly reduced in the 45KO cells. To quantify this signal, CTCF was calculated in Fiji from five randomly selected images for both WT and 45KO. This was divided by the number of nuclei in each field of view to give an average and is presented in Figure 3.13B as Tfn uptake relative to WT. A significant reduction of 40% was observed for the Tfn signal in 45KO cells, indicating a defect in CME.

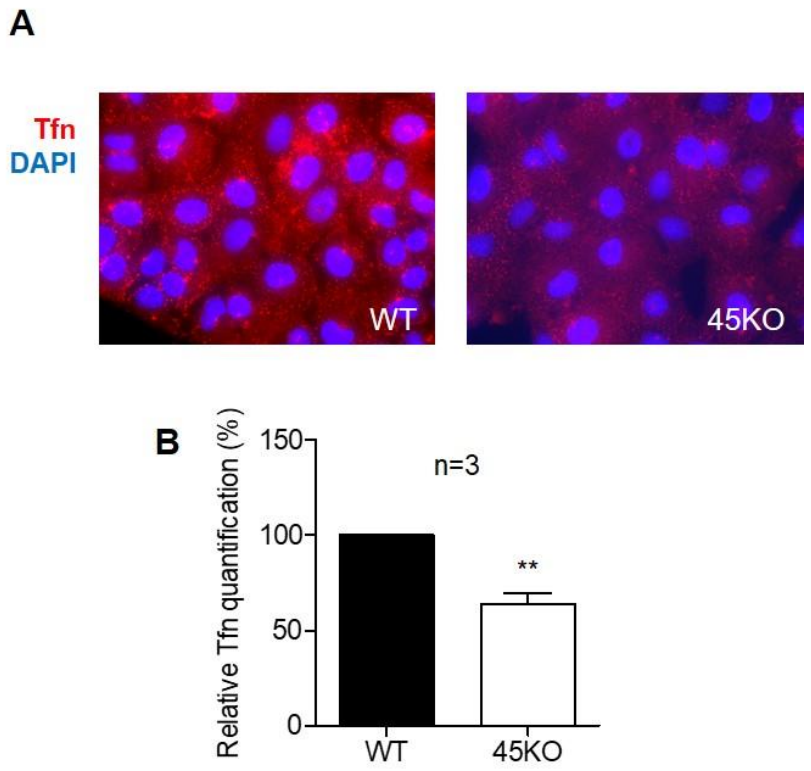

Figure 3.13. Transferrin uptake is inhibited in U2OS-45KO cells
(**A**) Representative images of U2OS-WT and -45KO cells treated with Alexa594-conjugated transferrin for 5 mins at 37°C. Cells were acid-washed to remove surface-bound transferrin, fixed and visualised by fluorescence microscopy. (**B**) CTCF was quantified using Fiji based on five random microscopic views and data are presented relative to WT (n=3). Error bars represent SD (paired, two-tailed student's t-test **p = 0.0078).

The endosome bypass assay demonstrated that the defect in alphavirus replication in 45KO cells can be partially recovered when bypassing the standard endosomal entry route. This indicated that USP45 played a role in virus entry. The results from the Tfn uptake assay support this finding by demonstrating that CME was less efficient in the 45KO cells than the WT.

3.7 Summary

USP45 was identified as a potential pro-viral DUB in an unbiased loss-of-function siRNA screen for the model alphavirus SFV. USP45 is poorly characterised, with the only suggested role at the start of this thesis in DNA repair. The role of USP45 in alphavirus replication was therefore further investigated in a USP45 knock-out cell line. U2OS cells that have targeted deletion of USP45 by CRISPR/Cas9 gene-editing, were utilised to confirm the initial observation from the siRNA screen, and then to establish the point during the virus lifecycle at which USP45 is required.

It was first important to confirm the genotype and phenotype of the WT and 45KO lines. Genotyping was achieved by sequencing a USP45 PCR product from both cell lines with primers designed to amplify across the expected region of USP45 mutation. This revealed that USP45 was knocked out due to a single thymine deletion at the end of exon 2, resulting in a frame-shift that introduces a premature stop codon. The 45KO clone used here contained a different mutation to that in the study reported by Perez-Oliva *et al*. It was therefore important to confirm lack of USP45 protein expression in the clone used in this thesis. Several commercially available antibodies were tested for immunoblotting, but these did not detect endogenous USP45. Therefore, protein expression was monitored by immunofluorescence using an antibody shown to detect endogenous USP45 (Perez-Oliva *et al.*, 2015). This demonstrated the efficiency of knock-out, as USP45 was detectable in WT cells but was absent in the 45KO cells. In addition, the phenotype of the U2OS cells was further analysed by monitoring growth over 96 hrs and it was confirmed that the 45KO cells grew more slowly than their WT equivalents.

Taken together, these data confirm the efficient deletion of USP45 in the KO cells which also results in slower cell growth.

Next, the effect of 45KO on cell viability was monitored to confirm the observations from the initial siRNA screen for SFV infection. The optimal number of cells per well was first tested by carrying out a cell viability assay in uninfected cells. This allowed for selection of a cell seeding density which would provide the capacity to reliably measure potential increases in cell viability. The cell viability assay was then repeated with the U2OS WT and 45KO cell lines infected with SFV. This confirmed that there were significantly more viable 45KO cells following infection with SFV than WT cells. To examine if this effect was also observed for CHIKV, WT and 45KO cells were infected with either SFV or CHKV then CPE monitored visually at 24 hrs p.i.. This revealed that WT cells displayed substantial CPE following both SFV and CHIKV infection, which was markedly reduced in the 45KO cells. These data confirm the pro-viral role for USP45 in alphavirus infection using an alternative model for USP45 loss-of-function.

In order to begin to define at which point in the virus lifecycle USP45 could be playing a role, assays to examine progressively earlier stages of virus replication were utilised. First, qPCR analysis of viral RNA production, following infection with either SFV or CHIKV, demonstrated that significantly less viral RNA was produced in the 45KO cells compared to WT. Next, WT and 45KO cells were infected with SFV or CHIKV and total protein extracts immunoblotted for viral proteins. The 45KO cells produced significantly less viral proteins following infection with either SFV or CHIKV, which was indicative of a role for USP45 early in infection.

The assays used to this point were based on monitoring events that occur late in the alphavirus replication cycle. To begin to explore earlier stages of the virus lifecycle, plaque formation of both SFV and CHIKV in WT and 45KO cells was monitored. For both viruses there was a significant reduction in plaque formation in the 45KO cells. Furthermore, although a mixed plaque phenotype was observed, there did not appear to be any obvious differences in plaque size. Taken together, these data point towards

a defect early in the virus lifecycle. To determine whether this defect was common to other non-related viruses, plaque formation by VACV and syncytia formation by RSV was also monitored in the WT and 45KO cells. In contrast, no significant differences in plaque or syncytia formation was observed for either viruses, thus suggesting a defect specific to alphaviruses. To complement these data, the percentage of CHIKV infected cells in the presence or absence of USP45 was monitored by immunofluorescence staining. Again, a significant reduction in the number of infected cells in the absence of USP45 was observed, strengthening the evidence for a role of USP45 early in virus infection.

To test if virus entry was defective in 45KO cells, the effect of bypassing the normal endosomal viral entry route was monitored. When WT and 45KO cells were incubated with CHIKV at pH 5.5 there was no significant difference in the percentage of infected cells. This was suggestive of a role for USP45 in virus entry, therefore this mechanism was further investigated. The Tfn uptake assay was utilised to directly monitor CME, the primary mechanism of entry for alphaviruses. Uptake of a labelled Tfn was reduced in 45KO cells compared to WT, supporting a role for USP45 in CME.

In summary, this chapter has shown that USP45 plays an important role in the alphavirus lifecycle. Progressively earlier stages of the alphavirus lifecycle were investigated as well as comparison with two unrelated viruses. Taken together, this has demonstrated that USP45 is important for alphavirus entry through its involvement in the CME pathway.

Chapter 4: Analysis of the use of activity based probes as a measure of deubiquitylase activity following alphavirus infection

4.1 Introduction

To date the techniques used to identify DUBs as therapeutic targets in virus infections have typically been based on loss-of-function phenotypes. Commonly used techniques include RNA interference (RNAi) or Clustered Regularly Interspaced Short Palindromic Repeats (CRISPR) screening methods. RNAi screens such as siRNA knockdown have been described in section 3.1 and while these have proven useful they have their limitations. For example, efficient knock-down can be difficult if the transcript has a high turnover or the protein has a long half-life (Mohr *et al.*, 2010; Boettcher & McManus, 2015). There is also the risk of off-target effects with unrelated genes being down-regulated creating a false-positive result (Jackson *et al.*, 2003). One way in which this is thought to occur is through hybridisation of the guide strand of RNAi, largely through the seed region, with non-target transcripts thus leading to their suppression (Jackson *et al.*, 2003, 2006*b*). However, another way this can occur is through saturating the endogenous RNAi machinery, which can result in global perturbations in gene expression. This includes potential upregulation of off-target genes due to subversion of the RNAi machinery by artificially introduced siRNAs (Khan *et al.*, 2009). Another limitation is the observation that introduction of siRNAs can lead to the unintended induction of the non-specific interferon response (Sledz *et al.*, 2003). This is a particular issue when attempting to study virus replication, exemplified by the misinterpretation of the anti-viral effect of an siRNA on influenza replication (Robbins *et al.*, 2008). While chemical modifications and software developments to identify prevalent off-target sequences have reduced these risks, they remain limitations which must be taken into account (Arziman *et al.*, 2005; Jackson *et al.*, 2006*a*).

An alternative screening method, CRISPR, has addressed some of these issues as it has the ability to permanently knock-out the gene of interest with a reduced risk of off-target effects (Wang *et al.*, 2014). However, CRISPR technology lags behind RNAi and can be technically challenging, especially for large scale screens (Kampmann *et al.*, 2015). In addition, there can be general disadvantages to loss-of-function studies, such as being limited to certain cell lines which can be easily transfected. Importantly, if the ablation of the gene of interest is deleterious or lethal to the cells it is difficult to investigate further.

As described in section 1.4.3 the control of deubiquitinase activity is tightly regulated and changes can occur independently of the level of protein expression (Sahtoe & Sixma, 2015). Subtle changes in DUB activity could therefore have a considerable impact on a system but may be overlooked in loss of function studies. Recent advances in the ubiquitin field have provided novel tools to address this shortfall. DUB Activity Based Probes (ABPs) are useful tools which can not only be used to monitor DUB activity but have also been used to identify novel roles for DUBs as well as pathogen encoded DUBs (Ekkebus *et al.*, 2014).

In their infancy, ABPs consisted simply of a single full-length ubiquitin molecule with the C-terminal glycine residue replaced by an electrophile, such as ubiquitin-aldehyde (Ubal) or ubiquitin-nitrile (Ub-CN) (Hershko & Rose, 1987; Lam *et al.*, 1997). These proved to be important tools in mechanistic studies, indeed Ubal was utilised to solve the structure of a DUB in complex with Ub for the first time (Johnston *et al.*, 1999). However, the use of these early probes was limited as the binding reaction with DUBs is reversible and therefore not suitable for use with the strong reducing agents required in SDS-PAGE (Lam *et al.*, 1997). The development of irreversible DUB ABPs was subsequently achieved by Borodovsky *et al* through the introduction of a C-terminal vinyl methyl sulfone (VS) (Borodovsky *et al.*, 2001). For detection of the probe-bound proteins they radiodinated UbVS with Na[^{125}I], thus creating the first irreversible ABP, ^{125}I-Ub-VS. Using this probe, Borodovsky et al were the first to identify USP14 as a proteasomal associated DUB (Borodovsky *et al.*, 2001). In a later study, this group went

on to further develop these probes by also conjugating a hemagglutinin (HA) tag to aid visualisation. This not only provided a more convenient method for visualisation of labelled DUBs, but also allowed for immunoprecipitation studies to identify the tagged DUBs (Borodovsky *et al.*, 2002). In the same study, this group also compared the labelling efficiency of different electrophilic warheads by synthesising new probes. For example, probes with a vinyl methyl ester (VME) or bromoethyl (Br2) warheads, which have a higher electrophilicity than VS, were compared. Of the probes tested in this study, the Ha-Ub-VME probe exhibited the broadest labelling pattern (Borodovsky *et al.*, 2002). It was therefore predicted that increasing the electrophilic capability of the probes yet further would yield even greater binding efficiency. Thus, a new generation of probes was created with the warheads vinylethoxysulfone (OEtVS), β-lactone (Lac) or 2,6-trifluoromethylbenzyloxymethylketone (TF_3BOK). However, the increase in electrophilicity did not correspond to an increased binding capability, with the first generation probe, HA-Ub-VME, still providing the broadest binding pattern. It was suggested that this is likely caused by rapid hydrolysis of the probes during the labelling reaction due to their increased reactivity. Importantly, it was also noted that increasing the electrophilicity in the warhead resulted in reduced specificity, with other Ub-interacting enzymes, such as HECT E3 ligases, now being detected (Love *et al.*, 2009).

Work to continue improving these probes serendipitously lead to the synthesis of another warhead, propargyl amide (PA), which had both an improved electrophilicity and specificity (Ekkebus *et al.*, 2013). This was an important development as the probes synthesised to this point had binding preferences for USP and UCH DUBs (Ovaa *et al.*, 2004; Rolén *et al.*, 2006). However, the PA probe was shown to bind well to all the four families of cysteine proteases known at the time (Ekkebus *et al.*, 2013). Subsequently, the PA probe has been demonstrated to also bind to the more recently discovered cysteine protease DUBs, MINDYs and ZUFSPs. Indeed, it has positively aided the characterisation of these newly discovered DUBs (Abdul Rehman *et al.*, 2016; Haahr *et al.*, 2018; Kwasna *et al.*, 2018). While the PA warhead now potentially allows binding to the majority of DUBs, these probes

cannot bind to the JAMM family which contain a zinc ion in place of the cysteine residue (described in more detail in section 1.4.2). It has also been noted that these ABPs bind non-catalytic cysteine residues. Consequently, probe binding is not necessarily indicative of DUB activity, for example in the case of OTUB1 an ABP was shown to bind to a non-catalytic cysteine residue, rather than the active site (Wang *et al.*, 2009). In addition, there have been reports that the ABP can stimulate realignment of the active site for some DUBs, for example USP7 and USP14 (Hu *et al.*, 2002, 2005). Thus, when referring to probe bound proteins they should be considered 'probe reactive' rather than 'active' until binding location and mechanism has been elucidated. It also clear that careful optimisation of the reaction is required to measure activity rather than total protein.

Further advances were made by improving the efficiency of synthesis for the ABPs. Classically, ABPs were synthesised through intein chemistry by expressing an N-terminally tagged HA-tagged Ub (HAUb) lacking Gly76 in *E. coli*. The appropriate reactive group was then chemically ligated via a trans-thioesterified intermediate (Borodovsky *et al.*, 2002). The intein approach is laborious and limited with regards to the potential tags which can be used. Synthesising ABPs in this way was also not conducive to large scale production of probes. Therefore, to overcome these issues total chemical synthesis of ubiquitin followed by introduction of specific tags and warheads on a resin scaffold was utilised. This not only permitted ease of scaling up synthesis but also allowed for unlimited modifications, thereby greatly increasing the potential experimental applications of ABPs (El Oualid *et al.*, 2010; de Jong *et al.*, 2012).

Indeed, ABPs have demonstrated their versatility through their utilisation in a range of experimental situations. For example, in the comparison of DUB activity and expression levels in normal versus diseased states. Using HA-Ub-VME and HA-Ub-Br2 probes, the activity levels of USP5, -7, -9, -13, -15 and -22 was shown to increase upon infection with EBV (Ovaa *et al.*, 2004). However, ABPs have yet to be used to monitor DUBs in alphavirus infection. ABPs have also proven instrumental in the identification and characterisation of virally encoded DUBs (section 1.5.3), for

example HSV-1 UL36 and adenovirus Avp (Balakirev *et al.*, 2002; Kattenhorn *et al.*, 2005). Alphaviruses possess a cysteine protease, nsP2, but this has not previously been monitored for potential DUB activity (Ramakrishnan *et al.*, 2017).

4.2 Aims

ABPs have been shown to be powerful tools in identifying DUBs involved in virus infections. However, they have yet to be used in the context of alphavirus infection to study virus-host interactions. Furthermore, to date there has been no experimental data published to indicate whether the cysteine protease of alphaviruses could act as a DUB. Considering the potential for novel therapeutics against DUBs this could be an effective method of identifying targets for future investigation. Thus, the aims of this chapter were:

1. To first optimise the use of ABPs for future screening protocols (Chapter 5) to ensure the maximum number of DUBs can be identified.
2. To investigate whether the CHIKV cysteine protease, nsP2, possesses DUB activity.

4.3 Optimisation of the use of ABPs as a screening method in HeLa cells

The DUB ABPs used in this study contain three key features: a targeting element (VME or PA), a reactive group (ubiquitin) and a reporter tag (HA) (Figure 4.1). It was first necessary to optimise the probing conditions to ensure the maximum number of DUBs could be detected. Two ABPs, with different electrophilic warheads, were tested during optimisation, HA-Ub-VME and HA-Ub-PA.

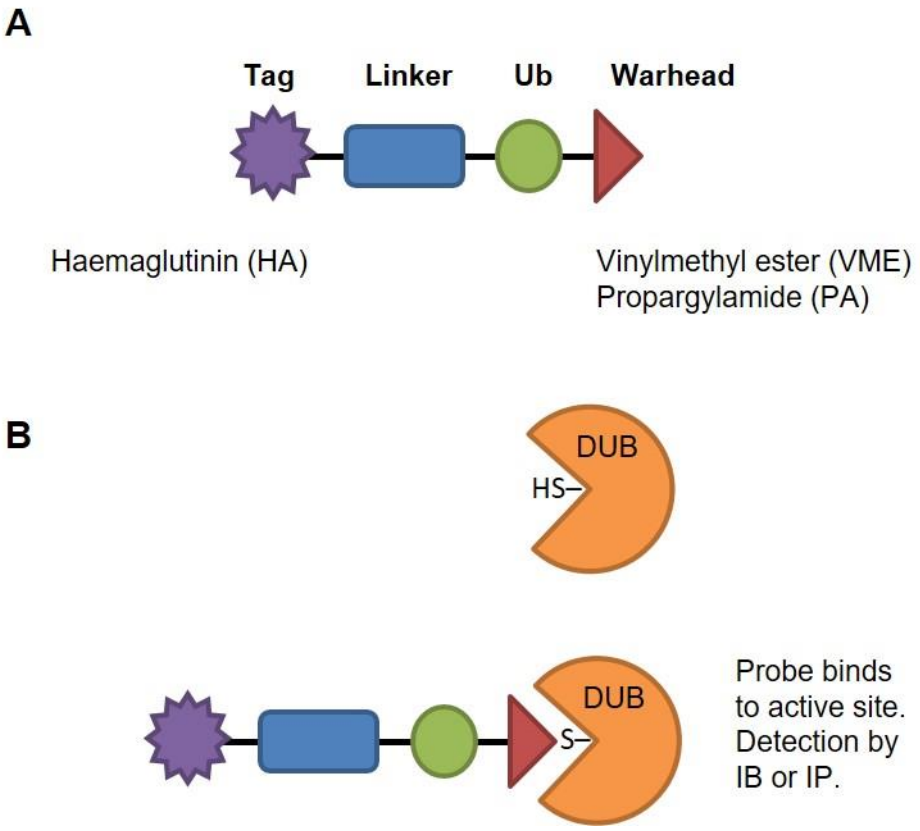

Figure 4.1. Schematic representation of structure and mechanism of action for DUB ABPs
(**A**) The DUB ABPs used in this study contain a ubiquitin molecule as the core targeting element to which an electrophilic warhead (VME or PA) is conjugated. A HA tag is attached to the ubiquitin molecule via a linker. (**B**) The warhead of the ABP reacts with the thiol group of the catalytic cysteine. A covalent thioether attachment is formed allowing for detection by immunoblot (IB) or pull-down of probe-bound proteins by immunoprecipitation (IP). Figure adapted from Hewings *et al.* (2017)

In order to detect changes in probe-reactivity it was important to incubate with the optimal concentration of probe. If the concentration of probe was too high it would have been hard to see differences if the signal became saturated. However, a probe concentration which was too low could have limited the reaction, meaning less abundant or reactive proteins were overlooked. Thus, a comparison of probe concentrations (probe: protein lysate ratio) from 2.5 ng probe/ 1 µg protein (1:400) to 200 ng probe/ 1 µg protein (1:50) was performed. Following a constant incubation time of 15

mins, cells were harvested for immunoblot with an anti-HA antibody to detect the N-terminal HA tag. The profiles of detected proteins for each probe are shown in Figure 4.2.

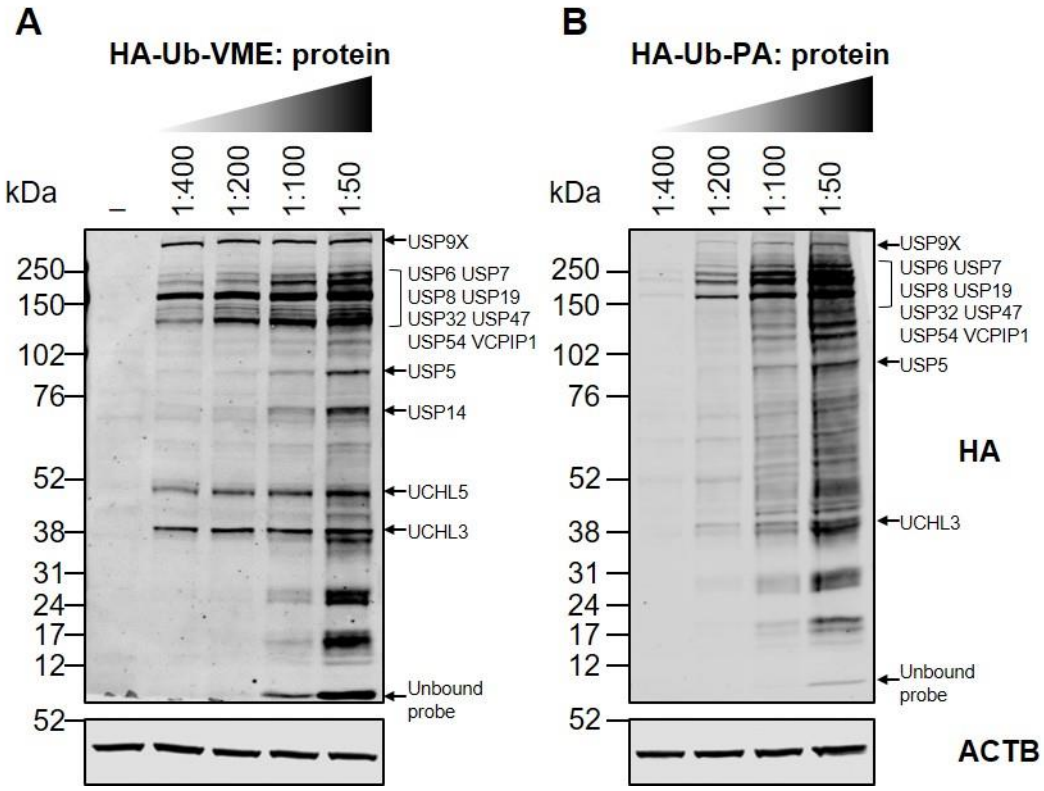

Figure 4.2. Optimisation of probe: protein ratio for HeLa cell lysate
The optimal probe: protein ratio was determined by incubating a set concentration of non-denatured HeLa cell lysate with increasing amounts of either (**A**) HA-Ub-VME or (**B**) HA-Ub-PA probe: Probe/ lysate mixtures were incubated at 37˚C with constant shaking for 15 mins, before being resolved on 4-12% SDS-PAGE gradient gels, and immunoblotted for the HA tag. Protein loading was monitored by immunoblotting for ACTB. Predicted DUB candidates for specific bands or regions are indicated. Unbound probe is also highlighted.

The VME probe (Figure 4.2A) bound to fewer proteins in total compared to the PA probe (Figure 4.2B), as seen in lanes 1:50 for each probe. However, for some proteins the VME probe bound much more efficiently that the PA probe, with strong HA-immunoreactive bands visible even at the lowest concentration (1:400). For example, the VME probe had clear binding preference for certain proteins, such as the HA-immunoreactive bands at ~38 and ~52kDa, which are much stronger at the lower

concentrations when compared to the PA probe. The ABPs have a molecular weight of approximately 10kDa. Thus, modification with the probes is expected to increase the molecular weight of a DUB by 10kDa, resulting in slower migration through the gel matrix. Predictions as to what these bands are can therefore be made based on their molecular weight. For example, the highest band above 250kDa could be the DUB USP9X, the band at ~38kDa could be UCHL3 and the ~52kDa band could be one of the proteasomal DUBs, UCHL5. Two bands which were more prominent in the VME probed samples at higher concentrations, compared to PA, are the HA-immunoreactive bands in the regions below the 102kDa and 76kDa marker. The lower of these two bands could be one of the other proteasomal DUBs, USP14. The higher band, below 102kDa, could be the highly abundant DUB, USP5. There was also a region of intense binding between 150-250kDa for both probes which was likely to be due to the lower resolution of larger proteins as well as there being several DUBs expected at these sizes. For example, the DUBs USP6, USP7, USP8, USP19, USP32, USP47, USP54 and VCPIP1, when tagged with a probe, would all be expected to be present in this size range. To confirm the identification of these putative DUBs, probing with specific antibodies would be required but was not done here.

At the lower probe concentrations (1:400 and 1:200), many of the bands which were observed with a higher concentration of probe, were no longer visible. It was therefore decided that these concentrations were not suitable for detecting changes in probe-reactivity as the reaction was limited by lack of probe. However, at the highest concentration of probe (1:50), for both VME and PA, many of the HA-immunoreactive bands were saturated and unbound probe was clearly visible at ~10kDa. This can also be seen when comparing the intensity plots for the two ABPs (Figure 4.3). These plots represent the intensity of the signal from the HA-immunoreactive bands. While the plots for HA-Ub-VME (Figure 4.3A) appear very similar for the 1:400 and 1:200 probe ratios, there are clearly new peaks visible at 1:100 that increase in intensity at 1:50. These represent proteins that may be less abundant in the lysate and/or less reactive towards the ABP. For HA-Ub-PA (Figure 4.3B), a similar pattern is seen with additional peaks becoming

apparent as the probe concentration increases. A probe: protein ratio of 1:100 was therefore considered the optimal concentration for both VME and PA probes as, under these conditions, all possible bands were visible.

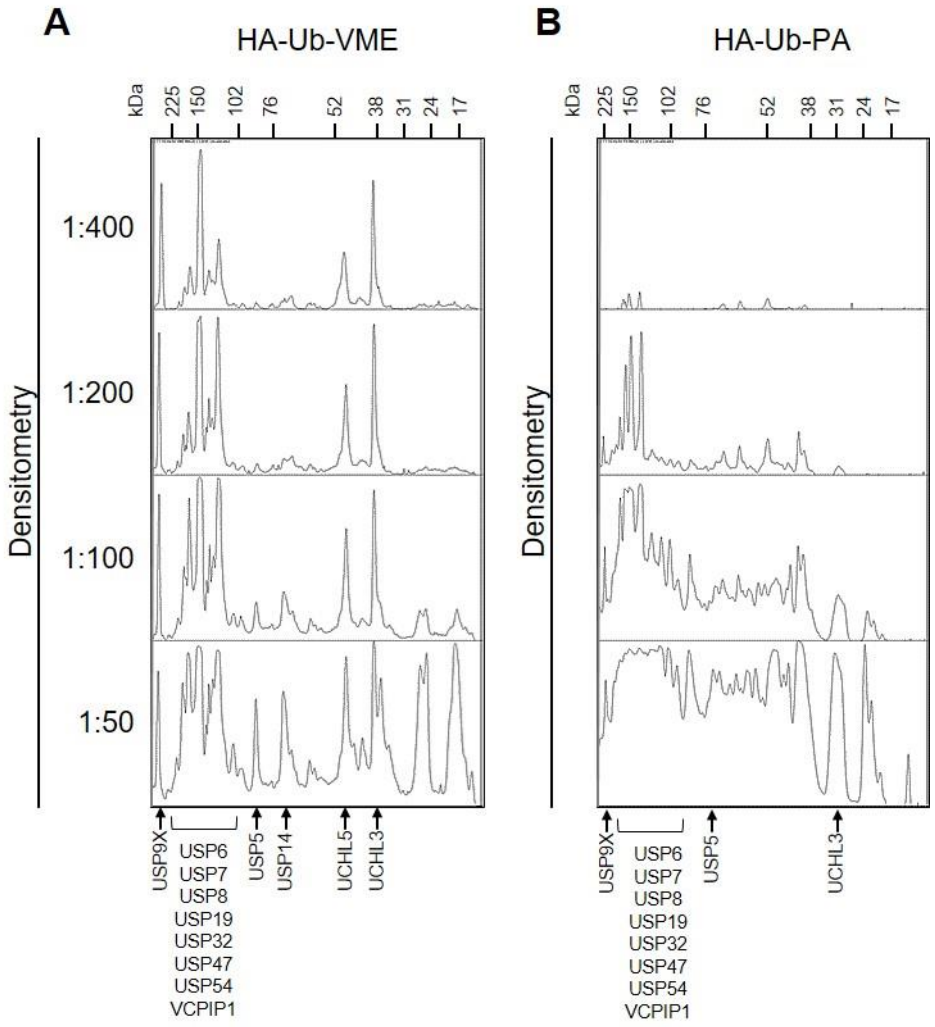

Figure 4.3. Intensity plots for probe-bound protein from optimisation of DUB ABP concentration
The intensity plots for HA immunoblots from figure 4.2 were generated in Fiji for HA-Ub-VME (**A**) and HA-Ub-PA (**B**). Predicted DUB candidates for specific peaks or regions are highlighted.

Using a probe: protein ratio of 1:100, the incubation time was then tested by incubating HeLa lysate with HA-Ub-VME or HA-Ub-PA for a range of times between 2 – 45 mins. Following visualisation by immunoblotting for

HA, it became apparent that there were differences in patterns for low and high molecular weight proteins as the incubation time increased, for both HA-Ub-VME (Figure 4.4A) and HA-Ub-PA (Figure 4.4B). While the bands representing larger proteins (above ~76 kDa) became more intense as the incubation time increased, the smaller proteins (below ~52 kDa) displayed the opposite pattern. The covalent binding of probes to the active site of DUBs inhibits their normal physiological function. Therefore, the decrease in intensity for some bands with longer incubation times may be as a result of changes in the stability or activity of these proteins following inactivation of probe-bound DUBs.

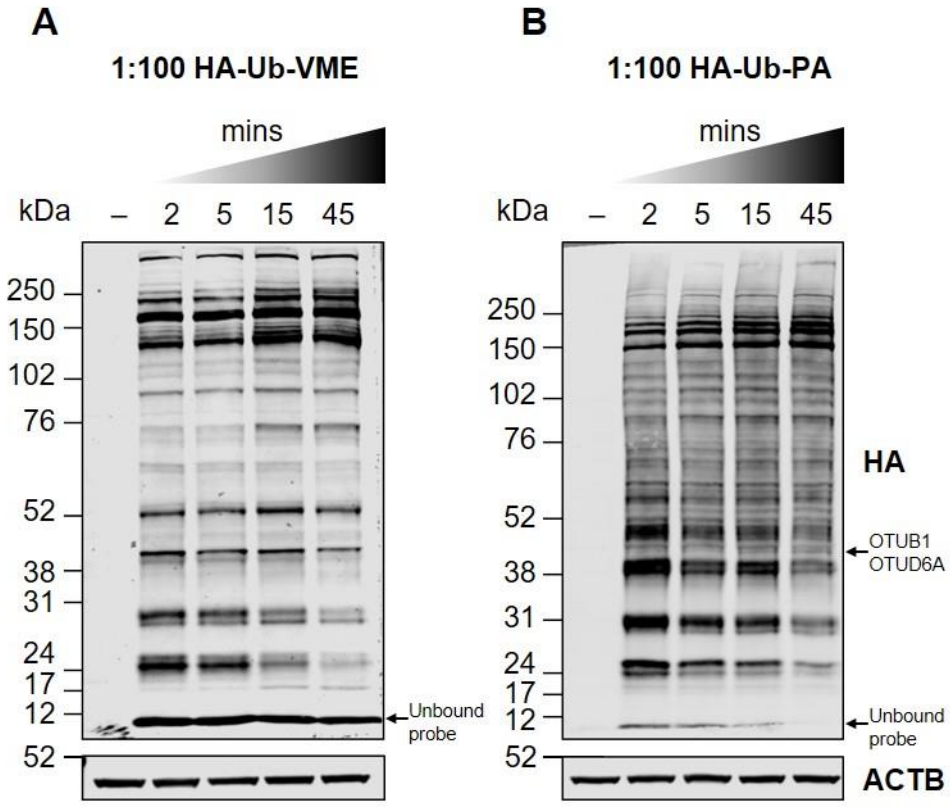

Figure 4.4. Optimisation of DUB ABP incubation times in HeLa cell lysate
The optimal incubation time for DUB ABPs in HeLa cell lysate was determined by incubating a set concentration of non-denatured HeLa cell lysate with either (**A**) HA-Ub-VME or (**B**) HA-Ub-PA probe at 1:100 (probe: protein) for increasing amounts of time. Probe/ lysate mixtures were incubated at 37°C with constant shaking for the stated time before being resolved on 4-12% SDS-PAGE gradient gels, and immunoblotted for the HA tag. Protein loading was monitored by immunoblotting for ACTB. Predicted DUB candidates for the band indicated and unbound probe are highlighted.

The intensity plots for both VME (Figure 4.5A) and PA (Figure 4.5B) probes show initially strong binding at 2 mins and the same fluctuations of a decreasing and increasing binding intensity over time. Despite this trend for a decrease in intensity for smaller proteins as the incubation time increased, other bands could not be seen clearly with a short incubation time. For example, a band at approximately ~40kDa (Figure 4.4B), which is the around the predicted size for OTUB1 or OTUD6A, was seen more clearly with a 45 min incubation. In addition, no bands disappeared completely following a 45 min incubation with either the VME or PA probe. An incubation time of 45 mins and a probe: protein ratio of 1:100 was therefore selected as the optimal time for detecting the maximum number of probe-bound proteins.

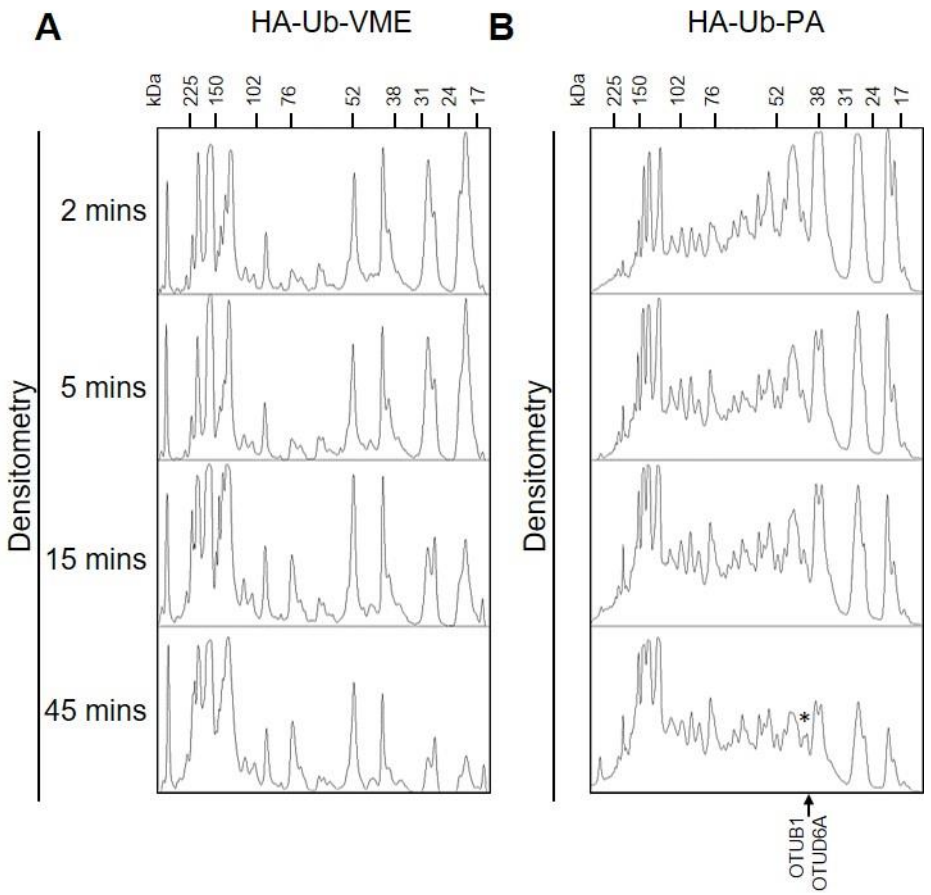

Figure 4.5. Intensity plots for probe-bound protein for optimisation of DUB ABP incubation times
The intensity plots for HA immunoblots from figure 4.5 were generated in Fiji for HA-Ub-VME (**A**) and HA-Ub-PA (**B**). Predicted DUB candidates for the peak indicated by a * are highlighted.

In summary, a range of probe concentrations and incubation times were tested to determine the optimal probing conditions in HeLa lysate to allow detection of the maximum number of DUBs in screening experiments. It was decided to use HA-Ub-PA for screening as this binds more proteins and would allow for retrieval of more DUBs from the lysate than HA-Ub-VME. For the incubation conditions, a concentration of 1:100 (probe: protein) and incubation time of 45 mins were selected. However, it was clear that individual DUBs have different probe-reactivity which would require specific optimisation if interrogating behaviour of a DUB using specific antibodies.

4.4 Profiling of probe-reactivity in SFV infected HeLa cells

It was next important to test this protocol in alphavirus infected cells which would also give an impression as to whether probe-reactivity is altered following infection, either by viral hijacking or for host defence. In this initial experiment, the model alphavirus SFV was used in order to establish the protocols for using ABPs in virus infected cells whilst working in CL2 conditions. HeLa cells were mock-infected or infected with SFV at an MOI of 10 then harvested at 1, 2 and 4 hrs p.i. for ABP assays. A short time-course was selected to monitor any changes in probe-reactivity during virus replication and to give a sense of how soon these changes may occur after virus infection. Lysate was then probed with HA-Ub-PA at 1:100 (probe: protein) for 45 mins, as per the optimised conditions described in section 4.3. Immunoblot analysis of HA was performed to provide a binding profile of probe reactive proteins (Figure 4.6A). Intensity plots were also produced to aid visualisation of changes in band intensities (Figure 4.6B).

As seen in the optimisation experiments with a 45 min incubation, probe binding was strongest for the larger molecular weight proteins. A very similar binding pattern for the PA probe was observed across the whole time-course of viral infection. However, a slight increase in HA intensity can be seen between mock infected and 1 hr p.i. with SFV. This is particularly noticeable for the two prominent bands above the 102kDa marker and is reflected in the intensity plot as higher peaks for this area. Some variation in

individual bands can also be seen at the 4 hr time-point. For example, the bands in the region ~52–76kDa appear to be weaker in the 4 hr lane compared to mock. Quantification of the HA signal normalised to ACTB (Figure 4.6C) revealed that, although minor, the total HA intensity was beginning to show a trend towards a decrease as the infection progressed. This suggested that the decrease in intensity of the HA-immunoreactive bands described above were due to changes in probe-reactivity and not simply due to minor loading differences.

As described above, it is also possible to make predictions as to which DUBs certain bands may represent, based on the predicted MW of the DUBs. For example, the strong bands above the 102kDa marker, alluded to above, could represent USP4, USP11 or USP15. These are DUBs with a predicted weight (+ABP) between 106-123kDa and have been shown to bind the ABPs well in previous studies (Ekkebus *et al.*, 2013). In addition, the bands between 52–76kDa could represent the DUBs OTUD3, MINDY1, OTUD1, USP14, USP30, USP3 or USP21. This could therefore suggest that these DUBs are increasing or decreasing in probe-reactivity, respectively, following alphavirus infection. To confirm this, predicted DUBs would need to be investigated with specific antibodies. However, as the aim of this experiment was simply to validate the protocols in virus-infected cells, this was not done here. In addition, as no extra bands were seen in virus infected samples, this suggests that alphaviruses do not encode a DUB that reacts with these ABPs.

To monitor virus replication, the expression of SFV nsP1 was also analysed by immunoblot using ACTB as a loading control (Figure 4.6D). SFV nsP1 expression was not detected at 1 or 2 hrs p.i. but by 4 hrs there was a strong band indicating good viral replication. Taken together, the data from cells infected with the model alphavirus, SFV, demonstrated that ABPs could be used in the context of alphavirus infection to measure probe-reactivity. These findings were therefore considered sufficient before moving on to the more clinically relevant CHIKV.

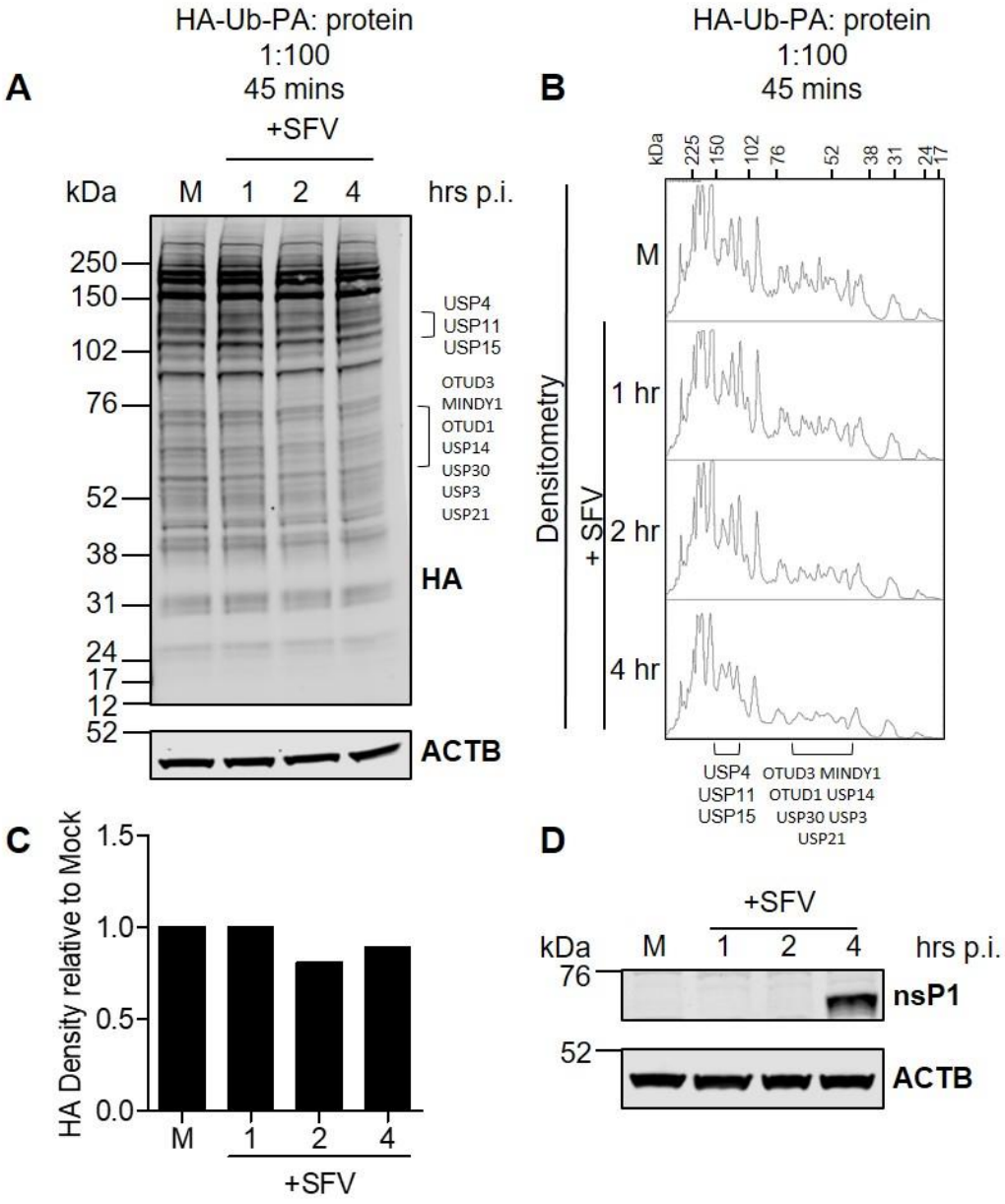

Figure 4.6. DUB reactivity profiling in SFV infected HeLa cells
HeLa cells were infected with SFV at an MOI of 10 and harvested at 1, 2, and 4 hrs p.i. (**A**) 15 µg of non-denatured HeLa lysate was incubated with HA-Ub-PA at 1:100 for 45 mins. Samples were resolved by SDS-PAGE on a 4-12% gradient gel and global DUB binding was visualised by immunoblotting for HA. Predicted DUB candidates are highlighted. (**B**) Intensity plots of HA immuno-staining were generated using Fiji. Predicted DUB candidates are highlighted. (**C**) Quantification of HA intensity plots, shown in part B, were calculated and normalised to ACTB. (**D**) Analysis of the SFV viral protein nsP1 was monitored by immunoblot.

4.5 Utilising ABPs to investigate potential deubiquitylase activity in CHIKV nsP2

4.5.1 Monitoring CHIKV infection in HeLa cells

Having established the techniques using SFV at CL2, this approach could now be used to study changes in probe-reactivity following CHIKV infection at CL3. It was first important to establish the appropriate conditions to monitor changes in probe-reactivity during CHIKV replication. HeLa cells were infected with CHIKV at 5 MOI and harvested for denaturing protein extraction at 2 hr intervals to a maximum of 10 hrs p.i.. CHIKV nsP1 expression was analysed as a measure of virus replication by immunoblotting (Figure 4.7A) then quantified using densitometry in Fiji (Figure 4.7B). CHIKV nsP1 expression could not be detected until 4 hrs p.i., but by 6 hrs high expression was observed. Expression then plateaued between 8 and 10 hrs p.i.. This is in line with published data showing that CHIKV nsP1 expression generally peaks at approximately 10 hrs p.i. while structural proteins continue to be produced, before reaching a maximum expression around 12 hrs p.i.. A shut-off of cellular translation and transcription has been shown to occur at 8 and 10 hrs p.i., respectively (Scholte *et al.*, 2013). Furthermore, the host cellular response to alphaviruses has been shown to be induced by 4 hrs p.i. (van Duijl-Richter *et al.*, 2015). For time-course experiments it was therefore decided to use time-points between 4 and 10 hrs p.i.. This would allow for analysis during active virus replication, incorporating both early and late stages, while also providing a good window for observing any host-cell responses.

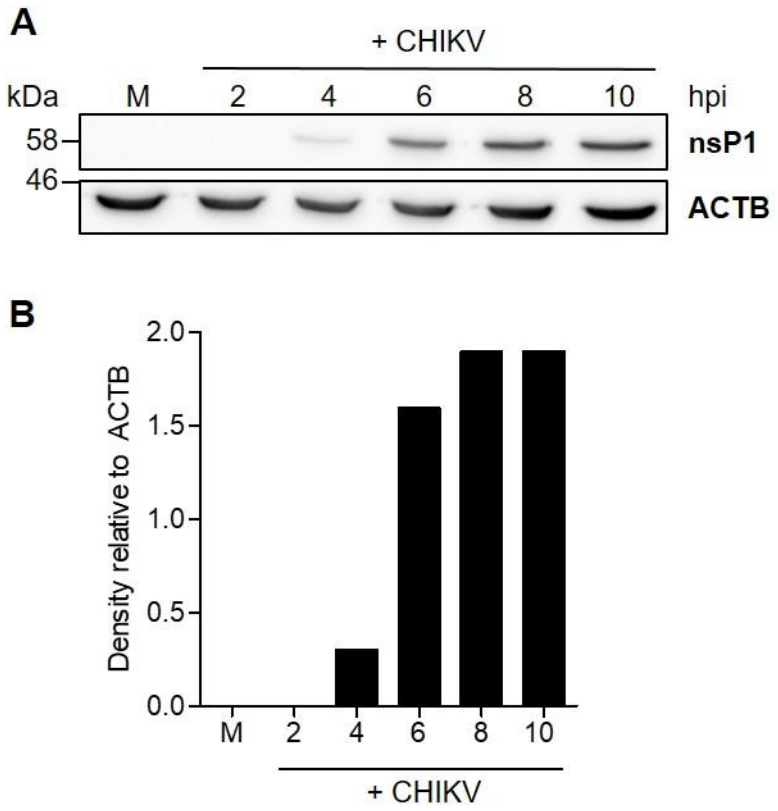

Figure 4.7. Monitoring CHIKV infection in HeLa cells
(**A**) HeLa cells were infected with CHIKV at an MOI of 5 and harvested at 2, 4, 6, 8 and 10 hrs p.i.. Protein was extracted for analysis of the CHIKV viral protein nsP1 by immunoblot. (**B**) Expression of CHIKV nsP1 was calculated using densitometry and is presented as density relative to ACTB.

4.5.2 Exploring deubiquitylase activity of CHIKV nsP2

As discussed in section 1.5.5 it is well known that viruses can encode their own proteins with DUB activity, in addition to manipulating host-cell DUBs. The alphavirus nsP2 is a cysteine protease and therefore the viral protein of interest when looking for DUB activity (Ramakrishnan *et al.*, 2017). To investigate the presence of alphavirus DUB activity, HeLa cells were mock-infected or infected with CHIKV at 5 MOI and harvested at 10 hrs post infection for non-denaturing lysis. A 10 hr time-point was chosen to allow sufficient production of viral protein to perform ABP assays with. The viral DUBs discovered to date can be categorised into several different DUB

family domains (Bailey-Elkin *et al.*, 2017). In addition, the ABPs have previously been shown to have different binding preferences for certain DUB families and DUBs themselves vary in their reactivity towards the probes. Thus, by using a range of incubation conditions with both HA-Ub-VME and HA-Ub-PA, there was a greater likelihood of being able to detect any DUB activity in nsP2. A short (5 min) and long (45 min) incubation time was utilised for each probe at a probe: protein ratio of 1:100 followed by immunoblot analysis of nsP2 and ACTB. As the probes are approximately 10kDa, any protein it binds therefore migrates slower through the gel matrix and appears ~10kDa heavier than its predicted weight. There were no apparent size shifts for CHIKV nsP2 following incubation with either HA-Ub-VME (Figure 4.8A) or HA-Ub-PA (Figure 4.8B) under any of the conditions tested.

As a positive control, the DUB USP15 was immunoblotted, as it is approximately the same size as nsP2 and is known to bind well to the ABPs. The expected size shift (marked with an *) can be seen for USP15 in Figure 4.8. For USP15, submaximal binding for both HA-Ub-VME and HA-Ub-PA can be seen at 5 mins which has become saturated at 45 mins with all available USP15 bound to the probe. This demonstrates that CHIKV nsP2 lacks probe reactivity under these conditions and is unlikely to have DUB activity. However, only one time-point p.i. was monitored here and it can therefore not be ruled out that there may be DUB activity at a different stage of infection.

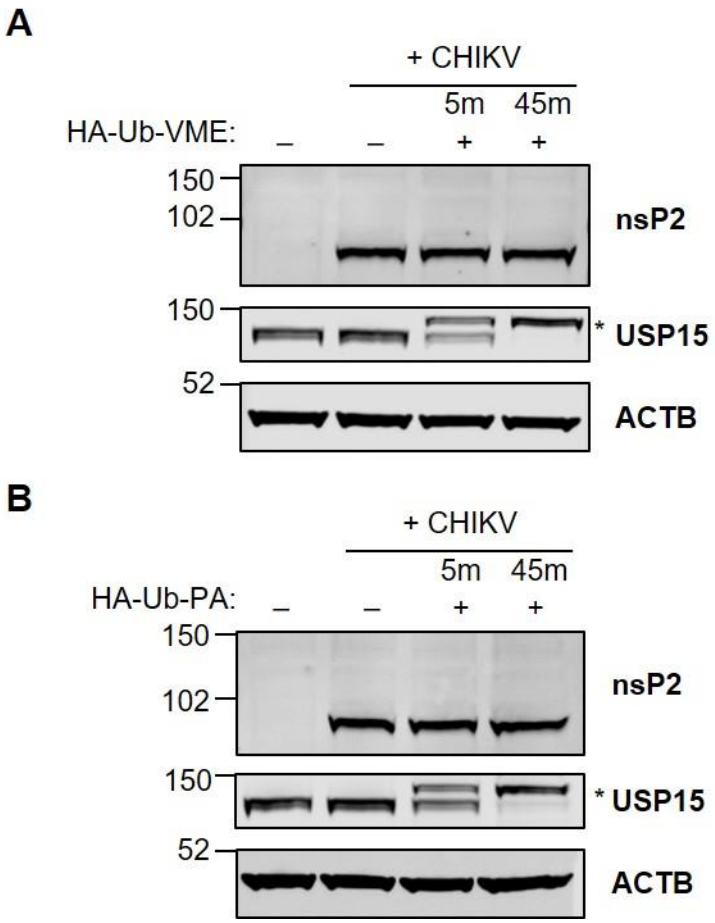

Figure 4.8. CHIKV nsP2 does react with the DUB ABPs HA-Ub-VME or HA-Ub-PA
HeLa cells were infected with CHIKV at an MOI of 5 and harvested 10 hrs p.i.. 15 µg of non-denatured HeLa lysate was probed for 5 and 45 mins at 1:100 with either HA-Ub-VME (**A**) or HA-Ub-PA (**B**). Samples were resolved by SDS-PAGE on a 4-12% gradient gel then nsP2, USP15 and ACTB were visualised by immunoblotting. * indicates the probe-bound protein.

4.6 Summary

ABPs have been shown to be powerful tools for identifying DUBs of therapeutic interest for virus infections while avoiding the inherent limitations of loss-of-function studies (Ovaa *et al.*, 2004; Mohr *et al.*, 2010). In addition, they have also been used to identify and characterise viral DUBs (Balakirev *et al.*, 2002; Abdul Rehman *et al.*, 2016; Kwasna *et al.*, 2018). However, ABPs have not previously been used in the context of alphavirus infection.

Therefore, it was necessary to optimise the incubation conditions for the two probes used in this thesis: HA-Ub-VME and HA-Ub-PA. Both the probe concentration (probe: protein ratio) and incubation time were tested in HeLa cell lysate. Probe binding was monitored by immunoblot analysis of the N-terminal HA tag and revealed differences in the binding profiles for each probe. A difference in binding patterns was also observed for high and low molecular weight proteins at different incubation times. This highlighted the need to further optimise the conditions for particular DUBs which are to be individually investigated. However, for initial screening experiments it was decided to continue with the PA probe at an incubation tine of 45 mins and a 1:100 (probe: protein) ratio.

This approach was next tested in lysate generated from HeLa cells infected with the model alphavirus, SFV. A short time-course was selected to provide an overview of changes in probe-reactivity following alphavirus replication during a phase of active viral replication. Overall, there was very little change in total probe reactivity over the course of infection. However, some changes for individual bands were visible suggesting that changes in probe-reactivity could be observed with this approach. Furthermore, comparison of the binding patterns from infected cell lysate revealed no obvious additional bands following SFV infection. This gave an initial indication that alphaviruses are unlikely to possess DUB activity within their viral proteins.

Following establishment and optimisation of these protocols at CL2 it was then possible to move into the more clinically relevant virus, CHIKV, at CL3. Firstly, the kinetics of CHIKV replication in HeLa cells was monitored to ensure a suitable time-course of infection was selected for observing changes in probe-reactivity. Immunoblot analysis of CHIKV nsP1 revealed that expression of this viral protein was clearly detectable after 4 hrs and peaks at approximately 8 hrs p.i.. This was used to decide an appropriate time-course for future experiments with CHIKV as between 4 and 10 hrs to enable monitoring of changes during active virus replication (see chapter 5).

Finally, both HA-Ub-VME and HA-Ub-PA were also used to probe for potential DUB activity in CHIKV nsP2. Protein lysate from HeLa cells infected with CHIKV for 10 hrs was probed with at 1:100 (probe: protein) for either 5 or 45 mins. By using a range of conditions it increased the probability of detecting any probe-reactivity in nsP2, as the different probes have alternative binding preferences depending on the structure of the active site. Under these conditions, no probe reactivity of nsP2 was detected while a host DUB, USP15, provided a positive control to demonstrate the probing experiment had worked. Whilst these results suggest that CHIKV is unlikely to encode a DUB, the possibility of probe-reactivity being detected with a different probe or at a different time p.i. cannot be ruled out.

Taken together, the work presented in this chapter enabled the optimisation for use of ABPs in screening experiments to monitor changes in probe-reactivity following alphavirus infection. These protocols were tested in lysate from HeLa cells infected with the model alphavirus, SFV, and confirmed the feasibility of this approach in a CL2 setting. The potential for CHIKV to encode its own DUB was also investigated using the ABPs and it appears unlikely that CHIKV encodes a viral DUB.

Chapter 5: Unbiased profiling of deubiquitylase probe-reactivity following Chikungunya virus infection using activity based proteomics

5.1 Introduction

The proteome was first described in 1996 by Wilkins *et al* and was used to refer to the complement of proteins expressed by the genome. Proteomics was therefore considered the study of proteins on a large scale (Wilkins *et al.*, 1996). In the intervening time this term has evolved to include not only the study of the protein complement of a cell, but a much more complex examination of protein biology. For example data can now be obtained for: different isoforms, modifications, structures and protein-protein interactions (Tyers & Mann, 2003; Aebersold & Mann, 2016). The most commonly used proteomic technique is mass spectrometry, which allows for a high-throughput investigation of all proteins within a system and has proved invaluable for unbiased screening at the protein level. By ionising a sample and measuring the number of ions at each mass: charge ratio, a detailed image of its composition can be obtained. Proteins in a sample can either be measured using “bottom-up” or “top-down” proteomics which utilise digested peptides or intact proteins, respectively (Kelleher *et al.*, 1999). Bottom-up analyses are more commonly used owing to the increased sensitivity, ease of automation and the availability of comprehensive analysis software. Typically, highly specific proteases which cleave at known amino-acid residues are used to create peptides. For example trypsin is often used which cleaves proteins at the C-terminal of every arginine and lysine residue. This creates a mixture of peptides approximately 20 residues in length which can be accurately identified (Aebersold & Mann, 2003; Vandermarliere *et al.*, 2013).

Mass spectrometry can be split into three main stages. Ionisation of a sample is the first stage and is responsible for adding charges to the molecules by removing one or more electrons. This charge allows the ions to

be deflected in the mass analyser, the second stage, which separates the sample. The extent to which ions are deflected is dependent on both their mass and charge. For example ions which are lighter or possess more positive charges are deflected to a greater degree than heavier ions or those with fewer positive charges. When the ions reach the third stage, the ion detector plate, an electrical current is produced which generates a mass: charge ratio spectra. To further analyse and identify the peptides in a sample, tandem mass spectrometry (MS/MS) can be used. This involves addition of a fragmentation step and further rounds of mass spectrometry. An MS/MS spectrum is then produced which can be compared against sequence databases in order to identify the proteins within a sample (Johnson *et al.*, 1990; Hunt *et al.*, 1992; Henzel *et al.*, 2003).

Further quantitative information can be obtained by using techniques which allow for multiplexing, where the mass: charge ratios for several samples can be compared simultaneously. A commonly used technique is Stable Isotope Labelling with Amino Acids in Cell Culture (SILAC). This is a non-radioactive method for labelling cells via metabolic incorporation of amino acids with different stable isotopes. For example, cells can be grown in media containing arginine labelled with carbon-13 (^{13}C) instead of the usual carbon-12 (^{12}C). Thus, as a six-carbon amino acid, arginine-containing peptides will be 6 Da heavier than their unlabelled equivalent. In triplexing experiments, amino acids can be made even heavier, for example by incorporation of nitrogen-15 (^{15}N) in place of the normal nitrogen-14 (^{14}N). In the case of arginine, a four-nitrogen amino acid, peptides will be 4 Da heavier than unlabelled peptides. Therefore, it is possible to have populations of cells labelled with light (^{12}C, ^{14}N), medium (^{13}C, ^{14}N) and heavy (^{13}C, ^{15}N) arginine. If trypsin is to be used in SILAC experiments to digest proteins, a mixture of isotopically labelled lysines and arginines are usually used. This ensures that each peptide will have a different isotopic mass owing to the fact that trypsin will cleave at every lysine and arginine residue (Ong *et al.*, 2002).

There have been several studies utilising a proteomics approach to study CHIKV in both experimentally infected cells or animals, and in patient-derived samples. The first study to perform a proteome analysis following

CHIKV infection identified several proteins that were differentially expressed in liver and brain tissue from mice. These could be functionally classified into different groups, predominantly: stress inflammation, apoptosis and energy metabolism (Dhanwani *et al.*, 2011). Another group performed a screen of CHIKV infected SILAC-labelled 293 cells and identified several proteins which exhibited changes in expression over the course of infection. The majority of these exhibited a decrease in abundance with the four most differentially expressed proteins identified as: RND3, DDX56, PLK1 and UBCH10 (Treffers *et al.*, 2015). Another study found 90 proteins to be significantly down regulated in CHIKV infected human microglial cells, including the E3 ligase BRE1B (Abere *et al.*, 2012). The first report of differential DUB expression following alphavirus infection also came from a proteomic screen. Fraisier and colleagues identified Usp13 as being down-regulated in mice following infection with CHIKV (Fraisier *et al.*, 2014). As well as proteome analysis in artificially infected samples, differential protein expression has also been monitored in clinical samples from infected patients. For example, Wikan *et al* compared the proteome of white blood cells extracted from patients with CHIKF and to febrile non-CHIKF patients. They identified 240 proteins which were upregulated in CHIKV infected patients and 68 proteins which were downregulated, many of which mapped to cellular signalling pathways. In addition, expression of proteins associated with inflammasome activation were linked to the severity of the disease (Wikan *et al.*, 2014).

The proteomic studies mentioned above have focussed on looking at the whole proteome which provides useful information about global changes in protein expression following infection. However, proteomics studies tend to identify the most abundant proteins within the proteome meaning less abundant proteins may be missed without enrichment strategies (Cho, 2007; Mulvey *et al.*, 2010). Taking a more targeted approach to look at specific groups of proteins can provide a more detailed insight of a system of interest. In addition, protein function can be regulated in a variety of ways other than changes in expression, for example through post-translational modifications, proteolytic cleavage or allosteric regulation (Kobe & Kemp, 1999). Novel

tools such as ABPs (described in chapter 4) have facilitated this by providing new methods of screening particular groups of proteins, such as DUBs. By combining the use of ABPs with a proteomic approach, it is possible to enrich a sample for probe-reactive proteins by pull-down in order to monitor changes in their reactivity or expression level. The use of ABPs could also indicate potential changes in activity and could therefore identify proteins for which their function may be altered, but not necessarily their abundance. This is an approach which has been gaining in popularity and has been used to identify DUBs involved in a range of diseases. For example, Ovaa and colleagues utilised ABPs to identify a number of DUBs upregulated in cancer or EBV infected cells (Ovaa *et al.*, 2004). Also, Kummari *et al* used ABPs to identify DUBs which were involved in inflammasome regulation during *Salmonella* infection of chicken macrophages (Kummari *et al.*, 2015). However, there are currently no examples of this approach being utilised in the context of alphavirus infection.

5.2 Aims

Combining ABPs with a proteomic approach provides a powerful unbiased technique to investigate the functionality of DUBs. Furthermore by incorporating SILAC-labelled cells it is possible to simultaneously quantify the peptides in a sample to provide a quantitative comparative analysis. Therefore, the aims of this chapter were:

1. To assess the enrichment of probe-reactive DUBs in uninfected HeLa cells for analysis by tandem mass spectrometry.
2. To monitor changes in probe-reactivity of DUBs in SILAC-labelled HeLa cells following CHIKV infection by tandem mass spectrometry.
3. To investigate the role of DUBs identified in aim 2 for their role during alphavirus infection.

5.3 Validation of mass spectrometry protocols in unlabelled HeLa cells

It was first important to carry out an initial screen to validate the immunoprecipitation and mass spectrometry approach to be used in this study. Identification of proteins through mass spectrometry typically requires large quantities of protein to ensure an accurate identification. It was therefore necessary to scale-up the ABP probing protocols used in chapter 4 in order to obtain sufficient protein. Here it was decided to use 500 µg protein based on examples from within published literature (Altun *et al.*, 2011; Ward *et al.*, 2016). An initial test of the probing and immunoprecipitation protocols was performed to ensure that the binding efficiency of the probes was not affected by this increase in scale and that the immunoprecipitation was efficiently enriching the sample for probe-bound proteins. The proteins eluted from the immunoprecipitation were then identified by mass spectrometry to confirm DUBs were detectable with this approach.

As described in chapter 4, each DUB is likely to have a different optimal probe reactivity which would require specific optimisation. However, the aim of the initial mass spectrometry experiments was to detect the maximum possible number of DUBs from the sample, thus allowing for identification of DUBs for further investigation. Therefore, the probing conditions were selected according to the optimised conditions described in section 4.3 for identification of the maximum number of DUBs. The HA-Ub-PA probe was used as this bound more targets in my earlier experiments (Figure 4.2B and 4.3B), and there are published findings demonstrating the ability of this probe to bind to all families of cysteine proteases (Ekkebus *et al.*, 2013; Abdul Rehman *et al.*, 2016; Haahr *et al.*, 2018; Kwasna *et al.*, 2018). Therefore, HeLa cell lysate was incubated with the HA-Ub-PA probe at 1:100 (probe: protein) for 45 mins. The reaction was terminated with SDS before anti-HA beads were used to immunoprecipitate probe-bound proteins from the lysate.

Samples were taken at each step of the immunoprecipitation protocol for immunoblot analysis of HA (Figure 5.1). This was to both confirm that

scaling-up of the probing protocols did not affect binding efficiency and that probe-bound proteins were sufficiently enriched from the lysate. The samples were taken from the: input, pre-clear, flow-through, washes 1-4, elution and stripped stages. Samples taken immediately after termination of the probing reaction, prior to immunoprecipitation, are termed 'input'. The input lane (2% of the total sample) exhibits a similar binding pattern as seen in the total HA profile plots in chapter 4 (Figure 4.4B). This indicates that scaling up the reaction for the mass spectrometry protocol does not affect the efficiency of probe binding and that the conditions are suitable for this experiment. The pre-clear lane (1.5% of the total sample) represents the stage at which the samples have been incubated with protein-G beads to remove potentially reactive non-specific components. Although the signal is slightly weaker, the binding is very similar to the input, demonstrating that very few probe-reactive proteins have been lost at this stage. Lanes 3-7 represent samples taken from the flow-through and washes following incubation of the lysate with anti-HA beads and should therefore have little or no HA signal. Indeed this is what is observed, confirming that the washes are not eluting any of the probe-reactive proteins from the beads. Following elution of the proteins from the beads another sample was taken and the immunoblot analysis demonstrates that a good proportion of probe-reactive proteins are present in the eluted sample. Furthermore, after stripping of the beads there is very weak HA signal. Although there is a strong band at ~30kDa in the 'stripped' lane this is likely to represent a highly abundant protein which is not completely removed from the beads. However, the presence of a strong band of equivalent size in the 'eluted' lane indicates that the majority of this protein was removed from the beads. This demonstrates that the elution was efficient at removing the majority of probe-reactive proteins from the beads. In addition, the input, preclear and flow-through samples show ACTB staining as expected, which is not visible in the other lanes. This confirms that the other non-probe-reactive proteins in the lysate have been removed by the immunoprecipitation protocol.

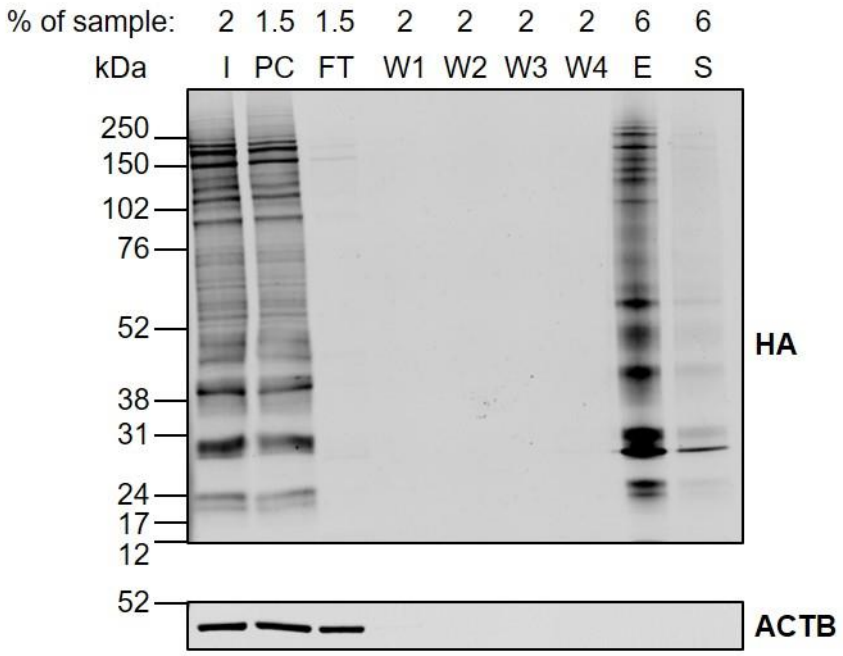

Figure 5.1. Analysis of immunoprecipitation to enrich for probe-bound proteins in unlabelled HeLa cells
Unlabelled HeLa cells were harvested and lysed under non-denaturing conditions and 500 µg lysate probed with Ha-Ub-PA at 1:100 for 45 mins. DUBs were enriched from the lysate by immunoprecipitation with anti-HA beads. Samples taken at each stage were separated on by SDS-PAGE on a 4-12% gradient gel followed by immunoblot for HA and ACTB. The % of sample taken at each stage is shown above each lane. I – input, PC – pre-clear, FT – flow-through, W1 – wash 1, W2 – wash 2, W3 – wash 3, W4 – wash 4, E – eluted, S – stripped.

Eluted proteins were then digested with trypsin and prepared for mass spectrometry. To identify probe-bound proteins the processed peptides were analysed by liquid chromatography tandem mass spectrometry (LC-MS/MS) on a LT Orbitrap XL mass spectrometer (University of Liverpool). This identified 65 probe-reactive proteins in total, of which 15 were DUBs (Appendix Table 1). Of the 50 other proteins identified, there were eight which were not identified as common contaminants from the agarose CRAPome (Mellacheruvu *et al.*, 2013). These could have been pulled down due to non-specific binding of the probes or as interactors with the DUBs, however they were not followed up further here. The DUBs are listed in Table 5.1 and the ranked intensities for each DUB presented in Figure 5.2A. Multiple peptides were identified for all DUBs except USP19 for which only

one peptide was detected. The DUBs identified represent three of the cysteine protease families: USP, UCH and OTU of which the USPs were most abundant (Figure 5.2B). As the USP family consists of the most members, this was in line with what would be expected. Furthermore, as described in section 4.1 these ABPs are not capable of reacting with JAMM domains therefore, as expected, no DUBs from this family were detected.

Table 5.1. DUBs bound to HA-Ub-PA identified by LC-MS/MS in unlabelled HeLa cells

DUB	Family	No. of peptides
OTUB1	OTU	5
OTUD6B	OTU	2
VCPIP1	OTU	2
UCHL3	UCH	6
UCHL5	UCH	11
USP19	USP	1
USP11	USP	4
USP8	USP	2
USP5	USP	25
USP14	USP	14
USP4	USP	6
USP9X	USP	22
USP7	USP	26
USP47	USP	6
USP15	USP	9

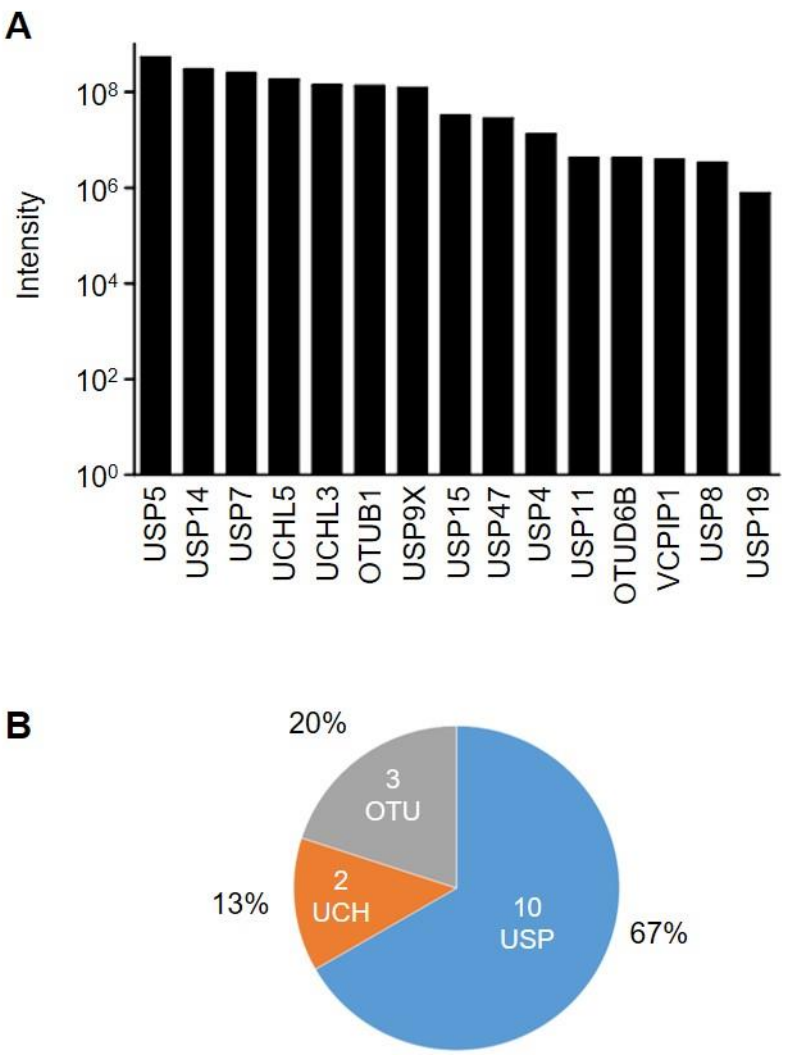

Figure 5.2. DUBs identified in unlabelled HeLa cells by MS
Unlabelled HeLa cells were harvested and lysed under non-denaturing conditions and 500 µg lysate probed with Ha-Ub-PA at 1:100 for 45 mins. DUBs were enriched from the lysate by immunoprecipitation with anti-HA beads. The samples were digested with trypsin and the peptides identified by LC-MS/MS analysis. Ranked intensities are presented in (**A**) and the proportion of DUB families identified are shown in (**B**).

In summary, the scaled-up protocols for ABP probing in HeLa cell lysate and subsequent pull-down of probe-bound proteins by immunoprecipitation were tested. This demonstrated that scaling-up of the ABP probing protocols did not affect probe-binding and that immunoprecipitation adequately enriched the sample for probe-bound proteins. Furthermore, the mass spectrometry analysis confirmed that DUBs from several cysteine protease families could be detected using this protocol.

The DUBs detected represent the three most abundant cysteine protease families and although there is an apparent bias towards USP DUBs, this is likely to be as this is the family with the most members. In addition, although fewer total DUBs were detected when compared to other studies, all of the DUBs identified here were also identified in HeLa cells by others using ABPs with a PA warhead (Lawson *et al.*, 2017; Gui *et al.*, 2018).

5.4 Monitoring changes in probe-reactivity in CHIKV infected SILAC-labelled cells

To identify changes in DUB probe-reactivity following CHIKV infection, mass spectrometry was coupled with SILAC. The outline for this approach is shown in Figure 5.3. Utilising a triplexed SILAC approach it was possible to use three different cell populations which are labelled with isotopically heavier arginine (R) and lysine (K). SILAC labelling efficiency had been tested and demonstrated that labelling of R and K was >97% (SILAC labelling and testing carried out by Fiona Hood). This allowed for a quantitative comparison of the mass: charge ratios of peptides from different cell populations. HeLa cells were pre-labelled with different SILAC isotopes for light (K0, R0), medium (K4, R6) or heavy (K8, R10) amino acids then maintained in the relevant media. In a triplex configuration, labelled cells were mock-infected or infected with CHIKV and harvested at 4, 6, 8 and 10 hrs p.i.. These time-points were selected to enable observation of probe-reactivity at various stages of the virus life-cycle. HeLa cells labelled with light amino acids were always designated as the mock-infected controls to allow for quantitative comparison of infected cells relative to mock. To achieve this for all time-points, two mock-infected samples were harvested to enable two groups of triplexed samples to be analysed. Group A contained mock, 4 hr and 6 hr samples then Group B contained mock, 8 hr and 10 hr samples. This was done on a large enough scale to provide 500 µg of protein lysate for probing with HA-Ub-PA. However, it should be noted that for experiment 3 the grouping was altered to take into account an issue with insufficient protein yield from one time-point (8 hr). Therefore, in experiment

3 the grouping was changed so that group 1 contained Mock, 4 hr and 10 hr (with the intended 500 µg of protein) while group 2 contained Mock, 6 hr and 8 hr (with 250 µg protein).

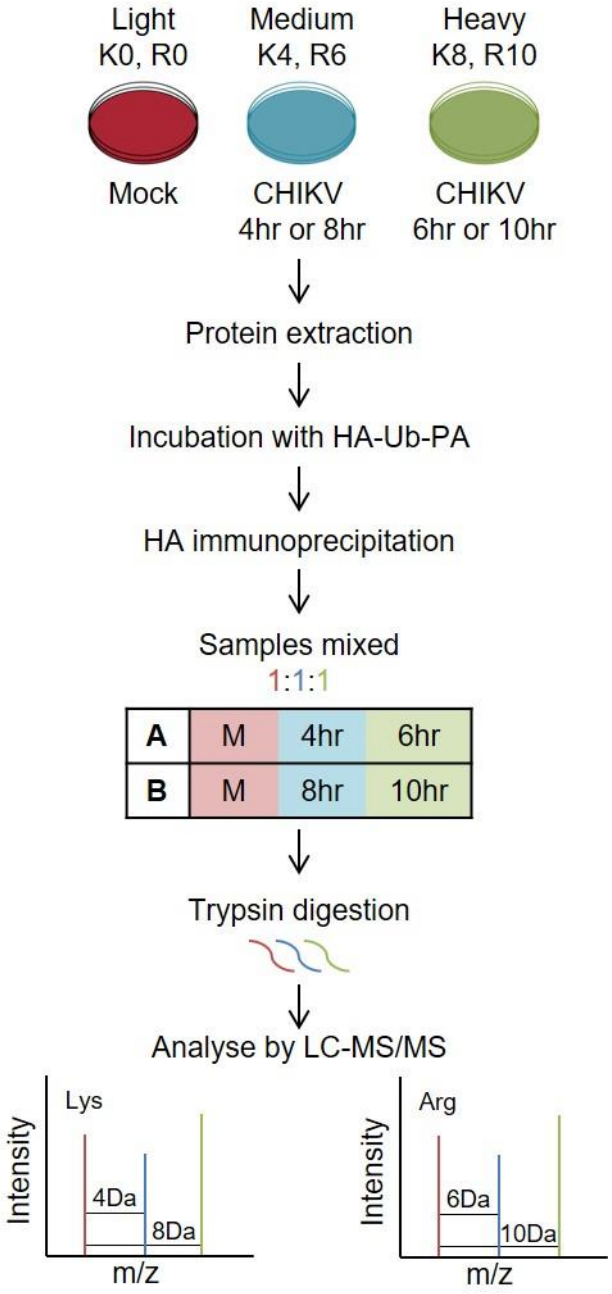

Figure 5.3. Schematic of experimental strategy to identify changes in probe-reactivity of DUBs following CHIKV infection
SILAC labelled HeLa cells were used to quantitatively analyse DUB probe-reactivity following CHIKV infection by LC-MS/MS using the ABP, HA-Ub-PA. Red, blue and green colours represent light, medium and heavy samples, respectively.

Immunoblotting was carried out for CHIKV nsP1 prior to processing for mass spectrometry to confirm that there was efficient virus infection. NsP1 was readily detected for each experiment, thus confirming that CHIKV replication has occurred (Figure 5.4). A similar pattern of nsP1 production was observed for each experiment, with nsP1 first being detected between 6 and 8 hrs p.i. and a strong band representing nsP1 at 10 hrs. However, there was some variation between experiments. For example, the 8 hr time-point exhibited varying intensities of nsP1 expression. In addition, experiment 3 was the only example of nsP1 being detected at 6 hrs p.i., albeit faintly, under these conditions. However, similar viral replication was visible for each experiment. It was therefore decided that this was sufficient to justify proceeding with analysis of the samples for probe-reactivity.

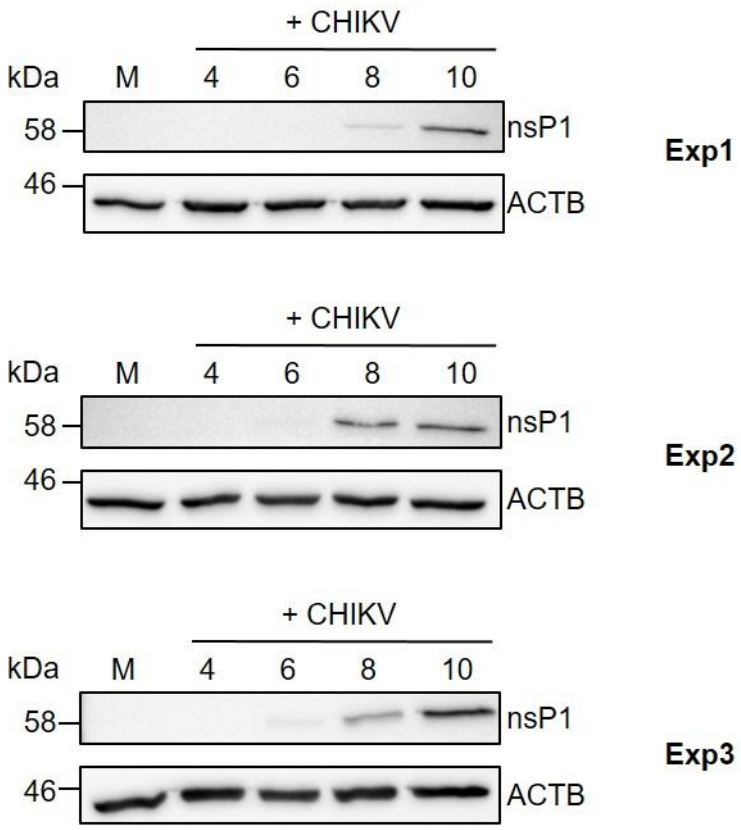

Figure 5.4. Monitoring of CHIKV nsP1 expression in SILAC labelled HeLa cells infected with CHIKV
SILAC labelled HeLa cells were mock infected or infected with CHIKV at 5 MOI then harvested at 4, 6, 8 or 10 hrs p.i.. Protein was extracted under non-denaturing conditions and CHIKV nsP1 protein was analysed by immunoblot. ACTB was used as a loading control. Each individual experiment is shown.

HeLa lysate was then incubated with HA-Ub-PA at 1:100 (probe: protein) for 45 mins to ensure that the maximum number of DUBs could be detected (as described in section 5.2). The reactions were terminated then HA immunoprecipitation used to enrich the samples for probe-bound proteins. Validation of the immunoprecipitation protocol was performed again here to confirm that probe-reactive proteins were being efficiently enriched from the lysate. Samples were taken at each stage of the immunoprecipitation protocol and immunoblot analysis for HA was performed. Figure 5.5 shows all the samples for group B from experiment 1 (Mock, 8 hrs and 10 hrs p.i.). The data are as described in section 5.3 and demonstrate that the immunoprecipitation protocol has worked efficiently. For the remaining experiments the elution samples (representing 6% of the total) were analysed together to confirm that there were probe-reactive proteins remaining prior to mass spectrometry analysis (Figure 5.6). All samples show strong HA signal and a similar pattern although there is some variation in intensity between experiments. However, as a quality control step the data demonstrated that the immunoprecipitation protocol had worked and was considered sufficient to send samples for mass spectrometry analysis.

Eluted proteins were digested with trypsin and prepared for mass spectrometry. In order to increase the number of detectable probe-bound proteins, samples were sent to Warwick Scientific Services for analysis on a higher resolution mass spectrometer. Here, analysis was performed by LC-MS/MS on an Orbitrap Fusion instrument (ThermoFisher) which is capable of generating spectra at a higher resolution than the LTQ Orbitrap XL (ThermoFisher) used in the preliminary experiment. This results in better definition between mass spectral peaks and improves the ability to distinguish peaks of similar a mass (Kelleher *et al.*, 1999; Kellmann *et al.*, 2009). RAW files were returned for analysis by MaxQuant. In total 192 probe-reactive proteins were identified, of which 24 were DUBs for which multiple peptides were identified (Appendix Table 2). This is an approximate 3-fold increase for total number of proteins and 1.5-fold increase for number of DUBs compared to samples analysed in-house (Table 5.1). From the

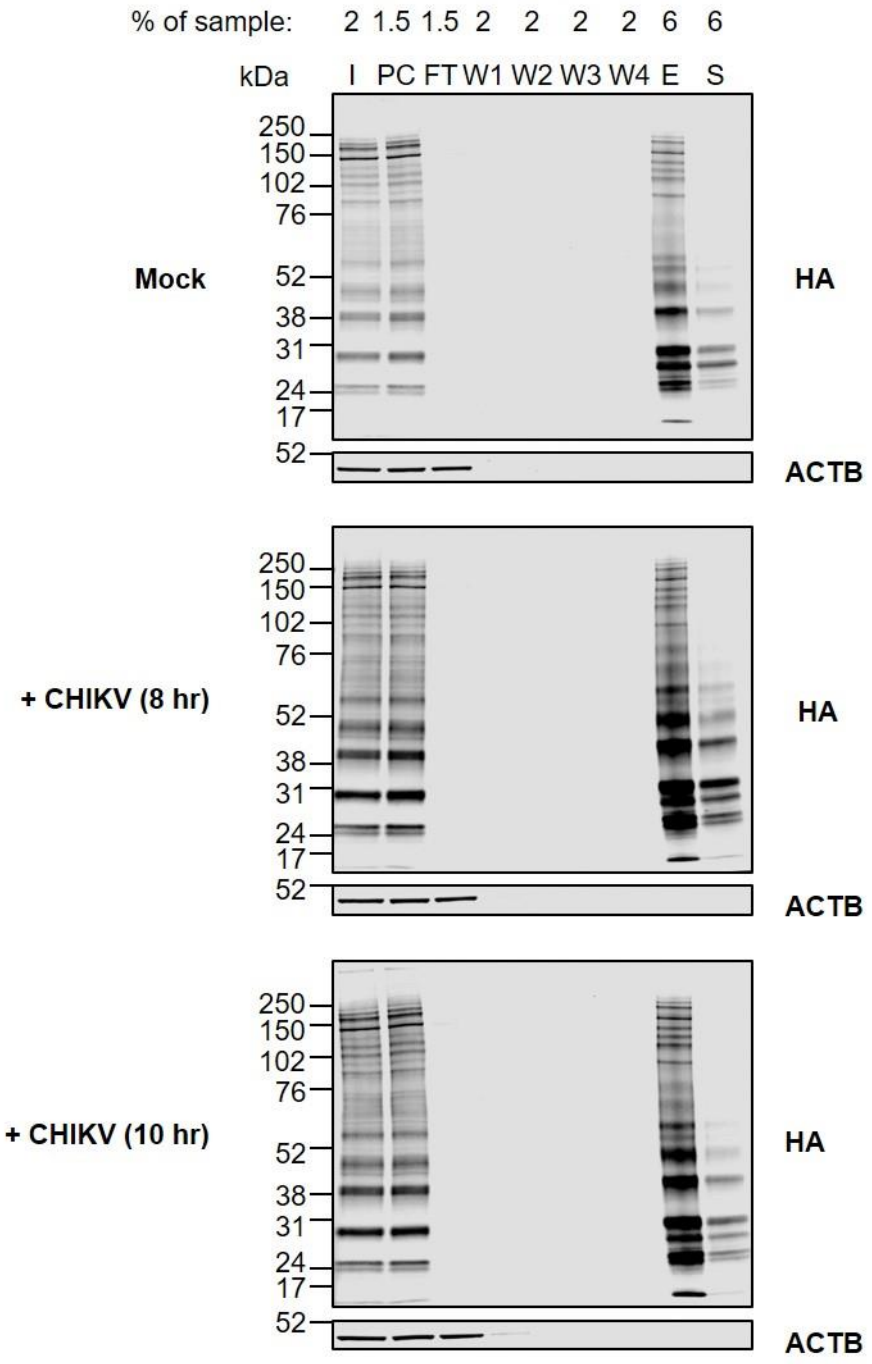

Figure 5.5. Analysis of efficiency of immunoprecipitation to enrich for DUBs in SILAC labelled HeLa cells

SILAC labelled HeLa cells were infected (or mock) with CHIKV at 5 MOI then harvested at 8 or 10 hrs p.i. and lysed under non-denaturing conditions. 500 µg lysate was probed with Ha-Ub-PA at 1:100 for 45 mins. DUBs were enriched from the lysate by immunoprecipitation with anti-HA beads. Samples taken at each stage were separated on by SDS-PAGE on a 4-12% gradient gel followed by immunoblot for HA and ACTB. The percentage of sample taken at each stage is shown above each lane. I – input, PC – pre-clear, FT – flow-through, W1 – wash 1, W2 – wash 2, W3 – wash 3, W4 – wash 4, E – eluted, S – stripped.

other proteins identified, once common contaminants of the agarose CRAPome (Mellacheruvu *et al.*, 2013) had been excluded, there were 10 proteins which could either be non-specific binders of the probes or DUB interactors. These were not investigated further here, however see section 6.5 for further discussion of these proteins. Furthermore, two different isoforms for UCHL5 were identified which have been labelled here as UCHL5_A and UCHL5_B. There are four known isoforms for UCHL5, the main one being Isoform 1 which is labelled as UCHL5_B in this data. For UCHL5_A there was insufficient information from the peptides detected to identify the isoform (Appendix Table 3).

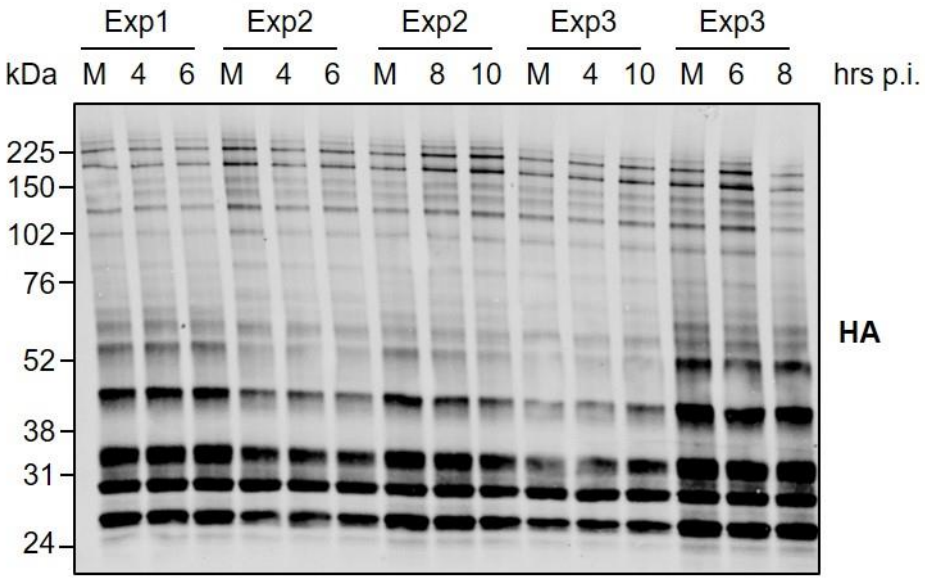

Figure 5.6. Analysis of proteins remaining in eluate following immunoprecipitation to enrich for DUBs in SILAC labelled HeLa cells
SILAC labelled HeLa cells were infected (or mock) with CHIKV at 5 MOI then harvested at 4, 6, 8 or 10 hrs p.i. and lysed under non-denaturing conditions. 500 µg lysate was probed with HA-Ub-PA at 1:100 for 45 mins. DUBs were enriched from the lysate by immunoprecipitation with anti-HA beads. Samples were taken following elution from the anti-HA beads, representing 6% of the total sample. Analysis was carried out by separating samples by SDS-PAGE on a 4-12% gradient gel, followed by immunoblot for HA.

The intensities for each DUB are presented in Figure 5.7A, and highlights an issue with experiment 3 as many of the DUBs were not detected in this experiment. In addition, the DUBs which were detected

consistently appeared at lower intensity in this experiment compared to experiments 1 and 2. A low protein yield for one of the samples in experiment 3 necessitated sending half the amount of protein for one half of

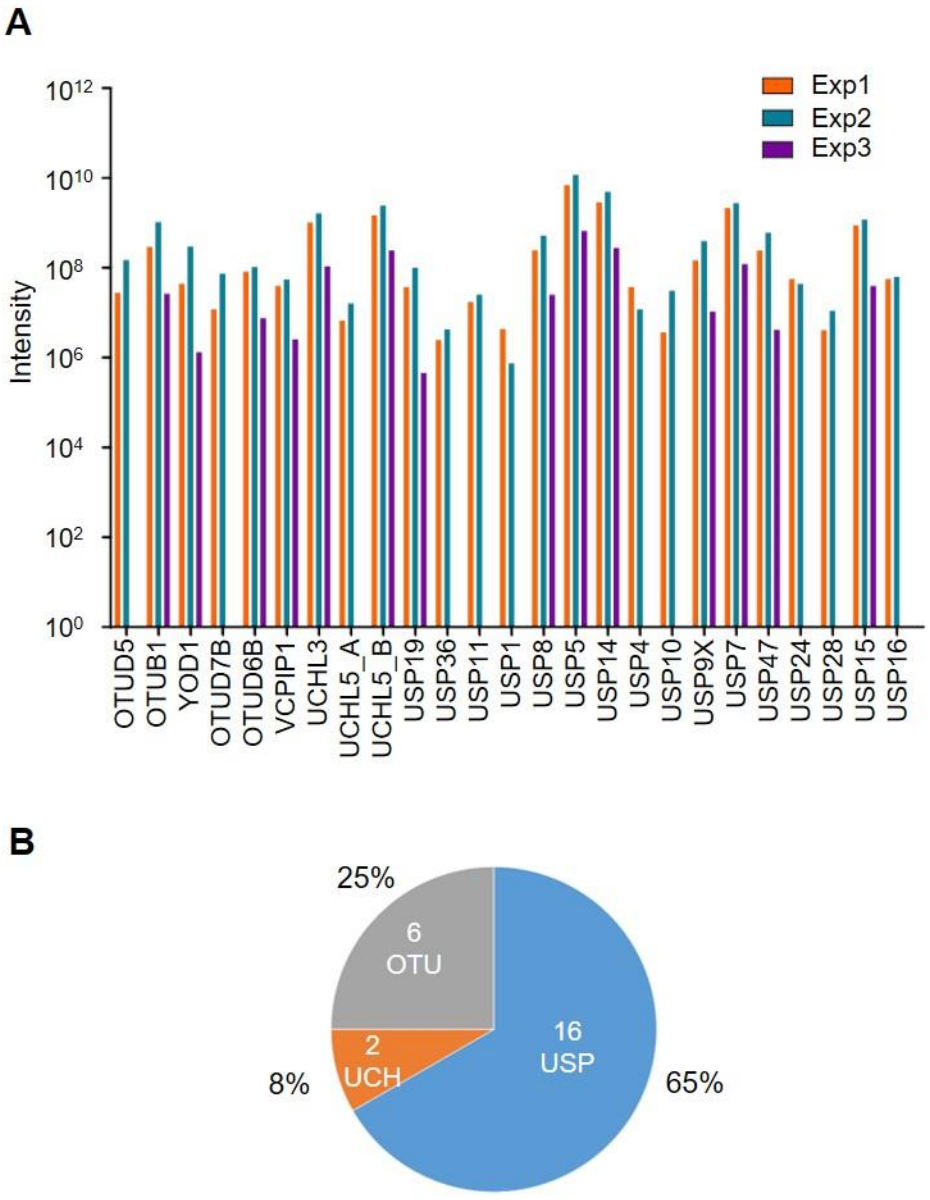

Figure 5.7. DUBs identified with probing with HA-Ub-PA in SILAC-labelled HeLa cells infected with CHIKV by LC-MS/MS
SILAC-labelled HeLa cells were infected with CHIKV, harvested at 4, 6, 8 and 10 hrs p.i. and lysed under non-denaturing conditions and 500 µg lysate probed with HA-Ub-PA at 1:100 for 45 mins. DUBs were enriched from the lysate by immunoprecipitation with anti-HA beads. The samples were digested with trypsin and the peptides identified by MS analysis. Intensities for each individual experiment are presented in (**A**) and the proportion of DUB families identified between all three experiments are shown in (**B**).

this experiment (as described above). Therefore, DUBs with a lower abundance are less likely to be pulled-down during the immunoprecipitation and detected by mass spectrometry. However, analysis of samples following elution from the anti-HA beads (Figure 5.6) appeared to show that there was sufficient protein remaining at that stage. It is therefore likely that an issue has occurred with this experiment in one of the latter stages of the protocol, such as during the preparation for mass spectrometry. The proportion of DUBs from each family are also shown in Figure 5.7B. Again USP DUBs were the most prevalent family with 16 identified, followed by OTU with 6 and UCH with 2 DUBs identified (Figure 5.7B).

For quantitative comparison of probe-reactivity of DUBs following CHIKV infection, the Log_2 mass:charge ratio was calculated for each time-point relative to mock-infected cells (Appendix Table 1). This is presented graphically in Figure 5.8 with Log_2 ratio plotted against Log_{10} intensity to provide an indication of the spread of the data. A shift to the left along the x-axis is representative of a decrease in probe-reactivity and a shift to the right represents an increase in probe-reactivity following CHIKV infection. The dashed lines indicate a 1.5-fold change. A notable observation when looking at these data was that substantially fewer DUBs were detected in experiment 3. This was not unexpected for half of experiment 3, due to the issue with protein yield for this experiment discussed above. However, the issue was not restricted to samples for which half the amount of protein was analysed (6 hr and 8 hr). The reduction in number of DUBs detected was also apparent in samples analysed with the intended quantity of protein (4 hr and 10 hr). This indicates that the lack of DUBs detected in experiment 3 was not solely due to low protein yield, but a more general defect for all samples within this experiment. However, for each experiment it was observed that the majority of DUBs fall within the dashed lines, indicating that probe-reactivity for most DUBs was not substantially altered. Furthermore DUBs which fall outside the 1.5-fold change parameters are generally decreasing in probe-reactivity, with a few exceptions. OTUD6B and VCPIP1 were the only two DUBs to exceed a 1.5-fold change in at least two experiments, displaying a decrease in each, with OTUD6B decreased in all three.

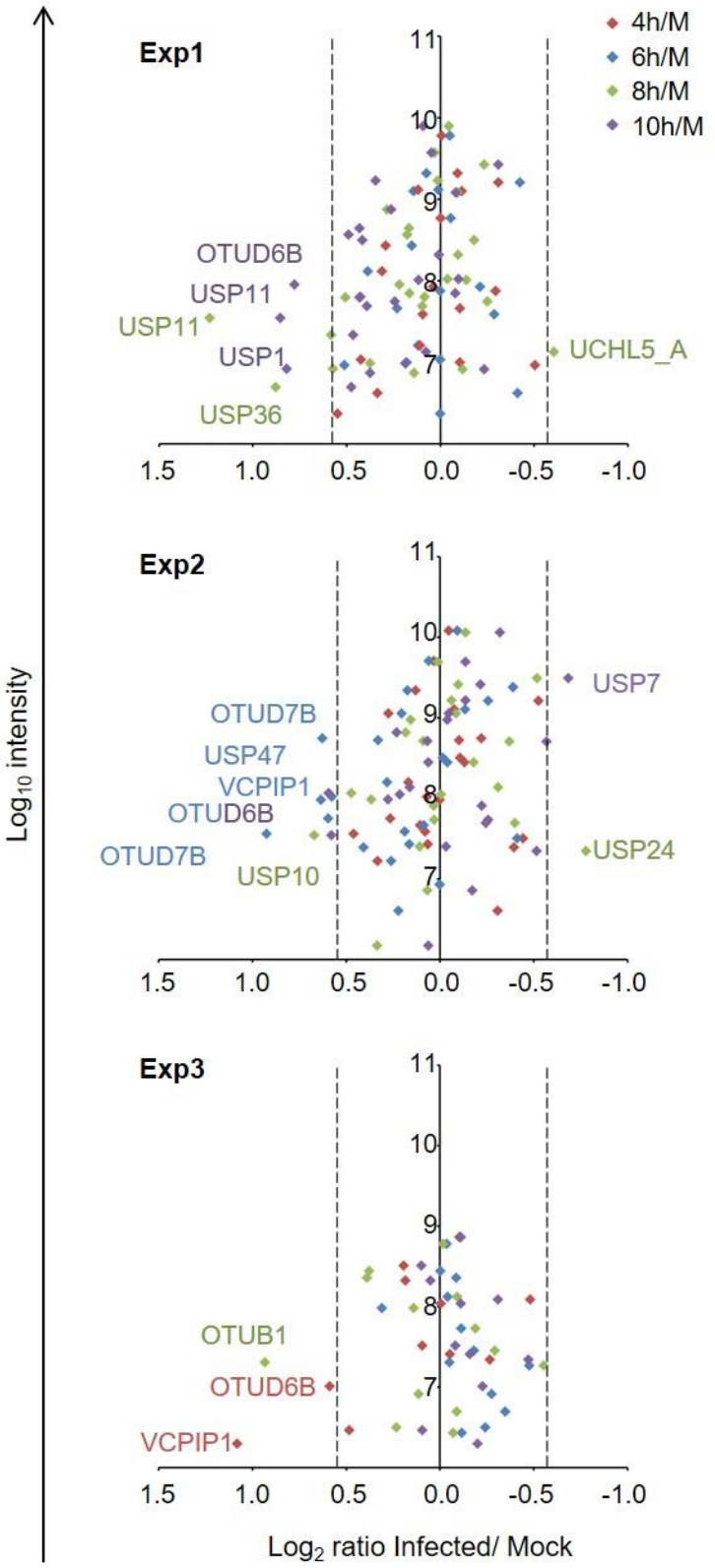

Figure 5.8. Analysis of DUB activity in SILAC labelled HeLa cells infected with CHIKV

SILAC labelled HeLa cells were infected (or mock infected) with CHIKV at 5 MOI then harvested at 4, 6, 8 or 10 hrs p.i. and lysed under non-denaturing

conditions. 500 µg lysate was probed with HA-Ub-PA at 1:100 for 45 mins. DUBs were enriched from the lysate by immunoprecipitation with anti-HA beads then digested with trypsin. Peptides were analysed by LC-MS/MS and identified by MaxQuant analysis. The Log_2 ratios (infected/ mock) and Log_{10} intensities for the DUBs detected are presented as scatter plots for each experiment with the dashed the lines representing a 1.5 fold-change increase or decrease. DUBs which exceed this threshold are labelled accordingly.

To visualise the data in another form, heat maps for each experiment were created in Multi-experiment Viewer: MeV 4.8 – Version 10.2 using the Log_2 ratios and are presented in Figure 5.9. This alternative method of visualising the data allows for observation of trends for each DUB between each of the three experiments. This further highlighted the issues with experiment 3, where only 13 DUBs were detected, compared to 24 or 23 DUBs in experiments 1 and 2, respectively. It was therefore decided to exclude experiment 3 from further analysis as it was clear there had been a more widespread issue with this experiment than protein yield alone. For experiments 1 and 2, although there is some variation in the extent to which the probe-reactivity for each DUB changes over time, they largely appeared to show the same trends. To aid identification of DUBs displaying a similar trend in changes for probe-reactivity, the Log_2 ratios were visualised by a box-and-whisker plot for each DUB from experiments 1 and 2 (Figure 5.10). This allowed for analysis for the response of each DUB, irrespective of time-point or experiment number, and highlighted certain DUBs exhibiting similar trends. For example, the DUBs USP9X, USP7 and USP24 all show a general trend to increase in probe-reactivity following CHIKV infection. In comparison, the DUBs OTUD7B, OTUD6B, USP19 and USP10 all show a general trend to decrease in probe-reactivity following CHIKV infection. There are also several examples of DUBs which do not appear to change in probe-reactivity over the time-course of infection, for example USP5, USP14 and USP15. Furthermore, the trends for USP11 appear to particularly variable due to the opposite response in experiment 1 and 2 (Figure 5.9). However, it should be stressed that statistical analysis could not be carried out following the issues with experiment 3 which necessitated its exclusion from the analysis.

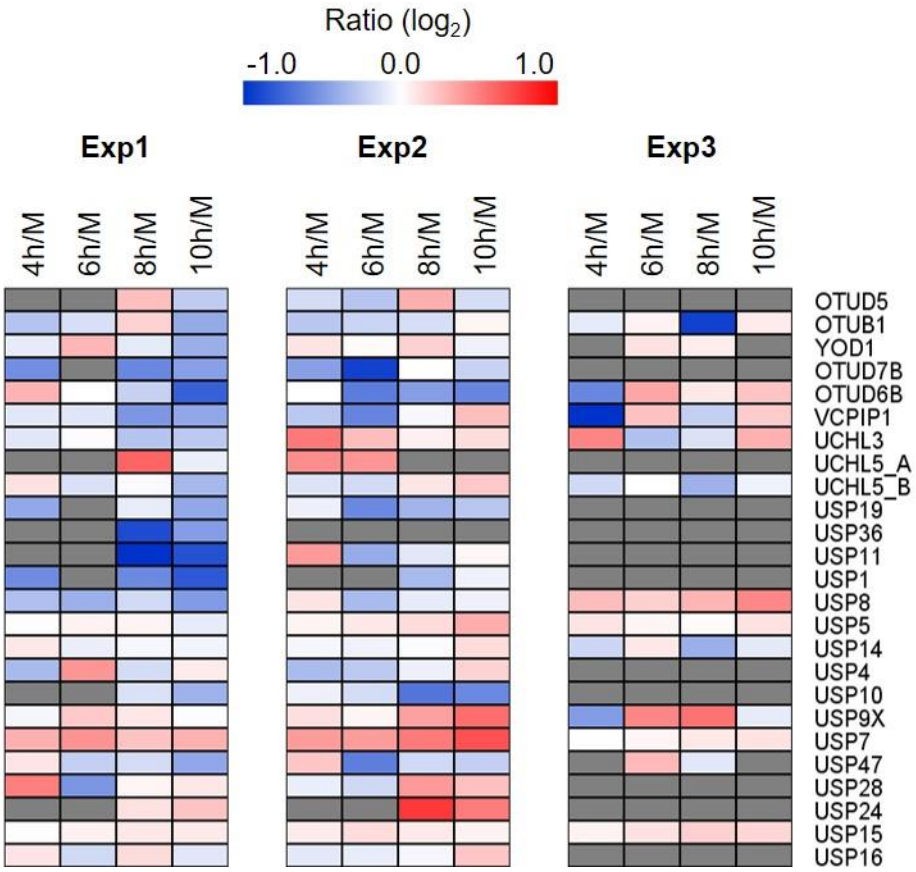

Figure 5.9 – Analysis of DUB activity in SILAC labelled HeLa cells infected with CHIKV

SILAC labelled HeLa cells were infected (or mock) with CHIKV at 5 MOI then harvested at 4, 6, 8 or 10 hrs p.i. and lysed under non-denaturing conditions. 500 µg lysate was probed with HA-Ub-PA at 1:100 for 45 mins. DUBs were enriched from the lysate by immunoprecipitation with anti-HA beads then digested with trypsin. Peptides were analysed by LC-MS/MS and identified by MaxQuant analysis. Log_2 DUB peptide ratios, relative to mock, are presented as heatmaps for each experiment using a blue-to-red colour scale to represent decreased and increased HA-Ub-PA reactivity respectively. Grey boxes indicate where a ratio could not be calculated.

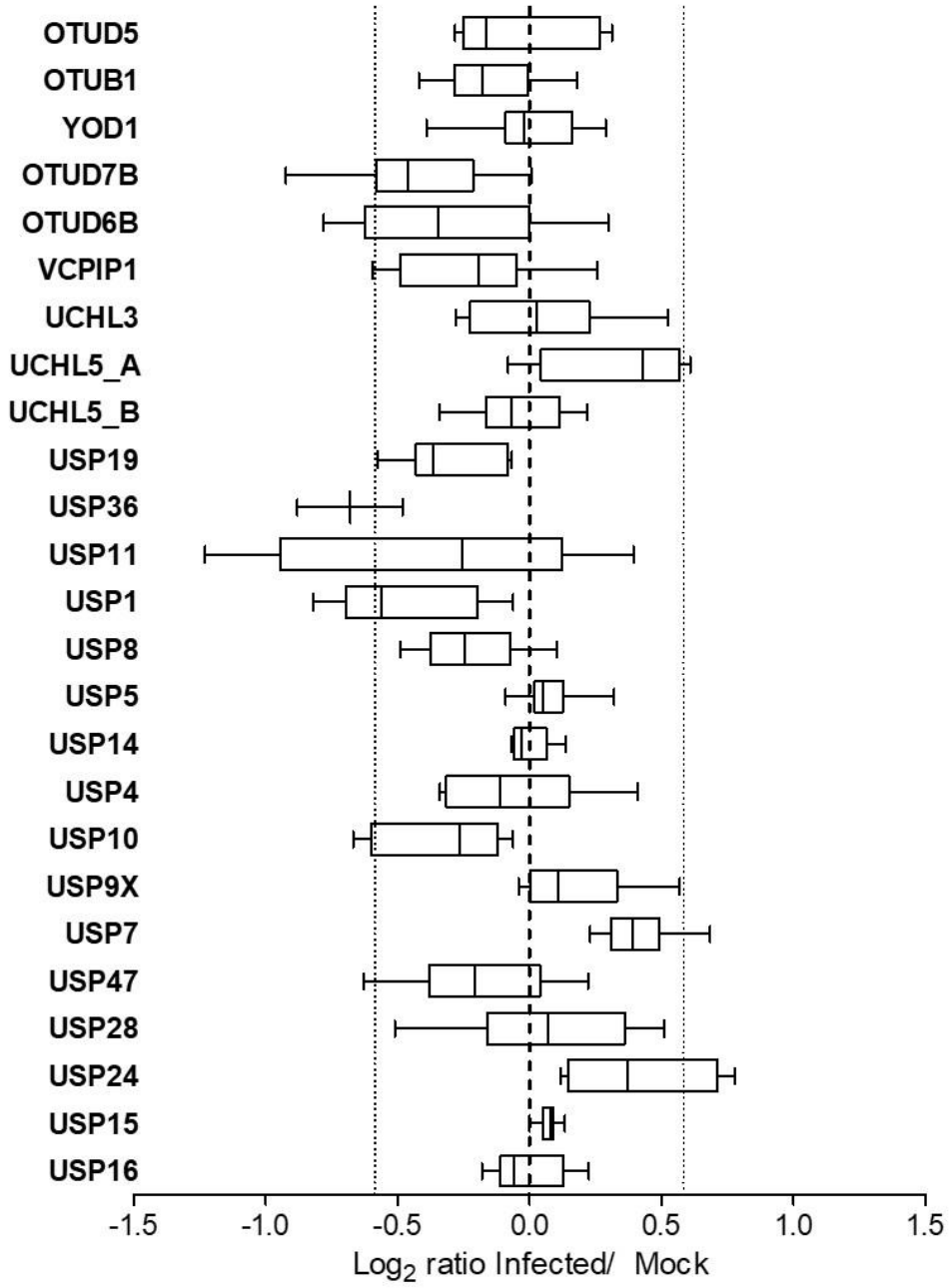

Figure 5.10. Box and whisker plot of probe-reactive DUBs in SILAC labelled HeLa cells infected with CHIKV

SILAC labelled HeLa cells were infected (or mock) with CHIKV at 5 MOI then harvested at 4, 6, 8 or 10 hrs p.i. and lysed under non-denaturing conditions. 500 µg lysate was probed with HA-Ub-PA at 1:100 for 45 mins. DUBs were enriched from the lysate by immunoprecipitation with anti-HA beads then digested with trypsin. Peptides were analysed by LC-MS/MS and identified by MaxQuant analysis. Log_2 DUB peptide ratios relative to mock for experiments 1 and 2 are presented as box-and-whisker plots. Boxes represent upper and lower quartiles and median. Whiskers show the minimum and maximum data points. The outer dashed lines represent a 1.5 fold-change increase or decrease in probe reactivity,

As discussed above, the mass spectrometry had yielded some variable results and experimental issues with experiment 3 necessitated its removal from the overall analysis. However, there were consistencies in the trends for some DUBs and it was therefore decided to select two for follow up experiments. This decision was based on selecting DUBs which had either shown an increase or decrease in probe-reactivity in order to look at both ends of the screen. Firstly, USP7 was selected having shown a similar pattern on the heat maps of increased probe-reactivity following CHIKV infection. It was also consistently showing a trend to increase in probe-reactivity at each time-point. Secondly, OTUD6B was chosen for follow-up as it was one of the few DUBs to exceed a 1.5-fold change in each experiment. Although the pattern for probe-reactivity over the time-course of infection is slightly different, this could reflect the slight differences in virus replication as indicated by the nsP1 blots (Figure 5.4). In experiment 1, there was only faint staining for nsP1 at 8 hrs compared to experiment 2 where the band for nsP1 is clearly visible by 8 hrs. The earlier production of nsP1 in experiment 2 could explain the earlier decrease in probe-reactivity for this experiment. OTUD6B was therefore selected in order to represent the decreased side of the screen.

5.5 Investigation of the potential pro- or anti-viral roles of USP7 and OTUD6B following alphavirus infection

The DUBs, USP7 and OTUD6B, were selected for follow-up from the mass spectrometry screening data described above as they represent targets from both sides of the screen (increase or decrease in probe-reactivity). These DUBs were the most consistent in their trends for both experiments, as demonstrated in Figures 5.8, 5.9 and 5.10. These data indicate a potential role for these DUBs in alphavirus infection which could be driven by either the virus or the host. To further investigate the potential pro- or anti-viral roles of these DUBs, it was decided to perform knock-down experiments, for both USP7 and OTUD6B, then monitor the effect on

alphavirus replication. For these experiments the model alphavirus, SFV, was used to give an initial overview before moving into the CHIKV system.

5.5.1 Monitoring the effect of USP7 siRNA knockdown on alphavirus replication

USP7 was knocked down in HeLa cells using two individual siRNAs for 72 hrs. An siControl (siC) transfection was also included as a control for non-targeting effects of siRNA transfection. Cells were harvested at 72 hrs post-transfection to monitor the efficiency of knock-down by immunoblotting for USP7 (Figure 5.11A). For the siC samples there was clear protein expression of USP7 which was then reduced for both USP7 siRNAs by approximately 90% (Figure 5.11B).

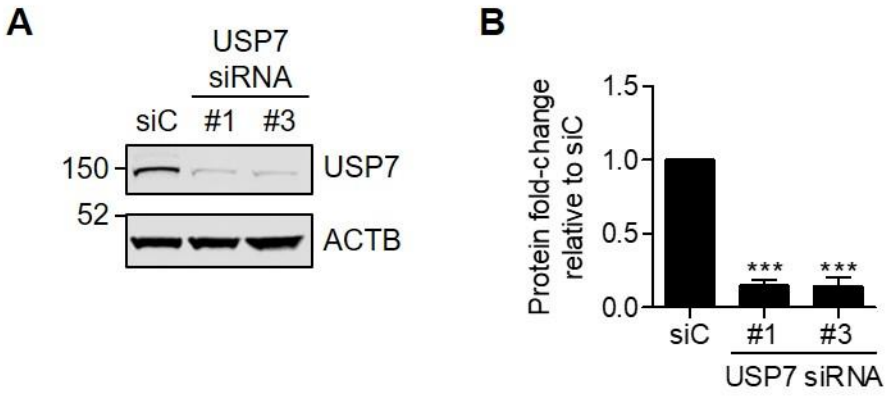

Figure 5.11. Monitoring efficiency of knock-down for USP7 in HeLa cells HeLa cells were reverse-transfected with USP7 siRNAs #1 and #3. A non-targeting siRNA (siC) was also used in each experiment. 72 hrs post-transfection, protein was extracted for immunoblot analysis for USP7 with ACTB as a loading control. A representative blot is shown in **(A).** Densitometry was used to quantify expression levels of USP7 normalised to ACTB and is presented as density relative to siC **(B).** Error bars represent SD, (one way ANOVA followed by Dunnet's multiple comparison test, *** $p < 0.001$).

To investigate the effect of USP7 knock-down on viral replication, in parallel, 72 hrs after knock-down HeLa cells were infected with SFV at 5 MOI. Infected cells were harvested 8 hrs p.i. for analysis of viral replication by qPCR. Briefly, RNA was extracted and used as a template to synthesise cDNA with oligo d(T) primers. Subsequently, levels of SFV genomic RNA

and the reference RNA, 18S, were analysed by qPCR. The fold-changes in viral genome levels relative to siC controls were calculated using the $2^{-\Delta\Delta Ct}$ method and are normalised to 18S (Figure 5.12). Following USP7 knock-down, a significant decrease in SFV replication can be seen for oligo #1 with a 2-fold reduction in SFV RNA relative to siC. However, for oligo #3, although there was a slight decrease in SFV RNA, the results were much more variable and are therefore not significant (Figure 5.12). The trend towards a decrease in viral replication upon USP7 knock-down was consistent with a potential pro-viral role, as suggested by the ABP screen. However, the evidence for a role for USP7 in alphavirus replication was not consistent between the two siRNAs, and it was therefore decided not to follow USP7 up any further.

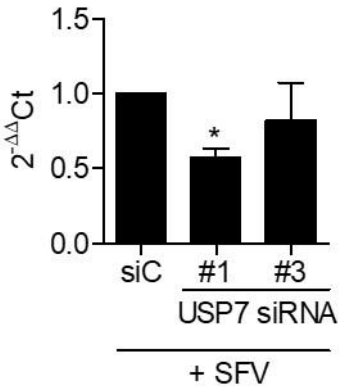

Figure 5.12. The effect of USP7 depletion on SFV replication
HeLa cells were reverse-transfected with USP7 siRNAs #1 and #3 for 72 hrs. An siC siRNA was also used in each experiment. Cells were infected with SFV at 5 MOI then harvested 8 hrs p.i. for qPCR analysis of SFV RNA. Fold-change of SFV RNA relative to siC, normalised to 18S, was calculated using the $2^{-\Delta\Delta Ct}$ method. Data from three independent experiments are shown. Error bars represent SD, (one way ANOVA followed by Dunnet's multiple comparison test, * $p < 0.05$).

5.5.2 Monitoring the effect of OTUD6B siRNA knockdown on alphavirus replication

The other DUB selected for further investigation from the mass spectrometry data was OTUD6B, which displayed a trend of decreased

probe-reactivity following virus infection. To further investigate this, the same approach of knocking-down OTUD6B followed by analysis of SFV replication was used. As before, HeLa cells were transfected with two individual siRNAs against OTUD6B as well as the control siC siRNA. The efficiency of knock-down was monitored 72 hrs after transfection by harvesting cells for immunoblot analysis of OTUD6B (Figure 5.13A). For siC transfected cells, good expression of OTUD6B protein was observed which was significantly reduced by approximately 75% following OTUD6B knock-down (Figure 5.13B).

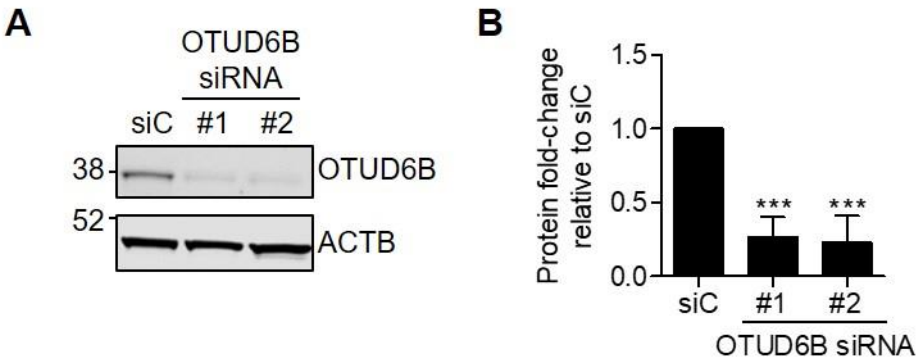

Figure 5.13. Monitoring efficiency of knock-down for OTUD6B in HeLa cells
HeLa cells were reverse-transfected with OTUD6B siRNAs #1 and #2. An siC siRNA was also used in each experiment. 72 hrs post-transfection, protein was extracted for immunoblot analysis for OTUD6B with ACTB as a loading control. A representative blot is shown in **(A).** Densitometry was used to quantify expression levels of OTUD6B normalised to ACTB and is presented as density relative to siC **(B).** Error bars represent SD, (one way ANOVA followed by Dunnet's multiple comparison test, *** $p < 0.001$).

The effect of OTUD6B knock-down on SFV replication was investigated in parallel by infecting HeLa cells with SFV at 5 MOI 72 hrs after OTUD6B knock-down. Infected cells were harvested 8 hrs p.i. and RNA extracted for qPCR analysis as above. Quantification of the fold-change in SFV genomic RNA relative to siC was calculated using the $2^{-\Delta\Delta Ct}$ method and was normalised to 18S (Figure 5.14). Here, a significant increase in SFV genome levels was observed for both OTUD6B oligos #1 and #3 with a 2.5- and 1.7-fold increase, respectively. It was therefore decided to take the

investigation for OTUD6B further and look at the effect of knock-down of this DUB on the clinically relevant, CHIKV.

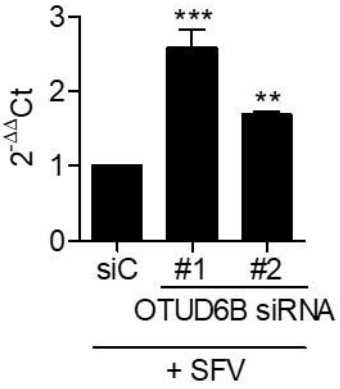

Figure 5.14. The effect of OTUD6B depletion on SFV replication
HeLa cells were reverse-transfected with OTUD6B siRNAs #1 and #2 for 72 hrs. An siC siRNA was also used in each experiment. Cells were infected with SFV at 5 MOI then harvested 8 hrs p.i. for qPCR analysis of SFV RNA. Fold-change of SFV RNA relative to siC, normalised to 18S, was calculated using the $2^{-\Delta\Delta Ct}$ method. Data from three independent experiments are shown. Error bars represent SD, (one way ANOVA followed by Dunnet's multiple comparison test, ** $p < 0.01$, *** $p < 0.001$).

HeLa cells were reverse transfected with two individual OTUD6B oligos or siC control as before. Again, efficiency of knock-down was monitored by immunoblotting for OTUD6B in samples harvested 72 hrs post-transfection (Figure 5.15A). Efficient knock-down of OTUD6B was achieved for this experiment with a reduction of approximately 85% (Figure 5.15B). The remaining cells were infected with CHIKV at 5 MOI, 72 hrs after knock-down, and then harvested for RNA extraction and qPCR analysis of CHIKV genomic RNA. The results from a single experiment are presented in Figure 5.15. A similar result to that seen for SFV genomic RNA was seen for CHIKV with an increase in viral replication following OTUD6B knock-down. A 2-fold increase in CHIKV RNA was observed for oligo#2 and is comparable to the 1.7-fold change seen with SFV. In contrast, for oligo#1 there was very little change in CHIKV RNA relative to siC with only a 1.2-fold increase. However, these data are from a single experiment and although no firm conclusions

can be drawn, it shows that CHIKV demonstrates a similar trend towards increased viral replication following OTUD6B knock-down. Taken together, these data suggest a potential anti-viral role for OTUD6B following CHIKV infection as ablation of this DUB was beneficial to viral replication.

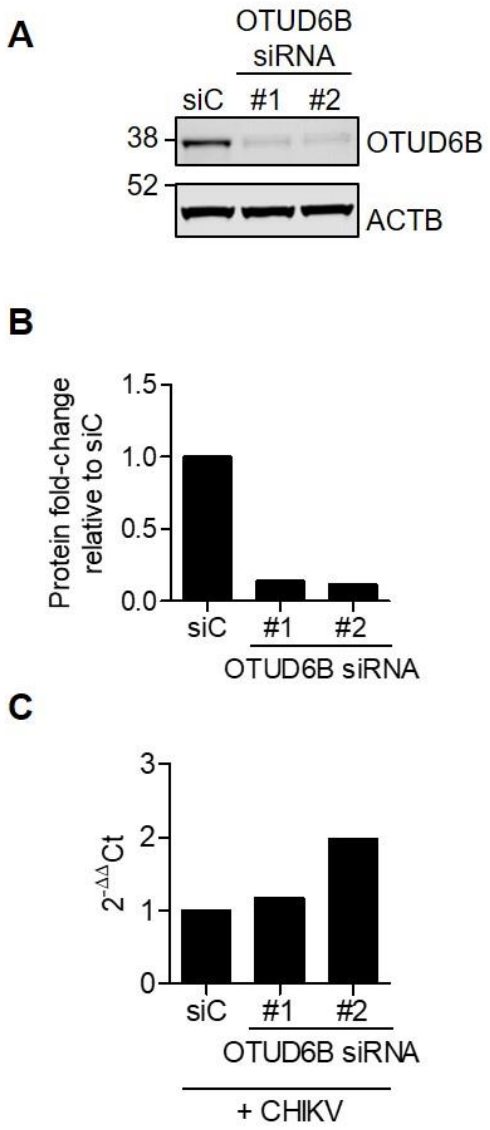

Figure 5.15. Monitoring efficiency of knock-down for OTUD6B in HeLa cells and the effect on CHIKV replication
HeLa cells were reverse-transfected with OTUD6B siRNAs #1 and #2 or an siC siRNA. Protein was extracted 72 hrs post-transfection for immunoblot analysis of OTUD6B (**A**). Densitometry was used to quantify expression levels of OTUD6B normalised to ACTB and is presented as density relative to siC (**B**). Cells were infected with CHIKV at 5 MOI, 72 hrs post-transfection. RNA was extracted 8 hrs p.i. for qPCR analysis of CHIKV RNA. The fold-change, normalised to 18S, was calculated using the $2^{-\Delta\Delta Ct}$ method and is presented as CHIKV RNA relative to siC (**C**). Data is from a single experiment.

5.6 Summary

Proteomic screens have proved invaluable in identifying proteins involved in alphavirus infections. However, pathway specific screens can provide a more detailed insight into a particular system. ABPs have proven to be useful tools to identify DUBs involved in a range of diseases and have also been used to demonstrate changes in activity which occur. However, this approach has yet to be utilised in the context of alphavirus infection. Therefore, the overall aim of this chapter was to identify DUBs which may play a role in alphavirus infection by combining the ABPs with a proteomic approach

The mass spectrometry screening approach used here was designed to detect changes in DUB probe-reactivity, thus giving an indication of potential changes in activity. However, binding conditions for each DUB would require specific optimisation. It was therefore decided to start with probing conditions which would favour identification of the maximum number of DUBs to identify DUBs for further investigation. According to the conditions optimised in chapter 4, HA-Ub-PA was the most suitable ABP for this aim with a probe: protein ratio of 1:100 and an incubation time of 45 mins. With these conditions it was likely that many of the changes observed would reflect changes in abundance rather than activity. However, for an initial screening this was considered an acceptable compromise as any DUBs identified at this stage would go on for further validation.

First, the immunoprecipitation and mass spectrometry approach to be used in screening for changes in probe-reactivity following CHIKV infection was validated. As accurate peptide identification by mass spectrometry requires large amounts of initial protein, it was necessary to scale-up the probing experiments used in chapter 4 to increase the protein yield. To confirm that this did not alter the binding patterns of the probe, samples were taken and analysed by immunoblot for the HA tag. The binding pattern of HA-Ub-PA in HeLa cells was the same as observed in chapter 4, thus confirming that increasing the scale of the reaction did not affect binding efficiency. Samples taken from each stage of the immunoprecipitation

demonstrated that the majority of probe-bound proteins were successfully enriched from the sample. Identification of these probe-bound proteins by trypsin digestion and subsequent mass spectrometry confirmed that DUBs could be detected using this approach. The DUBs identified here represented three of the cysteine protease families: USP, UCH and OTU, with most DUBs identified from the USP family. Although there was an apparent bias towards the USP DUBs, this is also the family with the most members and was therefore not wholly unexpected. In addition, no DUBs from the JAMM family were detected owing to their lack of a cysteine residue at their active site. Taken together, these data demonstrated that scaling-up the probing reaction did not affect ABP binding efficiency. This also acted as a preliminary test of the immunoprecipitation and mass spectrometry protocols, thereby confirming the feasibility of this approach for detecting DUBs.

To monitor changes in DUB probe-reactivity following CHIKV infection, SILAC-labelled cells were utilised. SILAC-labelled HeLa cells were mock-infected or infected with CHIKV and harvested at 4, 6, 8 and 10 hrs p.i.. Virus replication was monitored by immunoblotting for nsP1 for each experiment with good levels of viral replication in each case. Probe-bound proteins were enriched from the sample using the HA tag as a target for immunoprecipitation. Two groups of labelled cells in a triplex configuration were used to allow for monitoring of changes in DUB probe-reactivity at various stages of the virus lifecycle. For experiment 3, an insufficient protein yield necessitated using half the amount of protein than desired and altering the group configurations. For one group, the immunoprecipitation samples were analysed by immunoblot for HA, as previously described, and demonstrated that the immunoprecipitation was working well. The remaining elution samples from the immunoprecipitation were analysed by immunoblot analysis for HA. This demonstrated that there were probe-reactive proteins in the samples but also that there was some variation in the intensity between experiments.

Samples were sent to Warwick Scientific Services for analysis of probe-bound proteins following CHIKV infection as could be performed at a

higher resolution. This allowed for identification of nine more DUBs when compared to the DUBs identified in-house. However, the intensity of DUBs detected for each experiment revealed that for experiment 3, many of these DUBs were either not detected at all or at a lower intensity compared to the other experiments. Further analysis through quantitative comparison of the Log_2 ratios further confirmed the issue with this experiment 3 and it was consequently removed from further analysis. For the remaining experiments, quantitative comparison of the Log_2 ratios provided a kinetic analysis of changes in probe-reactivity over the course of CHIKV infection. Although there was some variation between experiments, two DUBs which demonstrated a similar pattern for both experiments were taken forward for further investigation. These were USP7 and OTUD6B which were selected to represent both sides of the screen with either an apparent increase or decrease in probe-reactivity, respectively.

To further investigate the potential role of USP7 and OTUD6B in alphavirus replication, siRNA knockdown experiments were performed. Knock-down of each of these DUBs with two individual siRNAs was followed by an 8 hour infection with SFV and subsequent analysis of viral genome replication by qPCR. For USP7, although there was a trend for a decrease in viral genome production following USP7 knock-down, the results were inconsistent and therefore not investigated further at this stage. For OTUD6B, a significant increase in SFV genome replication was observed for both siRNAs. Repeating this experiment with CHIKV appeared to confirm this trend, however firm conclusions could not be drawn as these results were obtained from a single experiment.

Taken together, this chapter has validated the use of ABPs to identify DUBs in CHIKV infected cells. Although some variation was observed between experiments, certain patterns could be identified and prompted further investigation of two DUBs: USP7 and OTUD6B. Analysis of these DUBs identified OTUD6B as a potential anti-viral DUB which may be down-regulated by CHIKV and warrants additional future investigation.

Chapter 6: Discussion

6.1 Overview

As a mosquito-borne alphavirus, CHIKV has been generating increasing concern as this re-emerging pathogen spreads worldwide. Large, ongoing outbreaks of CHIKV infection in Asia and the Americas are having a significant impact on the healthcare systems and economies of affected countries. There are two distinct phases of CHIKF: the acute and chronic phase. During the acute phase, patients present with high fever, skin rash and severe joint pain which, in the majority of patients, is self-limiting. However, there are increasing reports of more severe manifestations in certain high-risk groups such as neonates or those with underlying comorbidities. Some patients continue to suffer from the effects of CHIKV infection during the chronic phase with persistent joint pain which can last for months or years (Weaver & Forrester, 2015; Weaver & Lecuit, 2015). With no vaccines or antivirals currently available, the only treatment options are centred on relieving symptoms (Subudhi *et al.*, 2018). As obligate intracellular parasites, viruses are completely dependent on their host to replicate. Targeting host factors to counter virus infections is increasingly being seen as a promising therapeutic strategy due to the reduced risk of resistance developing. One cellular system which has been generating interest for drug development for a range of disorders is the ubiquitin system, in particular the DUBs (Colland, 2010; Farshi *et al.*, 2015). However, the role of DUBs in relation to alphavirus*es* remains poorly characterised. The overall aim of this thesis was therefore to investigate the involvement of DUBs in alphavirus infection.

6.2 Analysis of the role for USP45 in alphavirus infection

A number of genome-wide pathway-specific siRNA and CRISPR screens have previously focussed on alphavirus*es*, including CHIKV, SINV and VEEV (Ooi *et al.*, 2013; Radoshitzky *et al.*, 2016; Karlas *et al.*, 2016;

Zhang *et al.*, 2018*a*). DUBs were rare hits in these screens with only one screen using Sindbis virus and U2OS cells identifying DUBs amongst the hits, these being USP35, USP49 and USP9Y, but they were not validated in further experiments (Ooi *et al.*, 2013). Prior to this thesis, a targeted screen using a DUB siRNA library was performed to identify DUBs involved in the replication of the model alphavirus, SFV (Coombes *et al.*, 2019, unpublished). From this screen, several potential pro- and anti-viral DUBs were followed up in separate studies (Nubgan, 2017; King, 2018). For this work, USP45 was identified for follow-up as a poorly-characterised DUB with a potential pro-viral role.

Upon commencement of this thesis there was a single publication focussing on USP45. This established a role for USP45 in promoting DNA repair, in part through the interaction with ERCC1 (Perez-Oliva *et al.*, 2015). Additional studies have since been published demonstrating roles for USP45 in differentiation of the vertebrate retina as well as in cell migration (Toulis *et al.*, 2016; Yi *et al.*, 2018; Conte *et al.*, 2018). The most detailed of these investigations implicated USP45 as playing a role in cell migration as part of a protein complex including the protein, Spindly (Conte *et al.*, 2018). USP45 was not identified as playing a role in alphavirus infection in previous genome-wide screens despite being present in the libraries analysed (Ooi *et al.*, 2013; Zhang *et al.*, 2018*a*). However, it is likely that inherent pitfalls with large-scale screens such as false negatives, off-target effects or poor efficiency of depletion, contribute to the lack of identification of USP45 in these studies (Mohr *et al.*, 2010).

To further investigate the role of USP45 in alphavirus infection, a U2OS cell line with USP45 knocked-out by CRISPR/Cas9 was used alongside the parental WT cells. Perez-Oliva *et al* generated the USP45 knock-out cell line from U2OS cells with a gRNA targeting the end of exon 2 using NHEJ and kindly provided the clone used for this thesis. It should be noted that a different clone was used in this thesis compared to the original USP45 study (Perez-Oliva *et al.*, 2015). However, following confirmation of USP45 ablation by sequencing and immunofluorescent staining (section 3.3), this clone was deemed suitable for use in this thesis. A CRISPR/Cas9

knock-out system has a number of advantages over siRNA depletion. For example, siRNA results in partial depletion of the transcript, meaning that residual mRNA can still be translated (Boettcher & McManus, 2015). The efficiency of knockdown can also be limited if the protein has a long half-life or high turnover, as the protein will remain in the cell at close to normal levels (Hirsch, 2010). In addition, off-target effects can result in false-positives when non-targeted mRNAs have a partially complementary sequence to the guide strand (Jackson *et al.*, 2003; Ui-Tei *et al.*, 2008). In contrast, CRISPR depletion is capable of producing a complete and stable deletion of the target gene (Gilbert *et al.*, 2014; Boettcher & McManus, 2015).

The findings from the siRNA screen were first confirmed in the different cell background of WT and 45KO U2OS cells by monitoring cell viability following SFV infection. This was extended to CHIKV by observing the effect of USP45 KO on the extent of virus-induced CPE. Both assays confirmed the results from the screen by demonstrating an increase in cell viability and decrease in CPE following alphavirus infection when USP45 was absent (section 3.4). However, the cell viability assay is an indirect way of monitoring the effect on virus replication. In addition, the cell viability assays and CPE observations represent relatively late stages of virus replication, meaning that a role for USP45 could not be predicted from this data. Assays to monitor progressively earlier stages of alphavirus replication were therefore utilised in order to characterise the role USP45 was playing.

Firstly, analysis of the production of viral genomic RNA for both SFV and CHIKV revealed that viral replication was significantly inhibited in 45KO cells (section 3.5.1). Production of viral RNA (genomic and subgenomic) is dependent on formation of replication complexes formed by the nsPs. Therefore, to analyse a slightly earlier point in the virus lifecycle, expression of viral nsPs 1-3 was monitored in WT and 45KO cells following infection with both SFV and CHIKV. For both viruses there was a significant reduction in the level of nsP expression in 45KO cells. In addition, capsid protein expression was monitored for SFV. Although there was a decrease in capsid protein for SFV in 45KO cells, the difference here was not significant (section 3.5.2). Recent studies have suggested a role for the capsid protein of

incoming alphavirus nucleocapsid complexes in enhancing RNA stability and facilitating translation (Sokoloski *et al.*, 2017). It is therefore possible that detection of capsid protein remaining from the original inoculum masks the deficiency in production of capsid protein in 45KO cells to some extent.

Further analysis of the ability of SFV and CHIKV to infect WT and 45KO cells revealed that significantly fewer plaques were produced in 45KO cells following infection. In contrast, two unrelated viruses, RSV and VACV, were able to infect both cell lines equally well. For CHIKV the number of infected cells was also investigated by immunofluorescence and revealed a significant reduction in the number of infected 45KO cells compared to WT. These assays suggested a defect at an early stage during alphavirus infection in cells with USP45 loss-of-function (section 3.5.3). The primary mechanism of cell entry for CHIKV and SFV is by CME, which is in contrast to VACV and RSV which enter cells via macropinocytosis. The role of USP45 in virus entry was therefore investigated by testing the ability to bypass the normal alphavirus entry mechanism. Infecting WT cells with CHIKV resulted in similar numbers of infected cells under both normal and acidic conditions. However, infection of 45KO cells with CHIKV at a low pH resulted in an increase in the number of infected cells compared to infection at a neutral pH, thus supporting a role for USP45 in alphavirus entry (section 3.6.1). To directly investigate the role of USP45 in CME, a Tfn uptake assay was performed. This demonstrated that WT cells could efficiently internalise Tfn whereas uptake for 45KO cells was significantly lower (section 3.6.2). Taken together, these data point towards a role for USP45 in virus entry through its involvement in the CME pathway.

CME is thought to be the main mechanism mediating CHIKV entry into cells and has been investigated in a number of studies. For example, inhibition of CME using siRNAs targeting clathrin heavy chain (CHC), or with the inhibitor Pitstop2, was shown to significantly reduce CHIKV uptake into BSC-1 and HeLa cells (Hoornweg *et al.*, 2016*a*). Similarly, CHC depletion in U2OS and primary human umbilical vein endothelial cells resulted in inhibition of CHIKV infection (Ooi *et al.*, 2013). However, another study in 293T and HeLa cells demonstrated that siRNAs against CHC did not alter

CHIKV uptake, thereby suggesting a clathrin-independent mechanism of virus uptake (Bernard *et al.*, 2010). Here, uptake was reported to be dependent on Eps15, a mediator of both clathrin-dependent and –independent cell entry pathways (Sigismund *et al.*, 2005; Bernard *et al.*, 2010; Kirchhausen *et al.*, 2014). Although the majority of reports suggest that CHIKV entry occurs mainly via CME, it is likely that the route of virus uptake is, to some extent, dependent on the cell line. However, the deficiency in Tfn uptake in 45KO cells supports a role for USP45 in uptake of CHIKV via CME in U2OS cells.

Through the assays described above, it was apparent that while infection was significantly reduced, there was not a complete block of infection. In addition, bypassing the normal entry route for CHIKV did not completely rescue the infection defect in 45KO cells, as it has been shown to in other loss-of-function studies. For example, Hackett and colleagues demonstrated that bypassing the normal SINV entry route using this assay rescued the infection deficit in RNASEK depleted cells (Hackett *et al.*, 2015). It can therefore not be ruled out that USP45 may have an additional role at a step down-stream of virus entry. In addition, it may be that USP45 is not an absolute requirement for CME, rather it may play a role in making the process more efficient. It would therefore be of interest to see whether infection by other viruses which are known to use CME are also blocked in the absence of USP45. The ability of CHIKV to utilise different cellular receptors adds another level of complexity. To date, a number of cell-surface proteins have been reported to function as receptors for CHIKV (Wang *et al.*, 1992; Smit *et al.*, 2002; Klimstra *et al.*, 2003; La Linn *et al.*, 2005; van Duijl-Richter *et al.*, 2015). However, there appears to be a large degree of redundancy as infection can also occur in the absence of these molecules (van Duijl-Richter *et al.*, 2015). It is therefore likely that CHIKV receptors act mainly by facilitating the initial virus-cell contact and that specificity for a certain receptor may be of less importance. From the assays used here to investigate the role of USP45 in virus infection, the ability of CHIKV to bind to 45KO cells was not determined. It is therefore possible that USP45 could

also be involved upstream of CME play a role in virus binding and it would be of interest to investigate this in future work.

DUBs are known to play a number of roles during the endocytic process, primarily during the trafficking stages from the early through to late endosomes (Clague & Urbé, 2017). In the context of CME, DUB siRNA screens have been carried out focussing on EGFR trafficking, which is mediated through CME following stimulation with low doses of EGF. These studies in HeLa and KB cells identified USP9X and Cezanne-1 as playing a role in CME (Pareja *et al.*, 2012; Savio *et al.*, 2016). Although these groups did not identify USP45 in their screen, there was no assessment of the efficiency of USP45 depletion. Another example of a DUB shown to play a role in CME is USP17 (Jaworski *et al.*, 2014). In this instance, USP17 was found to be involved in recruitment of clathrin and other crucial components of CME to the plasma membrane (Barbieri *et al.*, 2001; Jaworski *et al.*, 2014). Studies in yeast also suggest that deubiquitylation of a homologue of Eps15, a scaffolding adaptor in CME, influences the formation of clathrin-coated vesicles (Weinberg & Drubin, 2014).

In the first screen of the DUB interaction landscape, Sowa and colleagues reported that USP45 interacts with a number of myosin proteins including MYH10 and MYH9 (Sowa *et al.*, 2009). Interestingly, these proteins have been identified as playing a critical role in CME in mammalian neurons and fibroblasts through their involvement in clathrin-coated pit curvature (Chandrasekar *et al.*, 2013, 2014). It is therefore feasible that USP45 could be part of a complex with myosin proteins which is important in the formation of clathrin-coated pits. Another recent study linked USP45 with Spindly and cell migration. While Spindly has not been reported to play a role in CME, it has been shown to localise to leading edges of cells and to interact with the dynein/ dynactin complex (Conte *et al.*, 2018). In this context, a dynein light chain protein has been reported to function in actin assembly during CME in yeast (Farrell *et al.*, 2017). There are conflicting reports for the involvement of actin assembly in mammalian endocytosis (Gottlieb *et al.*, 1993; Lamaze *et al.*, 1997). One study seeking to clarify these discrepancies suggested that while actin filament organisation is not

obligatory for CME, it can promote vesicle formation under certain conditions (Fujimoto *et al.*, 2000). Another group demonstrated the requirement of actin for internalisation of particularly large cargo such as VSV (Cureton *et al.*, 2009). It may be that uptake of CHIKV by CME requires a Spindly-dynein/dynactin complex in which USP45 plays a role, but this has yet to be investigated.

The study by Conte *et al.* also demonstrated that USP45 cleaves monoubiquitin and K48 linked poly-ubiquitin chains (Conte *et al.*, 2018). Monoubiquitin has been shown to have several roles such as: acting as an auto-inhibitory signal for proteins with UBDs, controlling cytoplasmic location of proteins and regulating protein complex formation (Pavri *et al.*, 2006; Fallon *et al.*, 2006; Wang *et al.*, 2013*b*). For example, monoubiquitylation of Eps15 has been shown to negatively regulate CME by preventing it from binding to its intended cargo, thereby delaying its uptake (Fallon *et al.*, 2006). CHIKV has been shown to be dependent on Eps15 for its uptake into 293T and HeLa cells (Bernard *et al.*, 2010). It is possible that monoubiquitylated Eps15 is a target for USP45 and that this DUB is required for efficient CME. Removal of K48-linked polyubiquitin chains and subsequent protection from degradation is the more classically associated role of DUBs (Xu *et al.*, 2009). Indeed, it is feasible that USP45 could be important for removal of K48 linked chains from a component of the CME pathway thereby stabilising it and promoting endocytosis.

6.3 Future work investigating the role of USP45 in alphavirus infection

As discussed in section 6.2, there are a number of avenues which would be of interest to explore in future work. Given the ability of CHIKV to enter cells via both clathrin-dependent and –independent mechanisms, it would be of interest to investigate the requirement of USP45 in different cell types. For example, CHIKV uptake into 293T cells has been suggested to occur in a clathrin-independent manner (Bernard *et al.*, 2010). Investigation of the requirement of USP45 for CHIKV uptake and replication in these cells

could help to clarify the question as to whether USP45 is important for alphavirus replication outside of its role in CME. Furthermore, whilst this data implicates USP45 in CME, a detailed mechanism was not investigated here. This could be further explored by monitoring the stability and recruitment of components of the CME pathway in 45KO cells, for example clathrin, Eps15 and AP-2. In addition, monitoring the ubiquitin status of these proteins could also provide clues as to the role of USP45 in CME given that USP45 has been suggested to have preferences for certain ubiquitin topologies (Conte *et al.*, 2018). It has also been implied that USP45 interacts with myosin II proteins, which have been implicated in CME, as well as Spindly, to promote cellular migration (Sowa *et al.*, 2009; Chandrasekar *et al.*, 2013, 2014; Conte *et al.*, 2018). Investigating the potential formation of a complex of these proteins at sites of CME could provide further mechanistic insight.

Another important experiment which would complement this work would be to transfect USP45 back into 45KO cells and see if this rescues a phenotype. Not only would this reinforce the findings of this thesis, but would also allow further exploration as to whether the requirement of USP45 in alphavirus entry was dependent on catalytic activity. Through transfection with plasmids encoding catalytically inactive USP45, or a variety of truncated proteins, it would be possible to determine the domains which are important for this phenotype. This would be an important aspect to address as DUBs have been shown to have both catalytic and non-catalytic roles (Zhang *et al.*, 2015; Wang *et al.*, 2017*a*). Unfortunately, despite several attempts to transfect USP45 plasmids into 45KO cells during this thesis, attempts to rescue the expression of USP45 were unsuccessful. However, work in two of the existing USP45 publications demonstrated that an active catalytic site was important for both its mode of action and binding (Perez-Oliva *et al.*, 2015; Conte *et al.*, 2018). It seems likely therefore that USP45 catalytic activity would also be required in this instance.

Taken together, this work is indicative of a new role for USP45 in alphavirus entry through its involvement in CME. Comprehensive biochemical and functional studies remain to be undertaken to further understand the role of USP45. However, with the increasing resources

focussing on DUBs as druggable targets, this study adds another cellular factor to the pool of potential anti-viral targets for this important infection.

6.4 The use of ABPs to monitor probe-reactivity in alphavirus infected cells

The remainder of this thesis explored the use of ABPs as a tool to monitor DUBs during alphavirus infection. ABPs can be used to monitor changes in expression and activity of both cellular and viral DUBs. However, this strategy had not previously been utilised in the context of alphavirus infection. Part of the aim of this project was therefore to generate the first unbiased global profile of DUB probe-reactivity during alphavirus infection. ABPs have been used to compare the expression and/or activity in normal and diseased states. For example, a study probing lysate of EBV infected cells and tumour lines demonstrated an increase in activity of the DUBs, USP5, -7, -9, -13, 15 and -22 (Ovaa *et al.*, 2004). In addition, UCHL1, UCHL3, USP7 and USP9X show enhanced activity following immortalisation of keratinocytes with HPV (Rolén *et al.*, 2006). Another aim of this thesis was to investigate the possibility of CHIKV encoding its own DUB. ABPs have successfully been used to identify and characterise viral DUBs in the past including for HSV-1 and adenovirus (Balakirev *et al.*, 2002; Kattenhorn *et al.*, 2005).

For this thesis, two ABPs with different electrophilic warheads, HA-Ub-VME and HA-Ub-PA, were tested for their suitability in monitoring changes in probe-reactivity following CHIKV infection. A comparison of both probe concentration and incubation time was first performed in HeLa cell lysate to identify suitable probing conditions. The most appropriate conditions to permit detection of the maximum number of DUBs, were decided to be with a probe: protein ratio of 1:100 and incubation time of 45 mins. The two different warheads tested here exhibit different binding preferences and reactivity. This is in line with what was expected when compared to other studies in HeLa cells using these probes (Lawson *et al.*, 2017; Gui *et al.*, 2018). The VME and PA warheads exhibit different binding preferences and

reactivity meaning they can be used to investigate different experimental questions. For example, while VME warheads do not bind well to all DUB families, their preference for USP and UCH DUBs makes them ideal tools for a targeted approach to investigate DUBs of this family (de Jong *et al.*, 2012). In contrast, the PA warheads bind well to all six cysteine protease DUBs and are therefore better suited for screening experiments (Ekkebus *et al.*, 2013; Abdul Rehman *et al.*, 2016; Kwasna *et al.*, 2018). This was confirmed during experiments to optimise the incubation conditions and can be seen through the different binding patterns for each probe. Consequently, it was decided to use the HA-Ub-PA probe for future screening experiments.

It was also noted during the optimisation of incubation times that there was a distinction in the binding of the probes to high and low molecular weight proteins over time. The larger proteins exhibited an increase in probe binding with longer incubation times, whereas the smaller proteins appeared to decrease in probe-reactivity. DUBs are known targets of ubiquitylation themselves which can result in either an increase or decrease in catalytic activity (Loch & Strickler, 2012; Haq & Ramakrishna, 2017). For example, ubiquitylation of the DUBs, ataxin-3 and USP25, was shown to increase their activity (Denuc *et al.*, 2009; Todi *et al.*, 2009). In comparison, ubiquitylation of UCHL1 was demonstrated to suppress catalytic activity by preventing binding to ubiquitylated targets (Meray & Lansbury, 2007). Ubiquitylation of DUBs can also result in their proteasomal degradation, as has been shown for USP19, which is also capable of stabilising itself through auto-deubiquitylation (Mei *et al.*, 2011). As the binding of probes to the active site of DUBs results in a covalent attachment, the catalytic activity of the DUB is therefore inhibited. It may be that as incubation with the probe progresses, the inability of DUBs to deubiquitylate themselves or other DUBs alters their activity or stabilisation.

This approach was then tested in virus infected cells by monitoring changes in probe-reactivity in lysate from HeLa cells infected with the model alphavirus, SFV. Over the course of a 4 hr infection there appeared to be very little change in overall probe-reactivity. However, certain bands were identified with potentially altered intensity demonstrating that the ABPs were

capable of detecting changes in reactivity using this setup. It could be that the changes in probe-reactivity do not occur this early in infection and indicated that using a longer time-course may be preferable for detecting changes in probe-reactivity in virus infected cells. In addition, although highly abundant proteins are readily detected using gel-based ABP approaches, using the same exposure, low-abundance proteins are likely to be masked. This issue is likely to be compounded by the known ability of ABPs to bind non-specifically to cysteine residues of non-DUBs (Wang *et al.*, 2009; Love *et al.*, 2009). Therefore, whilst immunoblot profiling of probe-reactive proteins within the proteome can provide an overview of global changes in probe-reactivity, individual DUBs cannot be accurately identified from these data.

As described in section 1.5.5, both DNA and RNA viruses have been shown to encode their own DUBs (Bailey-Elkin *et al.*, 2017). However, to date potential DUB activity in alphavirus*es* has not been investigated. As a cysteine protease, the alphavirus protein with the potential to act as a DUB is nsP2 (Ramakrishnan *et al.*, 2017). ABPs have previously aided identification of viral DUBs (Balakirev *et al.*, 2002; Kattenhorn *et al.*, 2005). It was therefore decided to utilise these probes to explore the potential of CHIKV to encode its own DUB. Both the VME and PA probes were used with a range of probing conditions in an attempt to identify any potential DUB activity in lysate from CHIKV infected HeLa cells. However, nsP2 reactivity with the probes was not detected under the conditions tested here, suggesting that CHIKV nsP2 does not act as a DUB. It should be noted however that nsP2 harvested at only one time-point p.i. (10 hr) was monitored here. A range of mechanisms for regulating cellular DUB activity have been described (section 1.4.3) and it is possible that viral DUB activity may also be dynamically regulated. For example, activity of pUL36, the viral DUB expressed by PRV, was shown to be differentially regulated during infection with DUB activity being dispensable for neurotropism but essential for neuroinvasion (Huffmaster *et al.*, 2015). Whilst the regulation of viral DUB activity has not been studied in as much detail as cellular DUBs, it is feasible that DUB activity may be detectable in CHIKV nsP2 at a different point of infection.

It has also been demonstrated that the structure of CHIKV nsP2 can vary depending on the strain. For example, nsP2 derived from the ECSA isolate of CHIKV was shown to differ from other CHIKV strains or alphavirus nsP2 proteases in the recognition of small peptide substrates (Saisawang *et al.*, 2015*b*). In addition, the catalytic dyad cysteine residue of CHIKV nsP2 has been shown to be interchangeable with a proximal serine residue. Further characterisation revealed that enzyme activity was retained upon replacement of the catalytic cysteine with alanine (Saisawang *et al.*, 2015*a*). However, this was not verified in cell-based experiments and another study showed that the cysteine residue was essential for CHIKV nsP2 activity (Rausalu *et al.*, 2016). Taken together, these studies highlight the potential variation in alphavirus nsP2 structure and function. Whilst the data presented in this thesis suggest that CHIKV nsP2 is not a DUB, the activity of viral enzymes is affected by multiple factors and using a single type of assay cannot provide firm conclusions.

6.5 Unbiased profiling of cellular DUBs following alphavirus infection

In order to accurately identify cellular DUBs which exhibited a change in reactivity to the probes after alphavirus infection, the use of ABPs was combined with mass spectrometry. By taking a targeted approach of combining ABPs with mass spectrometry it is possible to enrich and profile specific components of the proteome based on shared functional properties. An initial experiment to validate the immunoprecipitation and mass spectrometry approach to be used in this study confirmed that DUBs could be detected in HeLa cells and that scaling up the probing reactions did not affect probe binding. To monitor changes in probe-reactivity of DUBs following CHIKV infection, a triplexed SILAC approach was utilised and combined with identification by mass spectrometry. Although fewer total DUBs were detected here compared to other studies, all the DUBs identified in this thesis were also identified by others using a ubiquitin-based probe with a PA warhead in HeLa cells (Lawson *et al.*, 2017; Gui *et al.*, 2018). However,

it is likely that differences in experimental setup and probing conditions account for these discrepancies.

Whilst there were a total of 24 DUBs identified, there were also 167 other proteins identified. After excluding common contaminants from the agarose CRAPome (Mellacheruvu *et al.*, 2013), there were 10 other proteins which were pulled-down with the DUBs: IGHV1-45, JCHAIN, IGHG2, IGHA1, HSP90AB2P, KCNK1, EEF1A1P5, TMEM263, MYDGF and MMTAG2. Of these proteins, two were pseudogenes (HSP90ABP2P and EEF1A1P5) and three exhibited no real change over the course of infection (TMEM263, MYDGF and MMTAG2). However, there were also a number of proteins associated with immunoglobulin heavy chains (IGHV1-45, JCHAIN, IGHG2, and IGHA1), which all appear to decrease to some extent following CHIKV infection. Whilst production of immunoglobulins is traditionally associated with B lymphocytes and plasma cells, it is now clear that a number of non-lymphoid lineage cells also produce immunoglobulins (Qiu *et al.*, 2003; Chen *et al.*, 2009, 2010*c*; Niu *et al.*, 2012). This has also been reported in HeLa cells where expression of immunoglobulins was shown to enhance proliferation through activation of MAPK/ERK signalling pathways (Wang *et al.*, 2013*a*). Another protein identified in this group was KCNK1, a member of the potassium channel family. Although cellular potassium channels have not been implicated in alphavirus infections, they have been shown to be essential to some viruses. For example, Bunyamwera virus (BUNV) was shown to traffic through endosomes containing high concentrations of potassium ions. Transport of BUNV through endosomes was subsequently shown to be arrested following inhibition of cellular potassium channels (Hover *et al.*, 2016, 2018). It is possible that these proteins were detected due to non-specific binding of ABPs, for example to non-catalytic cysteine residues, or that they are potential DUB interactors. However, as these proteins do not exhibit similar changes in probe-reactivity as any of the DUBs, it is likely that these were pulled down due to non-specific binding and were therefore not investigated further.

A notable observation from the mass spectrometry data was that the majority of DUBs exhibited either no change or a decrease in probe reactivity

following CHIKV infection. This is in-line with other CHIKV proteomic studies performed *in vitro* which demonstrated that the majority of proteins exhibited a decrease in abundance following CHIKV infection (Abere *et al.*, 2012; Thio *et al.*, 2013). As CHIKV is known to cause transcriptional and translational shutoff, it is possible that the apparent decreased abundance of proteins represents natural degradation (Fros & Pijlman, 2016). Therefore, consideration should be given to the half-life of a protein to be sure it is being reduced as a result of viral infection and not simply degrading. However, although no DUBs exceeded the 1.5-fold change increase in more than one experiment, it was clear that not all DUBs were decreased following CHIKV infection. This suggests that virus induced changes are being detected with this approach.

In contrast to *in vitro* CHIKV studies, the trends for *in vivo* proteomic screens generally show the opposite effect with upregulation for the majority of proteins (Dhanwani *et al.*, 2011; Fraisier *et al.*, 2014). This could be as a result of the time-points utilised in these two different types of studies. *In vitro* experiments generally look at early time-points, before cellular apoptosis, whereas *in vivo* experiments typically monitor later time-points, after the onset of clinical symptoms (Dhanwani *et al.*, 2011; Thio *et al.*, 2013). One study which sought to further investigate this issue demonstrated *in vivo* that overall protein abundance before and after the onset clinical symptoms was decreased or increased, respectively (Fraisier *et al.*, 2014). It is therefore possible that DUBs which exhibited a decrease in probe-reactivity here could be increased at a later time-point, as was the case for αV/β1 integrins (Fraisier *et al.*, 2014).

The results from the mass spectrometry screen highlighted USP7 and OTUD6B for further investigation as they either demonstrated a trend to increase or decrease in probe-reactivity following CHIKV infection, respectively. USP7 is a DUB which is well known for its role in stabilising p53 and MDM2 to ensure an appropriate response to DNA damage (Li *et al.*, 2002; Brooks *et al.*, 2007). Indeed, USP7 is seen as a promising drug target for many cancers due to the strong p53 induction in the absence of this DUB (Brooks *et al.*, 2007; Fan *et al.*, 2013). However, USP7 was first identified as

a protein associated with HSV and is therefore also known as Herpesvirus Associated USP (HAUSP). Here it was shown to play an important role in stabilising the HSV protein, ICP0, in order to promote viral replication (Meredith *et al.*, 1994). Many additional roles have now been associated with USP7 in a range of diseases. For example, USP7 was shown to promote HIV infection through stabilising the viral Tat protein (Ali *et al.*, 2017). In addition a role in promoting the formation of inflammasomes in macrophages has been described (Palazón-Riquelme *et al.*, 2018). It was therefore feasible that USP7 could be involved in alphavirus infection as either a pro- or anti-viral DUB.

Thus, the potential role of USP7 was further investigated through monitoring the effect of USP7 siRNA knockdown on alphavirus replication. Although there was a trend towards a decrease in the level of replication of SFV following USP7 knock-down, the evidence was not consistent between the two siRNAs tested. This inconsistency between the siRNAs could be as a result of off-target effects (Khan *et al.*, 2009). However, it could also be that USP7 was a false positive from the mass spectrometry data. For example, the probe may have stimulated rearrangement of the USP7 active site to allow binding or USP7 may have been saturated under these conditions (Hu *et al.*, 2002, 2005). Whilst this may suggest that the abundance of USP7 increases after alphavirus infection, this does not reveal how the activity of USP7 changes after infection. USP7 activity regulation has shown to be regulated in range of ways, not associated with abundance. For example, through allosteric stabilisation by GMPS or through specific interactions with the target protein itself (Faesen *et al.*, 2011*a*; Cheng *et al.*, 2015; Kim *et al.*, 2019). It would therefore be of interest to repeat the probing experiment with conditions optimised for detecting changes in USP7 activity, not just abundance, following alphavirus infection.

The other DUB selected for follow-up was OTUD6B as it demonstrated a decrease in probe-reactivity following CHIKV infection. As described above, with proteins which appear to decrease following alphavirus infection, it is important to consider their half-life owing to the virus-induced translational shut-off. Although not investigated here, another study reported

OTUD6B as having a half-life of approximately 42 hrs (Sandoval *et al.*, 2013). It is therefore likely that the changes observed in OTUD6B probe-reactivity are not as a result of natural degradation following translational shut-off as the infection was only over the course of 10 hrs. With regards to the potential roles of OTUD6B, this remains a poorly characterised DUB compared to USP7. However, in one study it was shown to act as a negative regulator of cap-dependent protein translation by interacting with and destabilising the eIF4F initiation complex (Sobol *et al.*, 2017). OTUD6B has also been shown to be responsive to cytokine stimulation and is upregulated upon stimulation with IL-3, IL-4, IL-13 and GM-CSF in B-lymphocytes (Xu *et al.*, 2011). Interestingly, the role of OTUD6B appears to be dependent on the isoform present. There are three splice variants for OTUD6B with isoforms 1 and 3 behaving in a similar manner, whereas isoform 2 appears to behave differently. For example, OTUD6B-1 and -3 are thought to decrease protein translation and cell proliferation which is in contrast to OTUD6B-2 which appears to increase protein translation and cell proliferation (Sobol *et al.*, 2017).

As OTUD6B exhibited a consistent decrease in probe-reactivity following CHIKV infection, the potential role of OTUD6B in alphavirus infection was further investigated. Replication of SFV was significantly increased in OTUD6B depleted cells, which appears to also be the case for CHIKV infection. Although the mechanism for the role of OTUD6B in virus infection was not investigated here, it is feasible that OTUD6B is involved in the immune response (Xu *et al.*, 2011). OTUD6B may therefore be inhibited following infection as a viral strategy to dampen the cellular immune response. It would be of interest to further elucidate the role of OTUD6B in immune signalling in future work. In addition, the siRNAs used in this thesis target all three isoforms and it is therefore not possible to distinguish the effect of individual isoforms from this data. However, isoform-1 specific OTUD6B peptides were detected in the mass-spectrometry screen. Given the opposing role of different OTUD6B isoforms, it would be important to determine if there was a bias towards a particular isoform in alphavirus infection in any further work (Sobol *et al.*, 2017).

Taken together, the use of activity based proteomics to identify DUBs involved in alphavirus infection has highlighted a number of advantages compared to whole-proteome analysis. For example, whole proteome studies struggle to characterise all proteins, particularly those which are low abundance, and tend to only identify a few thousand of the most abundant proteins (Cho, 2007; Mulvey *et al.*, 2010). In addition, many proteins are regulated in a way which does not alter expression, for example through post-translational modifications or protein-protein interactions (section 1.4.3). A more targeted approach, such as utilisation of ABPs, allows for enrichment of the proteome based on shared functional properties (Evans & Cravatt, 2006). However, it should be noted that the conditions used in screening experiments with ABPs are not always conducive to monitoring changes in DUB activity. As each DUB displays differential binding preferences and reactivity to the probes, it is not possible to use one set of probing conditions to monitor activity in a screen (de Jong *et al.*, 2012; Ekkebus *et al.*, 2013). The ABP incubation conditions used for screening in this thesis were selected to provide an overview of changes in abundance for DUBs following CHIKV infection. Although not monitoring activity directly, this provides an insight into a group of proteins which are often overlooked and allows for identification of DUBs for further investigation.

Whilst it is clear that the use of ABPs in proteomics is a powerful tool for studying DUBs, there are also a number of limitations associated with this approach. For example, reactivity of ABPs towards DUBs is unequal meaning that DUBs which are unreactive toward the probe, such as the metalloprotease DUBs, will be overlooked (Hewings *et al.*, 2017). This can also lead to false negative results for the cysteine protease DUBs. For example, DUBs requiring substrate-assisted activation from a proximal ubiquitin, such as OTULIN, will not bind mono-ubiquitin ABPs (Keusekotten *et al.*, 2013). Conversely, there is also a risk of false positives. Binding of ABPs to some DUBs, for example USP7 and USP14, has been shown to induce a conformational change in the active site which realigns the catalytic triad (Hu *et al.*, 2002, 2005). In addition, the probes are known to bind to

non-catalytic cysteine residues of proteins and can lead to false positives (Wang *et al.*, 2009).

6.6 Future work utilising ABPs to investigate the role of DUBs in alphavirus infection

In addition to the future work described above, there are a number of additional avenues which would be of interest to explore with regards to using ABPs to investigate the role of DUBs in alphavirus infection. For example, the availability of cell permeable ABPs now permit analysis of DUBs in a more physiological setting. Lysis of cells tends to result in dilution of the cytoplasm and disrupts normal cellular organisation. Indeed, studies have shown substantial differences between ABP labelling in lysate or in live cells (Ward *et al.*, 2016; Gui *et al.*, 2018). When combined with potential compounds to target DUBs, competitive labelling can also provide characterisation of lead compounds (Kramer *et al.*, 2012; Ritorto *et al.*, 2014). In addition, second generation DUB ABPs which use di-ubiquitin as the targeting element could be used to provide a greater insight into the linkage specificity of DUBs. These probes could provide more detail on the binding mechanism as well as permitting analysis of DUBs which don't bind mono-ubiquitin probes. The increased specificity of di-ubiquitin probes towards DUBs could also reduce the likelihood of false-positives in screening experiments (Mulder *et al.*, 2014; Flierman *et al.*, 2016). Furthermore, in order to confirm that the probes are binding to the active site of DUBs, another important experiment to perform would be to compare probe binding of Cys-to-Ala DUB variants. This mutation should abolish DUB activity and probe binding should be inhibited. If this is not the case it could suggest an additional ubiquitin binding site near the reactive cysteine residue (Wang *et al.*, 2009).

6.7 Conclusions

Taken together, this study provides a greater understanding of the role of DUBs during alphavirus infection. Data demonstrating a role for USP45 in alphavirus entry indicated that this may be a candidate for consideration as a therapeutic target for alphavirus infection. In addition, the importance of utilising novel tools to monitor the ubiquitin system during alphavirus infection was highlighted by the use of ABPs. Utilising ABPs, it was demonstrated that CHIKV is unlikely to possess DUB activity. Furthermore, an alternative screening approach utilising ABPs was also exploited to identify DUBs playing a role in alphavirus infection by mass spectrometry. Two DUBs, USP7 and OTUD6B, were identified and taken forward for further analysis. Developing a greater understanding of the role of host proteins in alphavirus infection may lead to the development of novel strategies to combat these re-emerging viruses. The work presented in this thesis contributes to mounting evidence of the importance of DUBs to both normal cellular physiology, as well as viral replication and could help to inform future investigations.

References

Abdelnabi R, Jochmans D, Verbeken E, Neyts J & Delang L (2018). Antiviral treatment efficiently inhibits chikungunya virus infection in the joints of mice during the acute but not during the chronic phase of the infection. *Antiviral Res* **149,** 113–117.

Abdul Rehman SA, Kristariyanto YA, Choi S-Y, Nkosi PJ, Weidlich S, Labib K, Hofmann K & Kulathu Y (2016). *MINDY-1 Is a Member of an Evolutionarily Conserved and Structurally Distinct New Family of Deubiquitinating Enzymes*.

Abere B, Wikan N, Ubol S, Auewarakul P, Paemanee A, Kittisenachai S, Roytrakul S & Smith DR (2012). Proteomic analysis of chikungunya virus infected microgial cells ed. Ng Fong Poh L. *PLoS One* **7,** e34800.

Acevedo N, Waggoner J, Rodriguez M, Rivera L, Landivar J, Pinsky B & Zambrano H (2017). Zika virus, chikungunya virus, and dengue virus in cerebrospinal fluid from adults with neurological manifestations, Guayaquil, Ecuador. *Front Microbiol* **8,** 42.

Aebersold R & Mann M (2003). Mass spectrometry-based proteomics. *Nature* **422,** 198–207.

Aebersold R & Mann M (2016). Mass-spectrometric exploration of proteome structure and function. *Nature* **537,** 347–355. Available at: http://www.nature.com/articles/nature19949 [Accessed March 15, 2019].

Ahmad NA, Vythilingam I, Lim YAL, Zabari NZAM & Lee HL (2017). Detection of Wolbachia in aedes albopictus and their effects on chikungunya virus. *Am J Trop Med Hyg* **96,** 148–156.

Akahata W, Yang Z-Y, Andersen H, Sun S, Holdaway HA, Kong W-P, Lewis MG, Higgs S, Rossmann MG, Rao S & Nabel GJ (2010). A virus-like particle vaccine for epidemic Chikungunya virus protects nonhuman primates against infection. *Nat Med* **16,** 334–338.

Al-Hakim AK, Zagorska A, Chapman L, Deak M, Peggie M & Alessi DR (2008). Control of AMPK-related kinases by USP9X and atypical Lys 29 /Lys 33 -linked polyubiquitin chains. *Biochem J* **411,** 249–260.

Ali A, Raja R, Farooqui SR, Ahmad S & Banerjea AC (2017). USP7 deubiquitinase controls HIV-1 production by stabilizing Tat protein. *Biochem J* **474,** 1653–1668.

Aliota MT, Walker EC, Uribe Yepes A, Dario Velez I, Christensen BM & Osorio JE (2016). The wMel Strain of Wolbachia Reduces Transmission of Chikungunya Virus in Aedes aegypti ed. Armstrong PM. *PLoS Negl Trop Dis* **10,** e0004677.

Alphey L, Benedict M, Bellini R, Clark GG, Dame DA, Service MW & Dobson SL (2010). Sterile-Insect Methods for Control of Mosquito-Borne Diseases: An Analysis. *Vector-Borne Zoonotic Dis* **10,** 295–311.

Altun M, Kramer HB, Willems LI, McDermott JL, Leach CA, Goldenberg SJ, Kumar KGS, Konietzny R, Fischer R, Kogan E, MacKeen MM, McGouran J, Khoronenkova S V., Parsons JL, Dianov GL, Nicholson B & Kessler BM (2011). Activity-based chemical proteomics accelerates inhibitor development for deubiquitylating enzymes. *Chem Biol* **18,** 1401–1412.

Amaral JK, Sutaria R & Schoen RT (2018). Treatment of chronic chikungunya arthritis with methotrexate: a systematic review. *Arthritis Care Res (Hoboken)*; DOI: 10.1002/acr.23519.

An J, Mo D, Liu H, Veena MS, Srivatsan ES, Massoumi R & Rettig MB (2008). Inactivation of the CYLD deubiquitinase by HPV E6 mediates hypoxia-induced NF-kappaB activation. *Cancer Cell* **14,** 394–407.

Anyamba A, Small JL, Britch SC, Tucker CJ, Pak EW, Reynolds CA, Crutchfield J & Linthicum KJ (2014). Recent weather extremes and impacts on agricultural production and vector-borne disease outbreak patterns ed. Ikegami T. *PLoS One* **9,** e92538.

Arankalle VA, Shrivastava S, Cherian S, Gunjikar RS, Walimbe AM, Jadhav SM, Sudeep AB & Mishra AC (2007). Genetic divergence of Chikungunya viruses in India (1963-2006) with special reference to the 2005-2006 explosive epidemic. *J Gen Virol* **88,** 1967–1976.

Arziman Z, Horn T & Boutros M (2005). E-RNAi: A web application to design optimized RNAi constructs. *Nucleic Acids Res* **33,** W582-8.

Bailey-Elkin BA, Knaap RCM, Kikkert M & Mark BL (2017). Structure and Function of Viral Deubiquitinating Enzymes. *J Mol Biol* **429,** 3441–3470.

Baker RT & Board PG (1991). The human ubiquitin-52 amino acid fusion protein gene shares several structural features with mammalian ribosomal protein genes. *Nucleic Acids Res* **19,** 1035–1040.

Bakshi S, Holzer B, Bridgen A, McMullan G, Quinn DG & Baron MD (2013). Dugbe virus ovarian tumour domain interferes with ubiquitin/ISG15-regulated innate immune cell signalling. *J Gen Virol* **94,** 298–307.

Balakirev MY, Jaquinod M, Haas AL & Chroboczek J (2002). Deubiquitinating Function of Adenovirus Proteinase. *J Virol* **76,** 6323–6331.

Baravalle G, Schober D, Huber M, Bayer N, Murphy RF & Fuchs R (2005). Transferrin recycling and dextran transport to lysosomes is differentially affected by bafilomycin, nocodazole, and low temperature. *Cell Tissue Res* **320,** 99–113.

Barbieri MA, Heath CM, Peters EM, Wells A, Davis JN & Stahl PD (2001). Phosphatidylinositol-4-phosphate 5-Kinase-1β Is Essential for Epidermal Growth Factor Receptor-mediated Endocytosis. *J Biol Chem* **276,** 47212–47216.

Barretto N, Jukneliene D, Ratia K, Chen Z, Mesecar AD & Baker SC (2005). The papain-like protease of severe acute respiratory syndrome coronavirus has deubiquitinating activity. *J Virol* **79,** 15189–15198.

Barton DJ, Sawicki SG & Sawicki DL (1991). Solubilization and immunoprecipitation of alphavirus replication complexes. *J Virol* **65,** 1496–1506.

Bassetto M, De Burghgraeve T, Delang L, Massarotti A, Coluccia A, Zonta N, Gatti V, Colombano G, Sorba G, Silvestri R, Tron GC, Neyts J, Leyssen P & Brancale A (2013). Computer-aided identification, design and synthesis of a novel series of compounds with selective antiviral activity against chikungunya virus. *Antiviral Res* **98,** 12–18.

Baylis M (2017). Potential impact of climate change on emerging vector-borne and other infections in the UK. *Environ Heal* **16,** 112.

Békés M, Rut W, Kasperkiewicz P, Mulder MPC, Ovaa H, Drag M, Lima CD & Huang TT (2015). SARS hCoV papain-like protease is a unique Lys48 linkage-specific di-distributive deubiquitinating enzyme. *Biochem J* **468,** 215–226.

Benedict MQ & Robinson AS (2003). The first releases of transgenic mosquitoes: An argument for the sterile insect technique. *Trends Parasitol* **19,** 349–355.

Bernard E, Solignat M, Gay B, Chazal N, Higgs S, Devaux C & Briant L (2010). Endocytosis of chikungunya virus into mammalian cells: Role of clathrin and early endosomal compartments ed. Schwartz O. *PLoS One* **5,** e11479.

Bhalla N, Sun C, Metthew Lam LK, Gardner CL, Ryman KD & Klimstra WB (2016). Host translation shutoff mediated by non-structural protein 2 is a critical factor in the antiviral state resistance of Venezuelan equine encephalitis virus. *Virology* **496,** 147–165.

Bharaj P, Atkins C, Luthra P, Giraldo MI, Dawes BE, Miorin L, Johnson JR, Krogan NJ, Basler CF, Freiberg AN & Rajsbaum R (2017). The Host E3-Ubiquitin Ligase TRIM6 Ubiquitinates the Ebola Virus VP35 Protein and Promotes Virus Replication ed. Lyles DS. *J Virol* **91,** e00833-17.

Blanchette P, Cheng CY, Yan Q, Ketner G, Ornelles DA, Dobner T, Conaway RC, Conaway JW & Branton PE (2004). Both BC-Box Motifs of Adenovirus Protein E4orf6 Are Required To Efficiently Assemble an E3 Ligase Complex That Degrades p53. *Mol Cell Biol* **24,** 9619–9629.

Blot V, Perugi F, Gay B, Prévost M-C, Briant L, Tangy F, Abriel H, Staub O, Dokhélar M-C & Pique C (2004). Nedd4.1-mediated ubiquitination and subsequent recruitment of Tsg101 ensure HTLV-1 Gag trafficking towards the multivesicular body pathway prior to virus budding. *J Cell Sci* **117,** 2357–2367.

Boettcher M & McManus MT (2015). Choosing the Right Tool for the Job: RNAi, TALEN, or CRISPR. *Mol Cell* **58,** 575–585.

Boname JM & Lehner PJ (2011). What has the study of the K3 and K5 viral ubiquitin E3 ligases taught us about ubiquitin-mediated receptor regulation? *Viruses* **3,** 118–131.

Borgherini G, Poubeau P, Staikowsky F, Lory M, Moullec NL, Becquart JP, Wengling C, Michault A & Paganin F (2007). Outbreak of Chikungunya on Reunion Island: Early Clinical and Laboratory Features in 157 Adult Patients. *Clin Infect Dis* **44,** 1401–1407.

Borodovsky A, Kessler BM, Casagrande R, Overkleeft HS, Wilkinson KD & Ploegh HL (2001). A novel active site-directed probe specific for deubiquitylating enzymes reveals proteasome association of USP14. *EMBO J* **20,** 5187–5196.

Borodovsky A, Ovaa H, Kolli N, Gan-Erdene T, Wilkinson KD, Ploegh HL & Kessler BM (2002). Chemistry-based functional proteomics reveals novel members of the deubiquitinating enzyme family. *Chem Biol* **9,** 1149–1159.

Boutell C, Canning M, Orr A & Everett RD (2005). Reciprocal activities between herpes simplex virus type 1 regulatory protein ICP0, a ubiquitin E3 ligase, and ubiquitin-specific protease USP7. *J Virol* **79,** 12342–12354.

Boutell C, Sadis S & Everett RD (2002). Herpes Simplex Virus Type 1 Immediate-Early Protein ICP0 and Its Isolated RING Finger Domain Act as Ubiquitin E3 Ligases In Vitro. *J Virol* **76,** 841–850.

Breakwell L, Dosenovic P, Karlsson Hedestam GB, D'Amato M, Liljestrom P, Fazakerley J & McInerney GM (2007). Semliki Forest Virus Nonstructural Protein 2 Is Involved in Suppression of the Type I Interferon Response. *J Virol* **81,** 8677–8684.

Bremm A & Komander D (2011). Emerging roles for Lys11-linked polyubiquitin in cellular regulation. *Trends Biochem Sci* **36,** 355–363. Available at: http://www.ncbi.nlm.nih.gov/pubmed/21641804 [Accessed December 3, 2018].

Brinkmann V, Billich A, Baumruker T, Heining P, Schmouder R, Francis G, Aradhye S & Burtin P (2010). Fingolimod (FTY720): discovery and development of an oral drug to treat multiple sclerosis. *Nat Rev Drug Discov* **9,** 883–897.

Briolant S, Garin D, Scaramozzino N, Jouan A & Crance JM (2004). In vitro inhibition of Chikungunya and Semliki Forest viruses replication by antiviral compounds: Synergistic effect of interferon-α and ribavirin combination. *Antiviral Res* **61,** 111–117.

De Brito CAA (2017). Alert: Severe cases and deaths associated with Chikungunya in Brazil. *Rev Soc Bras Med Trop* **50,** 585–589. Available at: http://www.scielo.br/scielo.php?script=sci_arttext&pid=S0037-86822017000500585&lng=en&tlng=en [Accessed November 27, 2017].

Broeckel R et al. (2017). Therapeutic administration of a recombinant human monoclonal antibody reduces the severity of chikungunya virus disease in rhesus macaques ed. Powers AM. *PLoS Negl Trop Dis* **11,** e0005637.

Brooks CL, Li M, Hu M, Shi Y & Gu W (2007). The p53–Mdm2–HAUSP complex is involved in p53 stabilization by HAUSP. *Oncogene* **26,** 7262–7266.

Burt FJ, Chen W, Miner JJ, Lenschow DJ, Merits A, Schnettler E, Kohl A, Rudd PA, Taylor A, Herrero LJ, Zaid A, Ng LFP & Mahalingam S (2017). Chikungunya virus: an update on the biology and pathogenesis of this emerging pathogen. *Lancet Infect Dis* **17,** e107–e117.

Cai J, Liu T, Jiang X, Guo C, Liu A & Xiao X (2017). Downregulation of USP18 inhibits growth and induces apoptosis in hepatitis B virus-related hepatocellular carcinoma cells by suppressing BCL2L1. *Exp Cell Res* **358,** 315–322.

Calba C, Guerbois-Galla M, Franke F, Jeannin C, Auzet-Caillaud M, Grard G, Pigaglio L, Decoppet A, Weicherding J, Savaill MC, Munoz-Riviero M, Chaud P, Cadiou B, Ramalli L, Fournier P, Noël H, De Lamballerie X, Paty MC & Leparc-Goffart I (2017). Preliminary report of an autochthonous chikungunya outbreak in France, July to September 2017. *Eurosurveillance* **22,** 5–10.

Carey DE (1971). Chikungunya and dengue: A case of mistaken identity? *J Hist Med Allied Sci* **XXVI,** 243–262.

CDC (2018). Countries and territories where chikungunya cases have been reported* (as of May 29, 2018). Available at: https://www.cdc.gov/chikungunya/geo/index.html [Accessed May 31, 2018].

Chan MWY, Wei SH, Wen P, Wang Z, Matei DE, Liu JC, Liyanarachchi S, Brown R, Nephew KP, Yan PS & Huang TH-M (2005). Hypermethylation of 18S and 28S ribosomal DNAs predicts progression-free survival in patients with ovarian cancer. *Clin Cancer Res* **11,** 7376–7383.

Chanda E, Ameneshewa B, Mihreteab S, Berhane A, Zehaie A, Ghebrat Y & Usman A (2015). Consolidating strategic planning and operational frameworks for integrated vector management in Eritrea. *Malar J* **14,** 488.

Chandrasekar I, Goeckeler ZM, Turney SG, Wang P, Wysolmerski RB, Adelstein RS & Bridgman PC (2014). Nonmuscle myosin II is a critical regulator of clathrin-mediated endocytosis. *Traffic* **15,** 418–432.

Chandrasekar I, Huettner JE, Turney SG & Bridgman PC (2013). Myosin II Regulates Activity Dependent Compensatory Endocytosis at Central Synapses. *J Neurosci* **33,** 16131–16145.

Chang L-J, Dowd KA, Mendoza FH, Saunders JG, Sitar S, Plummer SH, Yamshchikov G, Sarwar UN, Hu Z, Enama ME, Bailer RT, Koup RA, Schwartz RM, Akahata W, Nabel GJ, Mascola JR, Pierson TC, Graham BS & Ledgerwood JE (2014). Safety and tolerability of chikungunya virus-like particle vaccine in healthy adults: a phase 1 dose-escalation trial. *Lancet (London, England)* **384,** 2046–2052.

de Chassey B, Meyniel-Schicklin L, Vonderscher J, André P & Lotteau V (2014). Virus-host interactomics: New insights and opportunities for antiviral drug discovery. *Genome Med* **6,** 115. Available at: http://www.ncbi.nlm.nih.gov/pubmed/25593595 [Accessed December 31, 2018].

Chau V, Tobias JW, Bachmair A, Marriott D, Ecker DJ, Gonda DK & Varshavsky A (1989). A multiubiquitin chain is confined to specific lysine in a targeted short-lived protein. *Science* **243,** 1576–1583.

Chavoshi S, Egorova O, Lacdao IK, Farhadi S, Sheng Y & Saridakis V (2016). Identification of kaposi sarcoma herpesvirus (KSHV) vIRF1 protein as a novel interaction partner of human deubiquitinase USP7. *J Biol Chem* **291,** 6281–6291.

Chen CI, Clark DC, Pesavento P, Lerche NW, Luciw PA, Reisen WK & Brault AC (2010*a*). Comparative pathogenesis of epidemic and enzootic Chikungunya viruses in a pregnant Rhesus macaque model. *Am J Trop Med Hyg* **83,** 1249–1258.

Chen R, Mukhopadhyay S, Merits A, Bolling B, Nasar F, Coffey LL, Powers A, Weaver SC & Ictv Report Consortium (2018). ICTV Virus Taxonomy Profile: Togaviridae. *J Gen Virol* **99,** 761–762.

Chen R, Zhang L, Zhong B, Tan B, Liu Y & Shu H-B (2010*b*). The ubiquitin-specific protease 17 is involved in virus-triggered type I IFN signaling. *Cell Res* **20,** 802–811.

Chen X, Yang X, Zheng Y, Yang Y, Xing Y & Chen Z (2014). SARS coronavirus papain-like protease inhibits the type I interferon signaling pathway through interaction with the STING-TRAF3-TBK1 complex. *Protein Cell* **5,** 369–381.

Chen Z, Huang X, Ye J, Pan P, Cao Q, Yang B, Li Z, Su M, Huang C & Gu J (2010*c*). Immunoglobulin G is present in a wide variety of soft tissue tumors and correlates well with proliferation markers and tumor grades. *Cancer* **116,** 1953–1963.

Chen Z, Qiu X & Gu J (2009). Immunoglobulin expression in non-lymphoid lineage and neoplastic cells. *Am J Pathol* **174,** 1139–1148.

Cheng J, Yang H, Fang J, Ma L, Gong R, Wang P, Li Z & Xu Y (2015). Molecular mechanism for USP7-mediated DNMT1 stabilization by acetylation. *Nat Commun* **6,** 7023.

Chenon M, Camborde L, Cheminant S & Jupin I (2012). A viral deubiquitylating enzyme targets viral RNA-dependent RNA polymerase and affects viral infectivity. *EMBO J* **31,** 741–753.

Cherry S (2009). What have RNAi screens taught us about viral-host interactions? *Curr Opin Microbiol* **12,** 446–452.

Cho WCS (2007). Proteomics Technologies and Challenges. *Genomics, Proteomics Bioinforma* **5,** 77–85.

Choi HK, Lu G, Lee S, Wengler G & Rossmann MG (1997). Structure of semliki forest virus core protein. *Proteins Struct Funct Genet* **27,** 345–359.

Choi HK, Tong L, Minor W, Dumas P, Boege U, Rossmann MG & Wengler G (1991). Structure of Sindbis virus core protein reveals a chymotrypsin-like serine proteinase and the organization of the virion. *Nature* **354,** 37–43.

Chow A, Her Z, Ong EKS, Chen JM, Dimatatac F, Kwek DJC, Barkham T, Yang H, Rénia L, Leo YS & Ng LFP (2011). Persistent arthralgia induced by Chikungunya virus infection is associated with interleukin-6 and granulocyte macrophage colony-stimulating factor. *J Infect Dis* **203,** 149–157.

Christodoulou M (2011). Biological vector control of mosquito-borne diseases. *Lancet Infect Dis* **11,** 84–85.

Chu H, Das SC, Fuchs JF, Suresh M, Weaver SC, Stinchcomb DT, Partidos CD & Osorio JE (2013). Deciphering the protective role of adaptive immunity to CHIKV/IRES a novel candidate vaccine against Chikungunya in the A129 mouse model. *Vaccine* **31,** 3353–3360.

Chua HH, Abdul Rashid K, Law WC, Hamizah A, Chem YK, Khairul AH & Chua KB (2010). A fatal case of chikungunya virus infection with liver involvement. *Med J Malaysia* **65,** 83–84.

Chusri S, Siripaitoon P, Hirunpat S & Silpapojakul K (2011). Case reports of neuro-chikungunya in Southern Thailand. *Am J Trop Med Hyg* **85,** 386–389.

Ciechanover A, Elias S, Heller H & Hershko A (1982). “Covalent affinity” purification of ubiquitin-activating enzyme. *J Biol Chem* **257,** 2537–2542.

Ciechanover A, Heller H, Katz-Etzion R & Hershko A (1981). Activation of the heat-stable polypeptide of the ATP-dependent proteolytic system. *Proc Natl Acad Sci U S A* **78,** 761–765.

Clague MJ, Barsukov I, Coulson JM, Liu H, Rigden DJ & Urbé S (2013). Deubiquitylases from genes to organism. *Physiol Rev* **93,** 1289–1315.

Clague MJ, Heride C & Urbé S (2015). The demographics of the ubiquitin system. *Trends Cell Biol* **25,** 417–426. Available at: https://www.sciencedirect.com/science/article/pii/S0962892415000549 [Accessed December 3, 2018].

Clague MJ & Urbé S (2017). Integration of cellular ubiquitin and membrane traffic systems: focus on deubiquitylases. *FEBS J* **284,** 1753–1766.

Clague MJ, Urbé S & Komander D (2019). Breaking the chains: deubiquitylating enzyme specificity begets function. *Nat Rev Mol Cell Biol*1.

Colland F (2010). The therapeutic potential of deubiquitinating enzyme inhibitors. *Biochem Soc Trans* **38,** 137–143.

Colland F, Formstecher E, Jacq X, Reverdy C, Planquette C, Conrath S, Trouplin V, Bianchi J, Aushev VN, Camonis J, Calabrese A, Borg-Capra C, Sippl W, Collura V, Boissy G, Rain J-C, Guedat P, Delansorne R & Daviet L (2009). Small-molecule inhibitor of USP7/HAUSP ubiquitin protease stabilizes and activates p53 in cells. *Mol Cancer Ther* **8,** 2286–2295.

Conte C, Griffis ER, Hickson I & Perez-Oliva AB (2018). USP45 and Spindly are part of the same complex implicated in cell migration. *Sci Rep* **8,** 14375.

Coombes N, Nugban A, King S, Wali M, Khandaker S, Hendrickse T, Conway L, Galbraith S, Coulson JM & Blake N (2019). The deubiquitylase USP45 plays a key role in entry of Chikungunya virus via clathrin mediated endocytosis.

Coombs KM & Brown DT (1989). Form-determining functions in Sindbis virus nucleocapsids: nucleosomelike organization of the nucleocapsid. *J Virol* **63,** 883–891.

Coscoy L & Ganem D (2001). A viral protein that selectively downregulates ICAM-1 and B7-2 and modulates T cell costimulation. *J Clin Invest* **107,** 1599–1606.

Couderc T, Chrétien F, Schilte C, Disson O, Brigitte M, Guivel-Benhassine F, Touret Y, Barau G, Cayet N, Schuffenecker I, Desprès P, Arenzana-Seisdedos F, Michault A, Albert ML & Lecuit M (2008). A mouse model for Chikungunya: Young age and inefficient type-I interferon signaling are risk factors for severe disease. *PLoS Pathog* **4,** e29.

Couderc T, Khandoudi N, Grandadam M, Visse C, Gangneux N, Bagot S, Prost J & Lecuit M (2009). Prophylaxis and Therapy for Chikungunya Virus Infection. *J Infect Dis* **200,** 516–523.

Cross RK (1983). Identification of a unique guanine-7-methyltransferase in Semliki forest virus (SFV) infected cell extracts. *Virology* **130,** 452–463.

Cureton DK, Massol RH, Saffarian S, Kirchhausen TL & Whelan SPJ (2009). Vesicular Stomatitis Virus Enters Cells through Vesicles Incompletely Coated with Clathrin That Depend upon Actin for Internalization ed. Young JAT. *PLoS Pathog* **5,** e1000394.

Darling S (2017). Profiling deubiquitylase activity during the cell cycle reveals phosphorylation-dependent regulation of USP7 activity at G1/S (Thesis).

Das PK, Puusepp L, Varghese FS, Utt A, Ahola T, Kananovich DG, Lopp M, Merits A & Karelson M (2016). Design and validation of novel chikungunya virus protease inhibitors. *Antimicrob Agents Chemother* **60,** 7382–7395.

Denuc A, Bosch-Comas A, Gonzàlez-Duarte R & Marfany G (2009). The UBA-UIM domains of the USP25 regulate the enzyme ubiquitination state and modulate substrate recognition. *PLoS One* **4,** e5571.

Dhanwani R, Khan M, Alam SI, Rao PVL & Parida M (2011). Differential proteome analysis of Chikungunya virus-infected new-born mice tissues reveal implication of stress, inflammatory and apoptotic pathways in disease pathogenesis. *Proteomics* **11,** 1936–1951.

Dubey C, Croft M & Swain SL (1995). Costimulatory requirements of naive CD4+ T cells. ICAM-1 or B7-1 can costimulate naive CD4 T cell activation but both are required for optimum response. *J Immunol* **155,** 45–57.

Dubrulle M, Mousson L, Moutailier S, Vazeille M & Failloux AB (2009). Chikungunya virus and Aedes mosquitoes: Saliva is infectious as soon as two days after oral infection ed. Baylis M. *PLoS One* **4,** e5895.

van Duijl-Richter MKS, Hoornweg TE, Rodenhuis-Zybert IA & Smit JM (2015). Early Events in Chikungunya Virus Infection-From Virus CellBinding to Membrane Fusion. *Viruses* **7,** 3647–3674.

Edelman R, Tacket CO, Wasserman SS, Bodison SA, Perry JG & Mangiafico JA (2000). Phase II safety and immunogenicity study of live chikungunya virus vaccine TSI-GSD-218. *Am J Trop Med Hyg* **62,** 681–685.

Edelmann MJ, Iphöfer A, Akutsu M, Altun M, di Gleria K, Kramer HB, Fiebiger E, Dhe-Paganon S & Kessler BM (2009). Structural basis and specificity of human otubain 1-mediated deubiquitination. *Biochem J* **418,** 379–390.

Edwards CJ, Welch SR, Chamberlain J, Hewson R, Tolley H, Cane PA & Lloyd G (2007). Molecular diagnosis and analysis of Chikungunya virus. *J Clin Virol* **39,** 271–275.

Ekkebus R, Flierman D, Geurink PP & Ovaa H (2014). Catching a DUB in the act: Novel ubiquitin-based active site directed probes. *Curr Opin Chem Biol* **23,** 63–70.

Ekkebus R, van Kasteren SI, Kulathu Y, Scholten A, Berlin I, Geurink PP, de Jong A, Goerdayal S, Neefjes J, Heck AJR, Komander D & Ovaa H (2013). On terminal alkynes that can react with active-site cysteine nucleophiles in proteases. *J Am Chem Soc* **135,** 2867–2870.

Elbashir SM, Harborth J, Lendeckel W, Yalcin A, Weber K & Tuschl T (2001). Duplexes of 21-nucleotide RNAs mediate RNA interference in cultured mammalian cells. *Nature* **411,** 494–498.

Elliott PR, Nielsen S V., Marco-Casanova P, Fiil BK, Keusekotten K, Mailand N, Freund SM V, Gyrd-Hansen M & Komander D (2014). Molecular basis and regulation of OTULIN-LUBAC interaction. *Mol Cell* **54,** 335–348.

Erasmus JH, Auguste AJ, Kaelber JT, Luo H, Rossi SL, Fenton K, Leal G, Kim DY, Chiu W, Wang T, Frolov I, Nasar F & Weaver SC (2017). A chikungunya fever vaccine utilizing an insect-specific virus platform. *Nat Med* **23,** 192–199.

Evans MJ & Cravatt BF (2006). Mechanism-based profiling of enzyme families. *Chem Rev* **106,** 3279–3301. Available at: http://pubs.acs.org/doi/abs/10.1021/cr050288g [Accessed August 5, 2016].

Faesen AC, Dirac AMG, Shanmugham A, Ovaa H, Perrakis A & Sixma TK (2011*a*). Mechanism of USP7/HAUSP activation by its C-Terminal ubiquitin-like domain and allosteric regulation by GMP-synthetase. *Mol Cell* **44,** 147–159.

Faesen AC, Luna-Vargas MPA, Geurink PP, Clerici M, Merkx R, Van Dijk WJ, Hameed DS, El Oualid F, Ovaa H & Sixma TK (2011*b*). The differential modulation of USP activity by internal regulatory domains, interactors and eight ubiquitin chain types. *Chem Biol* **18,** 1550–1561.

Fallon L, Bélanger CML, Corera AT, Kontogiannea M, Regan-Klapisz E, Moreau F, Voortman J, Haber M, Rouleau G, Thorarinsdottir T, Brice A, van Bergen en Henegouwen PMP & Fon EA (2006). A regulated interaction with the UIM protein Eps15 implicates parkin in EGF receptor trafficking and PI(3)K-Akt signalling. *Nat Cell Biol* **8,** 834–842.

Fan Y-H, Cheng J, Vasudevan S a, Dou J, Zhang H, Patel RH, Ma IT, Rojas Y, Zhao Y, Yu Y, Shohet JM, Nuchtern JG, Kim ES & Yang J (2013). USP7 inhibitor P22077 inhibits neuroblastoma growth via inducing p53-mediated apoptosis. *Cell Death Dis* **4,** e867.

Fan Y, Mao R, Yu Y, Liu S, Shi Z, Cheng J, Zhang H, An L, Zhao Y, Xu X, Chen Z, Kogiso M, Zhang D, Zhang H, Zhang P, Jung JU, Li X, Xu G & Yang J (2014). USP21 negatively regulates antiviral response by acting as a RIG-I deubiquitinase. *J Exp Med* **211,** 313–328.

Farrell KB, McDonald S, Lamb AK, Worcester C, Peersen OB & di Pietro SM (2017). Novel function of a dynein light chain in actin assembly during clathrin-mediated endocytosis. *J Cell Biol* **216,** 2565–2580.

Farshi P, Deshmukh RR, Nwankwo JO, Arkwright RT, Cvek B, Liu J & Dou QP (2015). Deubiquitinases (DUBs) and DUB inhibitors: a patent review. *Expert Opin Ther Pat* **25,** 1191–1208.

Fielding AB, Willox AK, Okeke E & Royle SJ (2012). Clathrin-mediated endocytosis is inhibited during mitosis. *Proc Natl Acad Sci* **109,** 6572–6577.

Fiil BK, Damgaard RB, Wagner SA, Keusekotten K, Fritsch M, Bekker-Jensen S, Mailand N, Choudhary C, Komander D & Gyrd-Hansen M (2013). OTULIN Restricts Met1-Linked Ubiquitination to Control Innate Immune Signaling. *Mol Cell*; DOI: 10.1016/j.molcel.2013.06.004.

Fire A, Xu S, Montgomery MK, Kostas SA, Driver SE & Mello CC (1998). Potent and specific genetic interference by double-stranded RNA in caenorhabditis elegans. *Nature* **391,** 806–811.

Flierman D, Van Der Heden Van Noort GJ, Ekkebus R, Geurink PP, Mevissen TET, Hospenthal MK, Komander D & Ovaa H (2016). Non-hydrolyzable Diubiquitin Probes Reveal Linkage-Specific Reactivity of Deubiquitylating Enzymes Mediated by S2 Pockets. *Cell Chem Biol* **23,** 472–482.

Fong S-W, Kini RM & Ng LFP (2018). Mosquito Saliva Reshapes Alphavirus Infection and Immunopathogenesis. *J Virol* **92,** e01004-17.

Forrester NL, Palacios G, Tesh RB, Savji N, Guzman H, Sherman M, Weaver SC & Lipkin WI (2012). Genome-scale phylogeny of the alphavirus genus suggests a marine origin. *J Virol* **86,** 2729–2738.

Forsell K, Suomalainen M & Garoff H (1995). Structure-function relation of the NH2-terminal domain of the Semliki Forest virus capsid protein. *J Virol* **69,** 1556–1563.

Foy NJ, Akhrymuk M, Akhrymuk I, Atasheva S, Bopda-Waffo A, Frolov I & Frolova EI (2013). Hypervariable Domains of nsP3 Proteins of New World and Old World Alphaviruses Mediate Formation of Distinct, Virus-Specific Protein Complexes. *J Virol* **87,** 1997–2010.

Fragkoudis R, Breakwell L, McKimmie C, Boyd A, Barry G, Kohl A, Merits A & Fazakerley JK (2007). The type I interferon system protects mice from Semliki Forest virus by preventing widespread virus dissemination in extraneural tissues, but does not mediate the restricted replication of avirulent virus in central nervous system neurons. *J Gen Virol* **88,** 3373–3384.

Fraisier C et al. (2014). Kinetic Analysis of Mouse Brain Proteome Alterations Following Chikungunya Virus Infection before and after Appearance of Clinical Symptoms ed. Stewart JP. *PLoS One* **9,** e91397.

Frolov I, Garmashova N, Atasheva S & Frolova EI (2009). Random Insertion Mutagenesis of Sindbis Virus Nonstructural Protein 2 and Selection of Variants Incapable of Downregulating Cellular Transcription. *J Virol* **83,** 9031–9044.

Frolova EI, Gorchakov R, Pereboeva L, Atasheva S & Frolov I (2010). Functional Sindbis virus replicative complexes are formed at the plasma membrane. *J Virol* **84,** 11679–11695.

Fros J & Pijlman G (2016). Alphavirus Infection: Host Cell Shut-Off and Inhibition of Antiviral Responses. *Viruses* **8,** 166.

Fujimoto LM, Roth R, Heuser JE & Schmid SL (2000). Actin Assembly Plays a Variable, but not Obligatory Role in Receptor-Mediated Endocytosis. *Traffic* **1,** 161–171.

Gardner J, Anraku I, Le TT, Larcher T, Major L, Roques P, Schroder WA, Higgs S & Suhrbier A (2010). Chikungunya Virus Arthritis in Adult Wild-Type Mice. *J Virol* **84,** 8021–8032.

Gardner J, Rudd PA, Prow NA, Belarbi E, Roques P, Larcher T, Gresh L, Balmaseda A, Harris E, Schroder WA & Suhrbier A (2015). Infectious chikungunya virus in the saliva of mice, monkeys and humans ed. Ng LFP. *PLoS One* **10,** e0139481.

Garoff H & Simons K (1974). Location of the spike glycoproteins in the Semliki Forest virus membrane. *Proc Natl Acad Sci U S A* **71,** 3988–3992.

Gérardin P et al. (2014). Neurocognitive Outcome of Children Exposed to Perinatal Mother-to-Child Chikungunya Virus Infection: The CHIMERE Cohort Study on Reunion Island ed. Powers AM. *PLoS Negl Trop Dis* **8,** e2996.

Gérardin P, Guernier V, Perrau J, Fianu A, Le Roux K, Grivard P, Michault A, de Lamballerie X, Flahault A & Favier F (2008). Estimating Chikungunya prevalence in La Réunion Island outbreak by serosurveys: Two methods for two critical times of the epidemic. *BMC Infect Dis* **8,** 99.

Gibbons DL, Vaney MC, Roussel A, Vigouroux A, Reilly B, Lepault J, Kielian M & Rey FA (2004). Conformational change and protein-protein interactions of the fusion protein of Semliki Forest virus. *Nature* **427,** 320–325.

Gilbert LA, Horlbeck MA, Adamson B, Villalta JE, Chen Y, Whitehead EH, Guimaraes C, Panning B, Ploegh HL, Bassik MC, Qi LS, Kampmann M & Weissman JS (2014). Genome-Scale CRISPR-Mediated Control of Gene Repression and Activation. *Cell* **159,** 647–661.

Glickman MH & Adir N (2004). The Proteasome and the Delicate Balance between Destruction and Rescue. *PLoS Biol* **2,** e13.

Glomb-Reinmund S & Kielian M (1998). The role of low pH and disulfide shuffling in the entry and fusion of Semliki Forest virus and Sindbis virus. *Virology* **248,** 372–381.

Go YY, Balasuriya UBR & Lee C-K (2014). Zoonotic encephalitides caused by arboviruses: transmission and epidemiology of alphaviruses and flaviviruses. *Clin Exp Vaccine Res* **3,** 58.

Goldknopf IL, French MF, Musso R & Busch H (1977). Presence of protein A24 in rat liver nucleosomes. *Proc Natl Acad Sci U S A* **74,** 5492–5495.

Goldstein G, Scheid M, Hammerling U, Schlesinger DH, Niall HD & Boyse EA (1975). Isolation of a polypeptide that has lymphocyte-differentiating properties and is probably represented universally in living cells. *Proc Natl Acad Sci* **72,** 11–15.

Gomez De Cedrón M, Ehsani N, Mikkola ML, García JA & Kääriäinen L (1999). RNA helicase activity of Semliki Forest virus replicase protein NSP2. *FEBS Lett* **448,** 19–22.

González CM, Wang L & Damania B (2009). Kaposi's sarcoma-associated herpesvirus encodes a viral deubiquitinase. *J Virol* **83,** 10224–10233.

Goodbourn S, Fitzpatrick-Swallow V, Randall RE, Precious B & Childs K (2005). Simian Virus 5 V Protein Acts as an Adaptor, Linking DDB1 to STAT2, To Facilitate the Ubiquitination of STAT1. *J Virol* **79,** 13434–13441.

Goodwin CJ, Holt SJ, Downes S & Marshall NJ (1995). Microculture tetrazolium assays: a comparison between two new tetrazolium salts, XTT and MTS. *J Immunol Methods* **179,** 95–103.

Gorchakov R, Wang E, Leal G, Forrester NL, Plante K, Rossi SL, Partidos CD, Adams AP, Seymour RL, Weger J, Borland EM, Sherman MB, Powers AM, Osorio JE & Weaver SC (2012). Attenuation of Chikungunya Virus Vaccine Strain 181/Clone 25 Is Determined by Two Amino Acid Substitutions in the E2 Envelope Glycoprotein. *J Virol* **86,** 6084–6096.

Gottlieb TA, Ivanov IE, Adesnik M & Sabatini DD (1993). Actin microfilaments play a critical role in endocytosis at the apical but not the basolateral surface of polarized epithelial cells. *J Cell Biol* **120,** 695–710.

Gould E, Pettersson J, Higgs S, Charrel R & de Lamballerie X (2017). Emerging arboviruses: Why today? *One Heal* **4,** 1–13. Available at: https://www.sciencedirect.com/science/article/pii/S2352771417300137?via%3Dihub [Accessed April 23, 2018].

Gredmark S, Schlieker C, Quesada V, Spooner E & Ploegh HL (2007). A Functional Ubiquitin-Specific Protease Embedded in the Large Tegument Protein (ORF64) of Murine Gammaherpesvirus 68 Is Active during the Course of Infection. *J Virol* **81,** 10300–10309.

Grossi-Soyster EN, Cook EAJ, de Glanville WA, Thomas LF, Krystosik AR, Lee J, Wamae CN, Kariuki S, Fèvre EM & LaBeaud AD (2017). Serological and spatial analysis of alphavirus and flavivirus prevalence and risk factors in a rural community in western Kenya ed. Bingham A. *PLoS Negl Trop Dis* **11,** e0005998.

Grou CP, Pinto MP, Mendes A V., Domingues P & Azevedo JE (2015). The de novo synthesis of ubiquitin: Identification of deubiquitinases acting on ubiquitin precursors. *Sci Rep* **5,** 12836.

Gui W, Ott CA, Yang K, Chung JS, Shen S & Zhuang Z (2018). Cell-Permeable Activity-Based Ubiquitin Probes Enable Intracellular Profiling of Human Deubiquitinases. *J Am Chem Soc* **140,** 12424–12433.

Gustin JK, Moses A V., Früh K & Douglas JL (2011). Viral takeover of the host ubiquitin system. *Front Microbiol* **2,** 161.

Haahr P, Borgermann N, Guo X, Typas D, Achuthankutty D, Hoffmann S, Shearer R, Sixma TK & Mailand N (2018). ZUFSP Deubiquitylates K63-Linked Polyubiquitin Chains to Promote Genome Stability. *Mol Cell* **70,** 165–174.e6.

Hackett BA, Yasunaga A, Panda D, Tartell MA, Hopkins KC, Hensley SE & Cherry S (2015). RNASEK is required for internalization of diverse acid-dependent viruses. *Proc Natl Acad Sci* **112,** 7797–7802.

Hagglund R, Van Sant C, Lopez P & Roizman B (2002). Herpes simplex virus 1-infected cell protein 0 contains two E3 ubiquitin ligase sites specific for different E2 ubiquitin-conjugating enzymes. *Proc Natl Acad Sci* **99,** 631–636.

Hahn YS, Strauss EG & Strauss JH (1989). Mapping of RNA- temperature-sensitive mutants of Sindbis virus: assignment of complementation groups A, B, and G to nonstructural proteins. *J Virol* **63,** 3142–3150.

Hallengärd D, Lum F-M, Kümmerer BM, Lulla A, Lulla V, García-Arriaza J, Fazakerley JK, Roques P, Le Grand R, Merits A, Ng LFP, Esteban M & Liljeström P (2014). Prime-boost immunization strategies against Chikungunya virus. *J Virol* **88,** 13333–13343.

Hamilton AJ & Baulcombe DC (1999). A species of small antisense RNA in posttranscriptional gene silencing in plants. *Science* **286,** 950–952.

Hammon WM & Sather GE (1964). Virological Findings in the 1960 Hemorrhagic Fever Epidemic (dengue) in Thailand. *Am J Trop Med Hyg* **13,** 629–641.

Hanson RP, Sulkin SE, Beuscher EL, Hammon WM, McKinney RW & Work TH (1967). Arbovirus infections of laboratory workers. Extent of problem emphasizes the need for more effective measures to reduce hazards. *Science* **158,** 1283–1286.

Haq S & Ramakrishna S (2017). Deubiquitylation of deubiquitylases. *Open Biol*; DOI: 10.1098/rsob.170016.

Hardy JL, Houk EJ, Kramer LD & Reeves WC (1983). Intrinsic Factors Affecting Vector Competence of Mosquitoes for Arboviruses. *Annu Rev Entomol* **28,** 229–262.

Harrison V, Eckels K, Bartelloni P & Hampton C (1971). Production and evaluation of a formalin killed chikungunya vaccine. *J Immunol* **107,** 643–647.

Hawley RJ & Eitzen Jr EM (2001). Biological Weapons—a Primer for Microbiologists. *Annu Rev Microbiol* **55,** 235–253.

Hawman DW, Stoermer KA, Montgomery SA, Pal P, Oko L, Diamond MS & Morrison TE (2013). Chronic joint disease caused by persistent Chikungunya virus infection is controlled by the adaptive immune response. *J Virol* **87,** 13878–13888.

Health and Safety Executive (2013). *The Approved List of biological agents Advisory Committee on Dangerous Pathogens HSE Books Health and Safety Executive Health and Safety Executive*. Available at: www.nationalarchives.gov.uk/doc/open-government-licence/, [Accessed December 13, 2018].

Hefti E, Bishop DH, Dubin DT & Stollar V (1975). 5' nucleotide sequence of sindbis viral RNA. *J Virol* **17,** 149–159.

Helenius A, Kartenbeck J, Simons K & Fries E (1980). On the entry of Semliki forest virus into BHK-21 cells. *J Cell Biol* **84,** 404–420.

Henzel WJ, Watanabe C & Stults JT (2003). Protein identification: The origins of peptide mass fingerprinting. *J Am Soc Mass Spectrom* **14,** 931–942. Available at: https://www.sciencedirect.com/science/article/pii/S1044030503002149?via%3Dihub [Accessed November 1, 2018].

Her Z, Malleret B, Chan M, Ong EKS, Wong S-C, Kwek DJC, Tolou H, Lin RTP, Tambyah PA, Rénia L & Ng LFP (2010). Active infection of human blood monocytes by Chikungunya virus triggers an innate immune response. *J Immunol* **184,** 5903–5913.

Heride C, Urbé S & Clague MJ (2014). Ubiquitin code assembly and disassembly. *Curr Biol* **24,** R215-20.

Hershko A & Ciechanover A (1998). The ubiquitin system. *Annu Rev Biochem* **67,** 425–479.

Hershko A, Heller H, Elias S & Ciechanover A (1983). Components of ubiquitin-protein ligase system. Resolution, affinity purification, and role in protein breakdown. *J Biol Chem* **258,** 8206–8214.

Hershko A & Rose IA (1987). Ubiquitin-aldehyde: a general inhibitor of ubiquitin-recycling processes. *Proc Natl Acad Sci* **84,** 1829–1833.

Hewings DS, Flygare JA, Bogyo M & Wertz IE (2017). Activity-based probes for the ubiquitin conjugation–deconjugation machinery: new chemistries, new tools, and new insights. *FEBS J* **284,** 1555–1576.

Hirsch AJ (2010). The use of RNAi-based screens to identify host proteins involved in viral replication. *Future Microbiol* **5,** 303–311.

Ho Y-J, Wang Y-M, Lu J, Wu T-Y, Lin L-I, Kuo S-C & Lin C-C (2015). Suramin Inhibits Chikungunya Virus Entry and Transmission ed. Roques P. *PLoS One* **10,** e0133511.

Hoarau JJ et al. (2010). Persistent Chronic Inflammation and Infection by Chikungunya Arthritogenic Alphavirus in Spite of a Robust Host Immune Response. *J Immunol* **184,** 5914–5927.

Hoke CH, Pace-Templeton J, Pittman P, Malinoski FJ, Gibbs P, Ulderich T, Mathers M, Fogtman B, Glass P & Vaughn DW (2012). US Military contributions to the global response to pandemic chikungunya. *Vaccine* **30,** 6713–6720.

Holland Cheng R, Kuhn RJ, Olson NH, Rossmann^Hok-Kin Choi MG, Smith TJ & Baker TS (1995). Nucleocapsid and glycoprotein organization in an enveloped virus. *Cell* **80,** 621–630.

Holzer B, Bakshi S, Bridgen A & Baron MD (2011). Inhibition of interferon induction and action by the nairovirus nairobi sheep disease virus/Ganjam virus. *PLoS One* **6,** e28594.

Honig JE, Osborne JC & Nichol ST (2004). Crimean-Congo hemorrhagic fever virus genome L RNA segment and encoded protein. *Virology* **321,** 29–35.

Hoornweg TE, van Duijl-Richter MKS, Ayala Nuñez N V., Albulescu IC, van Hemert MJ & Smit JM (2016*a*). Dynamics of Chikungunya Virus Cell Entry Unraveled by Single-Virus Tracking in Living Cells ed. Lyles DS. *J Virol* **90,** 4745–4756.

Hoornweg TE, van Duijl-Richter MKS, Ayala Nuñez N V, Albulescu IC, van Hemert MJ & Smit JM (2016*b*). Dynamics of chikungunya virus cell entry unraveled by single virus tracking in living cells. *J Virol*JVI.03184-15-.

Hover S, Foster B, Fontana J, Kohl A, Goldstein SAN, Barr JN & Mankouri J (2018). Bunyavirus requirement for endosomal K+reveals new roles of cellular ion channels during infection ed. Whelan SPJ. *PLoS Pathog* **14,** e1006845.

Hover S, King B, Hall B, Loundras E-A, Taqi H, Daly J, Dallas M, Peers C, Schnettler E, McKimmie C, Kohl A, Barr JN & Mankouri J (2016). Modulation of Potassium Channels Inhibits Bunyavirus Infection. *J Biol Chem* **291,** 3411–3422.

Hu M, Li P, Li M, Li W, Yao T, Wu JW, Gu W, Cohen RE & Shi Y (2002). Crystal structure of a UBP-family deubiquitinating enzyme in isolation and in complex with ubiquitin aldehyde. *Cell* **111,** 1041–1054.

Hu M, Li P, Song L, Jeffrey PD, Chenova TA, Wilkinson KD, Cohen RE & Shi Y (2005). Structure and mechanisms of the proteasome-associated deubiquitinating enzyme USP14. *EMBO J* **24,** 3747–3756.

Hu X, Tian J, Kang H, Guo D, Liu J, Liu D, Jiang Q, Li Z, Qu J & Qu L (2017). Transmissible Gastroenteritis Virus Papain-Like Protease 1 Antagonizes Production of Interferon- β through Its Deubiquitinase Activity. *Biomed Res Int* **2017,** 7089091.

Huang OW, Ma X, Yin J, Flinders J, Maurer T, Kayagaki N, Phung Q, Bosanac I, Arnott D, Dixit VM, Hymowitz SG, Starovasnik MA & Cochran AG (2012). Phosphorylation-dependent activity of the deubiquitinase DUBA. *Nat Struct Mol Biol* **19,** 171–176.

Huang X & Dixit VM (2016). Drugging the undruggables: Exploring the ubiquitin system for drug development. *Cell Res* **26,** 484–498.

Huffmaster NJ, Sollars PJ, Richards AL, Pickard GE & Smith GA (2015). Dynamic ubiquitination drives herpesvirus neuroinvasion. *Proc Natl Acad Sci U S A* **112,** 12818–12823.

Huibregtse JM, Scheffner M, Beaudenon S & Howley PM (1995). A family of proteins structurally and functionally related to the E6-AP ubiquitin-protein ligase. *Proc Natl Acad Sci* **92,** 2563–2567.

Hunt DF, Henderson RA, Shabanowitz J, Sakaguchi K, Michel H, Sevilir N, Cox AL, Appella E & Engelhard VH (1992). Characterization of peptides bound to the class I MHC molecule HLA-A2.1 by mass spectrometry. *Science (80-)* **255,** 1261–1263.

Hyoung TK, Kwang PK, Lledias F, Kisselev AF, Scaglione KM, Skowyra D, Gygi SP & Goldberg AL (2007). Certain pairs of ubiquitin-conjugating enzymes (E2s) and ubiquitin-protein ligases (E3s) synthesize nondegradable forked ubiquitin chains containing all possible isopeptide linkages. *J Biol Chem* **282,** 17375–17386.

Inn K-S, Lee S-H, Rathbun JY, Wong L-Y, Toth Z, Machida K, Ou J-HJ & Jung JU (2011). Inhibition of RIG-I-mediated signaling by Kaposi's sarcoma-associated herpesvirus-encoded deubiquitinase ORF64. *J Virol* **85,** 10899–10904.

Ivanova L & Schlesinger MJ (1993). Site-directed mutations in the Sindbis virus E2 glycoprotein identify palmitoylation sites and affect virus budding. *J Virol* **67,** 2546–2551.

Jackson AL, Bartz SR, Schelter J, Kobayashi S V, Burchard J, Mao M, Li B, Cavet G & Linsley PS (2003). Expression profiling reveals off-target gene regulation by RNAi. *Nat Biotechnol* **21,** 635–637.

Jackson AL, Burchard J, Leake D, Reynolds A, Schelter J, Guo J, Johnson JM, Lim L, Karpilow J, Nichols K, Marshall W, Khvorova A & Linsley PS (2006*a*). Position-specific chemical modification of siRNAs reduces "off-target" transcript silencing. *RNA* **12,** 1197–1205.

Jackson AL, Burchard J, Schelter J, Chau BN, Cleary M, Lim L & Linsley PS (2006*b*). Widespread siRNA "off-target" transcript silencing mediated by seed region sequence complementarity. *RNA* **12,** 1179–1187.

Jarosinski K, Kattenhorn L, Kaufer B, Ploegh H & Osterrieder N (2007). A herpesvirus ubiquitin-specific protease is critical for efficient T cell lymphoma formation. *Proc Natl Acad Sci* **104,** 20025–20030.

Jaworski J, Vega M De, Fletcher SJ, Mcfarlane C, Greene MK, Smyth AW, Schaeybroeck S Van, James A, Scott CJ, Rappoport JZ & Burrows JF (2014). USP17 is required for clathrin mediated endocytosis of epidermal growth factor receptor. *Oncotarget* **5,** 6964–6975.

Jin S, Tian S, Chen Y, Zhang C, Xie W, Xia X, Cui J & Wang R-F (2016). USP19 modulates autophagy and antiviral immune responses by deubiquitinating Beclin-1. *EMBO J* **35,** 866–880.

Johansson MA, Powers AM, Pesik N, Cohen NJ & Erin Staples J (2014). Nowcasting the spread of Chikungunya Virus in the Americas ed. Ng LF. *PLoS One* **9,** e104915.

Johnson J V., Yost RA, Kelley PE & Bradford DC (1990). Tandem-in-Space and Tandem-in-Time Mass Spectrometry: Triple Quadrupoles and Quadrupole Ion Traps. *Anal Chem* **62,** 2162–2172.

Johnston SC, Riddle SM, Cohen RE & Hill CP (1999). Structural basis for the specificity of ubiquitin C-terminal hydrolases. *EMBO J* **18,** 3877–3887.

de Jong A, Merkx R, Berlin I, Rodenko B, Wijdeven RHM, El Atmioui D, Yalçin Z, Robson CN, Neefjes JJ & Ovaa H (2012). Ubiquitin-based probes prepared by total synthesis to profile the activity of deubiquitinating enzymes. *Chembiochem* **13,** 2251–2258.

Jose J, Snyder JE & Kuhn RJ (2009). A structural and functional perspective of alphavirus replication and assembly. *Future Microbiol* **4,** 837–856.

Josseran L, Paquet C, Zehgnoun A, Caillere N, Le Tertre A, Solet J-L & Ledrans M (2006). Chikungunya Disease Outbreak, Reunion Island. *Emerg Infect Dis* **12,** 1994–1995.

Kahn JS, Schnell MJ, Buonocore L & Rose JK (1999). Recombinant Vesicular Stomatitis Virus Expressing Respiratory Syncytial Virus (RSV) Glycoproteins: RSV Fusion Protein Can Mediate Infection and Cell Fusion. *Virology* **254,** 81–91.

Kam Y-W, Lee WWL, Simarmata D, Harjanto S, Teng T-S, Tolou H, Chow A, Lin RTP, Leo Y-S, Renia L & Ng LFP (2012*a*). Longitudinal Analysis of the Human Antibody Response to Chikungunya Virus Infection: Implications for Serodiagnosis and Vaccine Development. *J Virol* **86,** 13005–13015.

Kam YW, Simarmata D, Chow A, Her Z, Teng TS, Ong EKS, Rénia L, Leo YS & Ng LFP (2012*b*). Early appearance of neutralizing immunoglobulin G3 antibodies is associated with chikungunya virus clearance and long-term clinical protection. *J Infect Dis* **205,** 1147–1154.

Kamgang B, Marcombe S, Chandre F, Nchoutpouen E, Nwane P, Etang J, Corbel V & Paupy C (2011). Insecticide susceptibility of Aedes aegypti and Aedes albopictus in Central Africa. *Parasites and Vectors* **4,** 79.

Kampmann M, Horlbeck MA, Chen Y, Tsai JC, Bassik MC, Gilbert LA, Villalta JE, Kwon SC, Chang H, Kim VN & Weissman JS (2015). Next-generation libraries for robust RNA interference-based genome-wide screens. *Proc Natl Acad Sci* **112,** E3384–E3391.

Karim R, Tummers B, Meyers C, Biryukov JL, Alam S, Backendorf C, Jha V, Offringa R, van Ommen GJB, Melief CJM, Guardavaccaro D, Boer JM & van der Burg SH (2013). Human Papillomavirus (HPV) Upregulates the Cellular Deubiquitinase UCHL1 to Suppress the Keratinocyte's Innate Immune Response ed. Hiscott J. *PLoS Pathog* **9,** e1003384.

Karlas A, Berre S, Couderc T, Varjak M, Braun P, Meyer M, Gangneux N, Karo-Astover L, Weege F, Raftery M, Schönrich G, Klemm U, Wurzlbauer A, Bracher F, Merits A, Meyer TF & Lecuit M (2016). A human genome-wide loss-of-function screen identifies effective chikungunya antiviral drugs. *Nat Commun* **7,** 11320.

Karpe YA & Lole KS (2011). Deubiquitination activity associated with hepatitis E virus putative papain-like cysteine protease. *J Gen Virol* **92,** 2088–2092.

van Kasteren PB, Bailey-Elkin BA, James TW, Ninaber DK, Beugeling C, Khajehpour M, Snijder EJ, Mark BL & Kikkert M (2013). Deubiquitinase function of arterivirus papain-like protease 2 suppresses the innate immune response in infected host cells. *Proc Natl Acad Sci U S A* **110,** E838-47.

van Kasteren PB, Beugeling C, Ninaber DK, Frias-Staheli N, van Boheemen S, Garcia-Sastre A, Snijder EJ & Kikkert M (2012). Arterivirus and nairovirus ovarian tumor domain-containing Deubiquitinases target activated RIG-I to control innate immune signaling. *J Virol* **86,** 773–785.

van Kasteren PB, Knaap RCM, van den Elzen P, Snijder EJ, Balasuriya UBR, van den Born E & Kikkert M (2015). In vivo assessment of equine arteritis virus vaccine improvement by disabling the deubiquitinase activity of papain-like protease 2. *Vet Microbiol* **178,** 132–137.

Kattenhorn LM, Korbel GA, Kessler BM, Spooner E & Ploegh HL (2005). A Deubiquitinating Enzyme Encoded by HSV-1 Belongs to a Family of Cysteine Proteases that Is Conserved across the Family Herpesviridae. *Mol Cell* **19,** 547–557.

Kelleher NL, Lin HY, Valaskovic GA, Aaserud DJ, Fridriksson EK & McLafferty FW (1999). Top down versus bottom up protein characterization by tandem high-resolution mass spectrometry. *J Am Chem Soc* **121,** 806–812.

Kellmann M, Muenster H, Zomer P & Mol H (2009). Full Scan MS in Comprehensive Qualitative and Quantitative Residue Analysis in Food and Feed Matrices: How Much Resolving Power is Required? *J Am Soc Mass Spectrom* **20,** 1464–1476.

Kessler BM, Mariola B & Edelmann J (2011). PTMs in Conversation: Activity and Function of Deubiquitinating Enzymes Regulated via Post-Translational Modifications. *Cell Biochem Biophys* **60,** 21–38.

Ketscher L, Hannß R, Morales DJ, Basters A, Guerra S, Goldmann T, Hausmann A, Prinz M, Naumann R, Pekosz A, Utermöhlen O, Lenschow DJ & Knobeloch K-P (2015). Selective inactivation of USP18 isopeptidase activity in vivo enhances ISG15 conjugation and viral resistance. *Proc Natl Acad Sci* **112,** 1577–1582.

Keusekotten K, Elliott PR, Glockner L, Fiil BK, Damgaard RB, Kulathu Y, Wauer T, Hospenthal MK, Gyrd-Hansen M, Krappmann D, Hofmann K & Komander D (2013). OTULIN Antagonizes LUBAC Signaling by Specifically Hydrolyzing Met1-Linked Polyubiquitin. *Cell* **153,** 1312–1326.

Khan AA, Betel D, Miller ML, Sander C, Leslie CS & Marks DS (2009). Transfection of small RNAs globally perturbs gene regulation by endogenous microRNAs. *Nat Biotechnol* **27,** 549–555.

Kielian MC, Marsh M & Helenius A (1986). Kinetics of endosome acidification detected by mutant and wild-type Semliki Forest virus. *EMBO J* **5,** 3103–3109.

Kim J-H, Luo J-K & Zhang D-E (2008). The level of hepatitis B virus replication is not affected by protein ISG15 modification but is reduced by inhibition of UBP43 (USP18) expression. *J Immunol* **181,** 6467–6472.

Kim RQ, Geurink PP, Mulder MPC, Fish A, Ekkebus R, El Oualid F, van Dijk WJ, van Dalen D, Ovaa H, van Ingen H & Sixma TK (2019). Kinetic analysis of multistep USP7 mechanism shows critical role for target protein in activity. *Nat Commun* **10,** 231.

King S (2018). The Role of the Deubiquitylase UCHL3 During Alphavirus Infection (Thesis).

Kirchhausen T, Owen D & Harrison SC (2014). Molecular structure, function, and dynamics of clathrin-mediated membrane traffic. *Cold Spring Harb Perspect Biol* **6,** a016725.

Kirisako T, Kamei K, Murata S, Kato M, Fukumoto H, Kanie M, Sano S, Tokunaga F, Tanaka K & Iwai K (2006). A ubiquitin ligase complex assembles linear polyubiquitin chains. *EMBO J* **25,** 4877–4887.

Klimstra WB, Nangle EM, Smith MS, Yurochko AD & Ryman KD (2003). DC-SIGN and L-SIGN can act as attachment receptors for alphaviruses and distinguish between mosquito cell- and mammalian cell-derived viruses. *J Virol* **77,** 12022–12032.

Klimstra WB, Ryman KD & Johnston RE (1998). Adaptation of Sindbis virus to BHK cells selects for use of heparan sulfate as an attachment receptor. *J Virol* **72,** 7357–7366.

Van Der Knaap JA, Kumar BRRP, Moshkin YM, Langenberg K, Krijgsveld J, Heck AJR, Karch F & Verrijzer CP (2005). GMP synthetase stimulates histone H2B deubiquitylation by the epigenetic silencer USP7. *Mol Cell* **17,** 695–707.

Knight RL, Schultz KLW, Kent RJ, Venkatesan M & Griffin DE (2009). Role of N-Linked Glycosylation for Sindbis Virus Infection and Replication in Vertebrate and Invertebrate Systems. *J Virol* **83,** 5640–5647.

Kobe B & Kemp BE (1999). Active site-directed protein regulation. *Nature* **402,** 373–376.

Kolokoltsov AA, Fleming EH & Davey RA (2006). Venezuelan equine encephalitis virus entry mechanism requires late endosome formation and resists cell membrane cholesterol depletion. *Virology* **347,** 333–342.

Komander D & Barford D (2008). Structure of the A20 OTU domain and mechanistic insights into deubiquitination. *Biochem J* **409,** 77–85.

Komander D, Lord CJ, Scheel H, Swift S, Hofmann K, Ashworth A & Barford D (2008). The Structure of the CYLD USP Domain Explains Its Specificity for Lys63-Linked Polyubiquitin and Reveals a B Box Module. *Mol Cell* **29,** 451–464.

Komander D, Reyes-Turcu F, Licchesi JDF, Odenwaelder P, Wilkinson KD & Barford D (2009). Molecular discrimination of structurally equivalent Lys 63-linked and linear polyubiquitin chains. *EMBO Rep* **10,** 662–662.

Kong L, Shaw N, Yan L, Lou Z & Rao Z (2015). Structural view and substrate specificity of papain-like protease from avian infectious bronchitis virus. *J Biol Chem* **290,** 7160–7168.

Kramer HB, Nicholson B, Kessler BM & Altun M (2012). Detection of ubiquitin-proteasome enzymatic activities in cells: Application of activity-based probes to inhibitor development. *Biochim Biophys Acta - Mol Cell Res* **1823,** 2029–2037.

Krzyzaniak MA, Zumstein MT, Gerez JA, Picotti P & Helenius A (2013). Host Cell Entry of Respiratory Syncytial Virus Involves Macropinocytosis Followed by Proteolytic Activation of the F Protein ed. Pekosz A. *PLoS Pathog* **9,** e1003309.

Kulcsar KA, Baxter VK, Greene IP & Griffin DE (2014). Interleukin 10 modulation of pathogenic Th17 cells during fatal alphavirus encephalomyelitis. *Proc Natl Acad Sci* **111,** 16053–16058.

Kumari P, Saha I, Narayanan A, Narayanan S, Takaoka A, Kumar NS, Tailor P & Kumar H (2017). Essential role of HCMV deubiquitinase in promoting oncogenesis by targeting anti-viral innate immune signaling pathways. *Cell Death Dis* **8,** e3078.

Kummari E, Alugubelly N, Hsu C-Y, Dong B, Nanduri B & Edelmann MJ (2015). Activity-Based Proteomic Profiling of Deubiquitinating Enzymes in Salmonella-Infected Macrophages Leads to Identification of Putative Function of UCH-L5 in Inflammasome Regulation ed. Chakravortty D. *PLoS One* **10,** e0135531.

Kuo S-C, Wang Y-M, Ho Y-J, Chang T-Y, Lai Z-Z, Tsui P-Y, Wu T-Y & Lin C-C (2016). Suramin treatment reduces chikungunya pathogenesis in mice. *Antiviral Res* **134,** 89–96.

Kwasna D, Abdul Rehman SA, Natarajan J, Matthews S, Madden R, De Cesare V, Weidlich S, Virdee S, Ahel I, Gibbs-Seymour I & Kulathu Y (2018). Discovery and Characterization of ZUFSP/ZUP1, a Distinct Deubiquitinase Class Important for Genome Stability. *Mol Cell* **70,** 150–164.e6.

Labadie K, Larcher T, Joubert C, Mannioui A, Delache B, Brochard P, Guigand L, Dubreil L, Lebon P, Verrier B, de Lamballerie X, Suhrbier A, Cherel Y, Le Grand R & Roques P (2010). Chikungunya disease in nonhuman primates involves long-term viral persistence in macrophages. *J Clin Invest* **120,** 894–906.

Laherty CD, Hu HM, Opipari AW, Wang F & Dixit VM (1992). The Epstein-Barr virus LMP1 gene product induces A20 zinc finger protein expression by activating nuclear factor ??B. *J Biol Chem* **267,** 24157–24160.

Lai Z, Ferry K V., Diamond MA, Wee KE, Kim YB, Ma J, Yang T, Benfield PA, Copeland RA & Auger KR (2001). Human mdm2 Mediates Multiple Mono-ubiquitination of p53 by a Mechanism Requiring Enzyme Isomerization. *J Biol Chem* **276,** 31357–31367.

Lake MW, Wuebbens MM, Rajagopalan K V. & Schindelin H (2001). Mechanism of ubiquitin activation revealed by the structure of a bacterial MoeB–MoaD complex. *Nature* **414,** 325–329.

Lam YA, Xu W, DeMartino GN & Cohen RE (1997). Editing of ubiquitin conjugates by an isopeptidase in the 26S proteasome. *Nature* **385,** 737–740.

Lamaze C, Fujimoto LM, Yin HL & Schmid SL (1997). The actin cytoskeleton is required for receptor-mediated endocytosis in mammalian cells. *J Biol Chem* **272,** 20332–20335.

Lampio A, Kilpeläinen I, Pesonen S, Karhi K, Auvinen P, Somerharju P & Kääriäinen L (2000). Membrane binding mechanism of an RNA virus-capping enzyme. *J Biol Chem* **275,** 37853–37859.

Lanciotti RS & Valadere AM (2014). Transcontinental movement of Asian Genotype Chikungunya virus. *Emerg Infect Dis* **20,** 1400–1402. Available at: http://www.ncbi.nlm.nih.gov/pubmed/25076384 [Accessed December 13, 2018].

Lautscham G, Mayrhofer S, Taylor G, Haigh T, Leese A, Rickinson A & Blake N (2001). Processing of a multiple membrane spanning Epstein-Barr virus protein for CD8(+) T cell recognition reveals a proteasome-dependent, transporter associated with antigen processing-independent pathway. *J Exp Med* **194,** 1053–1068.

Lavorgna A & Harhaj EW (2012). An RNA Interference Screen Identifies the Deubiquitinase STAMBPL1 as a Critical Regulator of Human T-Cell Leukemia Virus Type 1 Tax Nuclear Export and NF- B Activation. *J Virol* **86,** 3357–3369.

Lawson AP, Bak DW, Alexander Shannon D, Long MJC, Vijaykumar T, Yu R, El Oualid F, Weerapana E, Hedstrom L, Lawson AP, Bak DW, Alexander Shannon D, Long MJC, Vijaykumar T, Yu R, El Oualid F, Weerapana E & Hedstrom L (2017). Identification of deubiquitinase targets of isothiocyanates using SILAC-assisted quantitative mass spectrometry. *Oncotarget* **8,** 51296–51316.

Lee JI, Sollars PJ, Baver SB, Pickard GE, Leelawong M & Smith GA (2009). A herpesvirus encoded deubiquitinase is a novel neuroinvasive determinant. *PLoS Pathog* **5,** e1000387.

Lee MJ, Lee B-H, Hanna J, King RW & Finley D (2011). Trimming of Ubiquitin Chains by Proteasome-associated Deubiquitinating Enzymes. *Mol Cell Proteomics* **10,** R110.003871.

Lee S, Owen KE, Choi HK, Lee H, Lu G, Wengler G, Brown DT, Rossmann MG & Kuhn RJ (1996). Identification of a protein binding site on the surface of the alphavirus nucleocapsid and its implication in virus assembly. *Structure* **4,** 531–541.

Lee WWL, Teo T-H, Her Z, Lum F-M, Kam Y-W, Haase D, Rénia L, Rötzschke O & Ng LFP (2015). Expanding regulatory T cells alleviates chikungunya virus-induced pathology in mice. *J Virol* **89,** 7893–7904.

Lehoux M, Gagnon D & Archambault J (2014). E1-Mediated Recruitment of a UAF1-USP Deubiquitinase Complex Facilitates Human Papillomavirus DNA Replication. *J Virol* **88,** 8545–8555.

Levitt NH, Ramsburg HH, Hasty SE, Repik PM, Cole FE & Lupton HW (1986). Development of an attenuated strain of chikungunya virus for use in vaccine production. *Vaccine* **4,** 157–162.

Li G & Rice CM (1993). The signal for translational readthrough of a UGA codon in Sindbis virus RNA involves a single cytidine residue immediately downstream of the termination codon. *J Virol* **67,** 5062–5067.

Li L, Lei Q-S, Zhang S-J, Kong L-N & Qin B (2016). Suppression of USP18 Potentiates the Anti-HBV Activity of Interferon Alpha in HepG2.2.15 Cells via JAK/STAT Signaling. *PLoS One* **11,** e0156496.

Li M, Chen D, Shiloh A, Luo J, Nikolaev AY, Qin J & Gu W (2002). Deubiquitination of p53 by HAUSP is an important pathway for p53 stabilization. *Nature* **416,** 648–653.

Li Y-G, Siripanyaphinyo U, Tumkosit U, Noranate N, A-nuegoonpipat A, Tao R, Kurosu T, Ikuta K, Takeda N & Anantapreecha S (2013). Chikungunya virus induces a more moderate cytopathic effect in mosquito cells than in mammalian cells. *Intervirology* **56,** 6–12.

Liao T-LL, Wu C-YY, Su W-CC, Jeng K-SS & Lai MMC (2010). Ubiquitination and deubiquitination of NP protein regulates influenza A virus RNA replication. *EMBO J* **29,** 3879–3890.

Liljeström P & Garoff H (1991). Internally located cleavable signal sequences direct the formation of Semliki Forest virus membrane proteins from a polyprotein precursor. *J Virol* **65,** 147–154.

Liljeström P, Lusa S, Huylebroeck D & Garoff H (1991). In vitro mutagenesis of a full-length cDNA clone of Semliki Forest virus: the small 6,000-molecular-weight membrane protein modulates virus release. *J Virol* **65,** 4107–4113.

Lim EXY, Lee WS, Madzokere ET & Herrero LJ (2018). Mosquitoes as suitable vectors for alphaviruses. *Viruses*; DOI: 10.3390/v10020084.

Lin D, Zhang M, Zhang M-X, Ren Y, Jin J, Zhao Q, Pan Z, Wu M, Shu H-B, Dong C & Zhong B (2015). Induction of USP25 by viral infection promotes innate antiviral responses by mediating the stabilization of TRAF3 and TRAF6. *Proc Natl Acad Sci U S A* **112,** 11324–11329.

Lin R-J, Chu J-S, Chien H-L, Tseng C-H, Ko P-C, Mei Y-Y, Tang W-C, Kao Y-T, Cheng H-Y, Liang Y-C & Lin S-Y (2014). MCPIP1 Suppresses Hepatitis C Virus Replication and Negatively Regulates Virus-Induced Proinflammatory Cytokine Responses. *J Immunol* **193,** 4159–4168.

Lin RJ, Chien HL, Lin SY, Chang BL, Yu HP, Tang WC & Lin YL (2013). MCPIP1 ribonuclease exhibits broad-spectrum antiviral effects through viral RNA binding and degradation. *Nucleic Acids Res* **41,** 3314–3326.

La Linn M, Eble JA, Lübken C, Slade RW, Heino J, Davies J & Suhrbier A (2005). An arthritogenic alphavirus uses the α1β1 integrin collagen receptor. *Virology* **336,** 229–239.

La Linn M, Gardner J, Warrilow D, Darnell GA, McMahon CR, Field I, Hyatt AD, Slade RW & Suhrbier A (2001). Arbovirus of Marine Mammals: a New Alphavirus Isolated from the Elephant Seal Louse, Lepidophthirus macrorhini. *J Virol* **75,** 4103–4109.

Loch CM & Strickler JE (2012). A microarray of ubiquitylated proteins for profiling deubiquitylase activity reveals the critical roles of both chain and substrate. *Biochim Biophys Acta - Mol Cell Res* **1823,** 2069–2078.

Lombardi C, Ayach M, Beaurepaire L, Chenon M, Andreani J, Guerois R, Jupin I & Bressanelli S (2013). A compact viral processing proteinase/ubiquitin hydrolase from the OTU family. *PLoS Pathog* **9,** e1003560.

Long KM, Whitmore AC, Ferris MT, Sempowski GD, McGee C, Trollinger B, Gunn B & Heise MT (2013). Dendritic Cell Immunoreceptor Regulates Chikungunya Virus Pathogenesis in Mice. *J Virol* **87,** 5697–5706.

Lounibos LP & Kramer LD (2016). Invasiveness of aedes aegypti and aedes albopictus and vectorial capacity for chikungunya virus. *J Infect Dis* **214,** S453–S458.

Love KR, Pandya RK, Spooner E & Ploegh HL (2009). Ubiquitin C-terminal electrophiles are activity-based probes for identification and mechanistic study of ubiquitin conjugating machinery. *ACS Chem Biol* **4,** 275–287.

Lü S & Wang J (2013). The resistance mechanisms of proteasome inhibitor bortezomib. *Biomark Res* **1,** 13.

Lu YE, Cassese T & Kielian M (1999). The cholesterol requirement for sindbis virus entry and exit and characterization of a spike protein region involved in cholesterol dependence. *J Virol* **73,** 4272–4278.

Lu YE, Eng CH, Shome SG & Kielian M (2001). In vivo generation and characterization of a soluble form of the Semliki forest virus fusion protein. *J Virol* **75,** 8329–8339.

Lu YE & Kielian M (2000). Semliki Forest Virus Budding: Assay, Mechanisms, and Cholesterol Requirement. *J Virol* **74,** 7708–7719.

Lum FM, Couderc T, Chia BS, Ong RY, Her Z, Chow A, Leo YS, Kam YW, Rénia L, Lecuit M & Ng LFP (2018). Antibody-mediated enhancement aggravates chikungunya virus infection and disease severity. *Sci Rep* **8,** 1860.

Lum L, Ng CJ & Khoo EM (2014). Managing dengue fever in primary care: A practical approach. *Malaysian Fam physician Off J Acad Fam Physicians Malaysia* **9,** 2–10.

Lumsden WH (1955). An epidemic of virus disease in Southern Province, Tanganyika Territory, in 1952-53. II. General description and epidemiology. *Trans R Soc Trop Med Hyg* **49,** 33–57.

Lund PK, Moats-Staats BM, Simmons JG, Hoyt E, D'Ercole AJ, Martin F & Van Wyk JJ (1985). Nucleotide sequence analysis of a cDNA encoding human ubiquitin reveals that ubiquitin is synthesized as a precursor. *J Biol Chem* **260,** 7609–7613.

Malim MH (2009). APOBEC proteins and intrinsic resistance to HIV-1 infection. *Philos Trans R Soc B Biol Sci* **364,** 675–687.

Manasanch EE & Orlowski RZ (2017). Proteasome inhibitors in cancer therapy. *Nat Rev Clin Oncol* **14,** 417–433. Available at: http://www.nature.com/doifinder/10.1038/nrclinonc.2016.206 [Accessed December 9, 2018].

Manganaro L, Pache L, Herrmann T, Marlett J, Hwang Y, Murry J, Miorin L, Ting AT, König R, García-Sastre A, Bushman FD, Chanda SK, Young JAT, Fernandez-Sesma A & Simon V (2014). Tumor suppressor cylindromatosis (CYLD) controls HIV transcription in an NF-κB-dependent manner. *J Virol* **88,** 7528–7540.

Marsh M & Helenius A (1980). Adsorptive endocytosis of Semliki Forest virus. *J Mol Biol* **142,** 439–454.

Mashtalir N, Daou S, Barbour H, Sen NN, Gagnon J, Hammond-Martel I, Dar HH, Therrien M & Affar EB (2014). Autodeubiquitination protects the tumor suppressor BAP1 from cytoplasmic sequestration mediated by the atypical ubiquitin ligase UBE2O. *Mol Cell* **54,** 392–406.

Mavalankar D, Shastri P & Raman P (2007). Chikungunya epidemic in India: a major public-health disaster. *Lancet Infect Dis* **7,** 306–307.

Mayle KM, Le AM & Kamei DT (2012). The intracellular trafficking pathway of transferrin. *Biochim Biophys Acta - Gen Subj* **1820,** 264–281.

McClain DJ, Pittman PR, Ramsburg HH, Nelson GO, Rossi CA, Mangiafico JA, Schmaljohn AL & Malinoski FJ (1998). Immunologic Interference from Sequential Administration of Live Attenuated Alphavirus Vaccines. *J Infect Dis* **177,** 634–641.

McFee RB (2018). Selected mosquito-borne illnesses-Chikungunya. *Disease-a-Month* **64,** 222–234.

McGraw EA & O'Neill SL (2013). Beyond insecticides: New thinking on an ancient problem. *Nat Rev Microbiol* **11,** 181–193.

McLellan L, Forder C, Cranston A, Harrigan J & Jacq X (2016). Activity based profiling of deubiquitylating enzymes and inhibitors in animal tissues. In *Methods in Molecular Biology*, pp. 411–419. Available at: http://link.springer.com/10.1007/978-1-4939-3756-1_27 [Accessed April 25, 2017].

Mehle A, Strack B, Ancuta P, Zhang C, McPike M & Gabuzda D (2004). Vif Overcomes the Innate Antiviral Activity of APOBEC3G by Promoting Its Degradation in the Ubiquitin-Proteasome Pathway. *J Biol Chem* **279,** 7792–7798.

Mei Y, Hahn AA, Hu S & Yang X (2011). The USP19 Deubiquitinase Regulates the Stability of c-IAP1 and c-IAP2. *J Biol Chem* **286,** 35380–35387.

Mellacheruvu D et al. (2013). The CRAPome: a contaminant repository for affinity purification–mass spectrometry data. *Nat Methods* **10,** 730–736.

Mellman I, Fuchs R & Helenius A (1986). Acidification of the Endocytic and Exocytic Pathways. *Annu Rev Biochem* **55,** 663–700.

Melton J V, Ewart GD, Weir RC, Board PG, Lee E & Gage PW (2002). Alphavirus 6K proteins form ion channels. *J Biol Chem* **277,** 46923–46931.

Meray RK & Lansbury PT (2007). Reversible monoubiquitination regulates the Parkinson disease-associated ubiquitin hydrolase UCH-L1. *J Biol Chem* **282,** 10567–10575.

Mercer J & Helenius A (2008). Vaccinia virus uses macropinocytosis and apoptotic mimicry to enter host cells. *Science (80-)* **320,** 531–535.

Mercer J, Knebel S, Schmidt FI, Crouse J, Burkard C & Helenius A (2010). Vaccinia virus strains use distinct forms of macropinocytosis for host-cell entry. *Proc Natl Acad Sci* **107,** 9346–9351.

Meredith M, Orr A & Everett R (1994). Herpes simplex virus type 1 immediate-early protein Vmw110 binds strongly and specifically to a 135-kDa cellular protein. *Virology* **200,** 457–469.

Meulmeester E, Kunze M, Hsiao HH, Urlaub H & Melchior F (2008). Mechanism and Consequences for Paralog-Specific Sumoylation of Ubiquitin-Specific Protease 25. *Mol Cell* **30,** 610–619.

Mevissen TET, Hospenthal MK, Geurink PP, Elliott PR, Akutsu M, Arnaudo N, Ekkebus R, Kulathu Y, Wauer T, El Oualid F, Freund SM V, Ovaa H & Komander D (2013). OTU deubiquitinases reveal mechanisms of linkage specificity and enable ubiquitin chain restriction analysis. *Cell* **154,** 169–184.

Mielech AM, Kilianski A, Baez-Santos YM, Mesecar AD & Baker SC (2014). MERS-CoV papain-like protease has deISGylating and deubiquitinating activities. *Virology* **450–451,** 64–70.

Miner JJ, Cook LE, Hong JP, Smith AM, Richner JM, Shimak RM, Young AR, Monte K, Poddar S, Crowe JE, Lenschow DJ & Diamond MS (2017). Therapy with CTLA4-Ig and an antiviral monoclonal antibody controls chikungunya virus arthritis. *Sci Transl Med* **9,** eaah3438.

Miner JJ, Yeang HXA, Fox JM, Taffner S, Malkova ON, Oh ST, Kim AHJ, Diamond MS, Lenschow DJ & Yokoyama WM (2015). Brief report: Chikungunya viral arthritis in the United States: A mimic of seronegative rheumatoid arthritis. *Arthritis Rheumatol* **67,** 1214–1220.

Mohammad Arif K (2017). Update Management of Chikungunya. *Faridpur Med Coll J* **12,** 82–85.

Mohr S, Bakal C & Perrimon N (2010). Genomic Screening with RNAi: Results and Challenges. *Annu Rev Biochem* **79,** 37–64.

Morrison TE, Oko L, Montgomery SA, Whitmore AC, Lotstein AR, Gunn BM, Elmore SA & Heise MT (2011). A mouse model of chikungunya virus-induced musculoskeletal inflammatory disease: evidence of arthritis, tenosynovitis, myositis, and persistence. *Am J Pathol* **178,** 32–40.

Mukhopadhyay S, Zhang W, Gabler S, Chipman PR, Strauss EG, Strauss JH, Baker TS, Kuhn RJ & Rossmann MG (2006). Mapping the structure and function of the E1 and E2 glycoproteins in alphaviruses. *Structure* **14,** 63–73.

Mulder MPC, El Oualid F, Ter Beek J & Ovaa H (2014). A native chemical ligation handle that enables the synthesis of advanced activity-based probes: Diubiquitin as a case study. *ChemBioChem* **15,** 946–949.

Mulvey C, Thur B, Crawford M & Godovac-Zimmermann J (2010). How Many Proteins are Missed in Quantitative Proteomics Based on MS/MS Sequencing Methods? *Proteomics Insights* **3,** 61–66.

Muturi EJ & Alto BW (2011). Larval Environmental Temperature and Insecticide Exposure Alter Aedes aegypti Competence for Arboviruses. *Vector-Borne Zoonotic Dis* **11,** 1157–1163.

Nakamura N & Hirose S (2008). Regulation of Mitochondrial Morphology by USP30, a Deubiquitinating Enzyme Present in the Mitochondrial Outer Membrane ed. Shaw J. *Mol Biol Cell* **19,** 1903–1911.

Nan Y, Yu Y, Ma Z, Khattar SK, Fredericksen B & Zhang Y-J (2014). Hepatitis E Virus Inhibits Type I Interferon Induction by ORF1 Products. *J Virol* **88,** 11924–11932.

Neefjes J, Jongsma MLM, Paul P & Bakke O (2011). Towards a systems understanding of MHC class i and MHC class II antigen presentation. *Nat Rev Immunol* **11,** 823–836. Available at: http://www.nature.com/articles/nri3084 [Accessed March 1, 2019].

Ng LC & Hapuarachchi HC (2010). Tracing the path of Chikungunya virus--evolution and adaptation. *Infect Genet Evol* **10,** 876–885.

Ng LFP, Chow A, Sun Y-J, Kwek DJC, Lim P-L, Dimatatac F, Ng L-C, Ooi E-E, Choo K-H, Her Z, Kourilsky P & Leo Y-S (2009). IL-1β, IL-6, and RANTES as Biomarkers of Chikungunya Severity ed. Unutmaz D. *PLoS One* **4,** e4261.

Nguyen PTV, Yu H & Keller PA (2015). Identification of chikungunya virus nsP2 protease inhibitors using structure-base approaches. *J Mol Graph Model* **57,** 1–8.

Nicholson LK, Wang C, Xi J & Begley TP (2001). Solution structure of ThiS and implications for the evolutionary roots of ubiquitin. *Nat Struct Biol* **8,** 47–51.

Nijman SMB, Luna-Vargas MPA, Velds A, Brummelkamp TR, Dirac AMG, Sixma TK & Bernards R (2005). A genomic and functional inventory of deubiquitinating enzymes. *Cell* **123,** 773–786.

Ning S & Pagano JS (2010). The A20 deubiquitinase activity negatively regulates LMP1 activation of IRF7. *J Virol* **84,** 6130–6138.

Niu N, Zhang J, Huang T, Sun Y, Chen Z, Yi W, Korteweg C, Wang J & Gu J (2012). IgG Expression in Human Colorectal Cancer and Its Relationship to Cancer Cell Behaviors ed. Hold GL. *PLoS One* **7,** e47362.

Nok AJ (2003). Arsenicals (melarsoprol), pentamidine and suramin in the treatment of human African trypanosomiasis. *Parasitol Res* **90,** 71–79.

Nubgan AS (2017). The Role of the Deubiquitylase MYSM1 During Alphavirus Infection (Thesis).

Ohtake F, Saeki Y, Sakamoto K, Ohtake K, Nishikawa H, Tsuchiya H, Ohta T, Tanaka K & Kanno J (2015). Ubiquitin acetylation inhibits polyubiquitin chain elongation. *EMBO Rep* **16,** 192–201.

Ong RY, Lum FM & Ng LFP (2014). The fine line between protection and pathology in neurotropic flavivirus and alphavirus infections. *Future Virol* **9,** 313–330.

Ong S-E, Blagoev B, Kratchmarova I, Kristensen DB, Steen H, Pandey A & Mann M (2002). Stable isotope labeling by amino acids in cell culture, SILAC, as a simple and accurate approach to expression proteomics. *Mol Cell Proteomics* **1,** 376–386.

Ooi YS, Stiles KM, Liu CY, Taylor GM & Kielian M (2013). Genome-Wide RNAi Screen Identifies Novel Host Proteins Required for Alphavirus Entry ed. Dermody TS. *PLoS Pathog* **9,** 1–10.

Osei Kuffour E, Schott K, Jaguva Vasudevan AA, Holler J, Schulz WA, Lang PA, Lang KS, Kim B, Häussinger D, König R & Münk C (2018). USP18 (UBP43) Abrogates p21-Mediated Inhibition of HIV-1. *J Virol*JVI.00592-18.

El Oualid F, Merkx R, Ekkebus R, Hameed DS, Smit JJ, de Jong A, Hilkmann H, Sixma TK & Ovaa H (2010). Chemical synthesis of ubiquitin, ubiquitin-based probes, and diubiquitin. *Angew Chem Int Ed Engl* **49,** 10149–10153.

Ovaa H, Kessler BM, Rolén U, Galardy PJ, Ploegh HL & Masucci MG (2004). Activity-based ubiquitin-specific protease (USP) profiling of virus-infected and malignant human cells. *Proc Natl Acad Sci U S A* **101,** 2253–2258.

PAHO (2018). Epidemic Diseases - Chikungunya in the Americas. Available at: http://ais.paho.org/phip/viz/ed_chikungunya_amro.asp [Accessed May 31, 2018].

Palazón-Riquelme P, Worboys JD, Green J, Valera A, Martín-Sánchez F, Pellegrini C, Brough D & López-Castejón G (2018). USP7 and USP47 deubiquitinases regulate NLRP3 inflammasome activation. *EMBO Rep* **19,** e44766.

Panas MD, Schulte T, Thaa B, Sandalova T, Kedersha N, Achour A & McInerney GM (2015). Viral and cellular proteins containing FGDF motifs bind G3BP to block stress granule formation. *PLoS Pathog* **11,** e1004659.

Panda D, Fernandez DJ, Lal M, Buehler E & Moss B (2017). Triad of human cellular proteins, IRF2, FAM111A, and RFC3, restrict replication of orthopoxvirus SPI-1 host-range mutants. *Proc Natl Acad Sci* **114,** 3720–3725.

Panda S, Nilsson JA & Gekara NO (2015). Deubiquitinase MYSM1 Regulates Innate Immunity through Inactivation of TRAF3 and TRAF6 Complexes. *Immunity* **43,** 647–659.

Pareja F, Ferraro DA, Rubin C, Cohen-Dvashi H, Zhang F, Aulmann S, Ben-Chetrit N, Pines G, Navon R, Crosetto N, Köstler W, Carvalho S, Lavi S, Schmitt F, Dikic I, Yakhini Z, Sinn P, Mills GB & Yarden Y (2012). Deubiquitination of EGFR by Cezanne-1 contributes to cancer progression. *Oncogene* **31,** 4599–4608.

Partidos CD, Paykel J, Weger J, Borland EM, Powers AM, Seymour R, Weaver SC, Stinchcomb DT & Osorio JE (2012). Cross-protective immunity against o'nyong-nyong virus afforded by a novel recombinant chikungunya vaccine. *Vaccine* **30,** 4638–4643.

Pavri R, Zhu B, Li G, Trojer P, Mandal S, Shilatifard A & Reinberg D (2006). Histone H2B Monoubiquitination Functions Cooperatively with FACT to Regulate Elongation by RNA Polymerase II. *Cell* **125,** 703–717.

Peng J, Schwartz D, Elias JE, Thoreen CC, Cheng D, Marsischky G, Roelofs J, Finley D & Gygi SP (2003). A proteomics approach to understanding protein ubiquitination. *Nat Biotechnol* **21,** 921–926.

Perera R, Owen KE, Tellinghuisen TL, Gorbalenya AE & Kuhn RJ (2001). Alphavirus Nucleocapsid Protein Contains a Putative Coiled Coil -Helix Important for Core Assembly. *J Virol* **75,** 1–10.

Perez-Oliva AB, Lachaud C, Szyniarowski P, Muñoz I, Macartney T, Hickson I, Rouse J & Alessi DR (2015). USP45 deubiquitylase controls ERCC1-XPF endonuclease-mediated DNA damage responses. *EMBO J* **34,** 326–343.

Perwitasari O, Bakre A, Mark Tompkins S & Tripp RA (2013). siRNA genome screening approaches to therapeutic drug repositioning. *Pharmaceuticals* **6,** 124–160.

Petitdemange C, Wauquier N, Devilliers H, Yssel H, Mombo I, Caron M, Nkoghé D, Debré P, Leroy E & Vieillard V (2016). Longitudinal Analysis of Natural Killer Cells in Dengue Virus-Infected Patients in Comparison to Chikungunya and Chikungunya/Dengue Virus-Infected Patients ed. Michael SF. *PLoS Negl Trop Dis* **10,** e0004499.

Pietilä MK, van Hemert MJ & Ahola T (2018). Purification of highly active alphavirus replication complexes demonstrates altered fractionation of multiple cellular membranes. *J Virol* **92,** JVI.01852-17.

Pim D, Collins M & Banks L (1992). Human papillomavirus type 16 E5 gene stimulates the transforming activity of the epidermal growth factor receptor. *Oncogene* **7,** 27–32.

Pingen M, Bryden SR, Pondeville E, Schnettler E, Kohl A, Merits A, Fazakerley JK, Graham GJ & McKimmie CS (2016). Host Inflammatory Response to Mosquito Bites Enhances the Severity of Arbovirus Infection. *Immunity* **44,** 1455–1469.

Plante K, Wang E, Partidos CD, Weger J, Gorchakov R, Tsetsarkin K, Borland EM, Powers AM, Seymour R, Stinchcomb DT, Osorio JE, Frolov I & Weaver SC (2011). Novel chikungunya vaccine candidate with an ires-based attenuation and host range alteration mechanism ed. Heise M. *PLoS Pathog* **7,** e1002142.

Powers AM, Brault AC, Shirako Y, Strauss EG, Kang W, Strauss JH & Weaver SC (2001). Evolutionary relationships and systematics of the alphaviruses. *J Virol* **75,** 10118–10131.

Puiprom O, Morales Vargas RE, Potiwat R, Chaichana P, Ikuta K, Ramasoota P & Okabayashi T (2013). Characterization of chikungunya virus infection of a human keratinocyte cell line: Role of mosquito salivary gland protein in suppressing the host immune response. *Infect Genet Evol* **17,** 210–215.

Pyeon D, Timani KA, Gulraiz F & Park I-W (2016). Function of Ubiquitin (Ub) Specific Protease 15 (USP15) in HIV-1 Replication and Viral Protein Degradation. *Virus Res* **223,** 161–169.

Qian Y et al. (2016). USP16 Downregulation by Carboxyl-terminal Truncated HBx Promotes the Growth of Hepatocellular Carcinoma Cells. *Sci Rep* **6,** 1–12.

Qiu X, Zhu X, Zhang L, Mao Y, Zhang J, Hao P, Li G, Lv P, Li Z, Sun X, Wu L, Zheng J, Deng Y, Hou C, Tang P, Zhang S & Zhang Y (2003). Human epithelial cancers secrete immunoglobulin g with unidentified specificity to promote growth and survival of tumor cells. *Cancer Res* **63,** 6488–6495.

Querido E, Blanchette P, Yan Q, Kamura T, Morrison M, Boivin D, Kaelin WG, Conaway RC, Conaway JW & Branton PE (2001). Degradation of p53 by adenovirus E4orf6 and E1B55K proteins occurs via a novel mechanism involving a Cullin-containing complex. *Genes Dev* **15,** 3104–3117.

R Bron JMWHGJW (1993). Membrane fusion of Semliki Forest virus in a model system: correlation between fusion kinetics and structural changes in the envelope glycoprotein. *EMBO J* **12,** 693. Available at: /pmc/articles/PMC413255/?report=abstract [Accessed January 21, 2016].

Radoshitzky SR et al. (2016). siRNA Screen Identifies Trafficking Host Factors that Modulate Alphavirus Infection. *PLoS Pathog* **12,** e1005466.

Ramakrishnan C, Kutumbarao NHV, Suhitha S & Velmurugan D (2017). Structure–function relationship of Chikungunya nsP2 protease: A comparative study with papain. *Chem Biol Drug Des* **89,** 772–782.

Rashad AA, Neyts J, Leyssen P & Keller PA (2018). A reassessment of mycophenolic acid as a lead compound for the development of inhibitors of chikungunya virus replication. *Tetrahedron* **74,** 1294–1306.

Rathore APS, Haystead T, Das PK, Merits A, Ng ML & Vasudevan SG (2014). Chikungunya virus nsP3 & nsP4 interacts with HSP-90 to promote virus replication: HSP-90 inhibitors reduce CHIKV infection and inflammation in vivo. *Antiviral Res* **103,** 7–16.

Ratia K, Kilianski A, Baez-Santos YM, Baker SC & Mesecar A (2014). Structural Basis for the Ubiquitin-Linkage Specificity and deISGylating Activity of SARS-CoV Papain-Like Protease ed. Rey FA. *PLoS Pathog* **10,** e1004113.

Ratia K, Pegan S, Takayama J, Sleeman K, Coughlin M, Baliji S, Chaudhuri R, Fu W, Prabhakar BS, Johnson ME, Baker SC, Ghosh AK & Mesecar AD (2008). A noncovalent class of papain-like protease/deubiquitinase inhibitors blocks SARS virus replication. *Proc Natl Acad Sci U S A* **105,** 16119–16124.

Rausalu K, Utt A, Quirin T, Varghese FS, Žusinaite E, Das PK, Ahola T & Merits A (2016). Chikungunya virus infectivity, RNA replication and non-structural polyprotein processing depend on the nsP2 protease's active site cysteine residue. *Sci Rep* **6,** 37124.

Ravichandran R & Manian M (2008). Ribavirin therapy for Chikungunya arthritis. *J Infect Dev Ctries* **2,** 140–142.

Redman KL & Rechsteiner M (1989). Identification of the long ubiquitin extension as ribosomal protein S27a. *Nature* **338,** 438–440.

Reiley W, Zhang M, Wu X, Granger E & Sun SC (2005). Regulation of the deubiquitinating enzyme CYLD by IkappaB kinase gamma-dependent phosphorylation. *Mol Cell Biol* **25,** 3886–3895.

Ren Y, Zhao P, Liu J, Yuan Y, Cheng Q, Zuo Y, Qian L, Liu C, Guo T, Zhang L, Wang X, Qian G, Li L, Ge J, Dai J, Xiong S & Zheng H (2016). Deubiquitinase USP2a Sustains Interferons Antiviral Activity by Restricting Ubiquitination of Activated STAT1 in the Nucleus ed. Gaffen SL. *PLOS Pathog* **12,** e1005764.

Renault P, Solet JL, Sissoko D, Balleydier E, Larrieu S, Filleul L, Lassalle C, Thiria J, Rachou E, De Valk H, Ilef D, Ledrans M, Quatresous I, Quenel P & Pierre V (2007). A major epidemic of chikungunya virus infection on Réunion Island, France, 2005-2006. *Am J Trop Med Hyg* **77,** 727–731.

Reverdy C, Conrath S, Lopez R, Planquette C, Atmanene C, Collura V, Harpon J, Battaglia V, Vivat V, Sippl W & Colland F (2012). Discovery of specific inhibitors of human USP7/HAUSP deubiquitinating enzyme. *Chem Biol* **19,** 467–477.

Rezza G, Chen R & Weaver SC (2017). O'nyong-nyong fever: a neglected mosquito-borne viral disease. *Pathog Glob Health* **111,** 271–275. Available at: https://www.tandfonline.com/doi/full/10.1080/20477724.2017.1355431 [Accessed August 29, 2017].

Rice CM & Strauss JH (1981). Nucleotide sequence of the 26S mRNA of Sindbis virus and deduced sequence of the encoded virus structural proteins. *Proc Natl Acad Sci U S A* **78,** 2062–2066.

Richardson PG et al. (2005). Bortezomib or High-Dose Dexamethasone for Relapsed Multiple Myeloma. *N Engl J Med* **352,** 2487–2498.

Rigau-Pérez JG, Ayala-López A, García-Rivera EJ, Hudson SM, Vorndam V, Reiter P, Cano MP & Clark GG (2002). The reappearance of dengue-3 and a subsequent dengue-4 and dengue-1 epidemic in Puerto Rico in 1998. *Am J Trop Med Hyg* **67,** 355–362.

Ritorto MS, Ewan R, Perez-Oliva AB, Knebel A, Buhrlage SJ, Wightman M, Kelly SM, Wood NT, Virdee S, Gray NS, Morrice NA, Alessi DR & Trost M (2014). Screening of DUB activity and specificity by MALDI-TOF mass spectrometry. *Nat Commun* **5,** 4763.

Robbins M, Judge A, Ambegia E, Choi C, Yaworski E, Palmer L, McClintock K & MacLachlan I (2008). Misinterpreting the Therapeutic Effects of Small Interfering RNA Caused by Immune Stimulation. *Hum Gene Ther* **19,** 991–999.

Robinson MC (1955). An epidemic of virus disease in Southern Province, Tanganyika territory, in 1952–1953. *Trans R Soc Trop Med Hyg* **49,** 28–32.

Robzyk K, Recht J & Osley MA (2000). Rad6-dependent ubiquitination of histone H2B in yeast. *Science (80-)* **287,** 501–504.

Rochlin I, Ninivaggi D V., Hutchinson ML & Farajollahi A (2013). Climate Change and Range Expansion of the Asian Tiger Mosquito (Aedes albopictus) in Northeastern USA: Implications for Public Health Practitioners ed. Oliveira PL. *PLoS One* **8,** e60874.

Rolén U, Kobzeva V, Gasparjan N, Ovaa H, Winberg G, Kisseljov F & Masucci MG (2006). Activity profiling of deubiquitinating enzymes in cervical carcinoma biopsies and cell lines. *Mol Carcinog* **45,** 260–269.

Roman-Sosa G & Kielian M (2011). The Interaction of Alphavirus E1 Protein with Exogenous Domain III Defines Stages in Virus-Membrane Fusion. *J Virol* **85,** 12271–12279.

Rossini G, Gaibani P, Vocale C, Finarelli AC & Landini MP (2016). Increased number of cases of Chikungunya virus (CHIKV) infection imported from the Caribbean and Central America to northern Italy, 2014. *Epidemiol Infect*1–5.

Roy CJ, Adams AP, Wang E, Plante K, Gorchakov R, Seymour RL, Vinet-Oliphant H & Weaver SC (2014). Chikungunya vaccine candidate is highly attenuated and protects nonhuman primates against telemetrically monitored disease following a single dose. *J Infect Dis* **209,** 1891–1899.

Rubach JK, Wasik BR, Rupp JC, Kuhn RJ, Hardy RW & Smith JL (2009). Characterization of purified Sindbis virus nsP4 RNA-dependent RNA polymerase activity in vitro. *Virology* **384,** 201–208.

Rueda LM, Patel KJ, Axtell RC & Stinner RE (1990). Temperature-dependent development and survival rates of Culex quinquefasciatus and Aedes aegypti (Diptera: Culicidae). *J Med Entomol* **27,** 892–898.

Rulli NE, Rolph MS, Srikiatkhachorn A, Anantapreecha S, Guglielmotti A & Mahalingam S (2011). Protection from arthritis and myositis in a mouse model of acute chikungunya virus disease by bindarit, an inhibitor of monocyte chemotactic protein-1 synthesis. *J Infect Dis* **204,** 1026–1030.

Rupp JC, Jundt N & Hardy RW (2011). Requirement for the Amino-Terminal Domain of Sindbis Virus nsP4 during Virus Infection. *J Virol* **85,** 3449–3460.

Rupp JC, Sokoloski KJ, Gebhart NN & Hardy RW (2015*a*). Alphavirus RNA synthesis and non-structural protein functions. *J Gen Virol* **96,** 2483–2500.

Rupp JC, Sokoloski KJ, Gebhart NN & Hardy RW (2015*b*). Alphavirus RNA synthesis and nonstructural protein functions. *J Gen Virol* **96,** 2483–2500.

Sahadeo NSD, Allicock OM, De Salazar PM, Auguste AJ, Widen S, Olowokure B, Gutierrez C, Valadere AM, Polson-Edwards K, Weaver SC & Carrington CVF (2017). Understanding the evolution and spread of chikungunya virus in the Americas using complete genome sequences. *Virus Evol*; DOI: 10.1093/ve/vex010.

Sahtoe DD & Sixma TK (2015). Layers of DUB regulation. *Trends Biochem Sci* **40,** 456–467.

Saisawang C, Saitornuang S, Sillapee P, Ubol S, Smith DR & Ketterman AJ (2015*a*). Chikungunya nsP2 protease is not a papain-like cysteine protease and the catalytic dyad cysteine is interchangeable with a proximal serine. *Sci Rep* **5,** 17125.

Saisawang C, Sillapee P, Sinsirimongkol K, Ubol S, Smith DR & Ketterman AJ (2015*b*). Full length and protease domain activity of chikungunya virus nsP2 differ from other alphavirus nsP2 proteases in recognition of small peptide substrates. *Biosci Rep* **35,** 1–9.

Saito S, Murata T, Kanda T, Isomura H, Narita Y, Sugimoto A, Kawashima D & Tsurumi T (2013). Epstein-Barr virus deubiquitinase downregulates TRAF6-mediated NF-κB signaling during productive replication. *J Virol* **87,** 4060–4070.

Sanchez-San Martin C, Nanda S, Zheng Y, Fields W & Kielian M (2013). Cross-Inhibition of Chikungunya Virus Fusion and Infection by Alphavirus E1 Domain III Proteins. *J Virol* **87,** 7680–7687.

Sandoval PC, Slentz DH, Pisitkun T, Saeed F, Hoffert JD & Knepper MA (2013). Proteome-wide measurement of protein half-lives and translation rates in vasopressin-sensitive collecting duct cells. *J Am Soc Nephrol* **24,** 1793–1805.

Sarkar JK, Chatterjee SN, Chakravarti SK & Mitra AC (1965). Chikungunya Virus Infection with Haemorrhagic Manifestations. *Indian J Med Res* **53,** 921–925.

Savio MG, Wollscheid N, Cavallaro E, Algisi V, Di Fiore PP, Sigismund S, Maspero E & Polo S (2016). USP9X Controls EGFR Fate by Deubiquitinating the Endocytic Adaptor Eps15. *Curr Biol* **26,** 173–183.

Sawicki DL & Sawicki SG (1980). Short-lived minus-strand polymerase for Semliki Forest virus. *J Virol* **34,** 108–118.

Saxena N & Kumar V (2014). The HBx oncoprotein of hepatitis B virus deregulates the cell cycle by promoting the intracellular accumulation and re-compartmentalization of the cellular deubiquitinase USP37 ed. Bouchard MJ. *PLoS One* **9,** e111256.

Schaeffer V, Akutsu M, Olma MH, Gomes LC, Kawasaki M & Dikic I (2014). Binding of OTULIN to the PUB Domain of HOIP Controls NF-κB Signaling. *Mol Cell* **54,** 349–361.

Scheffner M, Werness BA, Huibregtse JM, Levine AJ & Howley PM (1990). The E6 oncoprotein encoded by human papillomavirus types 16 and 18 promotes the degradation of p53. *Cell* **63,** 1129–1136.

Schilte C, Staikowsky F, Staikovsky F, Couderc T, Madec Y, Carpentier F, Kassab S, Albert ML, Lecuit M & Michault A (2013). Chikungunya virus-associated long-term arthralgia: a 36-month prospective longitudinal study. *PLoS Negl Trop Dis* **7,** e2137.

Schlieker C, Korbel GA, Kattenhorn LM & Ploegh HL (2005). A deubiquitinating activity is conserved in the large tegument protein of the herpesviridae. *J Virol* **79,** 15582–15585.

Schlieker C, Weihofen WA, Frijns E, Kattenhorn LM, Gaudet R & Ploegh HL (2007). Structure of a herpesvirus-encoded cysteine protease reveals a unique class of deubiquitinating enzymes. *Mol Cell* **25,** 677–687.

Schmid MA, Glasner DR, Shah S, Michlmayr D, Kramer LD & Harris E (2016). Mosquito Saliva Increases Endothelial Permeability in the Skin, Immune Cell Migration, and Dengue Pathogenesis during Antibody-Dependent Enhancement ed. Heise MT. *PLoS Pathog* **12,** e1005676.

Schmid S, Fuchs R, Kielian M, Helenius A & Mellman I (1989). Acidification of endosome subpopulations in wild-type Chinese hamster ovary cells and temperature-sensitive acidification-defective mutants. *J Cell Biol* **108,** 1291–1300.

Schmid SL, Fuchs R, Male P & Mellman I (1988). Two distinct subpopulations of endosomes involved in membrane recycling and transport to lysosomes. *Cell* **52,** 73–83.

Schmittgen TD & Livak KJ (2008). Analyzing real-time PCR data by the comparative C(T) method. *Nat Protoc* **3,** 1101–1108.

Scholte FEM, Tas A, Martina BEE, Cordioli P, Narayanan K, Makino S, Snijder EJ & van Hemert MJ (2013). Characterization of synthetic Chikungunya viruses based on the consensus sequence of recent E1-226V isolates. *PLoS One* **8,** e71047.

Scholte FEM, Zivcec M, Dzimianski J V, Deaton MK, Spengler JR, Welch SR, Nichol ST, Pegan SD, Spiropoulou CF & Bergeron É (2017). Crimean-Congo Hemorrhagic Fever Virus Suppresses Innate Immune Responses via a Ubiquitin and ISG15 Specific Protease. *Cell Rep* **20,** 2396–2407.

Sefton BM (1977). Immediate glycosylation of Sindbis virus membrane proteins. *Cell* **10,** 659–668.

Semenza JC, Lindgren E, Balkanyi L, Espinosa L, Almqvist MS, Penttinen P & Rocklöv J (2016). Determinants and drivers of infectious disease threat events in europe. *Emerg Infect Dis* **22,** 581–589.

Seol JH, Feldman RMR, Zachariae W, Shevchenko A, Correll CC, Lyapina S, Chi Y, Galova M, Claypool J, Sandmeyer S, Nasmyth K, Shevchenko A & Deshaies RJ (1999). Cdc53/cullin and the essential Hrt1 RING-H2 subunit of SCF define a ubiquitin ligase module that activates the E2 enzyme Cdc34. *Genes Dev* **13,** 1614–1626.

Sette P, Nagashima K, Piper RC & Bouamr F (2013). Ubiquitin conjugation to Gag is essential for ESCRT-mediated HIV-1 budding. *Retrovirology* **10,** 79.

Setz C, Friedrich M, Rauch P, Fraedrich K, Matthaei A, Traxdorf M & Schubert U (2017). Inhibitors of deubiquitinating enzymes block HIV-1 replication and augment the presentation of gag-derived MHC-I epitopes. *Viruses* **9,** 222.

Sheehy AM, Gaddis NC, Choi JD & Malim MH (2002). Isolation of a human gene that inhibits HIV-1 infection and is suppressed by the viral Vif protein. *Nature* **418,** 646–650.

Shirako Y & Strauss JH (1994). Regulation of Sindbis virus RNA replication: uncleaved P123 and nsP4 function in minus-strand RNA synthesis, whereas cleaved products from P123 are required for efficient plus-strand RNA synthesis. *J Virol* **68,** 1874–1885.

Sieczkarski SB & Whittaker GR (2003). Differential requirements of Rab5 and Rab7 for endocytosis of influenza and other enveloped viruses. *Traffic* **4,** 333–343. Available at: http://www.ncbi.nlm.nih.gov/pubmed/12713661 [Accessed November 26, 2018].

Sigismund S, Woelk T, Puri C, Maspero E, Tacchetti C, Transidico P, Di Fiore PP & Polo S (2005). Clathrin-independent endocytosis of ubiquitinated cargos. *Proc Natl Acad Sci U S A* **102,** 2760–2765.

Simon F et al. (2015). French guidelines for the management of chikungunya (acute and persistent presentations). November 2014. *Médecine Mal Infect* **45,** 243–263.

Sledz CA, Holko M, De Veer MJ, Silverman RH & Williams BRG (2003). Activation of the interferon system by short-interfering RNAs. *Nat Cell Biol* **5,** 834–839.

Smit JM, Waarts B-L, Kimata K, Klimstra WB, Bittman R & Wilschut J (2002). Adaptation of alphaviruses to heparan sulfate: interaction of Sindbis and Semliki forest viruses with liposomes containing lipid-conjugated heparin. *J Virol* **76,** 10128–10137.

Smith SA et al. (2015). Isolation and characterization of broad and ultrapotent human monoclonal antibodies with therapeutic activity against chikungunya virus. *Cell Host Microbe* **18,** 86–95.

Sobol A, Askonas C, Alani S, Weber MJ, Ananthanarayanan V, Osipo C & Bocchetta M (2017). Deubiquitinase OTUD6B Isoforms Are Important Regulators of Growth and Proliferation. *Mol Cancer Res* **15,** 117–127.

Sokoloski KJ, Nease LM, May NA, Gebhart NN, Jones CE, Morrison TE & Hardy RW (2017). Identification of Interactions between Sindbis Virus Capsid Protein and Cytoplasmic vRNA as Novel Virulence Determinants ed. Cherry S. *PLoS Pathog* **13,** e1006473.

Sompallae R, Gastaldello S, Hildebrand S, Zinin N, Hassink G, Lindsten K, Haas J, Persson B & Masucci MG (2008). Epstein-barr virus encodes three bona fide ubiquitin-specific proteases. *J Virol* **82,** 10477–10486.

Sourisseau M et al. (2007). Characterization of reemerging chikungunya virus. *PLoS Pathog* **3,** 0804–0817.

Sowa ME, Bennett EJ, Gygi SP & Harper JW (2009). Defining the Human Deubiquitinating Enzyme Interaction Landscape. *Cell* **138,** 389–403.

Spuul P, Balistreri G, Kaariainen L & Ahola T (2010). Phosphatidylinositol 3-Kinase-, Actin-, and Microtubule-Dependent Transport of Semliki Forest Virus Replication Complexes from the Plasma Membrane to Modified Lysosomes. *J Virol* **84,** 7543–7557.

Spuul P, Salonen A, Merits A, Jokitalo E, Kaariainen L & Ahola T (2007). Role of the Amphipathic Peptide of Semliki Forest Virus Replicase Protein nsP1 in Membrane Association and Virus Replication. *J Virol* **81,** 872–883.

Straight SW, Hinkle PM, Jewers RJ & McCance DJ (1993). The E5 oncoprotein of human papillomavirus type 16 transforms fibroblasts and effects the downregulation of the epidermal growth factor receptor in keratinocytes. *J Virol* **67,** 4521–4532.

Strauss EG, Rice CM & Strauss JH (1983). Sequence coding for the alphavirus nonstructural proteins is interrupted by an opal termination codon. *Proc Natl Acad Sci U S A* **80,** 5271–5275.

Strauss EG, Rice CM & Strauss JH (1984). Complete nucleotide sequence of the genomic RNA of Sindbis virus. *Virology* **133,** 92–110.

Strauss JH & Strauss EG (1994). The alphaviruses: gene expression, replication, and evolution. *Microbiol Rev* **58,** 806.

Su Z-J, Cao J-S, Wu Y, Chen W, Lin X & Wu Y-L (2017). Deubiquitylation of hepatitis B virus X protein (HBx) by ubiquitin-specific peptidase 15 (USP15) increases HBx stability and its transactivation activity. *Nat Publ Gr* **7,** 1–11.

Subudhi BB, Chattopadhyay S, Mishra P & Kumar A (2018). Current strategies for inhibition of Chikungunya infection. *Viruses* **10,** 235.

Suhrbier A, Jaffar-Bandjee M-C & Gasque P (2012). Arthritogenic alphaviruses--an overview. *Nat Rev Rheumatol* **8,** 420–429.

Sun C, Schattgen SA, Pisitkun P, Jorgensen JP, Hilterbrand AT, Wang LJ, West JA, Hansen K, Horan KA, Jakobsen MR, O'Hare P, Adler H, Sun R, Ploegh HL, Damania B, Upton JW, Fitzgerald KA & Paludan SR (2015). Evasion of Innate Cytosolic DNA Sensing by a Gammaherpesvirus Facilitates Establishment of Latent Infection. *J Immunol* **194,** 1819–1831.

Sun H, Zhang Q, Jing Y-Y, Zhang M, Wang H-Y, Cai Z, Liuyu T, Zhang Z-D, Xiong T-C, Wu Y, Zhu Q-Y, Yao J, Shu H-B, Lin D & Zhong B (2017*a*). USP13 negatively regulates antiviral responses by deubiquitinating STING. *Nat Commun* **8,** 15534.

Sun X, Feng W, Guo Y, Wang Q, Dong C, Zhang M, Guan Z & Duan M (2017*b*). MCPIP1 attenuates the innate immune response to influenza A viruse by suppressing RIG-I expression in lung epithelial cells. *J Med Virol*; DOI: 10.1002/jmv.24944.

Sun Z, Chen Z, Lawson SR & Fang Y (2010). The Cysteine Protease Domain of Porcine Reproductive and Respiratory Syndrome Virus Nonstructural Protein 2 Possesses Deubiquitinating and Interferon Antagonism Functions. *J Virol* **84,** 7832–7846.

Swaney DL, Beltrao P, Starita L, Guo A, Rush J, Fields S, Krogan NJ & Villén J (2013). Global analysis of phosphorylation and ubiquitylation cross-talk in protein degradation. *Nat Methods* **10,** 676–682.

Takkinen K, Peranen J & Kaariainen L (1991). Proteolytic processing of Semliki Forest virus-specific non-structural polyprotein. *J Gen Virol* **72,** 1627–1633.

Tanikawa T, Uchida Y & Saito T (2017). Replication of a low-pathogenic avian influenza virus is enhanced by chicken ubiquitin-specific protease 18. *J Gen Virol* **98,** 2235–2247.

Teng T-S, Kam Y-W, Lee B, Hapuarachchi HC, Wimal A, Ng L-C & Ng LFP (2015). A Systematic Meta-analysis of Immune Signatures in Patients With Acute Chikungunya Virus Infection. *J Infect Dis* **211,** 1925–1935.

Teo T-H, Her Z, Tan JJL, Lum F-M, Lee WWL, Chan Y-H, Ong R-Y, Kam Y-W, Leparc-Goffart I, Gallian P, Rénia L, de Lamballerie X & Ng LFP (2015). Caribbean and La Réunion Chikungunya Virus Isolates Differ in Their Capacity To Induce Proinflammatory Th1 and NK Cell Responses and Acute Joint Pathology ed. Dermody TS. *J Virol* **89,** 7955–7969.

Teo T-H, Lum F-M, Claser C, Lulla V, Lulla A, Merits A, Renia L & Ng LFP (2013). A Pathogenic Role for CD4+ T Cells during Chikungunya Virus Infection in Mice. *J Immunol* **190,** 259–269.

Teo TH, Chan YH, Lee WWL, Lum FM, Amrun SN, Her Z, Rajarethinam R, Merits A, Rötzschke O, Rénia L & Ng LFP (2017). Fingolimod treatment abrogates chikungunya virus-induced arthralgia. *Sci Transl Med* **9,** eaal1333.

Thaa B, Biasiotto R, Eng K, Neuvonen M, Götte B, Rheinemann L, Mutso M, Utt A, Varghese F, Balistreri G, Merits A, Ahola T & McInerney GM (2015). Differential Phosphatidylinositol-3-Kinase-Akt-mTOR Activation by Semliki Forest and Chikungunya Viruses Is Dependent on nsP3 and Connected to Replication Complex Internalization. *J Virol* **89,** 11420–11437.

Thiboutot MM, Kannan S, Kawalekar OU, Shedlock DJ, Khan AS, Sarangan G, Srikanth P, Weiner DB & Muthumani K (2010). Chikungunya: A potentially emerging epidemic? *PLoS Negl Trop Dis*; DOI: 10.1371/journal.pntd.0000623.

Thio CL-P, Yusof R, Abdul-Rahman PSA & Karsani SA (2013). Differential proteome analysis of chikungunya virus infection on host cells. *PLoS One* **8,** e61444.

Tjaden NB, Suk JE, Fischer D, Thomas SM, Beierkuhnlein C & Semenza JC (2017). Modelling the effects of global climate change on Chikungunya transmission in the 21st century. *Sci Rep* **7,** 3813.

Todi S V, Winborn BJ, Scaglione KM, Blount JR, Travis SM & Paulson HL (2009). Ubiquitination directly enhances activity of the deubiquitinating enzyme ataxin-3. *EMBO J* **28,** 372–382.

Toulis V, Garanto A & Marfany G (2016). Combining zebrafish and mouse models to test the function of deubiquitinating enzyme (Dubs) genes in development: Role of USP45 in the retina. *Methods Mol Biol* **1449,** 85–101.

Tran HJTT, Allen MD, Löwe J & Bycroft M (2003). Structure of the Jab1/MPN Domain and Its Implications for Proteasome Function. *Biochemistry* **42,** 11460–11465.

Treffers EE, Tas A, Scholte FEM, Van MN, Heemskerk MT, de Ru AH, Snijder EJ, van Hemert MJ & van Veelen PA (2015). Temporal SILAC-based quantitative proteomics identifies host factors involved in chikungunya virus replication. *Proteomics* **15,** 2267–2280.

Tsetsarkin KA, Chen R, Sherman MB & Weaver SC (2011). Chikungunya virus: Evolution and genetic determinants of emergence. *Curr Opin Virol* **1,** 310–317.

Tsetsarkin KA, Vanlandingham DL, McGee CE & Higgs S (2007). A Single Mutation in Chikungunya Virus Affects Vector Specificity and Epidemic Potential. *PLoS Pathog* **3,** e201.

Tyers M & Mann M (2003). From genomics to proteomics. *Nature* **422,** 193–197.

Ui-Tei K, Naito Y, Nishi K, Juni A & Saigo K (2008). Thermodynamic stability and Watson-Crick base pairing in the seed duplex are major determinants of the efficiency of the siRNA-based off-target effect. *Nucleic Acids Res* **36,** 7100–7109.

Ulane CM & Horvath CM (2002). Paramyxoviruses SV5 and HPIV2 assemble STAT protein ubiquitin ligase complexes from cellular components. *Virology* **304,** 160–166.

Ulane CM, Rodriguez JJ, Parisien J-P & Horvath CM (2003). STAT3 Ubiquitylation and Degradation by Mumps Virus Suppress Cytokine and Oncogene Signaling. *J Virol* **77,** 6385–6393.

Umashankar M, Sanchez-San Martin C, Liao M, Reilly B, Guo A, Taylor G & Kielian M (2008). Differential Cholesterol Binding by Class II Fusion Proteins Determines Membrane Fusion Properties. *J Virol* **82,** 9245–9253.

Underwood KW, Andemariam B, McWilliams GL & Liscum L (1996). Quantitative analysis of hydrophobic amine inhibition of intracellular cholesterol transport. *J Lipid Res* **37,** 1556–1568.

VanderLinden RT, Hemmis CW, Schmitt B, Ndoja A, Whitby FG, Robinson H, Cohen RE, Yao T & Hill CP (2015). Structural Basis for the Activation and Inhibition of the UCH37 Deubiquitylase. *Mol Cell* **57,** 901–911.

Vandermarliere E, Mueller M & Martens L (2013). Getting intimate with trypsin, the leading protease in proteomics. *Mass Spectrom Rev* **32,** 453–465.

Vasiljeva L, Merits A, Auvinen P & Kääriäinen L (2000). Identification of a novel function of the Alphavirus capping apparatus. RNA 5'-triphosphatase activity of Nsp2. *J Biol Chem* **275,** 17281–17287.

Veiga IB, Jarosinski KW, Kaufer BB & Osterrieder N (2013). Marek's disease virus (MDV) ubiquitin-specific protease (USP) performs critical functions beyond its enzymatic activity during virus replication. *Virology* **437,** 110–117.

Venturi G, Di Luca M, Fortuna C, Remoli ME, Riccardo F, Severini F, Toma L, Del Manso M, Benedetti E, Caporali MG, Amendola A, Fiorentini C, De Liberato C, Giammattei R, Romi R, Pezzotti P, Rezza G & Rizzo C (2017). Detection of a chikungunya outbreak in central Italy, August to September 2017. *Eurosurveillance* **22,** 11–14.

Vijay-kumar S, Bugg CE & Cook WJ (1987). Structure of ubiquitin refined at 1.8 Å resolution. *J Mol Biol* **194,** 531–544.

Vital EM & Emery P (2006). Abatacept in the treatment of rheumatoid arthritis. *Ther Clin Risk Manag* **2,** 365–375.

Volk SM, Chen R, Tsetsarkin KA, Adams AP, Garcia TI, Sall AA, Nasar F, Schuh AJ, Holmes EC, Higgs S, Maharaj PD, Brault AC & Weaver SC (2010). Genome-Scale Phylogenetic Analyses of Chikungunya Virus Reveal Independent Emergences of Recent Epidemics and Various Evolutionary Rates. *J Virol* **84,** 6497–6504.

Waarts BL, Bittman R & Wilschut J (2002). Sphingolipid and cholesterol dependence of alphavirus membrane fusion: Lack of correlation with lipid raft formation in target liposomes. *J Biol Chem* **277,** 38141–38147.

Wahid B, Ali A, Rafique S & Idrees M (2017). Global expansion of chikungunya virus: mapping the 64-year history. *Int J Infect Dis* **58,** 69–76. Available at: https://www.sciencedirect.com/science/article/pii/S1201971217300899#bib0120 [Accessed December 12, 2018].

Wahlberg JM & Garoff H (1992). Membrane fusion process of Semliki Forest virus I: Low pH-induced rearrangement in spike protein quaternary structure precedes virus penetration into cells. *J Cell Biol* **116,** 339–348.

Wang D, Fang L, Li P, Sun L, Fan J, Zhang Q, Luo R, Liu X, Li K, Chen H, Chen Z & Xiao S (2011*a*). The leader proteinase of foot-and-mouth disease virus negatively regulates the type I interferon pathway by acting as a viral deubiquitinase. *J Virol* **85,** 3758–3766.

Wang G, Chen G, Zheng D, Cheng G & Tang H (2011*b*). PLP2 of mouse hepatitis Virus A59 (MHV-A59) targets TBK1 to negatively regulate cellular type I interferon signaling pathway ed. Ryu W-S. *PLoS One* **6,** e17192.

Wang J, Lin D, Peng H, Huang Y, Huang J & Gu J (2013*a*). Cancer-derived immunoglobulin G promotes tumor cell growth and proliferation through inducing production of reactive oxygen species. *Cell Death Dis* **4,** e945.

Wang J, Liu Y, Tang L, Qi S, Mi Y, Liu D & Tian Q (2017*a*). Identification of candidate substrates of ubiquitin-specific protease 13 using 2D-DIGE. *Int J Mol Med* **40,** 47–56.

Wang J, Loveland AN, Kattenhorn LM, Ploegh HL & Gibson W (2006). High-molecular-weight protein (pUL48) of human cytomegalovirus is a competent

deubiquitinating protease: mutant viruses altered in its active-site cysteine or histidine are viable. *J Virol* **80,** 6003–6012.

Wang KS, Kuhn RJ, Strauss EG, Ou S & Strauss JH (1992). High-affinity laminin receptor is a receptor for Sindbis virus in mammalian cells. *J Virol* **66,** 4992–5001.

Wang P, Henning SM & Heber D (2010). Limitations of MTT and MTS-Based Assays for Measurement of Antiproliferative Activity of Green Tea Polyphenols ed. Deb S. *PLoS One* **5,** e10202.

Wang T, Wei JJ, Sabatini DM & Lander ES (2014). Genetic screens in human cells using the CRISPR-Cas9 system. *Science (80-)* **343,** 80–84.

Wang T, Yin L, Cooper EM, Lai MY, Dickey S, Pickart CM, Fushman D, Wilkinson KD, Cohen RE & Wolberger C (2009). Evidence for Bidentate Substrate Binding as the Basis for the K48 Linkage Specificity of Otubain 1. *J Mol Biol* **386,** 1011–1023.

Wang X, Jin C, Tang Y, Tang LY & Zhang YE (2013*b*). Ubiquitination of tumor necrosis factor receptor-associated factor 4 (TRAF4) by smad ubiquitination regulatory factor 1 (Smurf1) regulates motility of breast epithelial and cancer cells. *J Biol Chem* **288,** 21784–21792.

Wang X, Mazurkiewicz M, Hillert E-K, Olofsson MH, Pierrou S, Hillertz P, Gullbo J, Selvaraju K, Paulus A, Akhtar S, Bossler F, Khan AC, Linder S & D'Arcy P (2016). The proteasome deubiquitinase inhibitor VLX1570 shows selectivity for ubiquitin-specific protease-14 and induces apoptosis of multiple myeloma cells. *Sci Rep* **6,** 26979.

Wang X, Zhang L, Zhang Y, Zhao P, Qian L, Yuan Y, Liu J, Cheng Q, Xu W, Zuo Y, Guo T, Yu Z & Zheng H (2017*b*). JOSD1 Negatively Regulates Type-I Interferon Antiviral Activity by Deubiquitinating and Stabilizing SOCS1. *Viral Immunol* **30,** 342–349.

Ward JA, McLellan L, Stockley M, Gibson KR, Whitlock GA, Knights C, Harrigan JA, Jacq X & Tate EW (2016). Quantitative Chemical Proteomic Profiling of Ubiquitin Specific Proteases in Intact Cancer Cells. *ACS Chem Biol* **11,** 3268–3272.

Wauquier N, Becquart P, Nkoghe D, Padilla C, Ndjoyi-Mbiguino A & Leroy EM (2011). The acute phase of Chikungunya virus infection in humans is associated with strong innate immunity and T CD8 cell activation. *J Infect Dis* **204,** 115–123.

Weaver SC & Barrett ADT (2004). Transmission cycles, host range, evolution and emergence of arboviral disease. *Nat Rev Microbiol* **2,** 789–801. Available at: http://www.nature.com/articles/nrmicro1006 [Accessed December 12, 2018].

Weaver SC, Ferro C, Barrera R, Boshell J & Navarro J-C (2004). Venezuelan equine encephalitis. *Annu Rev Entomol* **49,** 141–174.

Weaver SC & Forrester NL (2015). Chikungunya: Evolutionary history and recent epidemic spread. *Antiviral Res* **120,** 32–39.

Weaver SC & Lecuit M (2015). Chikungunya Virus and the Global Spread of a Mosquito-Borne Disease ed. Campion EW. *N Engl J Med* **372,** 1231–1239.

Weber C, Büchner SM & Schnierle BS (2015). A Small Antigenic Determinant of the Chikungunya Virus E2 Protein Is Sufficient to Induce Neutralizing Antibodies which Are Partially Protective in Mice ed. Williams M. *PLoS Negl Trop Dis* **9,** e0003684.

Weinberg JS & Drubin DG (2014). Regulation of Clathrin-mediated endocytosis by dynamic ubiquitination and deubiquitination. *Curr Biol* **24,** 951–959.

Weinstock J, Wu J, Cao P, Kingsbury WD, McDermott JL, Kodrasov MP, McKelvey DM, Suresh Kumar KG, Goldenberg SJ, Mattern MR & Nicholson B (2012). Selective dual inhibitors of the cancer-related deubiquitylating proteases USP7 and USP47. *ACS Med Chem Lett* **3,** 789–792.

Welcker M & Clurman BE (2005). The SV40 large T antigen contains a decoy phosphodegron that mediates its interactions with Fbw7/hCdc4. *J Biol Chem* **280,** 7654–7658.

Wengler G, Gros C & Wengler G (1996). Analyses of the role of structural changes in the regulation of uncoating and assembly of alphavirus cores. *Virology* **222,** 123–132.

Wengler G, Koschinski A, Wengler G & Dreyer F (2003). Entry of alphaviruses at the plasma membrane converts the viral surface proteins into an ionpermeable pore that can be detected by electrophysiological analyses of whole-cell membrane currents. *J Gen Virol* **84,** 173–181. Available at: http://www.ncbi.nlm.nih.gov/pubmed/12533714 [Accessed November 26, 2018].

Wengler G, Würkner D & Wengler G (1992). Identification of a sequence element in the alphavirus core protein which mediates interaction of cores with ribosomes and the disassembly of cores. *Virology* **191,** 880–888.

Weston J, Villoing S, Bremont M, Castric J, Pfeffer M, Jewhurst V, McLoughlin M, Rodseth O, Christie KE, Koumans J & Todd D (2002). Comparison of Two Aquatic Alphaviruses, Salmon Pancreas Disease Virus and Sleeping Disease Virus, by Using Genome Sequence Analysis, Monoclonal Reactivity, and Cross-Infection. *J Virol* **76,** 6155–6163.

Wiborg O, Pedersen MS, Wind A, Berglund LE, Marcker KA & Vuust J (1985). The human ubiquitin multigene family: some genes contain multiple directly repeated ubiquitin coding sequences. *EMBO J* **4,** 755–759.

Wichit S, Hamel R, Bernard E, Talignani L, Diop F, Ferraris P, Liegeois F, Ekchariyawat P, Luplertlop N, Surasombatpattana P, Thomas F, Merits A, Choumet V, Roques P, Yssel H, Briant L & Miss? D (2017). Imipramine Inhibits Chikungunya Virus Replication in Human Skin Fibroblasts through Interference with Intracellular Cholesterol Trafficking. *Sci Rep* **7,** 3145.

Wickliffe KE, Williamson A, Meyer HJ, Kelly A & Rape M (2011). K11-linked ubiquitin chains as novel regulators of cell division. *Trends Cell Biol* **21,** 656–663. Available at: http://www.ncbi.nlm.nih.gov/pubmed/21978762 [Accessed December 3, 2018].

Wielgosz MM, Raju R & Huang H V (2002). Sequence Requirements for Sindbis Virus Subgenomic mRNA Promoter Function in Cultured Cells. *J Virol* **75,** 3509–3519.

Wikan N, Khongwichit S, Phuklia W, Ubol S, Thonsakulprasert T, Thannagith M, Tanramluk D, Paemanee A, Kittisenachai S, Roytrakul S & Smith DR (2014). Comprehensive proteomic analysis of white blood cells from chikungunya fever patients of different severities. *J Transl Med* **12,** 96.

Wilkins MR, Pasquali C, Appel RD, Ou K, Golaz O, Sanchez JC, Yan JX, Gooley AA, Hughes G, Humphery-Smith I, Williams KL & Hochstrasser DF (1996). From proteins to proteomes: Large scale protein identification by two-dimensional electrophoresis and amino acid analysis. *Bio/Technology* **14,** 61–65.

Wilkinson KD & Audhya TK (1981). Stimulation of ATP-dependent proteolysis requires ubiquitin with the COOH-terminal sequence Arg-Gly-Gly. *J Biol Chem* **256,** 9235–9241.

Willems WR, Kaluza G, Boschek CB, Bauer H, Hager H, Schütz HJ & Feistner H (1979). Semliki forest virus: Cause of a fatal case of human encephalitis. *Science (80-)* **203,** 1127–1129.

Wilson RC & Doudna JA (2013). Molecular Mechanisms of RNA Interference. *Annu Rev Biophys* **42,** 217–239.

Wimmer P & Schreiner S (2015). Viral Mimicry to Usurp Ubiquitin and SUMO Host Pathways. *Viruses* **7,** 4854–4877.

Wise de Valdez MR, Nimmo D, Betz J, Gong H-F, James AA, Alphey L & Black WC (2011). Genetic elimination of dengue vector mosquitoes. *Proc Natl Acad Sci* **108,** 4772–4775.

Woo JL & Berk AJ (2006). Adenovirus Ubiquitin-Protein Ligase Stimulates Viral Late mRNA Nuclear Export. *J Virol* **81,** 575–587.

Wu X, Zhang M & Sun S-C (2011). Mutual regulation between deubiquitinase CYLD and retroviral oncoprotein Tax. *Cell Biosci* **1,** 27.

Xia ZP, Sun L, Chen X, Pineda G, Jiang X, Adhikari A, Zeng W & Chen ZJ (2009). Direct activation of protein kinases by unanchored polyubiquitin chains. *Nature* **461,** 114–119.

Xing Y, Chen J, Tu J, Zhang B, Chen X, Shi H, Baker SC, Feng L & Chen Z (2013). The papain-like protease of porcine epidemic diarrhea virus negatively regulates type I interferon pathway by acting as a viral deubiquitinase. *J Gen Virol* **94,** 1554–1567.

Xu P, Duong DM, Seyfried NT, Cheng D, Xie Y, Robert J, Rush J, Hochstrasser M, Finley D & Peng J (2009). Quantitative Proteomics Reveals the Function of Unconventional Ubiquitin Chains in Proteasomal Degradation. *Cell* **137,** 133–145.

Xu Z, Zheng Y, Zhu Y, Kong X & Hu L (2011). Evidence for OTUD-6B Participation in B Lymphocytes Cell Cycle after Cytokine Stimulation ed. Umen JG. *PLoS One* **6,** e14514.

Yang X, Chen X, Bian G, Tu J, Xing Y, Wang Y & Chen Z (2014). Proteolytic processing, deubiquitinase and interferon antagonist activities of Middle East respiratory syndrome coronavirus papain-like protease. *J Gen Virol* **95,** 614–626.

Yao T, Song L, Jin J, Cai Y, Takahashi H, Swanson SK, Washburn MP, Florens L, Conaway RC, Cohen RE & Conaway JW (2008). Distinct modes of regulation of the Uch37 deubiquitinating enzyme in the proteasome and in the Ino80 chromatin-remodeling complex. *Mol Cell* **31,** 909–917.

Yasuda J, Nakao M, Kawaoka Y & Shida H (2003). Nedd4 Regulates Egress of Ebola Virus-Like Particles from Host Cells. *J Virol* **77,** 9987–9992.

Yasunaga J, Lin FC, Lu X & Jeang K-T (2011). Ubiquitin-Specific Peptidase 20 Targets TRAF6 and Human T Cell Leukemia Virus Type 1 Tax To Negatively Regulate NF-κB Signaling. *J Virol* **85,** 6212–6219.

Ye R, Su C, Xu H & Zheng C (2016). Herpes Simplex Virus 1 Ubiquitin-Specific Protease UL36 Abrogates NF-κB Activation in DNA Sensing Signal Pathway. *J Virol* **91,** e02417-16.

Ye Y & Rape M (2009). Building ubiquitin chains: E2 enzymes at work. *Nat Rev Mol Cell Biol* **10,** 755–764. Available at: http://www.nature.com/articles/nrm2780 [Accessed March 1, 2019].

Yeh HM, Yu CY, Yang HC, Ko SH, Liao CL & Lin YL (2013). Ubiquitin-specific protease 13 regulates IFN signaling by stabilizing STAT1. *J Immunol* **191,** 3328–3336.

Yi Z, Ouyang J, Sun W, Xiao X, Li S, Jia X, Wang P & Zhang Q (2018). Biallelic mutations in USP45, encoding a deubiquitinating enzyme, are associated with Leber congenital amaurosis. *J Med Genet*jmedgenet-2018-105709.

Yu L, Zhang X, Wu T, Wang Y, Meng J, Liu Q, Niu X & Wu Y (2017). The papain-like protease of avian infectious bronchitis virus has deubiquitinating activity. *Arch Virol* **162,** 1943–1950.

Yu X, Yu Y, Liu B, Luo K, Kong W, Mao P & Yu XF (2003). Induction of APOBEC3G Ubiquitination and Degradation by an HIV-1 Vif-Cul5-SCF Complex. *Science (80-)* **302,** 1056–1060.

Yuan WC, Lee YR, Lin SY, Chang LY, Tan YP, Hung CC, Kuo JC, Liu CH, Lin MY, Xu M, Chen ZJ & Chen RH (2014). K33-Linked Polyubiquitination of Coronin 7 by Cul3-KLHL20 Ubiquitin E3 Ligase Regulates Protein Trafficking. *Mol Cell* **54,** 586–600.

Zaim M, Aitio A & Nakashima N (2000). Safety of pyrethroid-treated mosquito nets. *Med Vet Entomol* **14,** 1–5.

Zhang B, Srirangam A, Potter DA & Roman A (2005). HPV16 E5 protein disrupts the c-Cbl-EGFR interaction and EGFR ubiquitination in human foreskin keratinocytes. *Oncogene* **24,** 2585–2588.

Zhang H, Wang D, Zhong H, Luo R, Shang M, Liu D, Chen H, Fang L & Xiao S (2015). Ubiquitin-specific Protease 15 Negatively Regulates Virus-induced Type I Interferon Signaling via Catalytically-dependent and -independent Mechanisms. *Sci Rep* **5,** 11220.

Zhang HM, Yang J, Sun HR, Xin X, Wang HD, Chen JP & Adams MJ (2007). Genomic analysis of rice stripe virus Zhejiang isolate shows the presence of an OTU-like domain in the RNA1 protein and a novel sequence motif conserved within the intergenic regions of ambisense segments of tenuiviruses. *Arch Virol* **152,** 1917–1923.

Zhang L, Zhou F, Drabsch Y, Gao R, Snaar-Jagalska BE, Mickanin C, Huang H, Sheppard KA, Porter JA, Lu CX & Ten Dijke P (2012). USP4 is regulated by AKT phosphorylation and directly deubiquitylates TGF-β type i receptor. *Nat Cell Biol* **14,** 717–726.

Zhang M, Lee AJ, Wu X & Sun S-C (2011*a*). Regulation of antiviral innate immunity by deubiquitinase CYLD. *Cell Mol Immunol* **8,** 502–504.

Zhang M, Zhang M-X, Zhang Q, Zhu G-F, Yuan L, Zhang D-E, Zhu Q, Yao J, Shu H-B & Zhong B (2016). USP18 recruits USP20 to promote innate antiviral response through deubiquitinating STING/MITA. *Cell Res* **26,** 1302–1319.

Zhang R, Kim AS, Fox JM, Nair S, Basore K, Klimstra WB, Rimkunas R, Fong RH, Lin H, Poddar S, Crowe JE, Doranz BJ, Fremont DH & Diamond MS (2018*a*). Mxra8 is a receptor for multiple arthritogenic alphaviruses. *Nature* **557,** 570–574.

Zhang W, Bailey-Elkin BA, Knaap RCM, Khare B, Dalebout TJ, Johnson GG, van Kasteren PB, McLeish NJ, Gu J, He W, Kikkert M, Mark BL & Sidhu SS (2017). Potent and selective inhibition of pathogenic viruses by engineered ubiquitin variants ed. Whelan SPJ. *PLoS Pathog* **13,** e1006372.

Zhang W, Mukhopadhyay S, Pletnev S V, Baker TS, Kuhn RJ & Rossmann MG (2002). Placement of the structural proteins in Sindbis virus. *J Virol* **76,** 11645–11658.

Zhang W, Sulea T, Tao L, Cui Q, Purisima EO, Vongsamphanh R, Lachance P, Lytvyn V, Qi H, Li Y & Ménard R (2011*b*). Contribution of active site residues to substrate hydrolysis by USP2: Insights into catalysis by ubiquitin specific proteases. *Biochemistry* **50,** 4775–4785.

Zhang X, Fugère M, Day R & Kielian M (2003). Furin Processing and Proteolytic Activation of Semliki Forest Virus. *J Virol* **77,** 2981–2989.

Zhang Y, Li LF, Munir M & Qiu HJ (2018*b*). RING-domain E3 ligase-mediated host-virus interactions: Orchestrating immune responses by the host and antagonizing immune defense by viruses. *Front Immunol* **9,** 1083.

Zheng D, Chen G, Guo B, Cheng G & Tang H (2008). PLP2, a potent deubiquitinase from murine hepatitis virus, strongly inhibits cellular type I interferon production. *Cell Res* **18,** 1105–1113.

Zheng N & Shabek N (2017). Ubiquitin Ligases: Structure, Function, and Regulation. *Annu Rev Biochem* **86,** 129–157.

Zheng Y, Liu Q, Wu Y, Ma L, Zhang Z, Liu T, Jin S, She Y, Li Y-P & Cui J (2018). Zika virus elicits inflammation to evade antiviral response by cleaving cGAS via NS1-caspase-1 axis. *EMBO J*e99347.

Zhong H, Wang D, Fang L, Zhang H, Luo R, Shang M, Ouyang C, Ouyang H, Chen H & Xiao S (2013). Ubiquitin-specific proteases 25 negatively regulates virus-induced type I interferon signaling ed. Ho W. *PLoS One* **8,** e80976.

Zhu H, Zheng C, Xing J, Wang S, Li S, Lin R & Mossman KL (2011). Varicella-Zoster Virus Immediate-Early Protein ORF61 Abrogates the IRF3-Mediated Innate Immune Response through Degradation of Activated IRF3. *J Virol* **85,** 11079–11089.

Appendix

Appendix Table 1. Proteins bound to HA-Ub-PA identified by LC-MS/MS in unlabelled HeLa cells		
Protein	**Peptides**	**CRAPome**
USP19	1	
USP8	2	
VCPIP1	2	
OTUD6B	2	
USP11	4	
USP4	6	
USP47	6	
USP15	9	
USP9X	22	
OTUB1	5	
UCHL3	6	
UCHL5	11	
USP7	26	
USP14	14	
USP5	25	
KYNU	1	No
IGHV1-45	1	No
TMEM71	1	No
CSF1	1	No
MYDGF	1	No
IGHG2	1	No
HSPA7	1	No
EEF1A1P5	5	No
PRDX1	3	Yes
RAN	3	Yes
GNB2L1	3	Yes
GAPDH	2	Yes
HNRNPH1	3	Yes
HSPA8	1	Yes
PRMT1	1	Yes
RPL8	1	Yes
RPL35	1	Yes
TUBA1B	2	Yes
HNRNPA1	1	Yes

OBSCN	1	Yes
EWSR1	1	Yes
UBB	7	Yes
RPL13	1	Yes
ZNF565	1	Yes
LDHA	2	Yes
KRT1	22	Yes
HSP90AB1	4	Yes
HSPA5	2	Yes
PKM	4	Yes
KCNA6	1	Yes
MSN	2	Yes
TARS	1	Yes
TKT	3	Yes
CPS1	1	Yes
HNRNPH3	1	Yes
PRDX2	2	Yes
HNRNPA3	2	Yes
HMGCS2	1	Yes
VCP	6	Yes
ACTG1	6	Yes
DCD	1	Yes
FSCN1	4	Yes
UGT3A2	1	Yes
TUBB	4	Yes
HUWE1	14	Yes
TMEM87A	1	Yes
PLBD2	1	Yes
TAF15	3	Yes
SMARCAD1	1	Yes
ANKFY1	4	Yes

Appendix Table 2. Log2 ratios of all proteins identified by mass spec in CHIKV infected HeLa cells with HA-Ub-PA in three individual experiments

			Exp1				Exp2				Exp3			
Protein	**Peptides**	**CRAPome**	**4h/M**	**6h/M**	**8h/M**	**10h/M**	**4h/M**	**6h/M**	**8h/M**	**10h/M**	**4h/M**	**6h/M**	**8h/M**	**10h/M**
OTUD5	7				0.25	-0.24	-0.17	-0.28	0.31	-0.16				
OTUB1	11		-0.29	-0.15	0.18	-0.42	-0.27	-0.20	-0.16	0.04	-0.09	0.05	-0.93	0.08
YOD1	9		-0.09	0.29	-0.09	-0.39	0.11	0.02	0.18	-0.06		0.12	0.07	
OTUD7B	6		-0.55		-0.58	-0.46	-0.46	-0.92	0.01	-0.21				
OTUD6B	8		0.30	0.00	-0.22	-0.78	0.00	-0.63	-0.47	-0.59	-0.59	0.35	0.09	0.23
VCPIP1	12		-0.11	-0.12	-0.51	-0.43	-0.26	-0.59	-0.03	0.26	-1.08	0.24	-0.23	0.20
UCHL3	10		-0.12	-0.01	-0.28	-0.26	0.53	0.26	0.06	0.14	0.48	-0.31	-0.14	0.31
UCHL5_A	19				0.61	-0.08	0.44	0.41						
UCHL5_B	19		0.12	-0.14	-0.01	-0.34	-0.13	-0.17	0.10	0.22	-0.18	0.00	-0.38	-0.05
USP19	12		-0.42		-0.08	-0.43	-0.07	-0.58	-0.37	-0.28				
USP36	2				-0.88	-0.48								
USP11	7				-1.23	-0.85	0.40	-0.41	-0.11	0.03				
USP1	4		-0.56		-0.57	-0.82			-0.33	-0.06				
USP8	33		-0.31	-0.39	-0.18	-0.49	0.10	-0.33	-0.09	-0.07	0.27	0.18	0.29	0.47
USP5	46		0.01	0.05	0.05	-0.09	0.05	0.09	0.14	0.32	0.10	0.04	0.02	0.11
USP14	34		0.09	-0.07	-0.03	-0.05	-0.03	-0.06	-0.01	0.14	-0.19	0.09	-0.39	-0.10
USP4	9		-0.34	0.41	-0.16	0.08	-0.33	-0.26	-0.07	0.17				
USP10	4				-0.14	-0.37	-0.06	-0.16	-0.67	-0.58				
USP9X	35		-0.04	0.21	0.09	-0.01	0.13	0.04	0.37	0.57	-0.48	0.48	0.55	-0.09
USP7	58		0.31	0.42	0.23	0.31	0.39	0.39	0.52	0.69	0.01	0.04	0.09	0.11
USP47	30		0.11	-0.23	-0.17	-0.43	0.22	-0.63	-0.18	-0.23		0.28	-0.11	
USP28	10		0.51	-0.51	0.04	0.10	-0.08	-0.19	0.40	0.25				

USP24	4				0.12	0.23			0.78	0.52				
USP15	40		0.00	0.06	0.09	0.08	0.08	0.13	0.09	0.05	0.05	0.11	0.19	0.16
USP16	13		0.10	-0.18	0.14	-0.11	-0.10	-0.08	-0.03	0.22				
IGHV1-45	1	No	-8.45		-8.55		-6.21	-4.10	-8.55					
JCHAIN	1	No									-3.25	-4.15	-2.73	-3.28
IGHG2	2	No	-7.30		-3.55		-3.82				-6.69			
IGHA1	3	No									-3.98			
HSP90AB2P	6	No	-0.84	-0.94	-1.21	-0.59	-0.96	-1.18	-1.21	-1.38				
KCNK1	1	No			-0.82	-0.80			-1.98	-1.92				
EEF1A1P5	15	No	-2.36	-2.50	-1.45	-1.87	-1.70	-1.95	-1.81	-2.02	-2.22	-2.38	-2.24	-2.96
TMEM263	1	No					0.35	0.71						
MYDGF	2	No	0.09	-0.21	0.33	0.40	0.45	0.43	0.46	0.55				
MMTAG2	1	No	0.28	-0.30										
HNRNPDL	1	Yes			0.17	0.85								
HNRNPDL	7	Yes			0.16	1.15								
RPL17	3	Yes			-0.56	-0.49	-0.27	-0.14	-1.75	-1.31				
HSPA4	3	Yes			0.04	-0.14	-0.82	-0.55	-0.65	-1.09				
YBX1	4	Yes	-0.12				-0.11	-0.38						
PRDX1	13	Yes	-0.76	-0.66	0.29	-0.09	0.41	0.01	-0.74	-0.74	-1.20	-1.02	-0.54	-1.09
RPS6	3	Yes			-0.87	-0.73	-0.24	-0.13	-0.87	-1.05				
RPL7	4	Yes			-0.54	-0.44	-0.45	-0.15	-1.70	-1.20				
EWSR1	4	Yes			-0.28	-0.35	1.71	0.76						
RPS7	3	Yes	-0.58	-1.00	-0.19	-0.16	-0.15	-0.19	-0.88	-1.02				

RAN	8	Yes	-1.09	-1.11	-0.29	-0.62	-0.44	-0.65	-0.92	-1.00	-0.92	-0.48	-0.19	-1.49
RPL37A	2	Yes			-0.33	-0.72	-0.60	-0.20	-0.77	-0.65				
RPL23	1	Yes			-0.79	-0.57	0.88	-0.29						
RPL24	3	Yes	-0.93	-0.13			-0.77	-0.63	-0.88	-0.23				
HNRNPAB	5	Yes	-0.89	-0.06	0.11	1.43	1.89	2.57	0.88	1.14				
RPS3A	4	Yes	-0.76	-1.58	-0.12	-0.47	0.09	-0.36	-1.31	-1.55				
HNRNPD	2	Yes			0.48	1.05								
SDHA	2	Yes	-0.18	-0.07	0.19	-0.34			-0.52	-1.21				
CCT5	2	Yes			-0.76	-1.21			-1.17					
RPL14	2	Yes			-0.59	-0.55	-0.17	-0.03	-1.45	-1.10				
RPS24	2	Yes			-0.10	-0.38	0.31	-0.28	-0.53	-0.75				
NACA	3	Yes			-0.26	-0.04								
HNRNPH1	3	Yes			-0.32	0.28								
DLD	1	Yes			0.78	0.87								
HSPA8	8	Yes	-1.16	-1.05	-1.22	-0.65	-0.69	-0.91	-1.77	-0.66				
PRMT1	4	Yes	0.52	-0.05	0.15	0.05			-0.04	-0.92				
RPL8	3	Yes	-0.47	3.15	-0.39	-0.35	-0.08	-0.14	-0.76	-0.90				
RPS3	7	Yes			-1.05	-0.73	-2.51	-1.64	-1.14	-1.42				
RPS2	4	Yes	-0.38	-0.44	-0.66	-0.84	-0.64	-0.86	-1.65	-1.63				
CFL1	1	Yes			-1.04	-0.53								
RPL35	1	Yes					-0.77	-0.70						
UBC	18	Yes	-6.76	-6.82	-4.30	-6.79	-6.23	-6.43	-7.13	-7.52	-6.82	-7.27	-7.62	-6.98
TUBA1C	11	Yes	-1.59	-2.01	-1.61	-1.75	-1.69	-2.00	-1.70	-1.86				
GANAB	3	Yes	-0.71	-0.49	0.17	0.25								
CCT2	4	Yes					-2.01	-3.12						
LYZ	3	Yes									-2.54		-2.60	

HNRNPA1	5	Yes			-0.38	0.81	0.56	0.36	-0.15	0.21				
PSMG1	1	Yes			-0.39	-0.71								
PPIA	2	Yes	-0.14	-0.51	-0.42	-0.16	0.42	-0.29	-1.14	-0.34				
RPL21	1	Yes					0.06	0.04	-0.32	-0.35				
RPL18	3	Yes	-0.38	-1.53	-0.33	-0.33	-0.19	-0.25	-0.45	-0.37				
RPS20	1	Yes			-1.41	-0.26								
SHMT2	2	Yes			-1.92	-2.00								
RPL28	2	Yes	-0.85	-0.72	-0.87	-0.94	0.10	-0.15	-0.66	-0.46				
RPL4	3	Yes	-0.24	-0.52	-0.63	-0.18	0.09	-0.21	-0.94	-0.42				
ITGA6	1	Yes			-3.18	-3.67								
RPL10	1	Yes					-0.12	0.14						
RPS15A	3	Yes			-0.06	-0.60	-0.32	0.49	-0.36	-0.16				
C1QBP	2	Yes	0.38	1.17	0.32	1.01								
DDX5	1	Yes			-0.53	-0.46								
ARHGDIA	1	Yes			-0.99	-1.75								
RPL13	2	Yes	-0.96	-0.48	-0.14	-0.73	0.04	-0.19	-0.67	-0.60				
H3F3B	2	Yes	-2.45		-3.68	-3.93								
RPS16	2	Yes	-1.03	-0.30										
RPS11	5	Yes			-0.57	-0.63	-0.82	-0.65	-1.01	-1.40				
RPS5	1	Yes							-1.56	-1.08				
UBA52	14	Yes											-1.19	
HNRNPR	5	Yes			-0.26	0.00					-0.80			-0.86
MGEA5	4	Yes			1.51	0.99			-0.52	-0.93				
CIAO1	1	Yes							-0.76	-0.75				
LDHA	7	Yes			-0.09	-0.01	0.38	0.44	0.09	-0.18				
PGK1	2	Yes			-1.31	-1.37								

ASS1	6	Yes			0.10	-0.10	0.78	0.26	-0.44	-0.28				
KRT1	59	Yes	-2.88	-3.31	-4.94	-4.62	-3.45	-4.00	-4.54	-4.84	-4.84	-2.16	-3.96	-4.98
GAPDH	13	Yes	-0.29	-0.56	-0.18	-0.25	0.00	0.16	-0.43	-0.31	-1.23	-1.54	-1.68	-1.59
ARG1	2	Yes									-3.17		-1.11	
ENO1	6	Yes	-0.92	0.15	-0.94	-0.83	-1.33	-1.97	-1.02	-1.00				
NPM1	5	Yes	-0.89	-1.14	-0.68	0.14	0.10	0.73	-0.85	-0.33				
LDHB	10	Yes	0.16	-0.23	0.07	-0.16	0.40	0.35	-0.09	0.00				
PFN1	4	Yes			-0.47	-0.38			-0.37	-0.44				
HSP90AA1	17	Yes			-1.98	-1.29	-2.17	-2.06	-2.28	-2.13				
HSP90AB1	24	Yes	-1.35	-2.35	-1.51	-0.88	-1.81	-2.06	-1.74	-1.93	-1.21	-0.48	-1.17	-1.61
HSPA1B	6	Yes			-0.05	0.61	0.17	1.71	-0.80	1.48				
HIST1H1E	6	Yes									0.06	-0.15	0.30	0.52
HSPA5	11	Yes	-1.33		-1.32	-0.49	-0.81	-1.50			-0.64		0.91	
PCNA	5	Yes			-0.14	-0.21	0.67	1.02	-0.36	-0.27				
EEF2	17	Yes	-1.24	-1.42	-0.89	-0.95	-0.16	-0.53	-0.51	-1.01				
MIF	1	Yes	-1.09	6.91	-0.29	4.45	-0.61	6.26	-0.68	5.78				
PKM	20	Yes	-2.19	-0.67	-1.66	-1.89	-1.34	-0.08	-1.73	-0.94	-1.57	-2.68	-1.90	-3.31
HSP90B1	22	Yes	-1.92	-2.92	-3.30	-2.33	-1.88	-2.86	-2.75	-4.31	-1.08			-1.89
AKR1B1	1	Yes					-1.17	-0.91						
HSPA6	4	Yes	-2.45	-2.75	-1.23	-0.70	-1.59	-1.66	-1.95	-1.52				
TCP1	6	Yes			-2.42	-1.99			-1.46	-2.35				
RPL35A	5	Yes			-0.89	-0.43	-0.27	-0.49	-1.04	-0.69				
HNRNPA2B1	13	Yes	-0.51	0.32	-0.31	0.46	0.87	1.11	0.34	0.47	-0.01	0.07	0.66	-0.22
PPIB	2	Yes			-0.84	-0.69								
AHCY	2	Yes			-0.69	-0.97								
MSN	2	Yes			0.24	-0.43	0.35	-0.39	-0.31	-0.45				

TARS	17	Yes	0.00	-0.05	0.20	0.29	0.67	0.30	-0.33	-0.70				
TKT	19	Yes	-0.52	-0.54	-0.12	0.11	0.02	0.41	-0.04	-0.18	-0.01	-0.47	-0.17	-0.11
PRDX3	6	Yes	0.53	0.62	1.06	0.77	1.02	1.17	-0.30	-0.06				
CPS1	37	Yes	0.54	0.68	0.73	0.86	1.12	1.76	0.42	0.29				
PRDX2	5	Yes	-1.07	3.55	0.38	0.06	0.48	1.77	-0.36	1.09				
KRT9	47	Yes	-3.22	-2.77	-3.76	-4.27	-2.82	-3.15	-2.95	-3.20	-4.36	-4.62	-2.31	-5.41
FUS	8	Yes	-1.09	-1.14	-1.31	-0.28	-0.17	-1.08	-0.20	-1.32	-0.71	-0.75	-0.32	-0.83
KRT2	60	Yes	-4.31	-3.14	-4.15	-5.17	-4.32	-3.88	-5.18	-4.70	-4.43	-6.42	-3.18	-5.96
RPL3	5	Yes	-0.56	-1.21	-0.30	-0.42	-0.37	-0.16	-0.58	-0.52				
EIF2S3	4	Yes	-0.61	-2.09	-0.71	-1.19	0.04	-0.41	-1.04	-1.61				
RPL5	6	Yes	-0.72	-1.87	-0.56	-0.40	-0.20	-0.21	-0.72	-0.89				
RPS9	6	Yes	-0.92	-0.46	-0.74	-0.80	-0.04	-1.02	-0.72	-1.01				
RPL29	2	Yes	-0.21	0.16	0.29	0.67	0.19	0.09	-1.07	-1.01	-1.01	0.01	0.59	0.44
FASN	3	Yes			-1.03	-0.91	-0.35	-0.54	-0.42	-0.65				
TUFM	3	Yes	-0.03	-0.60	0.35	-0.14								
SERPINH1	3	Yes			0.39	0.26			-0.22	0.25				
HNRNPA3	3	Yes			-0.11	0.47								
HNRNPF	3	Yes			-0.71	-0.03								
VCP	24	Yes	-1.40		-3.13	-3.58			-1.47	-2.97				
SEC13	1	Yes			0.30	0.31								
EIF4A1	8	Yes			-1.93	-2.23			-0.91					
RPL26	2	Yes			-0.39	-0.06	-0.47	-0.89	-1.25	-1.21				
RPL15	5	Yes	-0.36	-0.42	0.16	0.33	0.02	0.16	-0.53	-0.54		-0.39	-0.15	
RPL27	4	Yes	-1.34		-0.46	-0.78	0.08	0.26	-0.76	0.01				
RPS14	2	Yes	1.66		-0.37	-0.32								
RPS23	3	Yes	-0.58	-0.38	-0.66	-0.41	-0.37	-0.47	-0.73	-0.84				

RPS18	2	Yes			-1.63	-1.47	-0.16	-0.42	-1.24	-1.78				
RPS13	3	Yes	-1.62	-1.35	-1.27	-1.15	-0.78	-1.66	-2.25	-1.91				
RPS4X	5	Yes			-1.00	-0.72			-1.43	-1.57				
HIST1H4A	6	Yes	-5.00	-1.84	-3.65	-1.70			-5.62	-4.17				
RPL11	4	Yes	-0.90	-1.21	-0.38	-0.71	-0.25	0.13	-0.67	-0.72				
RPS27A	18	Yes	0.27	0.36	0.37	0.31	0.37	0.06	-0.40	-0.86				
GNB2L1	11	Yes	-0.65	-0.91	-0.47	-0.60	-0.47	-0.56	-0.59	-1.08	-0.49	-0.72	1.14	-0.23
ACTG1	16	Yes	-1.01	-1.42	-0.71	0.17	-1.11	-1.39	-1.78	-1.28	-0.87	-2.77	-1.84	-1.95
ACTA1	12	Yes			-0.95	0.27	-0.94	-0.97	-1.21	-0.54				
DCD	3	Yes	0.98		0.35		-0.69							
ARF1	4	Yes	-0.90	-1.54	-1.03	-0.94	-1.16	-1.96	-1.87	-2.31				
HNRNPU	14	Yes	-0.09	0.24	0.14	0.24	0.67	0.53	0.01	0.10	-0.51			0.09
RPL6	11	Yes	-0.52	-0.81	-0.10	0.01	0.12	-0.15	-0.88	-0.59				
ILF3	7	Yes			-0.42	-0.04								
HNRNPA0	2	Yes			0.31	0.13								
PRDX4	5	Yes	-1.12	-1.69	-0.70	-0.67	-0.76	-0.90	-1.13	-1.40				
EIF3I	3	Yes	-0.96	-0.10	0.09	0.10	0.04	-0.47	-0.33	-1.19				
PDIA6	2	Yes					4.01							
PCBP1	2	Yes					0.23	-0.74	0.07					
FSCN1	9	Yes	1.22	0.69	0.59	0.06	0.27	-0.03	-0.51	-1.28	0.38	-0.28	0.06	-0.90
C2CD3	1	Yes			-0.79	-0.14								
HSD17B10	1	Yes			-0.35	-0.18								
RBBP7	2	Yes			0.12	0.17								
TUBB	16	Yes	-1.65	-1.92	-1.61	-1.45	-1.81	-2.10	-1.98	-2.27	-0.49			-0.89
RPS8	5	Yes	-0.73	-1.32	-2.11	-2.23	-0.41	0.08	-0.63	-0.84	-0.64			-0.74
CAP1	2	Yes			-0.10	-0.76	-1.69	-0.49	-0.84	-1.12				

RPS27	3	Yes			-0.02	-0.65	-1.39	-0.68	-1.02	-1.25				
HNRNPK	1	Yes			-0.61	0.16								
KANK4	1	Yes			0.02	-0.31								
RPL7A	4	Yes	-0.52	-1.27	-0.24	0.07	-0.24	0.11	-0.98	-0.33				
SBSN	1	Yes			-2.10									
HUWE1	68	Yes	-0.12	-0.43	0.09	0.14	-0.17	-0.71	-0.09	-0.53	-0.37	-0.08	-0.65	-0.05
KRT77	11	Yes										-2.45	-0.16	
SREK1IP1	1	Yes	0.66	0.62			0.29	-0.27	-0.71	0.33				
TAF15	6	Yes	-0.25	-0.17	-0.75	-0.02	0.59	-0.15	-0.07	-1.12				
CACYBP	2	Yes							-0.07	-0.70				
CALML5	1	Yes									-2.10			
ANKFY1	34	Yes	0.23	-0.28	-0.33	-0.70	0.45	-0.16	0.15	-0.16	-0.07	1.26	-0.02	-0.34
CHORDC1	2	Yes							0.05	-1.01				
PA2G4	2	Yes			0.70	-0.49								
VPS26A	1	Yes			0.39	0.40								
HIST1H2BN	3	Yes			-1.12	-0.43								

Appendix Table 3. Peptides identified for each DUB with HA-Ub-PA by LC-MS/MS in SILAC labelled HeLa cells following CHIKV infection		
DUB	**No. of peptides**	**Peptide sequence**
OTUD5	7	ATDWEATNEAIEEQVAR AVADQVYGDQDMHEVVR DSGVVGARPR ESYLQWLR IEAMDPATVEQQEHWFEK NIHYNSVVNPNK TSEESWIEQQMLEDK
OTUB1	11	AFGFSHLEALLDDSK AFGFSHLEALLDDSKELQR EYAEDDNIYQQK FFEHFIEGGR GEGGTTNPHIFPEGSEPK IKDLHKK IQQEIAVQNPLVSER LELSVLYK LLTSGYLQR PGHYDILYK VYLLYRPGHYDILYK
YOD1	9	DGTHVLQGLSSR ELQGQIAAITGIAPGGQR ETGHTNFGEV ETLPVLTR FGEDAGYTK LIAQIVASDPDFYSEAILGK QFTDVNR SSPAFTKR VLLIYDGIHYDPLQR
OTUD7B	6	DLIEQSMLVALEQAGR EEQPTGPPAESR EQAVIPLTDSEYK GISHASSSIVSLAR GSKPGGVGTGLGGSSGTETLEK NWDVNAALSDFEQLR
OTUD6B	8	AIEDQLK ALSHILQTPIEIIQADSPPIIVGEEYSK HAYGLGEHYNSVTR HREELEQLK IAEAEIENLTGAR IDSVAVNISNLVLENQPPR LAQILAAR MEAVLTEELDEEEQLLRR
VCPIP1	12	AFLIEPEHVNTVGYGK DGPSSAPATPTK

		DQSTEQSPSDLPQR ITIEILK KHNTGTDFSNSSTK KNPDDYTPVNIDGAHAQR LLSPILAR NALLGVTGAPK NHYIPLVGIK SKAEGGQSAAAHSAHTVK VGDVQGQESESQLPTK VVHTILHQTAK
UCHL3	10	FLEESVSMSPEER FMERDPDELR KFLEESVSMSPEER MHFESGSTLK MHFESGSTLKK QLGLHPNWQFVDVYGMDPELLSMVPR SQGQDVTSSVYFMK VTHETSAHEGQTEAPSIDEK WLPLEANPEVTNQFLK YLENYDAIR
UCHL5_A	19	EEDAFHFVSYVPVNGR EFSQSFDAAMK FNLMAIVSDR FNLMAIVSDRK GAQVEEIWSLEPENFEK GLALSNSDVIR HNYLPFIMELLK KMIYEQK LDTIFFAK LKPVHGLIFLFK LYELDGLR NQMLIEEEVQK QLAEEPMDTDQGNSMLSAIQSEVAK QQMFEFDTK QVHNSFAR TLAEHQQLIPLVEK TSAKEEDAFHFVSYVPVNGR WQPGEEPAGSVVQDSR YKIENIR
UCHL5_B	19	EEDAFHFVSYVPVNGR EFSQSFDAAMK FNLMAIVSDR FNLMAIVSDRK GAQVEEIWSLEPENFEK GLALSNSDVIR HNYLPFIMELLK

		KMIYEQK LDTIFFAK LKPVHGLIFLFK LYELDGLR NQMLIEEEVQK QQMFEFDTK QVHNSFAR TLAEHQQLIPLVEK TSAKEEDAFHFVSYVPVNGR WQPGEEPAGSVVQDSR YKIENIR YSEGEIR
USP19	12	AGHSEHHPDLGPAAEAAASQGLGPGQAPEVAPTR FLVSVSK GEVGAGAGPGAQAGPSAK GTHHAFQPSK LFDDSTVTTVDESQVVTR LQEFVLVASK NDSFIVDLFQGQYK RGPPGLEDTTSK SEDTGLDSVATR VAVPTGPTPLDSTPPGGAPHPLTGQEEAR VLPVFYFAR VVVLEVQQRPQVPSVPISK
USP36	2	QTQATTLVHQIFGGYLR SFSYQLEALK
USP11	7	AAYVLFYQR ATVAANPAAAAAAVAAAAAVTEDREPQHEELPGLDSQWR EDIVVPVYLR NDSVIVDTFHGLFK VEVYPVELLLVR VIELPNIQK VLEVFFIPMDPR
USP1	4	EHQSLEENQR NVAELPTK VEESSEISPEPKTEMK YISENESPRPSQK
USP8	33	ALWTGQYR DLQIGTTLR ELYLSSSLK ELYTMMTDK FDDHEVSDISVSSVK FLDPITGTFR GEVAEEFGIIMK GSLENVLDSK

		GSLENVLDSKDK IHAETALLMEK IVPGLPSGWAK KKQEAEENEITEK KPTVTPTVNR KQEAEENEITEK LQTSVDFPLENLDLSQYVIGPK LRYEEAEVR MGPLNISTPVEPVAASK NISLIIMDAR NLNPVFGGSGPALTGLR NVPQIDR PAVASVPK QLNESIIVALFQGQFK QQQDYFHSILGPGNIK RQETGREDGGTLAK SDVSPIIQPVPSIK STGDVPHTSVTGDSGSGK STGDVPHTSVTGDSGSGKPFK STKPVVFSPTLMLTDEEK SYSSPDITQAIQEEEK SYSSPDITQAIQEEEKR SYVHSALK YKEENNDHLDDFK YVTVYNLIK
USP5	46	AELSEEALLSVLPTIR AVDWIFSHIDDLDAEAAMDISEGR DGLGGLPDIVR DLGYIYFYQR DRVTSAVEALLSADSASR DRVTSAVEALLSADSASRK EEDPATGTGDPPR EELLEYEEK ENLWLNLTDGSILCGR ETGYPLAVK EVQDGIAPR FASFPDYLVIQIK FASFPDYLVIQIKK FELDEDVK FTFGLDWVPK GHPEFSTNR GTGLQPGEEELPDIAPPLVTPDEPK IFQNAPTDPTQDFSTQVAK IGEWELIQESGVPLKPLFGPGYTGIR IVILPDYLEIAR KFTFGLDWVPK

		KLDVSIEMPEELDISQLR KQEVQAWDGEVR KYVDKLEK LAIGVEGGFDLSEEKFELDEDVK LDVSIEMPEELDISQLR LGHGLLSGEYSK LGHGLLSGEYSKPVPESGDGER LGHGLLSGEYSKPVPESGDGERVPEQK MALPELVR PVPESGDGERVPEQK QAEEEKMALPELVR QLDNPAR QQDAQEFFLHLINMVER RPKEEDPATGTGDPPR SAADSISESVPVGPK SSENPNEVFR TDKTMTELEIDMNQR TMTELEIDMNQR VDYIMQLPVPMDAALNK VDYIMQLPVPMDAALNKEELLEYEEK VTSAVEALLSADSASR VYLHLRR WVIYNDQK YFDGSGGNNHAVEHYR YVDKLEK
USP14	34	AQLFALTGVQPAR ASGEMASAQYITAALR CTESEEEEVTK DDDWGNIK DLFDSMDK EKFEGVELNTDEPPMVFK FDDDKVSIVTPEDILR FEGVELNTDEPPMVFK FKDLEDK FKDLEDKK GGTLKDDDWGNIK GGTLKDDDWGNIKIK ISRLPAYLTIQMVR KQDEWIK LEAIEDDSVK LEAIEDDSVKETDSSSASAATPSK LEAIEDDSVKETDSSSASAATPSKK LPAYLTIQMVR LQEEITK LRLQEEITK LSGGGDWHIAYVLLYGPR

		NGMTLLMMGSADALPEEPSAK PLYSVTVK QSPTLQR RKQDEWIK RVEIMEEESEQ SLIDQFFGVEFETTMK SSSSGHYVSWVK SSSSGHYVSWVKR SVPELKDALK SVPELKDALKR VLQQKLEAIEDDSVKETDSSSASAATPSK VSIVTPEDILR YLFTGLK
USP4	9	AAYVLFYQR ADTIATIEK DANGRPDAVVAK GAQWYLIDSR LFNIPAER LSGIAAENMVVADVYNHR NDSVIVDTFHGLFK VEVYLLELK YMSNTYEQLSK
USP10	4	DIRPGAAFEPTYIYR LPPVLVLHLK TAYLLYYR TVQDALESLVAR
USP9X	35	AQENYEGSEEVSPPQTK DDVFGYPQQFEDKPALSK DGLTISFTK DHEDYDPQTVR DSLHQPQYVEK ELDMEPYTVAGVAK ELLAFQTSEK EYNIGVLR HGNPEEEEWLTAER HLSFVVR ILTDEAVSGWK KEYNIGVLR KQNVQFMHNR LAEDDKDGVMAHK LAQQISDEASR LDDMINRPR LIGQLNLK LLLTAIGYGHVR LLQISSFNGK LQYYVPR

		LVGVLVHSGQASGGHYYSYIIQR LYSVVSQLIR NHQNLLDSLEQYVK NNFLPNADMETR NVHDLLAK RGAYLNALK SGGLPLVLSMLTR SPHVFYR TGETGIEETILEGHLGVTK VISSVSYYTHR VLGGSFADQK VVIQSNDDIASR WVVPVLPK YQYAELGK YSHVQEVQER
USP7	58	AGEQQLSEPEDMEMEAGDTDDPPR AGFIQDTSLILYEEVKPNLTER AVELGEK AVYMMPTEGDDSSK DDPENDNSELPTAK DFEPQPGNMSHPR DFEPQPGNMSHPRPWLGLDHFNK DGPGNPLR DLLQFFKPR EDYYDIQLSIK EEAIEHNYGGHDDDLSVR EEEITLYPDK ENDWGFSNFMAWSEVTDPEK EVFGTFGIPFLLR FAIVMMGR FDDDVVSR FDKDHDVMLFLK FEFPEQLPLDEFLQK FLTLPPVLHLQLMR FMYDPQTDQNIK FYPDRPHQK HNYEGTLR HQYINEDEYEVNLK HTGYVGLK IEEIPLDQVDIDKENEMLVTVAHFHK IHQGEHFR IINYRDDEK INDRFEFPEQLPLDEFLQK IQDYDVSLDK IQSLLDIQEK IQSLLDIQEKEFEK

		ISHLFFHK ITDFENR ITDFENRR ITQNPVINGNVALSDGHNTAEEDMEDDTSWR KHTGYVGLK KLYYQQLK KNIFESFVDYVAVEQLDGDNK LLEIVSYK LNTDPMLLQFFK LSEVLQAVTDHDIPQQLVER LWPMQAR LYYQQLK MNYFQVAK NIFESFVDYVAVEQLDGDNKYDAGEHGLQEAEK NSSLAEFVQSLSQTMGFPQDQIR PWLGLDHFNK REDYYDIQLSIK RPAMLDNEADGNK SDRREDYYDIQLSIK SEATFQFTVER SRYTYLEK SVPLALQR TIPNDPGFVVTLSNR VFYELQHSDKPVGTK VFYELQHSDKPVGTKK VLLDNVENK YDAGEHGLQEAEK
USP47	30	AEPYAADEGSGEGHK AESVAAPITVR AIETTDVTR AIHLPAETMR DGEQPQILLEDSSAGEDSVHDR DKTEELMELTDEQR EELIPQLR ELEQHIQTSDPENFQSEER FIGPLPR FLEVDEYPEHIK FLLDAVFAK ITLAAFK ITLNLPASTPVR IYLDGAPNKDLTQD KPDQVFQSYKPGEVMVK LDPFQEVVLESSSVDELR LFEDVANK LFVLLPEQSPVSYSK LSEISGIPLDDIEFAK

		QHLEPFVGVLSSHFK QTEQADLINELYQGK RFDFDYTTMHR SLSLQQQQDGDNGDSSK SMSQLAVLSR STETSDFENIESPLNER STYMFDLLLETR SVEAILEESTEKLK SYEGEEDTPMGLLLGGVK VHVVDLK VYASNQEFESVR
USP28	10	ASNGDITQAVSLLTDER EQTAQAIANTAR ESVIALYR FVDPSAALDLLK IPQMESSTNSSSQDYSTSQEPSVASSHGVR LLDPSAEIIVLK LPPVLTFELSR SSEEQQQDVSEFTHK TVTDEEINFVK VDGWPVGLK
USP24	4	QLHEITR VAVATILEK VLYNLEVLSSK VYDQTNPYTDVR
USP15	40	AAYVLFYQR ADTIDTIEK AEGGAADLDTQR EHLIDELDYILLPTEGWNK FSYVTPR HESVEYKPPK IFAMDENLSSIMER IFSIPDEK ISPSSLSNNYNNMNNR KGDTWYLVDSR KIFSIPDEK KIFSIPDEKETR KVVEQGMFVK LDLWSLPPVLVVHLK LVSWYTLMEGQEPIAR LYNLLLLR MDPLTKPMQYK MDPLTKPMQYKVVVPK MIVTDIYNHR NDSIIVDIFHGLFK NEDGTWPR

		NNTEDKLYNLLLLR NYDYSEPGR QDTFSGTGFFPLDR RNDSIIVDIFHGLFK SDIATLLK SFLALDWDPDLK SPGASNFSTLPK SYAELIK TLEVYLVR VEVYLTELK VVAEEAWENHLK VVAEEAWENHLKR WYYFDDSSVSTASEDQIVSK YFDENAAEDFEK YMSNTFEPLNKPDSTIQDAGLYQGQVLVIEQK YNLIAVSNHYGGMGGGHYTAFAK YQEELNFDNPLGMR YQMGDQNVYPGPIDNSGLLK YVGFDSWDK
USP16	13	DNGNIELENK GLEQGNLKK GYQQQDSQELLR KGLEQGNLK KGLEQGNLKK MIESVTDNQK NINMDNDLEVLTSSPTR SGHYTAYAK SNHISQEGVMHK TANSHLSNLVLHGDIPQDFEMESK VLNSQAYLLFYER VLYSLYGVVEHSGTMR YLLDGMR